

THESIS / THÈSE

DOCTOR OF SCIENCES

Plasticity of human indoleamine-2,3-dioxygenases 1 and 2 through a structural approach combining crystallography and Molecular Dynamics studies

MIRGAUX, Manon

Award date:
2022

Awarding institution:
University of Namur

[Link to publication](#)

General rights

Copyright and moral rights for the publications made accessible in the public portal are retained by the authors and/or other copyright owners and it is a condition of accessing publications that users recognise and abide by the legal requirements associated with these rights.

- Users may download and print one copy of any publication from the public portal for the purpose of private study or research.
- You may not further distribute the material or use it for any profit-making activity or commercial gain
- You may freely distribute the URL identifying the publication in the public portal ?

Take down policy

If you believe that this document breaches copyright please contact us providing details, and we will remove access to the work immediately and investigate your claim.



FACULTÉ
DES SCIENCES

Plasticity of human indoleamine-2,3-dioxygenases 1 and 2 through a structural approach combining crystallography and Molecular Dynamics studies

A thesis submitted by **Manon Mirgaux**
for the fulfillment of the requirements
for the degree of Doctor in Sciences

Thesis committee:

Yoann Olivier (Université de Namur, President of the jury)

Johan Wouters (Université de Namur, Advisor)

Geoffray Labar (Institut de recherche Labiris)

Laurence Leherte (Université de Namur)

Ute Röhrig (Swiss Institute of Bioinformatics)

René Wintjens (Université libre de Bruxelles)

November 2022

Université de Namur
FACULTÉ DES SCIENCES

Rue de Bruxelles 61, 5000 Namur, Belgique

Plasticity of human indoleamine-2,3-dioxygenases 1 and 2 through a structural approach combining crystallography and Molecular Dynamics studies by Manon

Mirgaux

Abstract

Recent researchs have highlighted the deregulation of enzyme levels for human indoleamine-2,3-dioxygenase 1 (hIDO1) and 2 (hIDO2) in high mortality pathologies such as cancer or Covid-19. As a result, hIDO1 has been intensively studied in the scientific community, with interest particularly directed towards drug design. However, in 2019, one of the most promising drugs failed in the clinical phase, challenging the knowledge about the protein. Conversely, hIDO2 is only minimally characterized in the literature. Few inhibitors have been developed for this target. Improving the understanding of these two enzymes is crucial to help design new drugs.

One of the most overlooked issues for hIDO1 and hIDO2 is the plasticity of both proteins. Recent research has highlighted the plasticity of the active site of hIDO1 and its potential involvement in activity. At present, the molecular bases associated to this plasticity remain unknown and the existence of such a mechanism in hIDO2 has not yet been proven. In this context, this work focuses on the structural and functional characterization of the proteins and the understanding of their plasticity. First, the two enzymes were characterized according to their physicochemical properties in order to compare them. Secondly, a multidisciplinary structural study, involving crystallography as well as Molecular Dynamics, has been performed on each target, in order to deepen the structural knowledge. Finally, with this new information, a model to explain the plasticity of each protein and the interactions between the two systems was proposed. Together, all these results improve the understanding of the two enzymes and form a solid basis for the development of new potential therapeutic tools.

Ph.D thesis in Sciences

Namur, November 2022

Université de Namur
FACULTÉ DES SCIENCES

Rue de Bruxelles 61, 5000 Namur, Belgique

**Étude de la plasticité des indoleamine-2,3-dioxygénases 1 et 2 humaine par une
approche structurale combinant la cristallographie et la Dynamique Moléculaire**

par **Manon Mirgaux**

Résumé

De récentes recherches ont mis en évidence la dérégulation des niveaux en enzymes indoleamine-2,3-dioxygénase humaine 1 (hIDO1) et 2 (hIDO2) dans des pathologies à mortalité élevée telles que le cancer ou la Covid-19. En conséquence, hIDO1 a été intensivement étudiée dans la communauté scientifique, avec un intérêt particulièrement orienté vers la conception de médicaments. Cependant, en 2019, un des médicaments les plus prometteurs a échoué en phase clinique, remettant en considération les connaissances sur la protéine. À l'inverse, hIDO2 n'est que très peu caractérisée dans la littérature. Peu d'inhibiteurs ont alors été développés pour cette cible. Améliorer la compréhension de ces deux enzymes est primordiale pour aider à la conception de nouveaux médicaments.

La plasticité du site actif de hIDO1 et son implication potentielle dans l'activité de la protéine a été mis en évidence depuis peu. À l'heure actuelle, les bases structurales et fonctionnelles de cette plasticité restent méconnues et l'existence d'une telle caractéristique dans hIDO2 n'a pas encore été prouvée. Dans ce contexte, ce travail s'intéresse à la caractérisation structurale des protéines et la compréhension de leur plasticité. Premièrement, les deux enzymes ont été caractérisées afin de pouvoir les comparer selon leurs propriétés physico-chimiques. Dans un deuxième temps, une étude pluridisciplinaire, faisant intervenir la cristallographie ainsi que la Dynamique Moléculaire, a été réalisée sur chaque cible. Enfin, avec ces nouvelles informations, un modèle d'explication de la plasticité de chaque protéine ainsi que des interactions entre les deux systèmes a pu être proposé. Ensemble, ces résultats améliorent la compréhension des deux enzymes et forment des bases solides au développement de nouveaux outils thérapeutiques potentiels.

Dissertation doctorale en Sciences

Namur, Novembre 2022

Acronyms

Acronyms	Signification
3HAA	3-hydroxyanthranilic Acid
3HK	3-Hydroxykynurenine
Ai	Absorbance ratio
ACMS	2-Amino-3-Carboxymuconic acid-6-Semialdehyde
AhR	Aryl hydrocarbon Receptor
AIDS	Acquired ImmunoDeficiency Syndrome
ALA	δ -aminolevulinic acid
AMS	2-Aminomuconic acid-6-Semialdehyde
cryo-EM	Cryogenic Electron Microscopy
C-term	C-terminal extremity
DNA	Deoxyribonucleic Acid
DSF	Differential Scanning Fluorimetry
D-Trp	D-Tryptophan
DTT	Dithiothreitol
GCN2	General Control Nondepressible 2
GMQE	Global Model Quality Estimate
<i>E. coli</i>	<i>Escherichia coli</i>
HEPES	4-(2-hydroxyethyl)-1-piperazineethanesulfonic acid
hIDO1	human Indoleamine-2,3-Dioxygenase 1
hIDO2	human Indoleamine-2,3-Dioxygenase 2
HIV	human Immunodeficiency Virus
HOMO	Highest Occupied π -orbitals
hTDO	human Tryptophan-2,3-Dioxygenase
IMAC	Immobilized Metal Affinity Chromatography
IPTG	Isopropyl β -D-1-thiogalactopyranoside
ITIMs	Immunoreceptor Tyrosine based Inhibitory Motifs
Ki	Inhibition constant
Km	Michaelis constant
KP	Kynurenine Pathway
KYN	L-Kynurenine
KynA	Kynureninc Acid
LB medium	Lysogeny broth medium
LUMO	Lowest Unoccupied π^* -orbitals
L-Trp	L-Tryptophan
mAbs	Monoclonal antibodies
MERS	Middle East Respiratory Syndrome
MD	Molecular Dynamics
MM-GBSA	Molecular mechanics with generalised Born and surface area solvation
mTORC1	mechanistic Target Of Rapamycin complex

Acronyms	Signification
NAD ⁺	Nicotinamide Adenine Dinucleotide
NCS	Non-crystalline symmetry
NFK	N-formyl-Kynurenine
NMR	Nuclear Magnetic Resonance
NMDA	N-methyl-D-aspartate
Nterm	N-terminal extremity
OX	Oxidized form
PA	Picolinic Acid
PBC	Periodic boundary conditions
PEG	Polyethylene Glycol
PDB	Protein Data Bank
PME	Particle Mesh Ewald
PX1	PROXIMA-1
PX2	PROXIMA-2
QA	Quinolinic Acid
RED	Reduced form
r.m.s.d	Root Mean Square Displacement
r.m.s.f	Root Mean Square Fluctuation
RNA	Ribonucleic Acid
ROS	Reactive Oxygen Species
SAXS	Small-angle X-ray scattering
SDS-PAGE	Sodium Dodecyl Sulfate–Polyacrylamide Gel Electrophoresis
T _m	Melting temperature
TRIS	Tris(hydroxymethyl)aminomethane
XA	Xanthurenic Acid
XRD	X-ray diffraction
WHO	World Health Organization

Dedicated to Tatave.

*“Went face to face with all our fears
Learned our lessons through the tears
Made memories we knew would never fade”*

Avicii - The Nights

Acknowledgements

Avertissement: Je ne sais pas la faire courte, on l'aura bien vu avec la taille de ce manuscrit. En conséquence, ces remerciements sont à mon image, trop long. Mais pour une fois, je pense que cela va vous plaire.

L'histoire que je raconte dans les lignes qui vont suivre ne commence pas un premier octobre 2019. Pour moi, le tout début de cette histoire est quand j'ai appris que j'avais obtenu ma bourse FNRS le 21 juin 2019. Sous la musique du Roi lion "Je voudrais déjà être roi", c'est alors lancée à 120 km/h au niveau de l'échangeur de Fleurus et au moment de me rabattre avec une voiture qui m'appartenait depuis 10 jours que j'ai reçu un des appels qui change une vie. Je ne citerais pas la personne, mais "Manon, tu l'as, jackpot, c'est mieux que gagner au loto". Peut-être que les premières personnes à remercier sont alors les automobilistes qui, ce jour-là, ont évité ma voiture afin que ma thèse dure plus que dix minutes. Faut dire que j'étais plus occupée à chanter, que dis-je hurler, les paroles dans ma 107. Autant dire que je n'ai pas été très concentrée par la suite pour vendre des sushis à mon job étudiant. À cette image, ma thèse a été une longue route, vécue à 100 à l'heure, sans trop de pauses sauf pour observer de nouveaux paysages. Il a fallu éviter les obstacles, les nids de poule où l'on risque de rester coincés et les feuilles qui s'écrasent sur le part-brise et qui empêchent de voir l'essentiel. Mais sur cette route, j'ai croisé des voitures nouvelles qui m'ont donné envie de les suivre, des automobilistes prêts à me dépanner quand je n'avais plus la force d'avancer, des aires de détente tenues par une main de maître par mes amis pour que je vienne m'y réchauffer sans devoir demander la raison de ma venue. C'est de toutes ces personnes que je vais vous parler.

*Pour remercier la première personne de cette thèse, je vais faire appel à une course que j'ai bien connue durant mon enfance. Au tour de France, avant les coureurs passe la caravane. Elle annonce le début de la course, apporte des forces et des cadeaux au public, mais montre également le chemin à suivre. Ma caravane lors de la course de ma thèse, c'est vous **Monsieur Wouters**. Une oreille toujours tendue pour écouter, vous m'avez donné l'opportunité*

*de traverser cette route pendant trois années. Merci de m'avoir transmis cette passion pour la cristallographie. Grâce à vous, j'ai pu me former à ce monde de la recherche et me surpasser en présentant mes résultats. Merci d'avoir pris le temps de me recevoir, plus ou moins tous les six mois, pour mes phases de doutes et de remises en question dramatiques. Merci également d'avoir lu et corrigé cette trop longue thèse de 365 pages, remerciements exclus. Il faut dire qu'avec 150 pages pour mon mémoire, j'avais déjà annoncé la couleur. Le co-passager de cette voiture a également été fondamental à mon développement scientifique et personnel. **Madame Leherte**, car je n'ai jamais su si je pouvais vous appeler Laurence, vous m'avez transmis, sans modération, toutes vos connaissances en Dynamique Moléculaire. C'est totalement à vous que revient l'attrait que j'ai développé pour ce domaine. Je retiendrais votre porte toujours ouverte, et votre personnalité toujours prête à répondre à mes questions et pleine d'imagination pour développer de nouvelles méthodes quand j'arrive avec mes idées farfelues. Merci également d'avoir pris de votre temps pour relire cette thèse, pour vos idées d'amélioration et vos conseils. Enfin, si je dois me souvenir de vous pour plus tard, je retiendrais qu'on peut négocier beaucoup de choses avec un paquet de souris à l'anis.*

*Pour qu'une voiture roule, elle a besoin de bons garagistes prêts à tester chaque paramètre. J'aimerais alors remercier les membres de mon jury en commençant par le chef d'équipe, **Prof. Yoann Olivier**. Monsieur le Président, merci d'avoir lu cette thèse et d'avoir accepté d'être à cette place aujourd'hui. J'ai tout de suite su que le fait de me poursuivre dans un laser game en criant "je vais te tuer Manon" préconisait un croisement de chemin un jour. Je ne retiendrais pas seulement que tu cours vite et que tu es assez menaçant avec un pistolet en main, mais que ça a toujours été agréable de te croiser dans le couloir. Merci pour tous les conseils durant la défense privée. J'aimerais aussi potentiellement te remercier pour ta patience. En effet, il faut savoir que le bureau de Mr Olivier est collé à la Nanodrop, machine que j'ai utilisée à de longues reprises en chantant beaucoup trop fort, et sûrement beaucoup trop faux, des chansons d'Angèle. Merci alors de ne t'être jamais plains pour ces concerts clandestins où tu étais auditeur à son insu. Ensuite, je souhaiterais remercier **Prof. Ute Röhrig**. Merci d'avoir accepté directement d'être dans mon comité d'accompagnement, et puis dans mon jury, pendant ces trois années. Merci pour nos discussions enrichissantes qui m'ont permis de faire progresser cette thèse. Merci pour votre relecture et vos suggestions. Pour moi, ça a été très inspirant de rencontrer une femme comme vous dans ce domaine. Cette équipe est encore composée de deux garagistes situés dans la périphérie de Bruxelles. À **Goeffrey Labar**, je souhaitais dire merci d'avoir accepté être dans mon jury et je lui souhaite beaucoup de force pour la suite. Enfin, **Prof. René Wintjens**, ça a été un plaisir de te côtoyer au long de ces trois années, pour parler*

de cristallographie, de cryo-EM, d'Alphafold ou encore des programmes de docking qui marche pas. Merci d'avoir accepté d'être dans ce jury, d'avoir toujours ouvert la porte de ton bureau (qui a changé de place, à retenir pour éviter de me retrouver dans le bureau d'un inconnu la prochaine fois) pour m'accueillir par un moment papote à chaque fois que je ramenaient des pucks. À tous, merci pour vos précieux conseils.

*Pour revenir à mon tour de France, une course ne se fait pas sans sponsors pour fournir la caravane. Sans **le FRS-FNRS**, rien de tout cela aurait été possible donc je tiens à les remercier chaleureusement de m'avoir fait confiance pendant ce projet de recherche. Merci à **l'UNamur** d'avoir été une seconde maison pour moi pendant des années avec la proximité de tous ces acteurs telle une petite famille. Particulièrement, merci aux instituts de recherches **NISM** et **NARILIS** de m'avoir accompagné financièrement quand je partais en vadrouille dans d'autres pays pour me former ou présenter mes recherches. Merci également d'avoir été attentif aux moindres prix, aux moindres réussites pour les publier dans vos "newsletters". Merci également au **CECI** pour les ressources computationnelles dont j'ai pu disposer durant mon travail. Mention spéciale à **Frédéric Wautelet** pour avoir été arrangeant que j'avais des délais impossibles à respecter. Ils ont partagé pendant tellement longtemps le même bureau qu'il paraît logique de les citer l'un après l'autre. Merci alors à **Laurent Demelenne** pour toute l'aide informatique que tu as pu m'apporter durant mes années de recherches. J'ai une grande pensée pour le **synchrotron SOLEIL**, et particulièrement à **Serena Sirigu**, **Bill Shepard**, **Pierre Legrand** et **Pierre Montaville** pour leurs précieux conseils lors des runs, leur aide lors du traitement des données pas toujours facile, et leur disponibilité pour toutes mes questions en début d'apprentissage. Merci également au laboratoire du **Prof. Raphaël Frédérick**, le **LDRI** et particulièrement **Marine Ancia**, qui m'a accueillie très gentiment pour mes manipulations de DSF. Enfin, merci à **l'URBM** et toute son équipe pour la possibilité de faire mes manipulations de biologie chez vous et parfois, avec vous. Vous êtes trop nombreux, mais je veux au moins citer **Aurélie**, **Elie**, **Pierre**, **Aish**, **Mathieu**, **Anthony** et **Pauline** pour avoir partagé ce bout de paillasse, pour m'avoir aidé quand la mutagenèse, les purifications de plasmides ou les phages me faisaient tourner la tête, pour m'avoir formé à vos différents instruments ou encore pour avoir soigné mes blessures quand je me transperce avec un berlin à 7h30 du matin pour bien commencer la journée. Merci au laboratoire de **Prof. Guillaume Berionni** pour les manipulations en Stopped-Flow. Particulièrement, merci à **Osi**, pour ton aide, qui rappelle les souvenirs de nos collocations étudiantes et de nos rapports de laboratoire. Enfin, je remercie la **VIB** et **Inge Van Molle** pour mon petit passage éclair pour m'essayer à la technique de l'ITC.*

Quand le trajet est long, il vaut mieux avoir de la bonne compagnie. Depuis longtemps, **le CBS** est MON labo. J'ai pu y voir passer des docs et les voir partir vers d'autres aventures, certains sont devenus postdoc. J'y ai croisé des étudiants, certains sont devenus doctorants. Ou encore des stagiaires, qui pour quelques d'entre eux sont après devenus des étudiants de l'UNamur. À tous, merci d'avoir été les éclaircies de mes journées d'averses. Merci pour nos fous-rires, merci pour nos discussions très profondes sur la beauté des chiffres pairs, et surtout, merci pour la quantité de nourriture partagée en cinq ans. Particulièrement, j'ai une pensée pour certaines de mes collèges. **Doc. Laurie**, doyenne du labo, merci pour nos discussions sur Vaasa et Vaika. Merci pour toutes tes idées quand je bloquais sur certains aspects de ma thèse, et merci pour cette mini parenthèse collaborative sur les ponts chalcogènes qui m'a permis de faire une pause bien nécessaire. **Doc. Elise**, danseuse endiablée à Just Dance, claudette de profession, et conductrice de folie à Mario Card, tu sais que tu es plus qu'une collègue pour moi et que ça a été, et restera, un plaisir de discuter de tout et de rien ensemble. Je sais que, qu'importe dans quel pays elle se trouvera, ta porte est toujours ouverte, et que je peux y sonner à n'importe quelle heure, également pour dormir après un synchrotron. Et tu sais que c'est réciproque. **Meg**, on n'a définitivement pas les mêmes goûts musicaux. Mais, toi, ton chignon à la Julien Doré et ton humour ont été une de mes plus belles découvertes de cette thèse. J'espère au moins qu'on mangera encore et encore des makimono, des Sothys, des Mex and Go, et autres crasses encore pour longtemps. Promis, on va te faire une tasse et tu vas beaucoup me manquer quand on ne sera plus des collèges. **Nikolay**, merci pour tes blagues scientifiques au moment des repas et pour ces tous ces modèles 3D que tu m'as fait pour mes conférences. Merci aussi à celles déjà parties vers d'autres aventures. **Doc. Kali**, tu as été la voix de la sagesse, pleine de conseils, et de bonnes remarques quand j'en avais besoin. Une pensée pour MisterCover, à jamais dans nos cœurs, toi-même, tu sais. **Doc. Marie**, tu as été mon encadrante et tu m'as toujours bien aiguillé quand j'avais un carrefour de possibilités à franchir. Merci pour nos discussions sur l'IND, pleines de nostalgies, et pour ce partage de l'amour de la bonne bouffe. **Nef**, mon acolyte de mémoire, je pense que si j'ai autant voulu faire une thèse, c'est pour tous ces bons moments qu'on a passés quand on était au labo, encore en statut d'enfants. C'est toujours un plaisir de te croiser et de parler ensemble. Tu as bien évolué pour un pokémon quand même, j'espère que la sauce du synchrotron restera à jamais dans ton cœur. Enfin, merci aux stagiaires et mémos que j'ai pu côtoyer: **Eddy** pour ton frac parlé et ton dynamisme, **Jeanne** pour ta folie, tes rires, parce que je sais que tu es une vraie avec ta Peugeot 107 et ces souvenirs au festival de Saint Louis. **Gilles**, fils adoptif qui peut s'endormir dans mon canapé avec Tanguy en regardant un film, merci pour les trajets Gembloux-Namur au goût de rap bien choisi, de débriefs de SNK, et de tes histoires d'amour parfois passionnelles,

mais surtout passionnantes. **Flo**, pas merci pour mon coccyx, tes lunettes cassées sans preuve que ce soit moi, le vin rouge hibou et le mélange qui en a découlé douloureusement. Merci à votre trio infernal qui m'a appris que je n'étais peut-être pas un ninja, à ces moments puzzles qui auront causé une ou deux arrivées tardives, car on ne part pas de Gembloux avant de trouver une pièce du puzzle. Merci pour vos folies capillaires réalisées sur mon trottoir.

Je sais que là, il y en a quatre qui se disent que je les ai oubliés. Comment j'oserai. Je ne peux pas écrire des remerciements de sept pages sans vous parler de mes étudiants, les miens, rien qu'à moi, mes enfants. **Berta, Robin, Tanguy, Martin**. Chacun, vous avez su apporter une brique de plus à l'édifice. Tous les jours n'ont pas été facile, parfois parce que j'abuse, mais je retiens que du positif de vous quatre. Pour vous avoir encadré, c'est douze bouteilles d'acide aminolévulinique consommées, 289 pages de mémoires et autres manuscrits rédigés, près de 1000 jours passés ensemble et des centaines d'essais de conditions cristallo réalisés. **Martin**, tu es arrivé à l'étape de fondation, à peine trois mois après le début de ma thèse. Il est difficile d'allier amitié et travail, mais tu m'as appris à être patiente et à m'adapter. Je suis fière de la direction que tu prends et je te souhaite que de la réussite. **Tanguy**, roi des Dráma Queens, fabriquant de gel en série, mon année à tes côtés a été plus qu'une année d'encadrement, mais un réel partage entre deux scientifiques. Tu es, et tu seras j'en suis sûre, un super encadrant et assistant. Merci d'avoir laissé l'hémime bronzer et toutes ces autres bêtises qui me font rire après coup. Longue vie à TDO et son odeur et aux pizzas quand ça diffracte. **Berta et Robin**, Dupont et Dupond de la cristallographie, un merci énorme pour tout le travail fourni, sans faillir, et plein de motivation. La tache était énorme, mais, même si IDO2 n'a jamais diffracté, pour moi, vous avez tout réussi. Robin, j'ai été épatée par la profondeur de nos discussions et ton perfectionnisme. Bonne chance pour le master. Berta, tu as été la bouffée d'air chaud de ma fin de thèse. J'ai hâte de venir te voir à Barcelone et vive le filet américain et le boudin. À tous, merci pour ces moments, merci pour ces sourires, merci pour ces "Team buildings". Les synchrotrons jusqu'au bout de la nuit ont été moins longs à vos côtés, les journées ont été plus ensoleillées et les matins ont été plus faciles (sauf pour Élise). Je vais citer des mots, totalement aléatoires pour certains, mais qui veulent dire tellement de choses pour moi: mur of shame, meringue italienne, avocat de la honte, petit vomi tactique de gastro avant les confs, apéro, Monsieur L. Profond que je remercie pour ces conseils en anglais, un tablier égal un gâteau, le soleil se lève à l'est sans oublier le front de Térese Bergfors.

Parmi tout le petit monde qu'on côtoie sur la route d'une thèse, il y a un second labo que je tiens à remercier. J'y ai toujours été accueillie comme chez moi, que ce soit pour poser des questions, faire des répets ou encore faire des débats dans la salle café. Le café, c'est très important là bas, je parle bien sûr du **LCT** mais aussi ces alumnis tel que **Jean** et **Christ**. Merci à tous ces membres et ces alumnis qui ont rendu ces moments chouettes en partage. Labo de mémoire, mais aussi labo de mes premiers pas en rhéto aux facs, je veux te remercier **Benoît** pour tout ce que tu m'as transmis avec les années. Elle est loin l'époque où je mangeais des ananas en boîte dans ton antichambre avant de faire le tour des labos. Non, maintenant, je la squatte pour faire des scans d'énergies, je ne sais pas si c'est mieux. Je pense que j'aurai toujours cette image de toi, penché en arrière, lunettes baissées sur le nez, quand je passe dans le couloir pour voir qui fait autant de bruits avec ces chaussures. C'est toujours une invitation pour venir causer cinq minutes avec toi. Merci pour tout. Il y en a un autre qui a été vraiment important pour moi dans ce labo, c'est le **Docteur Pierre Beaujean**. Je ne compte plus les fois où j'ai déboulé te voir au bureau, avec des questions les plus improbables les unes des autres. Mais, à chaque fois, sans exception, tu étais là. Encadrant de la première heure, collègue du **KapForScience**, j'ai traversé ces années depuis 2014 avec toi à tes côtés et il y a tellement de choses à dire que je n'ai définitivement pas la place. Merci pour tout. En parlant du **KapForScience**, je veux remercier toutes ces personnes que j'ai rencontrées en huit ans sur Namur par mes activités extrascolaires. Le **KFS**, l'**Akàp**, le cercle **Chigé**, la **Revue Science**, ça en fait du monde. **Loïc**, **Sma**, **Hélène**, **Lola**, **Julien**, **Nathan**, **Laurelène**, **François**, **Loïc la flèche**, j'oublie pleins de noms mais aucuns des moments passés avec vous. Promis, j'ai fini mon script et je ne le modifierais plus.

Au début de ces remerciements, je vous ai parlé d'aires de détente tenues par des amis sur lesquelles j'ai toujours su me changer les idées. **Charlotte** et **Mathilde**, mes deux **Totaly Spies**, **Mathilde** et **Romain**, **Calliope**, **Hermine** et **Husky**, c'est à vous que je m'adresse. Malgré la distance, toutes nos retrouvailles sont comme si on se quittait la veille. Merci pour tous ces moments, depuis tant d'années. Vous êtes mon équipe de choc, dans les bons comme les mauvais moments. J'ai tant de souvenirs qu'il serait indécent de tous les citer alors on va se contenter d'un grand calin et d'anecdotes encrées à jamais. Merci aussi à **Jess** et **Quentin** d'avoir été deux chouettes rencontres sur cette route, avec votre voiture atypique, cette passion pour Noël et les corgis. Merci à ma famille d'avoir aussi été cette bouchée d'oxygène: **Mamie Huguette**, **Mamie Annie**, **Marraine**, **Parrain**, **Cédric**, **Eve**, **Laura**, **Xavier**, **Maude**, **Sami**, **Ma tante**, **Mon Oncle**, mes deux merveilleuses filleules **Ambre** et **Eleonore**, **Louis** et **Adam** sans oublier **Papa**, **Maman**, **Fanny** et **Ugo**, merci pour votre soutien, toujours présent au

travers les années. Merci d'avoir cru en moi quand je vous ai dit que je voulais faire la chimie et que j'allais faire des cristaux comme ceux exposés dans ma chambre. Merci de ne pas avoir douté de moi quand moi-même j'en étais pas capable. Merci d'avoir eu les bons mots, au bon moment pour me demander comment j'allais. Enfin, quand il fallait me détendre, je pouvais compter sur mon rendez-vous synchro du mardi, voir du samedi. Merci à toute l'équipe, vous êtes des perles.

*Je ne peux pas terminer ces remerciements sans parler à ma famille. À **Vaasa**, une grosse touffe de poil qui est arrivée au bon moment pour me donner une dose d'amour inconditionnel, et des bonnes pauses entre la rédaction pour apprendre des chorées sur du Avicii. À toi, **Octave**, qui lit ces dernières lignes, parce que je sais que tu auras eu le courage de tout lire jusqu'au bout. Parce que le miel n'existe pas sans le vinaigre, parce que voyager est le meilleur apprentissage de la vie, parce que les lacs c'est trop le must, parce que tu roules trop vite dans les ronds-points et que tu brules le stop devant la maison à chaque fois, parce que "tu m'as sauvé d'tellement de mauvais choix", parce que tu as toujours su me rassurer, parce que tu as toujours une oreille pour m'écouter, même quand je hurle, parce que je trouve toujours avec toi une épaule sur laquelle me reposer depuis tant d'années. Pour de vrai, de vrai, de vrai, de vrai, de vrai, de vrai, merci.*

Enfin, je conclus ces remerciements pour toi qui lis ces lignes et que j'ai sans doute oublié. Il y en aura surement.

Alors, à toi, et bien d'autres complices, merci ...

Contents

Acknowledgements	xi
Preface	xxvii
I Introduction	1
1 The kynurenine pathway as a set of therapeutic targets	5
1.1 The fragility of human life	7
1.2 The kynurenine pathway	9
1.3 The proteins hIDO1 and hIDO2 as targets	11
1.3.1 hIDO1 and hIDO2 roles as an immunosuppressor in cancer . . .	11
The disease, its incidence and mechanism	11
Treatments	12
Implication of hIDO1	13
Implication of hIDO2	14
1.3.2 hIDO1 and hIDO2 roles in COVID-19 disease	15
The disease, its incidence and mechanism	15
Treatments	16
Implication of hIDO1	17
Implication of hIDO2	18
1.4 Development of inhibitors for hIDO1 and hIDO2	20
2 hIDO1 and hIDO2: identity cards	33
2.1 Introduction	35
2.2 State of the art of the knowledge about hIDO1	35
2.2.1 Heme cofactor and mechanism	35

2.2.2	Heme cofactor and physico-chemical properties	38
2.2.3	Known structural features of hIDO1	41
2.2.4	Grey areas and the beginning of difficulties	42
2.3	State of the art of the knowledge about hIDO2	44
3	Objectives and strategies	55
3.1	Objectives and strategies	57
II	Physico-chemical characterization of the two targets	61
4	Characterization of hIDO1	65
4.1	Introduction	67
4.2	Characterization of the cofactor incorporation	67
4.2.1	Definition of the absorbance ratio and relation with the holo protein ratio in solution	67
4.2.2	Peak attribution at 360nm	69
4.2.3	Lability/affinity evaluation of heme cofactor at 25 °C	75
4.3	Characterization of the protein stability	76
4.3.1	Principle of Differential Scanning Fluorimetry study	77
4.3.2	Effect of the redox environment on the stability	77
4.3.3	Effect of heme on the stability	80
4.4	Characterization of the protein activity	81
4.5	Intermediate conclusions	83
5	Characterization of hIDO2	85
5.1	Introduction	87
5.2	Characterization of the cofactor incorporation	87
5.3	Characterization of the lability of the cofactor	88
5.4	Characterization of the protein stability	90
5.5	Characterization of the protein activity	93
5.6	Intermediate conclusions	94
III	Comprehensive study of hIDO1 plasticity	95
6	The JK-loop plasticity study by means of crystallographic snapshots	99

6.1	Introduction	101
6.2	JK-loop behavior without ligand in the active site	101
6.2.1	Contextualizing the results	101
6.2.2	Quality of the refined structure	102
6.2.3	Description of the dimerization interface	103
6.2.4	Conformation of JK-loop	104
6.2.5	In summary	107
6.3	JK-loop behavior in the presence of L-Trp in the active site	107
6.3.1	Contextualizing the results	108
6.3.2	Positions of L-Trp inside the active site	108
6.3.3	Conformation of the JK-loop according to the L-Trp position	111
6.3.4	Influence of the JK-loop conformations on the cofactor affinity	114
6.3.5	In summary	114
6.4	JK-loop behavior in the presence of L-Kynurenine in the active site	115
6.4.1	Contextualizing the results	115
6.4.2	Overall characterization	116
6.4.3	Influence on the dynamic loop on presence of L-Kynurenine	117
6.4.4	In summary	118
6.5	Intermediate conclusions	119
7	The JK-loop plasticity study by Molecular Dynamics from crystallography snapshots	123
7.1	Introduction	125
7.2	JK-loop behavior without ligand in the active site	125
7.2.1	Structural comparison of the holo and apo forms	125
7.2.2	Contribution of MD simulation to the structural study	129
7.3	JK-loop behavior with L-Trp in the active site	129
7.3.1	Structural comparison of the different snapshots	130
7.3.2	Contribution of MD simulation to the structural study	133
7.4	JK-loop behavior with L-Kynurenine or NFK in the active site	135
7.4.1	Structural comparison of the NFK and the L-kynurenine	139
7.4.2	Contribution of MD simulation to the structural study	141
7.5	Intermediate conclusions	141

8	G261 to G265 as sensor of ligand entrance	147
8.1	Introduction	149
8.2	Highlighting of the different conformations collected	150
8.3	What's observed in other PDB structures?	154
8.3.1	Conformations for other ferrous proteins in the PDB	156
8.3.2	Conformations for other ferric proteins in the PDB	157
8.4	Intermediate conclusions	165
9	Plasticity outside the protein: discovery of an exo site	171
9.1	Introduction	173
9.1.1	Questioning the existence of an exo site in hIDO1	173
9.2	Occupancy of the exo site in the other PDB structures	176
9.3	Investigation of the exo site by Molecular Dynamics	178
9.3.1	Simulation with a L-Trp molecule	179
9.3.2	Simulation with a NFK molecule	183
9.4	Intermediate conclusions	186
IV	Comprehensive study of hIDO2 plasticity	189
10	Crystallization tests and construction optimization for hIDO2	193
10.1	Introduction	195
10.2	Crystallization assays of hIDO2 WT	195
10.3	Plasmid design to aid crystallization	197
10.3.1	Physico-chemical characterisations of new constructions	199
10.3.2	Crystallization assays on cleaved hIDO2 WT, truncated hIDO2 and truncated-cleaved hIDO2	201
10.3.3	What can you learn from this study?	203
10.4	Intermediate conclusions	203
11	Investigation of the hIDO2 structure by Molecular Dynamic and homology modeling	207
11.1	Introduction	209
11.2	Design of a homology model	209
11.3	Study of the JK-loop of hIDO2 with the heme cofactor	212
11.3.1	Influence of M350 on heme lability	218

11.3.2	Comparison of the holo and the apo form of hIDO2	220
11.3.3	Influence of the polymorphism on the lability	222
11.4	Study of the JK-loop with ligand in the active site	225
11.4.1	Docking of L-Trp into the active site of hIDO2	225
11.4.2	MD simulation of hIDO2 bound to L-Trp using docked poses . .	227
11.4.3	MD simulations of L-Trp bound to hIDO2 using hIDO1 data . .	228
11.5	Intermediate conclusions	230
V	Comparison of the two targets and discussion	233
12	Comparison of hIDO1 and hIDO2 and discussion	237
12.1	Introduction	239
12.2	Physico-chemical characterization of the two targets	239
12.2.1	Characterization of the cofactor incorporation	239
12.2.2	Characterization of the stability	241
12.2.3	Characterization of the activity	242
12.2.4	Conclusions of this physico-chemical comparison	243
12.3	Structural characterization of the two targets	244
12.3.1	Crystallization and global folding information	244
12.3.2	Study of the structural features of holo forms	247
12.3.3	Study of the structural features of apo forms	249
12.3.4	Study of the structural features of L-Trp bound forms	251
12.3.5	Study of binding sites outside the active site	253
12.4	hIDO2 acts as a pseudo-enzyme of hIDO1	253
VI	Conclusions and outlooks	257
13	Conclusions and outlook	261
13.1	To conclude	263
13.2	The plasticity of hIDO1	263
13.3	The plasticity of hIDO2	266
13.4	Comparison of the plasticity for hIDO1 and hIDO2	269
13.5	What to do in terms of prospects?	269
13.6	The final words	271

VII Appendices	273
A Materials and methods	275
A.1 Introduction	277
A.2 Proteins production and purification	277
A.2.1 Production of hIDO1 in a holo form	277
A.2.2 Production of hIDO1 in an apo form	279
A.2.3 Production of hIDO2 in a holo form	280
A.2.4 Production of hIDO2 in an apo form	282
A.3 Characterization of the cofactor incorporation	283
A.4 Characterization of the stability	283
A.5 Characterization of the activity	284
A.6 Characterization of the structure by crystallography	285
A.6.1 Crystallization assay of hIDO1	285
A.6.2 Co-crystallization assays of hIDO1	285
A.6.3 Crystallization screenings of hIDO2	286
A.6.4 X-ray collection and model refinement of hIDO1	286
A.7 Characterization by computational study	287
A.7.1 Analyses using MM-GBSA calculation of hIDO1	287
A.7.2 Binding site studies of hIDO1	287
A.7.3 Homology modeling of hIDO1	288
A.7.4 Homology modeling of hIDO2	288
A.7.5 Docking study of hIDO2	288
A.8 Characterization by Molecular Dynamics	289
A.8.1 Molecular Dynamics studies of hIDO1 in absence of ligand . . .	289
A.8.2 Molecular Dynamics studies of hIDO1 in presence of ligands . .	290
A.8.3 Molecular Dynamics studies of hIDO2 in absence of ligands . .	291
A.8.4 Molecular Dynamics studies of hIDO2 in presence of L-Trp . . .	291
B Methodological development for the fundamental study: definition of the histidine /heme link	297
B.1 Introduction	299
B.2 Influence of the covalent link on hIDO1	299
B.3 Influence of the covalent link on hIDO2	302
B.4 Conclusions of the appendix	307

C	Physico-chemical characterization of hIDO1 and hIDO2: Supporting information	311
C.1	Absorbance of free hemin in solution	313
C.2	UV-Visible absorption spectroscopy analyses of lability in hIDO1 at 25 °C	314
C.3	UV-Visible absorption spectroscopy analyses of lability in hIDO2 at 25 °C	315
D	Comprehensive study of hIDO1 plasticity: Supporting information	319
D.1	JK-loop plasticity study by means of crystallographic snapshots	321
D.1.1	JK-loop behavior without ligand in the active site	321
	Data-collection and refinement statistics of structure 7a62	321
	Interaction in the different dimerization interface	322
	Volume of pocket B as induced by the conformation of the JK-loop in 7a62	323
D.1.2	JK-loop behavior in the presence of L-Trp in the active site	324
	Data-collection and refinement statistics	324
	Relatives positions of L-Trp	325
D.1.3	JK-loop behavior in the presence of L-Kynurenine	326
	Data-collection and refinement statistics of structure 7zl2	326
D.2	The JK-loop plasticity study by MD from crystallography snapshots	328
D.2.1	JK-loop behavior without ligand in the active site	328
	Structural comparison of the holo/apo form	328
D.2.2	JK-loop behavior with NFK in the active site	329
D.3	G261 to G265 as sensor of ligand entrance	330
E	Comprehensive study of hIDO2 plasticity: Supporting information	337
E.1	Investigation of the hIDO2 structure by MD	339
E.1.1	Study of the JK-loop in the absence of ligand in the active site	339
E.1.2	Study of the JK-loop with M350I mutation	339
E.1.3	Influence of the polymorphism on the lability	340
E.2	Polarity changes between hIDO1 and hIDO2 in the sequence alignment	341
F	List of publications	343
F.1	Publications	345
F.2	Conferences	345
F.3	PDB structures	347
F.4	Prizes	347

F.5 Publications in web media 348

Preface

The thesis described in the present manuscript is the result of a three years work funded by an aspirant grant from the *Fond National de la Recherche Scientifique* (FRS-FNRS). During this thesis, three hemoproteins were studied: human Indoleamine-2,3-Dioxygenases 1 (hIDO1) and 2 (hIDO2) as well as human Tryptophan-2,3-Dioxygenase 2 (hTDO2). The three drug targets were then produced and purified in order to be characterized through a structural multidisciplinary approach. This manuscript was designed to present the results of hIDO1 and hIDO2. For this purpose, only the results obtained on the characterization steps are detailed. Specificities related to the production and purification of the proteins are mentioned in Appendix A.

After a brief introduction, the results of the thesis are organized in three parts, i.e., a first part dealing with the physicochemical characterization of the two therapeutic targets followed by two parts dealing with the structural study of hIDO1 and hIDO2 plasticities. In these parts, a multidisciplinary approach was used, combining characterization tools (UV-Visible absorption spectroscopy, DSF, enzymatic assays, etc.), crystallography, Molecular Dynamics and modeling tools such as MM-GBSA calculations or molecular docking. The methodology applied and details on practical aspects for these different methods is shown in Appendix A. In particular, the definition of constraints in the context of the Molecular Dynamics studies is discussed in detail in Appendix B. In the part named "Comprehensive study of hIDO1 plasticity", four chapters allow to highlight the multiple aspects of hIDO1 plasticity. The results contained in these chapters have been associated with two publications in scientific journals in 2020 and 2021. They have also been the object of a serie of presentations and posters in conferences throughout the thesis. These oral and written communications are listed in Appendix F. Only a few results of these chapters are not yet published. In particular, the results concerning the structures with L-Kynurenine (Chapter 6) and the

plasticity of the G261-G265 fragment (Chapter 8). Concerning the part named "Comprehensive study of hIDO2 plasticity", the results are presented in two chapters, one based on crystallization tests on the hIDO2 protein and the other on a computational chemistry analysis of the enzyme. Neither of these two chapters has been published before.

After detailed results collected during the research, the thesis continues with a part dealing with a discussion in the form of a comparison of the two proteins. Finally, a "conclusion and perspectives" part will allow us to review the discoveries made during the thesis and to open the door to new perspectives.

Part I

Introduction

*“Sans jamais dire où je vais
(Ce lion a une tête de mule!)
Je veux faire ce qu’il me plaît!”*

Le roi lion - Je voudrais déjà être roi

Chapter 1

The kynurenine pathway as a set of therapeutic targets

1.1 The fragility of human life

At the time of writing this introduction, almost eight billion people live on earth. [1] However, since the dawn of time, the worldwide existence has been weakened by the appearance of diseases. [2] In 2019, there were 55.4 million deaths worldwide. Of these, 55% are caused by one of the ten leading known causes of human death (Figure 1.1). These diseases are classed into three categories: communicable diseases (infectious and parasitic diseases, maternal, perinatal and nutritional conditions), noncommunicable (chronic) diseases, and injuries. [3] Noncommunicable diseases include all neurodegenerative diseases, cancers, cardiovascular diseases, chronic respiratory diseases, diabetes and mental disorders. [3] In 2019, seven of the ten leading causes of death in the world are classed in the second category, responsible for 44% of human deaths. If all known noncommunicable diseases are included, they are responsible for 74% of the world's deaths. [4] Cardiovascular diseases are well ahead of all other diseases in terms of mortality, causing nearly 16% of total deaths and 45% of deaths from noncommunicable diseases in 2019. [3, 4] Nowadays, cancer is the second leading cause of death worldwide with a percentage of 22% in 2019. [4, 5]

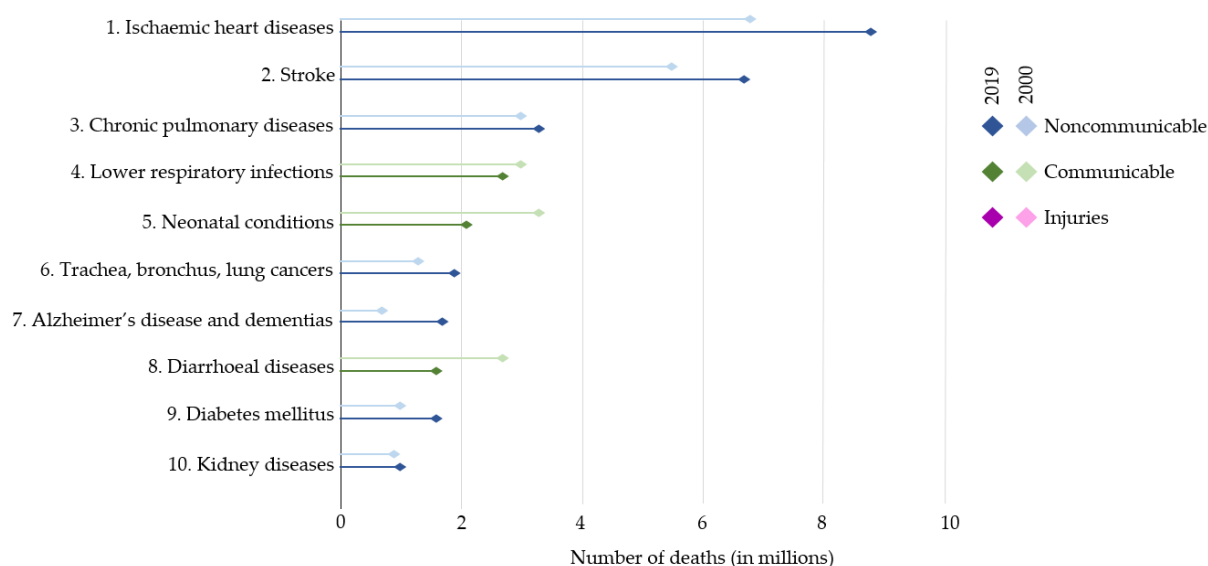


FIGURE 1.1: Distribution of human deaths worldwide among the ten leading causes of death on earth. Evolution of the figures between 2000 and 2019. Image inspired from the World Health Organization (WHO). [4] No cause of death by injury is in the top 10.

Although less important in the global death rate, communicable diseases are also a major cause of death leading to three of the top ten causes of death in 2019. [3, 4] Currently, 18.4% of deaths worldwide are associated with this kind of disease. This total of 10 million deaths per year is caused to 50% by the infectious and parasitic diseases, a figure that will increase in 2020 and 2021 due to the COVID-19 pandemic, 26% by respiratory infections and 20% by neonatal conditions (preterm birth complications, birth asphyxia, birth trauma, neonatal sepsis, infections or other). [4, 5] Historically, infectious and parasitic diseases were more dominant in pre-modern times with colonization. [2, 6] There exist five main types of pathogen agents: bacteria, viruses, prions, parasites and fungi. The progress of modern medicine allowed to counter most of them (tuberculosis, polio, smallpox, rabies, flu, tetanus or diphtheria). [2] Particularly, the vaccination, developed by Edward Jenner and Louis Pasteur, helps to drastically reduce the mortality. [7] In this way, diseases such as smallpox, in 1977, or polio were eradicated. [8, 9] Other effective treatments still appear in the last decades on the market in order to reduce the incidence of current communicable diseases such as human immunodeficiency virus/Acquired ImmunoDeficiency Syndrome (HIV/AIDS) [10–13], malaria [14–16] or leprosy [17, 18]. For example, HIV/AIDS declined to 19th place in 2019 (eighth place in 2000), reducing the number of deaths by 51%. [4] In spite of these advances, the 21st century has been also punctuated by the emergence or re-emergence of new infectious diseases [6] (COVID-19, Middle East Respiratory Syndrome (MERS), Ebola, influenza infections) and by the resistance to the treatment (tuberculosis [19, 20] or antibiotics bacteria resistance [21]). The COVID-19 pandemic alone has caused, at the time of writing, 6.5 million deaths. [22] Even if the WHO data for 2020 and 2021 are not yet published, a greater proportion of infectious diseases in the total deaths is expected, with an estimated excess mortality of 14.7 million people. [23]

Due to the causes of these diseases such as unhealthy nutrition, sedentary lifestyle, health problems, access to sexual protection means, hospital facility, etc., the distribution of the impact of noncommunicable and communicable diseases is not homogeneous in the world. At the beginning of the 21st century, industrialized countries are more likely to noncommunicable diseases while, in developing countries or low and middle-income countries, the mortality is mainly due to communicable diseases. This is mainly due to the "modern negative lifestyle" of developed countries. [24] However, this balance has been upset in recent years. Unfortunately, more and more developing

countries are also subject to an increase in cardiovascular diseases, cancer or diabetes historically associated with rich countries. [3] As far as developed countries are concerned, the appearance in December 2019 of the COVID-19 pandemic was one of the biggest infectious diseases of the last decades.

1.2 The kynurenine pathway

At the heart of these diseases, metabolic pathway disturbances are often the cause of large-scale effects on the human body. Among these pathways, a deregulation of the kynurenine pathway (KP) can be involved. [25–33] The KP (Figure 1.2) is a pathway responsible for the degradation of the majority of L-Tryptophan (95%), also named L-Trp and known as the least abundant essential amino acid in the human body [34–36] (with plasma concentrations of 40 μ M to 80 μ M [37]), into a series of metabolites such as Quinolinic acid (QA), 2-aminomuconic acid and Picolinic acid (PA). [34, 36] These molecules act as primordial precursors since they allow the subsequent formation of Nicotinamide adenine dinucleotide (NAD⁺) or Acetyl CoA. Secondary metabolites such as Anthranilic acid, Kynurenic acid (KynA, both formed from L-Kynurenine (KYN)) or Xanthurenic acid (XA, formed from 3-Hydroxykynurenine (3HK)) are also obtained. This pathway allows the formation of many neuroactive molecules such as neuroprotectors (KynA) or neurotoxic agents (QA, 3HK, and 3-Hydroxyanthranilic acid (3HAA)), allowing the control of the balance of these molecules in the body. [35, 38] Some of these molecules are also part of the class of immunomodulators such as KYN, KynA, 3HK, XA, 3HAA, QA, and PA. [34]

The kynurenine pathway allows the human body to perform many functions such as the detoxification of excess Tryptophan, the control of plasma Tryptophan availability, the control of hepatic heme biosynthesis, the influence on carbohydrate metabolism and the production of metabolites. The essential character of this route confers to it a central role in a lot of diseases, especially in disruption of immune response (cancer, HIV), cardiovascular diseases and neurological disorders (Alzheimer's disease, Parkinson's disease or Huntington's disease). [28, 35, 36, 39, 40] As these diseases are known to be among the most deadly in the world, the enthusiasm of the scientific community in the study of this metabolic pathway is clearly justified. Consequently, the enzymes of the kynurenine pathway are considered as a set of therapeutic targets.

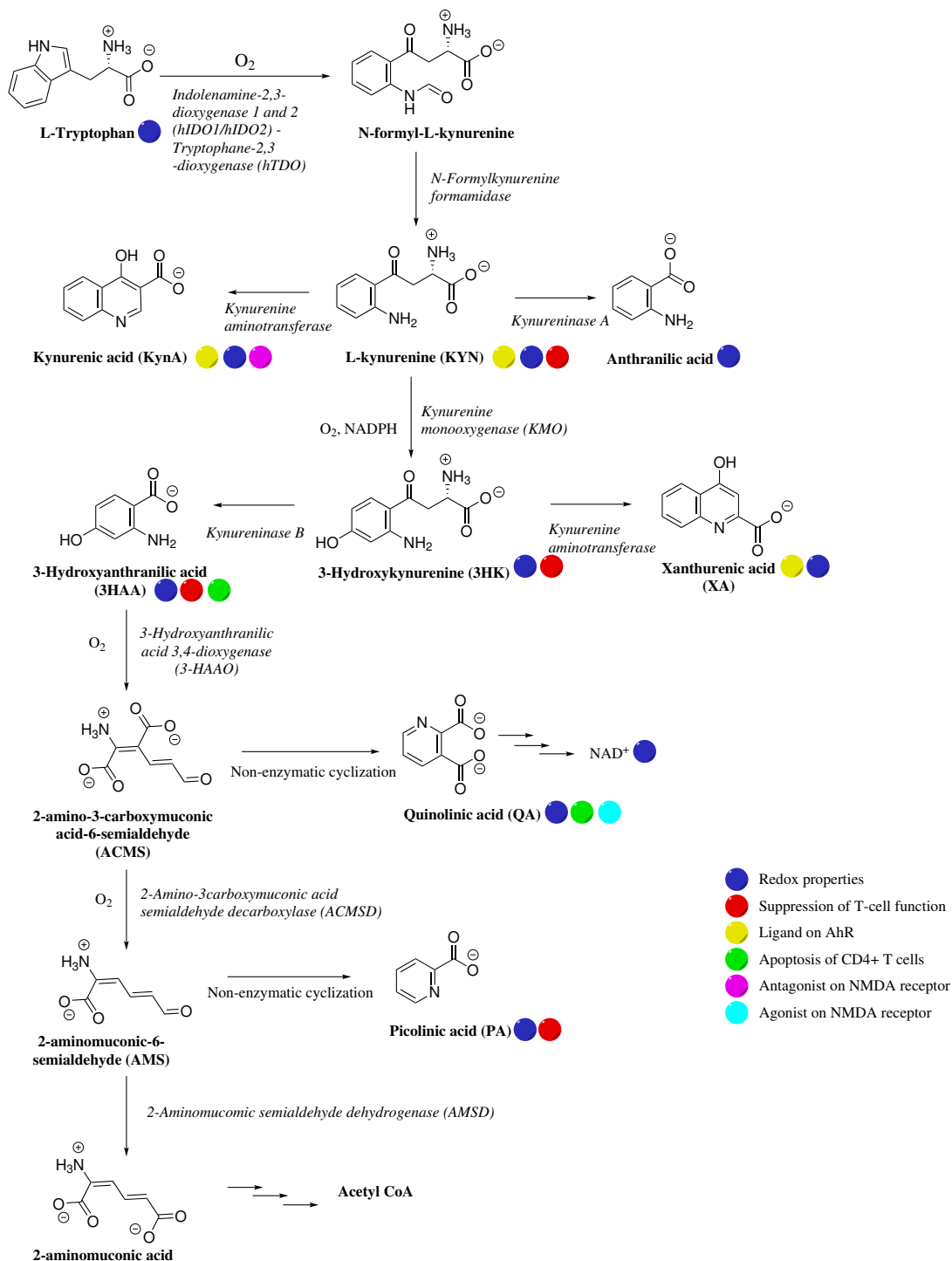


FIGURE 1.2: Kynurenine pathway and involved enzymes in each step. Inspired from schemes in [34–36]. Ahr = Aryl hydrocarbon Receptor, NMDA = N-methyl-D-aspartate.

The enzymes catalyzing these reactions are mainly overexpressed in the liver, but also appear elsewhere in case of immune system activation. [34] This is particularly the case for the enzymes human Indolenamine-2,3-dioxygenases 1 and 2 (hIDO1/hIDO2) governing the first, and rate limiting, reaction of the pathway. There is also a third enzyme which catalyzes this reaction: the human Tryptophan-2,3-dioxygenase (hTDO), expressed exclusively in the liver. This system with three enzymes capable of making one and the same reaction is the central object of the study carried out during the doctoral thesis.

1.3 The proteins hIDO1 and hIDO2 as targets

Due to their position in the first step of the pathway and the rate-limiting nature of this reaction, hIDO1 and hIDO2 are specifically known to be overexpressed in many diseases. [36, 41] For hIDO1, a multitude of articles mention its involvement in cancers, Alzheimer disease, cardiovascular diseases, depression, tuberculosis or diabetes. [28, 30, 32, 34, 41, 42] The protein is also involved in cases of early/mild pneumonia and long-term COVID-19 diseases. [43] For hIDO2, the scientific literature highlights its involvement in cancer [32, 44–46], autoimmune diseases [47] and recently in severe cases of COVID-19 disease. [33] The following sections detail two studies proving the implication of these two proteins in diseases and how their overexpression is a sign of poor prognosis for the patient. In this way, the manuscript focuses on the second largest noncommunicable disease (cancer) and a recent communicable disease (COVID-19).

1.3.1 hIDO1 and hIDO2 roles as an immunosuppressor in cancer

The disease, its incidence and mechanism

Cancer is defined as an abnormal, uncontrolled division of cells that have acquired one or more mutations. [48] In Belgium, in 2019, this type of disease led to nearly 27,300 deaths, i.e., one in four deaths, which makes it one of the major causes of death. [4] During the same year, there were 71,651 new cancers diagnosed. [49] For men, the three most common cancers are prostate, lung and colorectal cancer. For women, the podium differs slightly with breast cancer in first place, followed by lung cancer and, finally, colon cancer. The affected population is relatively old, since 69%

of women and 80% of men are older than 60 years at the time of diagnosis. [49] Different risk factors can lead to cancer, such as obesity, a poorly varied diet, a sedentary lifestyle, smoking, infections (hepatitis B, hepatitis C or human papillomavirus) or alcohol abuse. [48]

The starting point of all cancers is the initiation of a genetic change in a cell, either due to the mutation of a proto-oncogene, a gene with a role in the Deoxyribonucleic Acid (DNA) mutations repair or a tumor suppressor gene. [50, 51] In a healthy cell, it is not trivial to observe genetic mutations during cell division. When a mutation occurs, it can either be corrected or cell apoptosis is induced if the repair is impossible. The mechanism is changed in the case of a cancer cell. The cell repair or apoptosis are impaired leading to a proliferation of mutant cells. These mutant cells accumulate new uncorrected mutations, leading to the acquisition of primordial characteristics by cancer cells, such as resistance to cell death, dysfunction of mechanisms of cell growth regulation or the ability to over-activate some metabolic cascades. These characteristics are known as the cancer Hallmark. [50, 52] The metabolism is thus altered and it is possible for cancer cells to evade the immune system and inflammatory system. These characteristics guarantee cell survival, causing anarchic cell proliferation. This anarchic proliferation leads, in our body, to the formation of cluster of cells, called tumors. [50–52] Cancers are considered solid when they are abnormal cell growths in "solid" organs such as the breast or prostate, as opposed to leukemia, a cancer affecting the blood, which correspond to "liquid" cancers.

Treatments

Fortunately, treatments exist on the market to counter or mitigate the devastating effects of tumors on the body. The three main types of treatments are surgery¹, radiotherapy² and chemotherapy³. [53] Rarely administered alone, the cancer patient will then have to undergo a heavy treatment combining these techniques. Although effective enough to get rid of most tumors, these techniques have known disadvantages. The main is these techniques mostly treat the primary tumor. In particular, surgery is not possible if the tumor is difficult to reach, and not adapted to liquid cancers. Chemotherapy is not selective and also attacks the replication capacity of

¹Surgical operation to remove the tumor.

²Use of a high radiation source to lead to the destruction of the tumor.

³Treatment, at least of drugs, to kill cancer cells.

healthy cells in the body. [54] The side effects target on cells with a high replication rate, such as hematopoietic cells of the bone marrow, hair follicles, cells of the mouth, digestive tract and reproductive system. That leads to hair loss, nausea, skin reactions, easy bruising and bleeding, fertility problems or even infection. [55] Radiation therapy presents an inability to kill tumor cells when they are not visible on imaging scans or too big. It also does not work effectively when the tumor presents a lack of oxygenation. This treatment is also a time-consuming technique. [56, 57] As chemotherapy, this treatment leads to fatigue, hair loss, nausea, skin reactions, a weakening of the immune system or damage to surrounding tissues. [58] To reduce these side effects and better treat the patients, new therapies such as immunotherapy or targeted therapies become more of interest. [54, 59, 60] Targeted therapies is a treatment that targets receptors on tumor cells to inhibit abnormal cell growth and cancer spread. This is possible with monoclonal antibodies or with small molecule drugs, such as kinase inhibitors. [61] Immunotherapy is the use of a patient's own immunity, boosted or modified by a given treatment, to attack cancer cells. It is a complete technique, allowing the neutralization of both the primary tumor and the metastasis. In order to do this, immunotherapy will stimulate or complement the immune system by using lymphokines, vaccines, antibodies or immune checkpoint inhibitors. This technique considerably improves the quality of life of patients, with fewer side effects. In most cases, these are limited to an allergic reaction. [53, 59, 60] The problem with immunotherapy is that, in some cases of cancer, the cancer cells are resistant to the treatment by developing an immunosuppression phenomenon. A new strategy of this technique could be the inhibition of these immunosuppressive factors. This is a promising challenge in cancer research.

Implication of hIDO1

The intervention of hIDO1 is at the level of this immunosuppression problem. Various tumors such as colorectal cancer, pancreatic cancer, carcinomas and prostate cancer present this kind of resistance. [41, 42] In our body, the induction of hIDO1 is controlled, among others, by interferons. [62] It results in an inflammation signal. Naturally in our body, hIDO1 is present in order to regulate the immune system and introduce a tolerance of the T lymphocytes. That allows, for example, to avoid the rejection of a fetus. [32, 40] This mechanism is hijacked by cancer cells that over-express hIDO1 or secrete inflammatory cytokines to induce the protein expression.

[32, 40, 42, 63] A tolerance of tumor cells by our immune system is created.

The overexpression of hIDO1 occurs in more than 50% of human cancers. [64] In practice, this overexpression leads to the activation of the kynurenine pathway, to the decrease of local L-Tryptophan (L-Trp) and to the increase of the concentration of metabolites. [41, 62, 63] As a result, the lack of L-Trp leads to the inhibition of the mechanistic target of rapamycin (mTORC1) complex, which causes effector T cell autophagy, and activates general control nondepressible 2 (GCN2) kinase, leading to cell-cycle arrest of effector T cells by blocking their proliferation. [36, 40–42, 62] In parallel, the accumulation of kynurenine metabolites activates the transcription factor aryl hydrocarbon receptor (AhR), a ligand-gated transcription factor that is expressed in many immune cells and mediates a wide range of immunomodulatory. [62] An increase in regulatory T cells is observed and induces effector T-cell arrest. That causes an effect of regulation for growth promoting genes in cancer cells. As consequences, immune evasion and survival of cancer cells appear. [36, 42, 63, 65] In addition to these mechanisms, another action of hIDO1 is known at the level of the signaling pathways, independent from its catalytic function. This is due to the presence in its sequence of two immunoreceptor tyrosine based inhibitory motifs (ITIMs, ITIM1 and ITIM2) which can be modified by phosphorylation. After phosphorylation, these two motifs bind protein tyrosine phosphatases, (SHP-1 and SHP-2), and thus trigger an immunoregulatory signalling. [66–71]

Implication of hIDO2

The hIDO2 protein is induced by interferons but also by prostaglandin E2, IL-10, lipopolysaccharide and the AhR. [45] The overexpression of hIDO2 is to be less frequent than for hIDO1 [64, 72] and has been demonstrated in the case of non-small cell carcinoma, gastric cancers, colon cancers, renal cancers, pancreatic cancers and cervical cancer. [32, 45, 64, 73] The protein is upregulated in all cases, except for cervical cancers. The effect on the overexpression on cancer progression varies depending on the cancer type. [45, 64, 72, 74] In pancreatic cancer, hIDO2 silencing or inactivation following polymorphism forms (detailed in Chapter 2) leads to better patient survival, if combined with radiotherapy. [64, 75] Consequently, the understanding of the mode of application of this protein is a real challenge for cancer research.

For a long time, because of their homology and identical function (more explained in Chapter 2), it was thought that hIDO2 acted in a redundant manner with hIDO1 to induce immune system escape in cancer. However, while the escape from the immune system caused by hIDO1 was due to inflammatory cascades, the involvement of hIDO2 in cancer is more complex because this pharmaceutical target is not a representative participant in the enzymatic degradation reaction of L-Trp (see Chapter 2). It is therefore not responsible for metabolite formation and immune escape in the same way as hIDO1. [44, 72, 76] Regarding the possible signaling pathways of hIDO2, one of the two ITIMs motifs (ITIM1) is not retained. For the second (ITIM2), its role is still unknown. As a result, hIDO2 lacks signaling activity. [66, 70] Consequently, the role of this protein in cancer resistance is still being determined. There are several hypotheses to explain the action of hIDO2. The problem with the research on hIDO2 is that there is not much research and some of the articles are contradictory. [76] In a first hypothesis, Merlo *et al.* mentioned that hIDO2 works directly in B cells as a pro-inflammatory mediator, by means of a mechanism independent of hIDO1. [36, 76] In parallel, other papers suggest genetic and biochemical interactions between hIDO1 and hIDO2, which may influence IDO1-induced regulator T cells activation. [64, 70, 77] These claims are in contrast to those of Mellor *et al.* [45] Another influence of the protein may be that the enzyme acts as an upregulator of cytokine signaling. In addition to these effects, the involvement of the hIDO2 protein has been demonstrated in the promotion of cancer cell proliferation, survival and migration through a mechanism involving NAD⁺ production. [32, 45, 78] All this information highlights the mechanism of action of hIDO2 is not yet well understood. However, in view of the overexpression of this protein, its study is of great interest in cancer research.

1.3.2 hIDO1 and hIDO2 roles in COVID-19 disease

The disease, its incidence and mechanism

On a completely different note, COVID-19 is a recent disease. It appeared in December 2019 in China, then rapidly spread out to the rest of the world, causing the largest global pandemic in recent decades. Current data, often considered as underestimated, count 6.5 million deaths from the disease worldwide and 550 million cases. [79] In Belgium, there were 32 thousand deaths and more than 4.3 million cases. [80] At the time of writing, several waves of epidemics have hit countries around the globe

between 2020 and 2022. Mortality is most pronounced among the elderly but can also affect younger people. Obesity, diabetes, cardiovascular disease, immunodeficiency or cancer are factors leading to a higher risk of infection. [80]

COVID-19 disease is a disease caused by an infectious viral agent, SARS-CoV2. The infection results in a respiratory illness of low to moderate intensity. People with comorbidities can develop severe forms. Symptoms were variable throughout the epidemic depending on the type of infecting variants. Symptoms have included fever, cough, fatigue, loss of taste or smell, sore throat, headache, aches and pains, diarrhea, rash or discoloration of fingers or toes, redness or irritation of the eyes, difficulty breathing or shortness of breath, loss of speech, difficulty moving about or confusion and chest pain. [81] Post-acute sequelae, experiencing complications affecting different organs, called "Long COVID-19", have also been demonstrated in several patients, defined as a persistence of the symptoms of the disease after infection.

Treatments

COVID-19 has enabled a rapid and concerted research by the scientific community for new treatments. From the beginning of the pandemic, barrier measures and isolation were set up to limit the spread of the virus. Vaccines, allowing to increase the immunity of groups have been designated. These are mainly based on the detection of a protein, the spike protein, on the surface of the virus capsid, by antibodies and our immune system. It was in the context of the pandemic that the first messenger ribonucleic acid (RNA) vaccines came onto the market. [81] In 2022, drugs to improve the survival rate of severe cases of COVID-19 are put on the market. In particular, Molnupiravir is a new oral antiviral drug that reduces the replication of SARS-CoV2 in the body. [80] It is also possible to improve patient survival in a hospital setting with monoclonal antibodies (mAbs)⁴, Paxlovid⁵, Dexamethasone⁶, Tocilizumab⁷ and other interleukin-6 blockers, Tofacitinib⁸, Remdesivir⁹ and Baricitinib⁸. Currently,

⁴Authorized by the EMA, but they are not commercially available.

⁵Substance that blocks the activity of an enzyme needed by the virus to multiply, authorized in Europe.

⁶Anti-inflammatory and immunosuppressive in the form of corticosteroids.

⁷Immunosuppressant in the form of a humanized monoclonal antibody that blocks the action of interleukin-6 receptors.

⁸Immunomodulator blocking Janus Kinase responsible for transmission of inflammatory signals.

⁹An adenosine-like nucleotide analog that disrupts viral RNA polymerase, having already demonstrated an effect against Ebola, MERS or feline coronavirus.

only Remdesivir and Molnupiravir are available for sale in Belgium. [80]

Implication of hIDO1

One of the biomarkers to characterize the evolution of a disease is the level of L-Tryptophan and L-Kynurenine. In the case of COVID-19, the standard levels are altered, which highlights an involvement of the L-Kynurenine pathway in the disease. [43, 82] Kaplan-Meier analyses show that high L-Kynurenine level is one of the factors affecting the survival of patients. [82] To understand this phenomenon, the researchers looked at the level of the expression of enzymes of the kynurenine pathway. Immunohistochemistry analyses (Figure 1.3) highlight a significant proportion of hIDO1 in endothelial cells in early/mild pneumonia and long COVID-19 patients. However, this is not detected in severe or fatal cases of COVID-19. [43] It is therefore possible that the high levels of L-Kynurenine observed in the Kaplan-Meier curves are not solely due to hIDO1. This overexpression is interesting because endothelial cells include all the cells involved in vascularization and blood flow. They can, depending on the situation, secrete vasoconstrictor or vasodilator agents. It has been previously demonstrated that hIDO1 has a vasodilator effect. Particularly, with research on the placenta and the human fetus, overexpression of hIDO1 allows, in addition to inducing fetal immunotolerance, the regulation of blood flow to the placenta. [83] A similar phenomenon of vascular relaxation would therefore take place in the case of long COVID-19 and mild pneumonia. [43]

This phenomenon of vascular relaxation in early/mild pneumonia caused by COVID-19 could be explained by the activation of inflammatory signals, inducing the expression of hIDO1 and then the formation of metabolites as kynurenine or singlet molecular oxygen which relaxing actions on blood vessels. In this way, hIDO1 expression is a positive biomarker for blood vessel protection and limits the inflammation. [82] Furthermore, COVID-19 infection often goes hand in hand with the generation of oxidative stress, NO, or superoxide formation. Through its overexpression and generation of kynurenine, hIDO1 counteracts this harmful effect and acts as a local antioxidant defense. [82] Although the overexpression of hIDO1 in COVID-19 disease is an interesting defense action for our body, it can also be a double-edged sword since it leads, in a mechanism similar to the one described above for cancer, to immunotolerance of the virus. As research on COVID-19 is very new, it is too early to decide whether or not hIDO1 inhibition is necessary to improve treatment. [82]

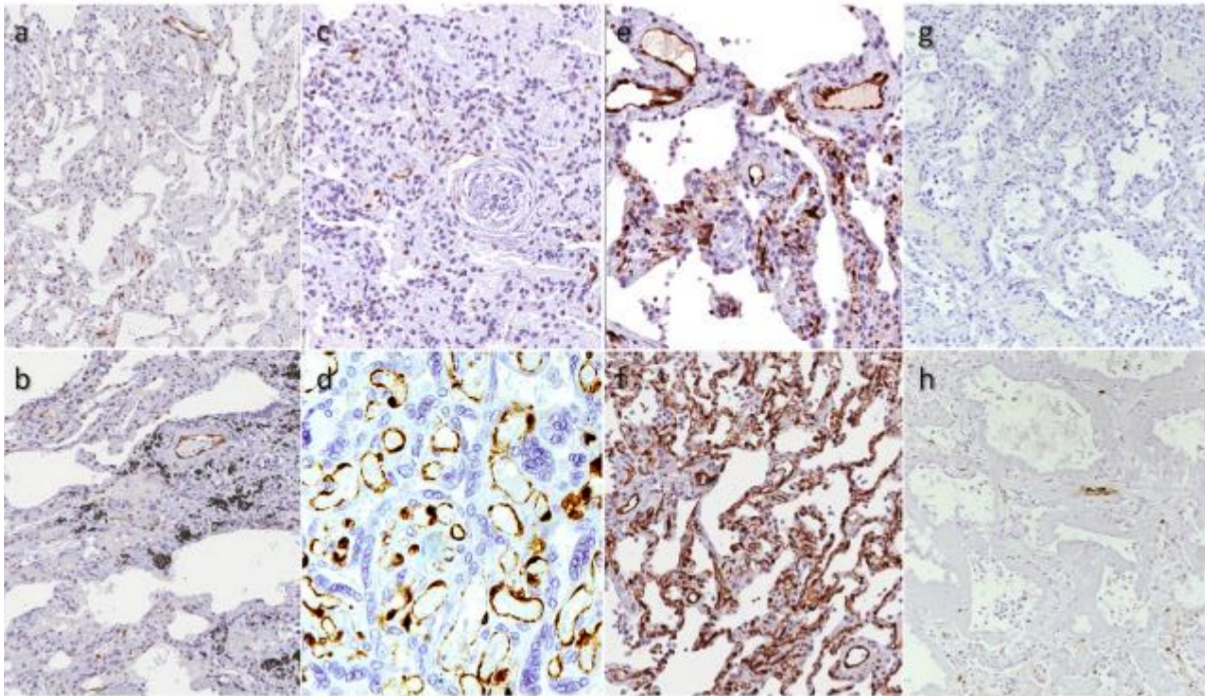


FIGURE 1.3: Expression of hIDO1 (in brown) in endothelial tissues (a,b) normal lung, (c) organizing pneumonia, (d) human placenta (e) COVID-19 early/mild pneumonia, (f) Post-COVID-19 pneumonia, (g,h) Severe COVID-19. Image from Chilosi *et al.* [43]

Implication of hIDO2

As mentioned before, the low expression of hIDO1 in severe or fatal COVID-19 cases does not explain the high L-Kynurenine concentration or the Kaplan-Meier curves. By means of immunohistochemistry, Guo *et al.* demonstrated the accumulation of metabolites of the kynurenine pathway (3-hydroxy-anthranilic acid and quinolinic acid) in the brain, lungs and heart of patients who died from severe forms of COVID-19, resulting from the overexpression of hIDO2 and not of hIDO1 (Figure 1.4). [33] In Figure 1.4, immunohistochemistry analyses demonstrate that hIDO1 expression mainly occurs in endothelial cells and in a disparate manner. Conversely, hIDO2 protein is largely overexpressed in the cytoplasm of interstitial cells, endothelial cells, and type 1 and type 2 pneumocytes. The overexpression of hIDO2 is correlated to the presence of autophagy and apoptosis indicators. [33]

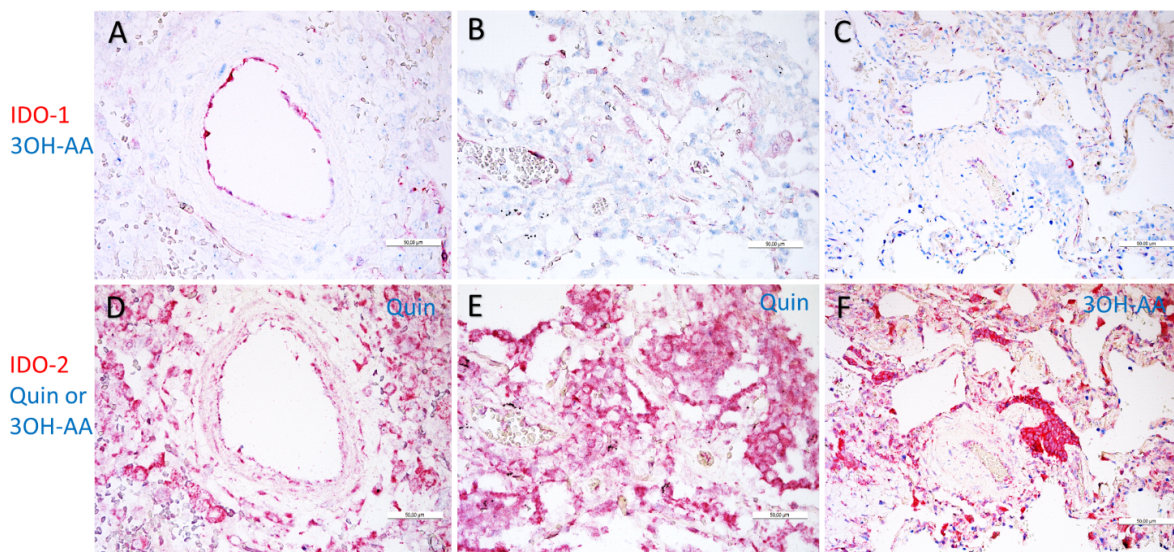


FIGURE 1.4: Distribution of hIDO1 and hIDO2 proteins in human lung tissues after severe cases of COVID-19. Autopsy lung tissue sections stained for hIDO1 or hIDO2 (in pink), and the kynurenine metabolites (3-hydroxy-anthranilic acid (3OH-AA) and quinolinic acid (QUIN), in blue).
Image from Guo *et al.* [33]

The imbalance between hIDO1/hIDO2 allows to switch into a protective vasodilatation to vascular dysfunction. This could lead to vascular inflammation and disruption of the endothelial homeostasis. [43] This phenomenon would be encouraged by the presence of pathological conditions (cardiovascular disease, diabetes, obesity, etc.), which also increases the chances of dysfunctions. [43] It is also possible that hIDO2 affects the patient's immunity, but this mechanism is still misunderstood. Chilosi *et al.* [43] explain the effect of hIDO2 as a positive feedback for hIDO1. Indeed, as hIDO2 is induced by AhR receptors, the low expression of hIDO1 leads, through the metabolic cascade of the kynurenine pathway, to the formation of metabolites and activates these receptors. They induce the expression of hIDO2, and help to the formation of new metabolites. This is correlated with a low level of L-Tryptophan at admission (30 μM), which is still decreasing at the time of death (25 μM). The concentration of the metabolites increases over time and when the death is coming. The overexpression of hIDO1 or hIDO2 is therefore a key factor in the evolution of the disease. [33]

1.4 Development of inhibitors for hIDO1 and hIDO2

With the two case studies detailed above, it is obvious that the inhibition of hIDO1 and hIDO2 could be a useful treatment tool for a huge panel of diseases. However, it will be necessary to choose these inhibitors carefully. Indeed, while in cancer, a dual inhibition of hIDO1 and hIDO2 could be desirable, the treatment of COVID-19 must be able to target only hIDO2. However, in order to choose the right inhibitor, knowing and differentiating the two therapeutic targets is crucial. This understanding could, in the future, reduce side effects.

Regarding drug development, over the years, hIDO1 inhibitors have been developed and entered in clinical trials (Indoximod, Epacadostat, EOS-200271, Navoximod, MMG-0752, LY3381916 and linrodostat). [84, 85] Figures 1.5 and 1.6 details some prototype inhibitors for hIDO1. These are separated into two main categories: holo inhibitors (Figure 1.5: Epacadostat, Navoximod, MMG-0752 or EOS-200271) and apo inhibitors (Figure 1.6 like linrodostat and LY3381916). Holo inhibitors bind into the active site of the enzyme in the presence of the heme cofactor (see Chapter 2). Whereas, apo inhibitors bind the enzyme without the cofactor. Holo inhibitors can then be classified into six categories, depending on the scaffold and the binding mode. The first category includes molecules with a [5,6]-fused heteroaromatic core (Figure 1.5, scaffold in red). In this category, three molecules are listed in clinical trials: Indoximod, EOS-200271 and NLG-802. This motif binds in the L-Trp pocket if hIDO1 is in oxygen-bound holo-IDO1 form. [36, 86]

The second category (Figure 1.5, scaffold in pink) corresponds to molecules with a hydroxyamidine moiety. This category includes Epacadostat and all its derivatives. [36, 87] This category is characterized by a binding to the ferrous iron complex, without dioxygen. The bond is established between the oxygen of the hydroxyl. [86] The third category has the particularity of having a phenylimidazole core (Figure 1.5, scaffold in green). These inhibitors bind the free ferric form of the enzyme via the imidazole nitrogen. The best known inhibitor in this category is Navoximod. [36, 86, 87] The fourth category contains the compounds with a 1,2,3-triazole or tetrazole motif (Figure 1.5, scaffold in orange). In this category, MMG-0752 is in clinical trials. This compound and analogues also bind to the free ferric form. The fifth category

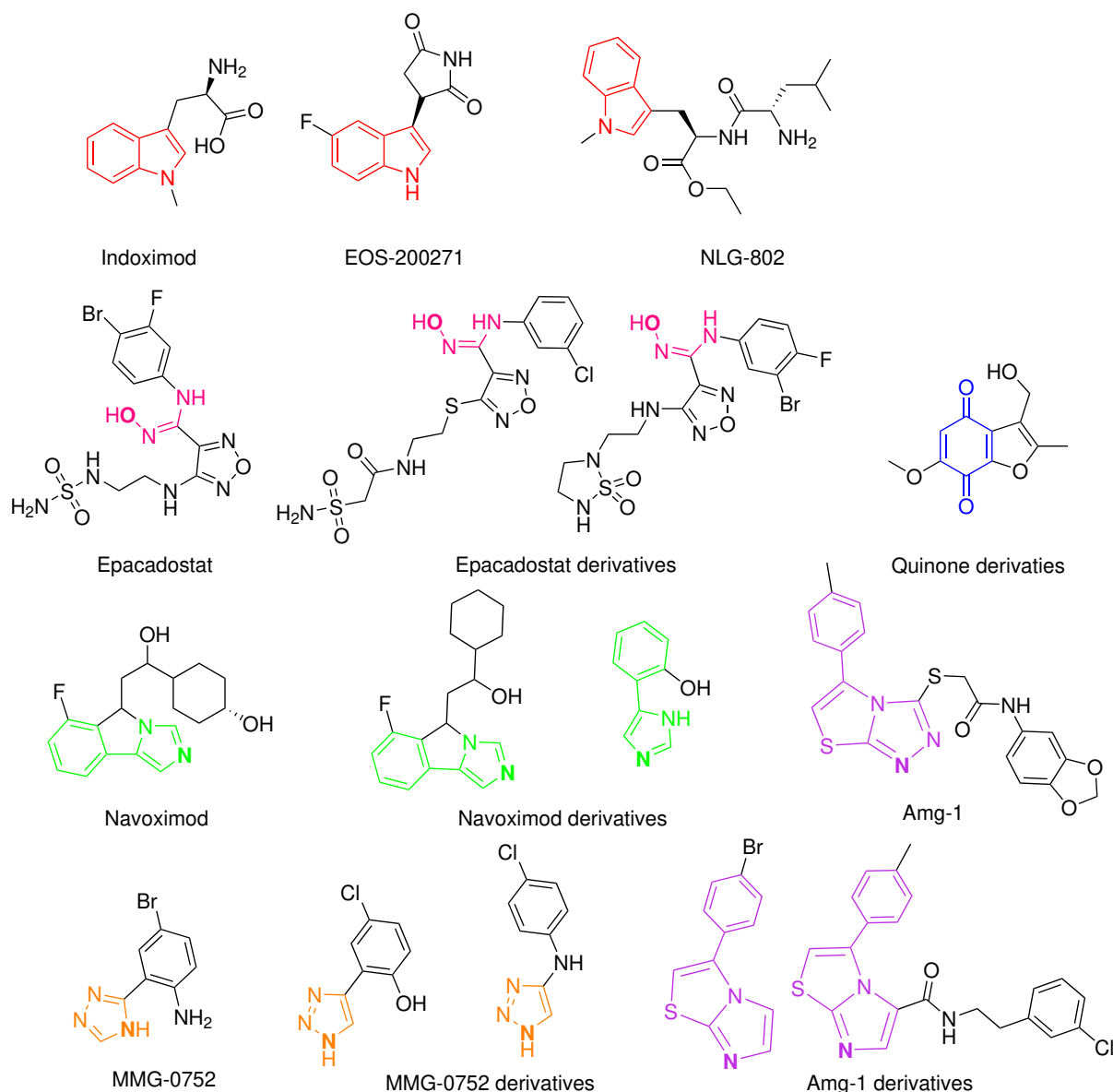


FIGURE 1.5: Non-exhaustive list of holo inhibitors developed against hIDO1. The atom binding the iron is in bold. [36, 86]

contains Amg-1 inhibitor (Figure 1.5, scaffold in purple) and analogs with imidazothiazole core. The binding locus between nitrogen atom to the iron of the cofactor. [88] The last category includes inhibitors with quinone or iminoquinone motifs (Figure 1.5, scaffold in blue). These molecules present redox activity. [36, 86, 87] In contrast, apo inhibitors have started to be developed quite recently and do not yet have strong patterning characteristics as shown in Figure 1.6.

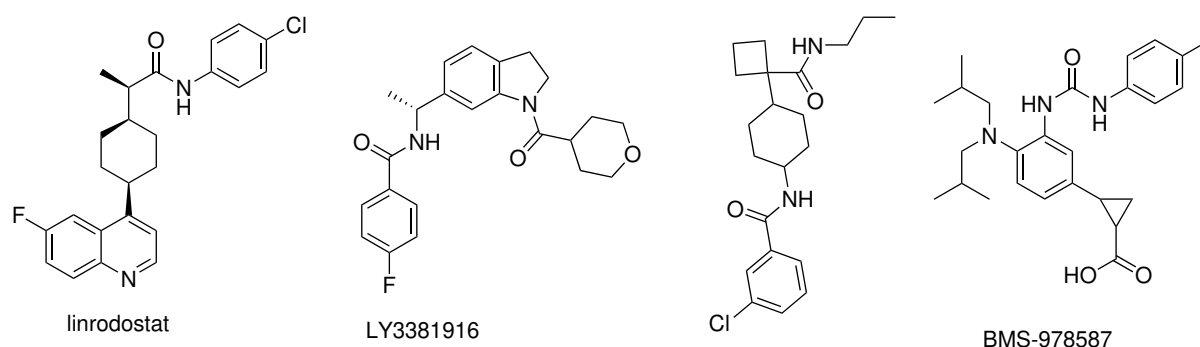


FIGURE 1.6: Non-exhaustive list of apo inhibitors developed against hIDO1. [36, 86]

Nevertheless, although there is a lot of research on the hIDO1 inhibition, no molecule has arrived on the market in the last 20 years. Unfortunately, the Epacadostat has recently failed in phase III of clinical trials, demonstrating that hIDO1 inhibition alone is not sufficient to solve the problem of immune escape. [85, 89, 90] This event has generated a reconsideration of the knowledge on the enzyme. A lack of information still exists for hIDO1, which is thought to be necessary to design new inhibitors.

Concerning hIDO2, the study of this protein is very limited. Only few molecules (Indoximod and 1,2,3-triazoles) are known to inhibit the enzyme. [91, 92] Recently, an attempt at a dual inhibitor, based on the epacadostat structure, has been proposed. [93, 94] However, since the low activity of hIDO2 compared to hIDO1 and the poorly understood role of the enzyme, it is therefore difficult to achieve such a potent active site inhibitor. Also, inhibiting the L-Trp binding site may not be the best strategy. At present, a fundamental study of hIDO2 to increase the knowledge of the enzyme (its mode of action and its structural features) is needed in order to target the protein efficiently.

Bibliography

- [1] Worldometer. Population mondiale, 1 June 2022. <https://www.worldometers.info>.
- [2] R. J. Dubos. The evolution of infectious diseases in the course of history. *Canadian Medical Association Journal*, 79(6):445, 1958.

- [3] A. Boutayeb. The double burden of communicable and non-communicable diseases in developing countries. *Transactions of the Royal society of Tropical Medicine and Hygiene*, 100(3):191–199, 2006.
- [4] World Health Organization. The top 10 causes of death, 4 December 2020. <http://www.who.int/>.
- [5] J. Elflein. Number of deaths caused by selected communicable diseases annually worldwide as of 2019 based on who numbers, 20 May 2022. <https://www.statista.com/>.
- [6] R. E. Baker, A. S. Mahmud, I. F. Miller, M. Rajeev, F. Rasambainarivo, B. L. Rice, S. Takahashi, A. J. Tatem, C. E. Wagner, L.-F. Wang, et al. Infectious disease in an era of global change. *Nature Reviews Microbiology*, 20:193–205, 2022.
- [7] Institut Pasteur. Troisième époque: 1877 - 1887 - jenner invente la vaccination, louis pasteur invente les vaccins, 20 May 2022. <https://www.pasteur.fr/>.
- [8] World Health Organization. Commemorating smallpox eradication – a legacy of hope, for covid-19 and other diseases, 8 May 2020. <http://www.who.int/>.
- [9] D. Antona. L'éradication des maladies infectieuses: l'exemple de la poliomyélite. *Médecine/Sciences*, 18(1):55–61, 2002.
- [10] T. Cihlar and M. Fordyce. Current status and prospects of hiv treatment. *Current Opinion in Virology*, 18:50–56, 2016.
- [11] R. K. Gupta, D. Peppas, A. L. Hill, C. Gálvez, M. Salgado, M. Pace, L. E. McCoy, S. A. Griffith, J. Thornhill, A. Alrubayyi, et al. Evidence for hiv-1 cure after ccr5 δ 32/ δ 32 allogeneic haemopoietic stem-cell transplantation 30 months post analytical treatment interruption: a case report. *The Lancet HIV*, 7(5):340–347, 2020.
- [12] University of California Los Angeles Health Sciences, editor. *UCLA Health at CROI: Presenting the case of a woman with HIV-1 in remission following specialized stem cell transplantation for leukemia*, 15 February 2022.
- [13] World Health Organization. Hiv/aids, 30 November 2021. <http://www.who.int/>.

- [14] B. Hanboonkunupakarn and N. J. White. Advances and roadblocks in the treatment of malaria. *British Journal of Clinical Pharmacology*, 88(2):374–382, 2022.
- [15] C. Antonio-Nkondjio, C. Ndo, F. Njiokou, J. D. Bigoga, P. Awono-Ambene, J. Etang, A. S. Ekobo, and C. S. Wondji. Review of malaria situation in cameroon: technical viewpoint on challenges and prospects for disease elimination. *Parasites & Vectors*, 12(1):1–23, 2019.
- [16] World Health Organization. Malaria, 6 December 2021. <http://www.who.int/>.
- [17] M. Fischer. Leprosy—an overview of clinical features, diagnosis, and treatment. *JDDG: Journal der Deutschen Dermatologischen Gesellschaft*, 15(8):801–827, 2017.
- [18] World Health Organization. Leprosy, 11 January 2022. <http://www.who.int/>.
- [19] M. D. Iseman. Treatment of multidrug-resistant tuberculosis. *New England Journal of Medicine*, 329(11):784–791, 1993.
- [20] World Health Organization et al. *WHO treatment guidelines for drug-resistant tuberculosis*. World Health Organization, 2016.
- [21] B. Talebi, A. Abadi, A. A. Rizvanov, T. Haertlé, and N. L. Blatt. World health organization report: current crisis of antibiotic resistance. *BioNanoScience*, 9(4):778–788, 2019.
- [22] Worldometer. Covid-19 coronavirus pandemic. <https://www.worldometers.info>.
- [23] World Health Organization. 14.9 million excess deaths associated with the covid-19 pandemic in 2020 and 2021, 5 May 2022. <http://www.who.int/>.
- [24] D. Cheta and A. Dragomir. The negative lifesyle and comtemporany diseases. *Romanian Journal of Diabetes Nutrition and Metabolic Diseases*, 15(1):1–4, 2008.
- [25] R. Kaddurah-Daouk, H. Zhu, S. Sharma, M. Bogdanov, S. G. Rozen, W. Matson, N. O. Oki, A. A. Motsinger-Reif, E. Churchill, Z. Lei, et al. Alterations in metabolic pathways and networks in alzheimer’s disease. *Translational Psychiatry*, 3(244):1–8, 2013.
- [26] P. C. Grayson, S. Eddy, J. N. Taroni, Y. L. Lightfoot, L. Mariani, H. Parikh, M. T. Lindenmeyer, W. Ju, C. S. Greene, B. Godfrey, et al. Metabolic pathways and

- immunometabolism in rare kidney diseases. *Annals of the Rheumatic Diseases*, 77(8):1226–1233, 2018.
- [27] P. Song, T. Ramprasath, H. Wang, and M.-H. Zou. Abnormal kynurenine pathway of tryptophan catabolism in cardiovascular diseases. *Cellular and Molecular Life Sciences*, 74(16):2899–2916, 2017.
- [28] D. C. Maddison and F. Giorgini. The kynurenine pathway and neurodegenerative disease. *Seminars in Cell & Developmental Biology*, 40:134–141, 2015.
- [29] G. J. Guillemin and B. J. Brew. Implications of the kynurenine pathway and quinolinic acid in alzheimer’s disease. *Redox Report*, 7(4):199–206, 2002.
- [30] J. S. Lott. The tryptophan biosynthetic pathway is essential for mycobacterium tuberculosis to cause disease. *Biochemical Society Transactions*, 48(5):2029–2037, 2020.
- [31] J. A. Khan, F. Forouhar, X. Tao, and L. Tong. Nicotinamide adenine dinucleotide metabolism as an attractive target for drug discovery. *Expert Opinion on Therapeutic Targets*, 11(5):695–705, 2007.
- [32] C. A. Opitz, L. F. Somarribas Patterson, S. R. Mohapatra, D. L. Dewi, A. Sadik, M. Platten, and S. Trump. The therapeutic potential of targeting tryptophan catabolism in cancer. *British Journal of Cancer*, 122(1):30–44, 2020.
- [33] L. Guo, B. Schurink, E. Roos, E. J. Nossent, J. W. Duitman, A. P. J. Vlaar, P. van der Valk, F. M. Vaz, S.-R. Yeh, Z. Geeraerts, et al. Indoleamine 2, 3-dioxygenase (ido)-1 and ido-2 activity and severe course of covid-19. *The Journal of Pathology*, 256(3):256–261, 2022.
- [34] A. Badawy. Kynurenine pathway of tryptophan metabolism: regulatory and functional aspects. *International Journal of Tryptophan Research*, 10:1–20, 2017.
- [35] R. S. Phillips, E. C. Iradukunda, T. Hughes, and J. P. Bowen. Modulation of enzyme activity in the kynurenine pathway by kynurenine monooxygenase inhibition. *Frontiers in Molecular Biosciences*, 6(3):1–9, 2019.
- [36] A. Dolšak, S. Gobec, and M. Sova. Indoleamine and tryptophan 2, 3-dioxygenases as important future therapeutic targets. *Pharmacology & Therapeutics*, 221(107746):1–23, 2021.

- [37] M. D. Armstrong and U. Stave. A study of plasma free amino acid levels. ii. normal values for children and adults. *Metabolism*, 22(4):561–569, 1973.
- [38] L. R. Kolodziej, E. M. Paleolog, and R. O. Williams. Kynurenine metabolism in health and disease. *Amino Acids*, 41(5):1173–1183, 2011.
- [39] D. H. Munn and A. L. Mellor. Indoleamine 2, 3 dioxygenase and metabolic control of immune responses. *Trends in Immunology*, 34(3):137–143, 2013.
- [40] A. L. Mellor, H. Lemos, and L. Huang. Indoleamine 2, 3-dioxygenase and tolerance: where are we now? *Frontiers in immunology*, 8(1360):1–6, 2017.
- [41] C. Uyttenhove, L. Pilotte, I. Théate, V. Stroobant, D. Colau, N. Parmentier, T. Boon, and B. J. Van den Eynde. Evidence for a tumoral immune resistance mechanism based on tryptophan degradation by indoleamine 2, 3-dioxygenase. *Nature Medicine*, 9(10):1269–1274, 2003.
- [42] G. C. Prendergast. Immune escape as a fundamental trait of cancer: focus on ido. *Oncogene*, 27(28):3889–3900, 2008.
- [43] M. Chilosì, C. Doglioni, C. Ravaglia, G. Martignoni, G. L. Salvagno, G. Pizzolo, V. Bronte, and V. Poletti. Unbalanced ido1/ido2 endothelial expression and skewed kynurenine pathway in the pathogenesis of covid-19 and post-covid-19 pneumonia. *Biomedicines*, 10(1332):1–24, 2022.
- [44] S. Löb, A. Königsrainer, D. Zieker, B. L. D. M. Brücher, H.-G. Rammensee, G. Opelz, and P. Terness. Ido1 and ido2 are expressed in human tumors: levo-but not dextro-1-methyl tryptophan inhibits tryptophan catabolism. *Cancer Immunology, Immunotherapy*, 58(1):153–157, 2009.
- [45] P. Li, W. Xu, F. Liu, H. Zhu, L. Zhang, Z. Ding, H. Liang, and J. Song. The emerging roles of ido2 in cancer and its potential as a therapeutic target. *Biomedicine & Pharmacotherapy*, 137:1–6, 2021.
- [46] A. A. Fatokun, N. H. Hunt, and H. J. Ball. Indoleamine 2, 3-dioxygenase 2 (ido2) and the kynurenine pathway: characteristics and potential roles in health and disease. *Amino Acids*, 45(6):1319–1329, 2013.
- [47] L. M. F. Merlo, J. Bowers, T. Stefanoni, G. V. Gordon, R. Getts, and L. Mandik-Nayak. The immunomodulating enzyme indoleamine 2, 3-dioxygenase 2 (ido2)

- as a target for therapy in autoimmune disease. *The Journal of Immunology*, 206(1):66, 2021.
- [48] Cancer Research UK. Together we will beat cancer, 2 June 2022. <http://www.cancerresearchuk.org>.
- [49] Belgian Cancer Registry. Les 10 tumeurs les plus fréquentes par sexe, 2 June 2022. <https://kankerregister.org>.
- [50] R. A. Weinberg and D. Hanahan. The hallmarks of cancer. *Cell*, 100(1):57–70, 2000.
- [51] J. Reece, L. A. Urry, M. L. Cain, S. A. Wasserman, P. V. Minorsky, and R. B. Jackson. *Campbell Biologie, 9th ed.* Pearson Boston, 2014.
- [52] D. Hanahan and R. A. Weinberg. Hallmarks of cancer: the next generation. *Cell*, 144(5):646–674, 2011.
- [53] M. Schuster, A. Nechansky, and R. Kircheis. Cancer immunotherapy. *Biotechnology Journal: Healthcare Nutrition Technology*, 1(2):138–147, 2006.
- [54] L. Falzone, S. Salomone, and M. Libra. Evolution of cancer pharmacological treatments at the turn of the third millennium. *Frontiers in Pharmacology*, 9(1300):1–26, 2018.
- [55] American Cancer Society. Radiation therapy side effects, 2 June 2022. <https://www.cancer.org/>.
- [56] Pancreatic Cancer UK. What are the advantages and disadvantages of radiotherapy?, 2 June 2022. <https://www.pancreaticcancer.org.uk/>.
- [57] National Cancer Institute. Side effects of cancer treatment, 2 June 2022. <https://www.cancer.gov/>.
- [58] J. L. Amiel, M. Sekiguchi, G. Daguet, S. Garattini, and V. Palma. Etude de l'effet immunodépresseur des composés chimiques utilisés en chimiothérapie anticancéreuse. *European Journal of Cancer*, 3(1):47–65, 1967.
- [59] K. Esfahani, L. Roudaia, N. Buhlaiga, S. V. Del Rincon, N. Papneja, and W. H. Miller. A review of cancer immunotherapy: from the past, to the present, to the future. *Current Oncology*, 27(2):87–97, 2020.

- [60] J. Zugazagoitia, C. Guedes, S. Ponce, I. Ferrer, S. Molina-Pinelo, and L. Paz-Ares. Current challenges in cancer treatment. *Clinical Therapeutics*, 38(7):1551–1566, 2016.
- [61] Y. T. Lee, Y. J. Tan, and C. E. Oon. Molecular targeted therapy: Treating cancer with specificity. *European journal of pharmacology*, 834:188–196, 2018.
- [62] B. W. Labadie, R. Bao, and J. J. Luke. Reimagining ido pathway inhibition in cancer immunotherapy via downstream focus on the tryptophan–kynurenine–aryl hydrocarbon axistrp–kyn–ahr immunotherapy. *Clinical Cancer Research*, 25(5):1462–1471, 2019.
- [63] G. C. Prendergast, C. Smith, S. Thomas, L. Mandik-Nayak, L. Laury-Kleintop, R. Metz, and A. J. Muller. Indoleamine 2, 3-dioxygenase pathways of pathogenic inflammation and immune escape in cancer. *Cancer Immunology, Immunotherapy*, 63(7):721–735, 2014.
- [64] A. Nevler, A. J. Muller, E. Sutanto-Ward, J. B. DuHadaway, K. Nagatomo, E. Londin, K. O’Hayer, J. A. Cozzitorto, H. Lavu, T. P. Yeo, et al. Host ido2 gene status influences tumor progression and radiotherapy response in kras-driven sporadic pancreatic cancersido2 polymorphisms affect pancreas cancer and radioresponse. *Clinical Cancer Research*, 25(2):724–734, 2019.
- [65] N. Venkateswaran and M. Conacci-Sorrell. Kynurenine: An oncometabolite in colon cancer. *Cell Stress*, 4(1):24, 2020.
- [66] F. Fallarino, U. Grohmann, and P. Puccetti. Indoleamine 2, 3-dioxygenase: from catalyst to signaling function. *European journal of immunology*, 42(8):1932–1937, 2012.
- [67] M. T. Pallotta, F. Fallarino, D. Matino, A. Macchiarulo, and C. Orabona. Ahr-mediated, non-genomic modulation of ido1 function. *Frontiers in immunology*, 5:497, 2014.
- [68] M. Liu, X. Wang, L. Wang, X. Ma, Z. Gong, S. Zhang, and Y. Li. Targeting the ido1 pathway in cancer: from bench to bedside. *Journal of hematology & oncology*, 11(1):1–12, 2018.

- [69] M. T. Pallotta, C. Orabona, C. Volpi, C. Vacca, M. L. Belladonna, R. Bianchi, G. Servillo, C. Brunacci, M. Calvitti, S. Bicciato, et al. Indoleamine 2, 3-dioxygenase is a signaling protein in long-term tolerance by dendritic cells. *Nature immunology*, 12(9):870–878, 2011.
- [70] G. Mondanelli, M. Mandarano, M. L. Belladonna, C. Suvieri, C. Pelliccia, G. Bellezza, A. Sidoni, A. Carvalho, U. Grohmann, and C. Volpi. Current challenges for ido2 as target in cancer immunotherapy. *Frontiers in immunology*, 12(679953):1–7, 2021.
- [71] E. Albin, V. Rosini, M. Gargaro, G. Mondanelli, M. L. Belladonna, M. T. Pallotta, C. Volpi, F. Fallarino, A. Macchiarulo, C. Antognelli, et al. Distinct roles of immunoreceptor tyrosine-based motifs in immunosuppressive indoleamine 2, 3-dioxygenase 1. *Journal of cellular and molecular medicine*, 21(1):165–176, 2017.
- [72] M. Mandarano, G. Bellezza, M. L. Belladonna, J. Vannucci, A. Gili, I. Ferri, C. Lupi, V. Ludovini, G. Falabella, G. Metro, et al. Indoleamine 2, 3-dioxygenase 2 immunohistochemical expression in resected human non-small cell lung cancer: a potential new prognostic tool. *Frontiers in Immunology*, 11(839):1–10, 2020.
- [73] J. Hascitha, R. Priya, S. Jayavelu, H. Dhandapani, G. Selvaluxmy, S. S. Singh, and T. Rajkumar. Analysis of kynurenine/tryptophan ratio and expression of ido1 and 2 mrna in tumour tissue of cervical cancer patients. *Clinical Biochemistry*, 49(12):919–924, 2016.
- [74] W. Yamasuge, Y. Yamamoto, H. Fujigaki, M. Hoshi, K. Nakamoto, K. Kunisawa, A. Mouri, T. Nabeshima, and K. Saito. Indoleamine 2, 3-dioxygenase 2 depletion suppresses tumor growth in a mouse model of lewis lung carcinoma. *Cancer Science*, 110(10):3061–3067, 2019.
- [75] A. K. Witkiewicz, C. L. Costantino, R. Metz, A. J. Muller, G. C. Prendergast, C. J. Yeo, and J. R. Brody. Genotyping and expression analysis of ido2 in human pancreatic cancer: a novel, active target. *Journal of the American College of Surgeons*, 208(5):781–787, 2009.
- [76] L. M. F. Merlo, J. B. DuHadaway, J. D. Montgomery, W.-D. Peng, P. J. Murray, G. C. Prendergast, A. J. Caton, A. J. Muller, and L. Mandik-Nayak. Differential roles of ido1 and ido2 in t and b cell inflammatory immune responses. *Frontiers in Immunology*, 11(1861):1–16, 2020.

- [77] R. Metz, C. Smith, J. B. DuHadaway, P. Chandler, B. Baban, L. M. F. Merlo, E. Pigott, M. P. Keough, S. Rust, A. L. Mellor, et al. Ido2 is critical for ido1-mediated t-cell regulation and exerts a non-redundant function in inflammation. *International Immunology*, 26(7):357–367, 2014.
- [78] Y. Liu, Y. Zhang, X. Zheng, X. Zhang, H. Wang, Q. Li, K. Yuan, N. Zhou, Y. Yu, N. Song, et al. Gene silencing of indoleamine 2, 3-dioxygenase 2 in melanoma cells induces apoptosis through the suppression of nad⁺ and inhibits in vivo tumor growth. *Oncotarget*, 7(22):32329–32340, 2016.
- [79] JHU CSSE. About novel coronavirus (covid-19) cases, provided by jhu csse, 5 July 2022. <https://github.com/CSSEGISandData/COVID-19>.
- [80] Sciensano. Coronavirus covid-19, 5 July 2022. <https://covid-19.sciensano.be/>.
- [81] World Health Organization. Coronavirus, 5 July 2022. <http://www.who.int/>.
- [82] H. Mangge, M. Herrmann, A. Meinitzer, S. Pailer, P. Curcic, Z. Sloup, M. Holter, and F. Prüller. Increased kynurenine indicates a fatal course of covid-19. *Antioxidants*, 10(1960):1–11, 2021.
- [83] P. Zardoya-Laguardia, A. Blaschitz, B. Hirschmugl, I. Lang, S. A. Herzog, L. Nikitina, M. Gauster, M. Häusler, M. Cervar-Zivkovic, E. Karpf, et al. Endothelial indoleamine 2, 3-dioxygenase-1 regulates the placental vascular tone and is deficient in intrauterine growth restriction and pre-eclampsia. *Scientific Reports*, 8(1):1–12, 2018.
- [84] Y. W. Moon, J. Hajjar, P. Hwu, and A. Naing. Targeting the indoleamine 2, 3-dioxygenase pathway in cancer. *Journal for Immunotherapy of Cancer*, 3(1):1–10, 2015.
- [85] G. C. Prendergast, W. J. Malachowski, A. Mondal, P. Scherle, and A. J. Muller. Indoleamine 2, 3-dioxygenase and its therapeutic inhibition in cancer. *International Review of Cell and Molecular Biology*, 336:175–203, 2018.
- [86] U. F. Röhrig, O. Michielin, and V. Zoete. Structure and plasticity of indoleamine 2, 3-dioxygenase 1 (ido1). *Journal of Medicinal Chemistry*, 64(24):17690–17705, 2021.
- [87] X.-X. Wang, S.-Y. Sun, Q.-Q. Dong, X.-X. Wu, W. Tang, and Y.-Q. Xing. Recent advances in the discovery of indoleamine 2, 3-dioxygenase 1 (ido1) inhibitors. *MedChemComm*, 10(10):1740–1754, 2019.

- [88] S. Tojo, T. Kohno, T. Tanaka, S. Kamioka, Y. Ota, T. Ishii, K. Kamimoto, S. Asano, and Y. Isobe. Crystal structures and structure–activity relationships of imidazothiazole derivatives as ido1 inhibitors. *ACS medicinal chemistry letters*, 5(10):1119–1123, 2014.
- [89] K. N. Pham, A. Lewis-Ballester, and S.-R. Yeh. Structural basis of inhibitor selectivity in human indoleamine 2, 3-dioxygenase 1 and tryptophan dioxygenase. *Journal of the American Chemical Society*, 141(47):18771–18779, 2019.
- [90] Y.-H. Peng, F.-Y. Liao, C.-T. Tseng, R. Kuppusamy, A.-S. Li, C.-H. Chen, Y.-S. Fan, S.-Y. Wang, M.-H. Wu, C.-C. Hsueh, et al. Unique sulfur–aromatic interactions contribute to the binding of potent imidazothiazole indoleamine 2, 3-dioxygenase inhibitors. *Journal of Medicinal Chemistry*, 63(4):1642–1659, 2020.
- [91] F. Qian, J. Liao, J. Vilella, R. Edwards, P. Kalinski, S. Lele, P. Shrikant, and K. Odunsi. Effects of 1-methyltryptophan stereoisomers on ido2 enzyme activity and ido2-mediated arrest of human t cell proliferation. *Cancer Immunology, Immunotherapy*, 61(11):2013–2020, 2012.
- [92] U. F. Röhrig, S. R. Majjigapu, D. Caldelari, N. Dilek, P. Reichenbach, K. Ascencao, M. Irving, G. Coukos, P. Vogel, V. Zoete, et al. 1, 2, 3-triazoles as inhibitors of indoleamine 2, 3-dioxygenase 2 (ido2). *Bioorganic & Medicinal Chemistry Letters*, 26(17):4330–4333, 2016.
- [93] X. He, G. He, Z. Chu, H. Wu, J. Wang, Y. Ge, H. Shen, S. Zhang, J. Shan, K. Peng, et al. Discovery of the first potent ido1/ido2 dual inhibitors: A promising strategy for cancer immunotherapy. *Journal of Medicinal Chemistry*, 64(24):17950–17968, 2021.
- [94] Y. Zhang, Z. Hu, J. Zhang, C. Ren, and Y. Wang. Dual-target inhibitors of indoleamine 2, 3 dioxygenase 1 (ido1): A promising direction in cancer immunotherapy. *European Journal of Medicinal Chemistry*, 238(114524):1–14, 2022.

Chapter 2

hIDO1 and hIDO2: identity cards

2.1 Introduction

Following the positioning of hIDO1 and hIDO2 as a pharmaceutical interest for the treatment of diseases such as cancer or Covid-19, many research groups have been interested in developing inhibitor molecules. However, this drug design effort has, at times, been done blindly since essential structural or functional information on the two targets was unknown. This chapter summarizes the knowledge and missing biophysical and biochemical information on hIDO1 and hIDO2.

2.2 State of the art of the knowledge about hIDO1

As described in Chapter 1, the protein hIDO1 (EC:1.13.11.52) is an immune checkpoint molecule and acts as a negative regulator of inflammation and immune activation. Intensively studied since the 21st century and the highlighting of importance in cancer research, its discovery by Hayaishi and coworkers dates to the sixties. [1, 2] It is an enzyme mainly expressed in mammals. In humans, it is found in a large number of body parts (lung, placenta, bones, skin, etc.) except in the liver.

2.2.1 Heme cofactor and mechanism

The hIDO1 protein is a monomeric hemoprotein, having a cofactor in the form of heme b in its active site. This heme group is essential to the proper functioning of the protein and governs a large number of physicochemical characteristics of this system. This complex porphyrin, where the variability of its electronic and chemical properties depends on the iron oxidation state, is represented at Figure 2.1, A. [3] The heme can be obtained by two ways: the food (red meat), and metabolic synthesis. [4] The formation of heme is performed in cells by the porphyrin pathway (Figure 2.1, C.). This metabolic pathway is initiated by δ -aminolevulinic acid (ALA) (Figure 2.1, B.). Its formation, from glycine and succinyl CoA, is the rate-limiting step of the porphyrin pathway. The pathway process takes place both in the mitochondria and in the cytoplasm. [3–6] Through its role as a cofactor of hemoproteins, heme controls a large number of functions in our body such as oxygen transport, drug and steroid metabolism, transcription regulation and signal translation. [4, 5]

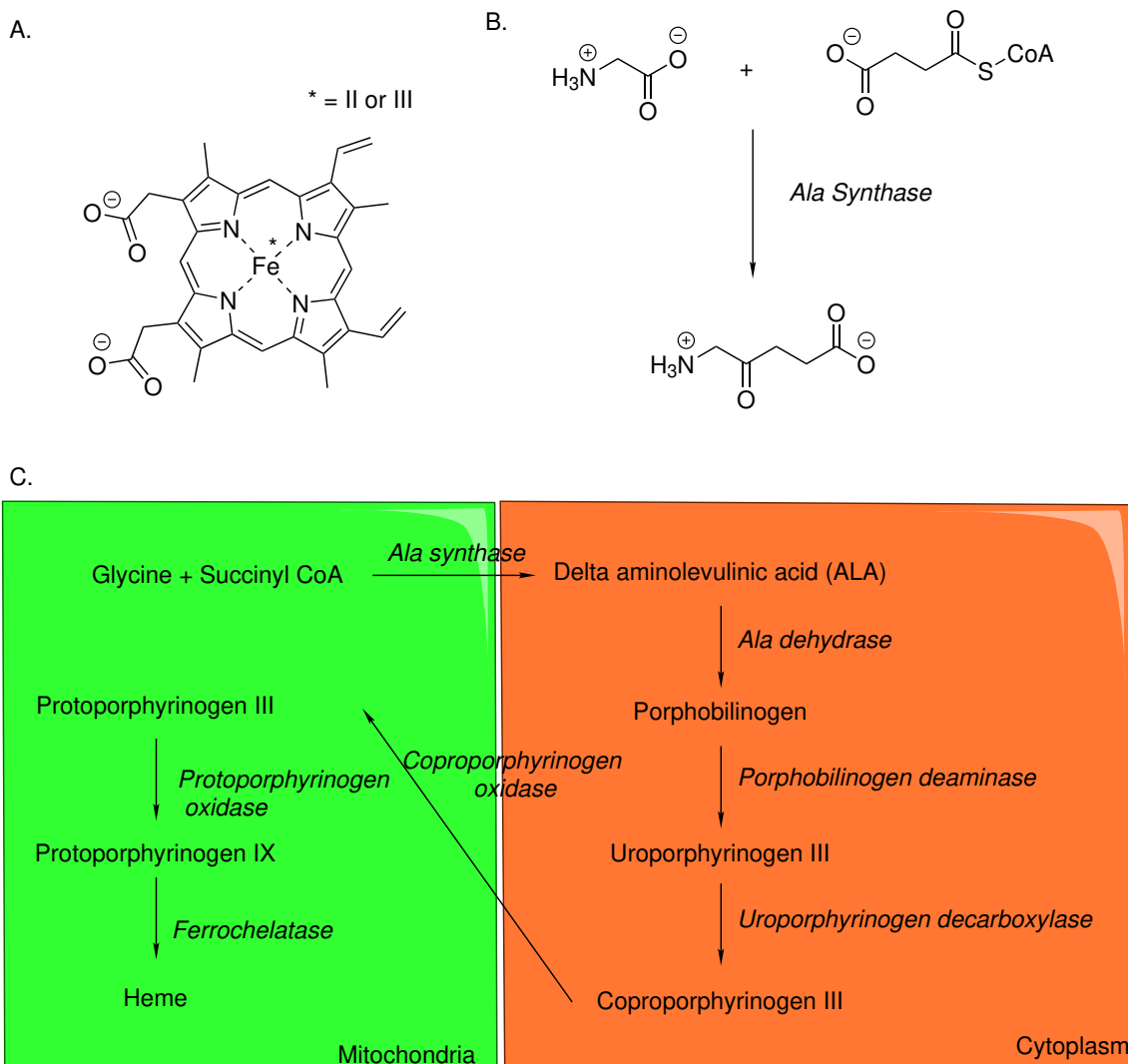


FIGURE 2.1: Focus on the heme b cofactor. A. Structure of heme b present in hIDO1. B. First step of the porphirin pathway and formation of δ -aminolevulinic acid. C. Schematic diagram of the porphyrin pathway.

Unfortunately, an abnormal concentration of free heme is harmful, and could induce cytosolic toxicity, such as reactive oxygen species (ROS) formation, and degradation of gram-positive bacteria of the intestinal flora. [5] Moreover, as other central compounds in biology, its use can be diverted in the case of cancers. It has been shown that a disturbance of free heme levels in our body (heme accumulation) is involved in tumors by promoting their proliferation and survival. [4, 7, 8] In particular, this gain in heme synthesis may contribute to increased activity of hemoproteins such as hIDO1 and hIDO2. [4]

Actually, the heme cofactor is essential to the mechanism of hIDO1, as described in Figure 2.2. In the latter, determined in 2016 by Basran *et al.*, the heme cofactor activates the dioxygen using a radical addition. Thus, using this activated molecule of O₂, hIDO1 converts L-Trp to N-formylkynurenine (NFK) by oxidative cleavage of the C2-C3 double bond of the indole moiety. [9–11] The radical addition of O₂ breaks the double bond of the indole to form a single bond and a radical on the C3 of L-Trp. The resulting intermediate is a peroxide on which the bond between the two oxygens will be broken to form an epoxide intermediate. The second oxygen then allows the opening of the epoxide, followed by the breaking of the bond between C2 and C3 and the formation of two carbonyls to form NFK.

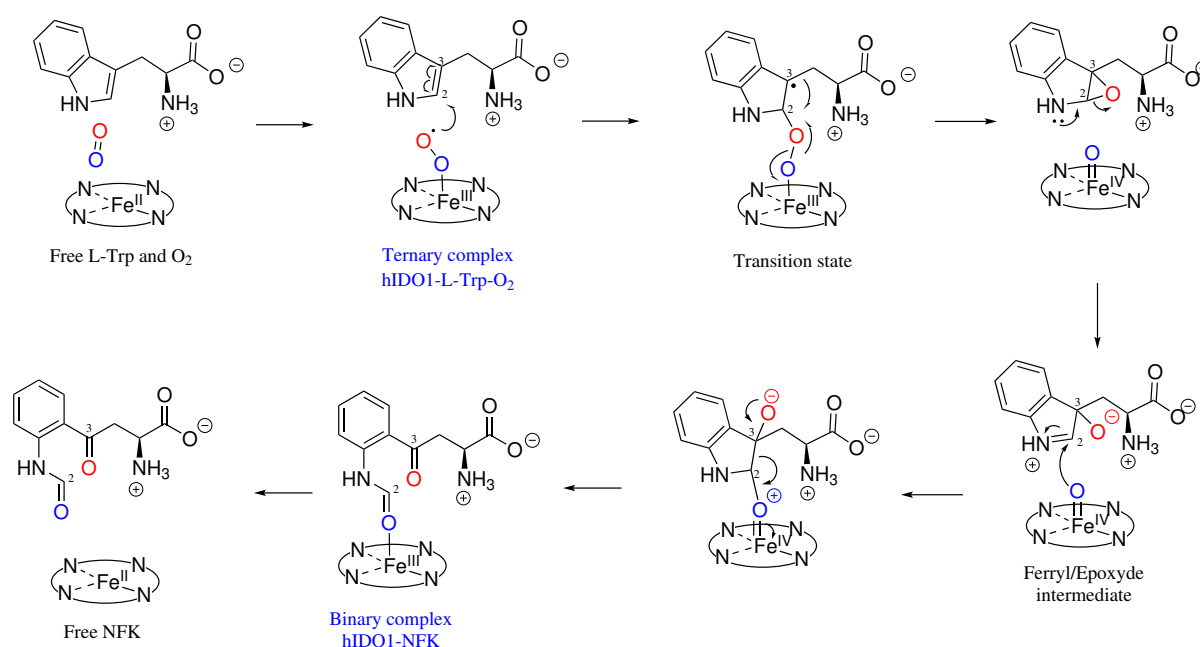


FIGURE 2.2: Mechanism of hIDO1 according to the hypothesis developed by Basran *et al.*. [9, 12]

The hIDO1 enzyme is not very specific to its substrate which leads to the possible catalysis of several indoleamine derivatives (L-Trp, D-Trp, serotonin, 5-hydroxy-L-Trp, etc.). For L-Trp, the current data shows an affinity of the protein for the substrate in the micro-molar range (Michaelis constant (K_m) of 40 μM). The enzymatic activity is also particular since an inhibition by the substrate is observed at high concentration. To explain this phenomenon, several hypotheses exist such as 1) the binding of L-Trp in an inhibitor site located near the heme binding pocket at a high concentration,

2) a ordered binding and a blocked access to the active site for dioxygen or 3) a ordered binding causing a disruption of the reduction potential. [13] At present, the last hypothesis is more accepted by the scientific community. According to this hypothesis, substrate inhibition is due to the preferential binding order of the two substrates. Indeed, oxygen binds first, which facilitates the binding of L-Tryptophan. [14–17] When substrate inhibition occurs at high concentrations of L-Trp, the binding order is reversed. [15] Due to this early binding of L-Trp, a modulation of the heme reduction potential is observed. This change could cause unfavourable O₂ binding by increasing the redox potential of the cofactor. [13] To perform the catalytic reaction, the heme must be in ferrous form at the beginning of the reaction cycle. To do this, traditionally, the hIDO1 activity assay is performed in a mixture of ascorbic acid and methylene blue to counteract the auto-oxidation of the protein. Catalase is also added to the mixture to avoid H₂O₂ poisoning of the active site. [14] Scientific evidence suggests that, *in vivo*, this is achieved with the help of cytochrome b5 and cytochrome P450 reductase with NADPH. [18]

2.2.2 Heme cofactor and physico-chemical properties

The presence of the heme cofactor in hIDO1 confers, in addition to its activity, a series of biophysical properties allowing the characterization of the protein state. Among these methods, an easy and inexpensive method, the UV-Visible absorption spectroscopy analysis, is possible. The analysis focuses on absorption bands typical of heme binding to the protein. These bands are known as the Soret band (maximum between 350 nm and 500 nm), also known as the B band, and the two Q bands (appearing between 500 nm and 750 nm), represented at Figure 2.3. The existence of the band is often shortened to Soret's band because of its highest intensity. [19, 20]

This spectral signature comes from the highly conjugated π -electron nature of the system. [19] The theory of four orbital determined by Gouterman is needed to understand this phenomenon. [19–23] In this theory, the heme electrons of the porphyrin can be simplified as two highest occupied π -orbitals (HOMOs) and two lowest unoccupied π^* -orbitals (LUMOs). In the case of a simple porphyrin (without any central ion), the different absorption bands on the UV-Visible absorption spectroscopy spectra come from the transitions between the two HOMOs and the two LUMOs orbitals (Figure 2.3, B.). [19, 22] The symmetry of these four orbitals are of type a_{1u} and a_{2u}

for HOMOs and of type eg_x and eg_y for LUMOs orbitals. The LUMO states are degenerated into two energy states. The Soret transition is characterized by a transition from a fundamental state (S_0) to the second energy state (S_2) of the LUMO while the Q bands are transitions from the fundamental state to the first energy level of the LUMO (S_0 to S_1). [19, 22]

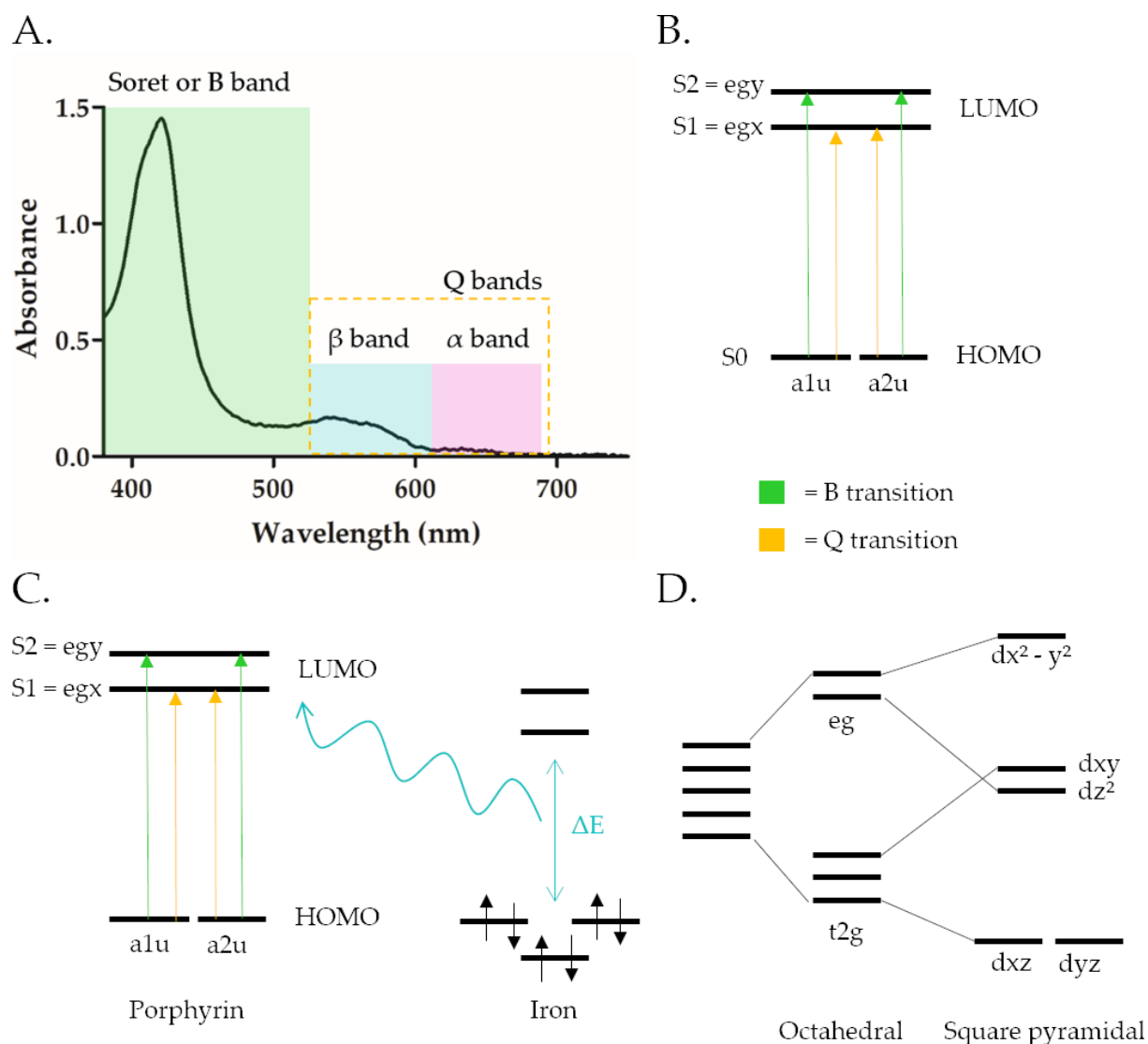


FIGURE 2.3: Four orbitals theory applied to heme b system. A. Typical spectral signature of hIDO1. Soret bands, β bands and α bands are respectively observed from left to right. B. Four orbital theory in case of porphyrins without central ion. C. Effect of iron on HOMO-LUMO gap from the porphyrin. D. Effect of symmetry on iron orbital.

As the model is complexed by adding a central iron into the phorphyrin, an interaction between the d-orbitals of the metal and the LUMOs of the porphyrins affect

the energy level between HOMOs and LUMOs (Figure 2.3, C.). Consequently, the type of oxidation state of the central atom or the presence of ligand impact on the interaction between the d-orbitals of the metal and the LUMOs of the porphyrin. This causes a maximum shift (nm) of the Soret band and the Q bands. In particular, it is known that the introduction of an iron (II) increases the HOMO-LUMO energy. Therefore, leading to a hypsochromic effect of the Soret band. The observed geometry is a square-pyramid. This increase will be even greater in the case of a Fe^{2+} atom bound to oxygen because the symmetry becomes octahedral (Figure 2.3, D.). [22] This type of reasoning can be used to explain the wavelength changes observed in the UV-Visible absorption spectroscopy spectra of hIDO1. In the protein system, it absorbs close to 406 nm for a ferric cofactor and 422 nm for a ferrous cofactor. It is also possible to determine if small organic molecules are bound via analysis of the maximum of the Soret band. In particular, the presence of oxygen bound to the central iron atom adapts the maximum of the Soret band at 412 nm while the presence of L-Trp in the active site changes the value at 415 nm.

UV-visible absorption spectroscopy analysis can also quantify the ratio of heme incorporation into the protein (absorbance around 400 nm/absorbance at 280 nm). The lability of the cofactor is an important point of hIDO1. In his paper, Nelp *et al.* argues that, unlike other hemoproteins, the binding of the heme to hIDO1 is a dynamic and reversible process. Consequently, the protein hIDO1 has less affinity for heme than myoglobin or hemoglobin. [24] Changes in the overall structure due to the cofactor lability are moderate. Nelp *et al.* also demonstrated the physiological relevance of the apo¹ form of hIDO1. They demonstrated that 85% of hIDO1 existed in the apo form in ovarian cancer cells. Therefore, it is one of the predominant forms. [24] The paper also shows that heme lability has a central role in post-translational regulation. Indeed, it has been shown that the lability of heme cofactor in hIDO1 is dependent on the redox state of the central ion. As the ferrous form has a tenfold higher affinity than the ferric form, the dynamic process of lability is no longer observed at the cellular level. Only the ferric form is labile. The presence of L-Trp also affects the lability of the cofactor on the ferrous active form. As hIDO1 accumulates in the ferric form when the L-Trp concentration is low, this could therefore be a self-regulatory mechanism to promote the apo form. This would explain why it is the majority form in cells. Finally, the study of the kinetics of the holo/apo transition demonstrates

¹Without cofactor or without binding between the protein and the cofactor.

a complex phenomenon, passing through intermediates and requiring more studies. [24]

2.2.3 Known structural features of hIDO1

Structural information on hIDO1 is extensive, but particularly focused on the active site and the L-Trp binding pocket. The two first crystallographic structures of hIDO1 were deposited by Sugimoto *et al.* in 2006. [25] These two co-crystals with 4-phenylimidazole or cyanide allowed a small revolution in the drug design world for hIDO1 inhibitors. Indeed, from this structure, the development of other inhibitors like navoximod was possible. This took some time (2016) to have an explosion of crystallographic data on the therapeutic target. At the present time, a total of 65 structures is present in the Protein Data Bank (PDB), more than three quarters are complexes with potential inhibitors. [13]

In all the reported structures, hIDO1 crystallizes with several molecules in the asymmetric unit, either as a dimer or as a dimer of dimer. This second case appears, in particular, with protein produced from plasmids including surface mutations (K116A, K117A). These mutations have allowed the generation of high-resolution structures (from 1.7 to 2.7 Å) soaked with L-Trp or inhibitors. [26] In the structure of hIDO1, each monomer is composed of two domains, i.e., the small domain (Figure 2.4, A., in pink) involving the N-terminal moiety and the large domain consisting in a bundle of 13 α -helices. The role of the small domain is then undetermined. The largest domain includes the catalytic core formed by the heme cofactor and the α -helices B (in purple), D (in orange), E (in green) and it is closed with the JK-loop (Q360 to G380, in blue) (Figure 2.4, A.). Before this thesis, the JK-loop had never been refined by crystallography and these conformations were unknown. Concerning the binding mode in the active site, a recent comprehensive review of crystallographic knowledge on hIDO1 has been performed by Röhrig *et al.*. [13] This describes the active site of hIDO1 in several pockets, respectively A, B, C, D and the heme pocket (Figure 2.4, B.). It was thus shown that the L-Tryptophan molecules observed in the literature tended to bind the A and B pockets of the protein. Before the beginning of our research, the L-Trp molecules listed in the literature were observed only in the so-called "reactive" position, i.e. perfectly oriented above the heme. These pockets A et B can also be occupied by holo inhibitors. Concerning the pocket D and the heme pocket, they are

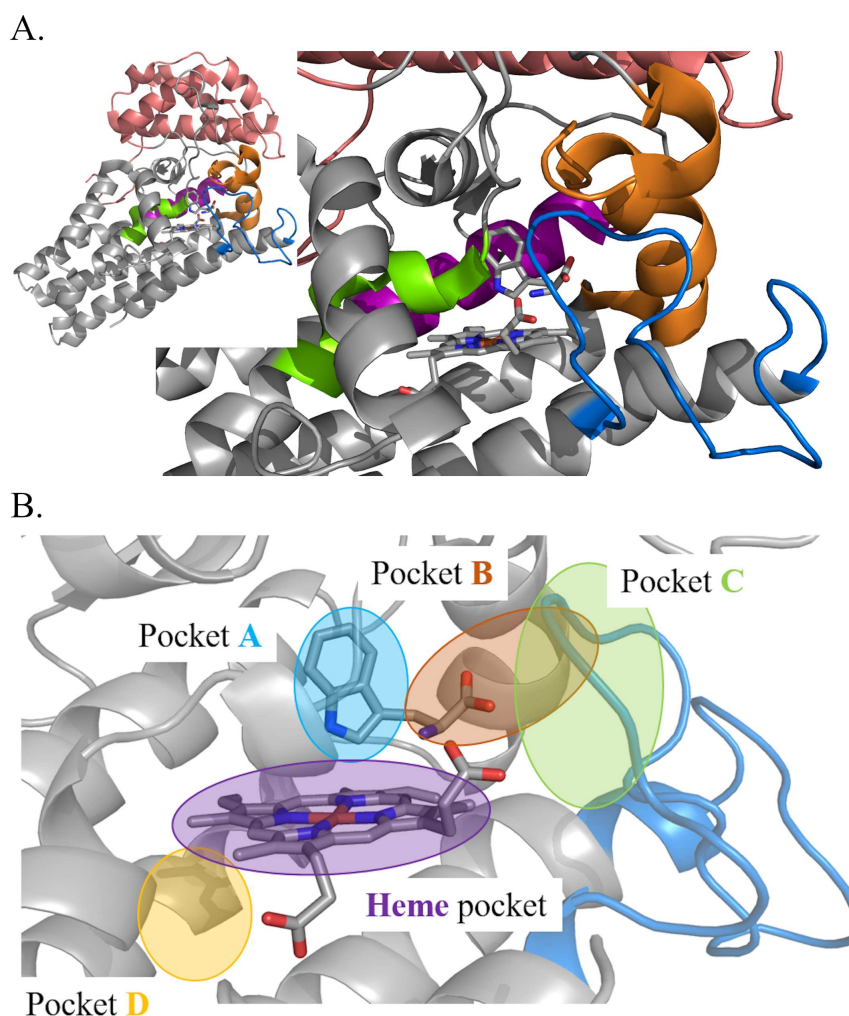


FIGURE 2.4: A. General structure of hIDO1. Zoom on the active site with the helix B (in purple), D (in orange), E (in green) and the JK-loop (in blue). Possible binding modes of inhibitors in the active site of hIDO1 (PDB code: 7nge). B. Pockets A, B, C, D and for the heme cofactor. [13]

occupied by the so-called apo inhibitors. The C pocket is rarely occupied, except by small solvent molecules.

2.2.4 Grey areas and the beginning of difficulties

As 2019 approaches and this thesis begins, new information is being collected on hIDO1. First, the clinical failure of Epacadostat [27] was announced in April 2018 at the ASCO conference, which generates a reconsideration of the knowledge on the protein. Several reasons have been put forward for this failure such as poor patient

selection [28], difficulty in targeting hIDO1 due to its involvement in signaling pathways [28] or metabolic adaptation due to hIDO1 inactivation promoting the serotonin pathway and NAD⁺ production resulting in reduced T cell proliferation and function. [29] In addition, the notion of protein plasticity and protein cofactor lability arrives at the heart of the problem. As a result of these new discoveries, it is clear that there are still grey areas in the understanding of the protein. Solving these grey areas could perhaps improve the design of drugs if the veil were lifted and thus avoid other failures like that of Epacadostat.

The first area to illuminate is the understanding of the plasticity of hIDO1 and its role in the level of activity. Some areas of the active site are known to exhibit plasticity, notably the loop (G261-G265) passing over the heme and closing the A pocket. However, the function of this fragment is not mentioned in the literature and only few articles focus on the subject. Substrate inhibition theories based on the binding in pocket D of L-Trp at high concentration are emerging in the laboratory of Pharm *et al.* [30] However, the density maps remain quite questionable as mentioned by some other groups. [13] In parallel of this, research proves that the enzyme plasticity is important because it could be involved in the arrival of the substrate or the inhibitor at the active site. Indeed, Molecular Dynamics studies of hIDO1 has shown that different binding states, never observed by crystallography, could exist for hIDO1. [31, 32] However, the duration of the dynamics production step (10 ns) does not allow a thorough study of the protein plasticity according to the behavior of the ligand over time. A more advanced study at the forefront of new methodological developments for hIDO1 is therefore needed. The best example of the dynamics of hIDO1 is the JK dynamic loop. This loop, located between residues Q360 and G380, is a loop closing the active site of hIDO1. It is partially refined in the crystallographic structures (at its C-terminal end, from G378 to G380). According to its conformation at the C-terminal part, JK-loop structures can be classified into three categories: a closed conformation², an intermediate conformation³ and an open conformation⁴. Only few information is referenced for this fragment. A Molecular Dynamics study exists. [33] This study shows the dynamic loop and confirms these three different exchangeable conformations for the C-terminal part (E375 to G380). For the N-terminal part (Q360 to L374),

²PDB entries 6pz1, 6e46, 6e35, 6cxu, 6cxv, 5whr, 6f0a, 5wmu, 5wmv, 5wmw and 5wmx

³PDB entries 6e43 chain B, 5etw chain A, 5ek2 chain B and 5ek3 chain B

⁴PDB entries 6e40 chain D, 6e41, 6e42 chain D, 6e44 chain B and 6e45 chain B

no predominant conformation is observed. Alvarez *et al.* [33] highlighted the involvement of the dynamic loop in substrate stabilization. In this case, the C-terminal part of the dynamic loop is stiffened by the positioning above the active site of L-Trp. The N-terminal part remains very mobile. Finally, the paper highlights the importance of one JK-loop amino acid, T379, in stabilizing the substrate. [33] These preliminary results are interesting but the dynamics studied are too short (45 ns) to see any loop folding movement. This highlights the importance to complete the study to better understand the function of the JK-loop, especially for the design of new protein inhibitors.

The second area of poor understanding of hIDO1 is the lability of its cofactor. As mentioned earlier, this concept developed by Nelp *et al.* was quite new at the beginning of the thesis. This news was supported by the release of a preprint by Ortiz-Meoz *et al.* [34] also describing this heme lability in the same period of time. The paper of Nelp *et al.* suggests the existence of intermediate states at the transition from the holo form to the apo form. These states are still unknown as well as the mechanism allowing the lability of the cofactor. It is therefore important to direct a more fundamental study of heme lability in hIDO1 to better understand this phenomenon and to assist in the design of new apo inhibitors.

2.3 State of the art of the knowledge about hIDO2

One of the last grey areas of hIDO1 is the understanding of its interaction with hIDO2. Indeed, the failure of Epacadostat could be due to a lack of understanding of the interaction between the two enzymes. Nonetheless, very little information is known about this second therapeutic target. Discovered in 2007 by Ball *et al.* [35, 36], the protein hIDO2 (EC:1.13.11) is encoded on chromosome 8, as hIDO1. Both proteins are paralogs, they probably come from an ancient gene duplication which occurred prior to the evolution of vertebrates. [35, 37–41] The expression of hIDO2 is more restricted than hIDO1 and remains confined to antigen presenting immune cells, liver, kidneys, brain and placenta. [36, 40, 42, 43] Several evidences shows that hIDO1 and hIDO2 do not have redundant functions. [36, 39–41, 43, 44] The role of hIDO2 would be more directed towards the regulation of the pro-inflammatory response and B lymphocytes. However, its role in immune function is still being determined. [43] The hIDO2 protein is composed of 420 amino acids and is predicted to be probably monomeric.

[45] For a long time, the sequence of hIDO2 was a source of discussion. The protein had two potential methionine starts (in position 1 and in position 14). Finally, it was shown that the active form of the protein was obtained only from the methionine start at position 14, with a total of 407 residues. [36, 40]

One of the well-known characteristics of hIDO2 is that it is a non active protein. [36, 37, 39, 43] The protein has very little affinity for L-Tryptophan, with a K_m (6.8 ± 0.9 mM) [45] that is not biologically relevant. [28, 36] As a consequence, hIDO2 is almost not involved in the catabolism of the amino acid.⁵ The protein hIDO2 could be a pseudoenzyme, also called "dead enzyme". [28, 47] Pseudoenzymes are a class of protein, representing 10% of the proteome, showing no or low enzymatic activity compared to a very close homologue. This lack of activity can be due to a lack of key amino acids in the enzyme. [47, 48] These incremental evolutionary changes do not change the overall fold of the protein, but influence the binding of the substrate or cofactor. Being a pseudoenzyme does not mean that hIDO2 is devoid of interest. A growing body of research has shown that pseudoenzymes are essential as biological regulators and to control the availability of substrates for their protein analogues.

The hypothesis of pseudoenzyme role for hIDO2 is mentioned by Chilosi *et al.* in 2022 and requires particular interest. This is consistent with previous studies performed by Lee *et al.* where it has been shown that hIDO2 can act as a negative regulator of hIDO1, competing for heme binding. [49] This research group found that cells expressing only hIDO1 produced large amounts of kynurenine ($65 \mu\text{M}$) while cells expressing only hIDO2 produced almost none (lower than $2 \mu\text{M}$). However, co-expression of the two proteins induces a decrease in kynurenine concentration ($56 \mu\text{M}$). The article postulates that this regulation of hIDO1 activity by hIDO2 would attenuate cell death since cells overexpressing both enzymes have a cell proliferation rate twice as high as cells with only hIDO1 expressed. For Lee *et al.* [49], it is possible that hIDO2 partially suppresses hIDO1 activity by competing for cofactor binding. This hypothesis is supported by the fact that the cofactor binding regions are less conserved regions between the two enzymes and that mutation of H347A abrogates the effect. [49] Other information for the activity of the enzyme is that the protein is less prone to auto-oxidation and can engage several catalytic cycles before being in

⁵However, a study shows that the ascorbic acid/MB complex, used in *in vitro* enzymatic assays, inhibits the enzyme. [46] According to the authors, the protein participates in the metabolism, *in vivo*.

the ferric form. [46]

```

      1      10      20      30      40      50
hIDO1  ...MAHAMENSWTISKELYHIDEEYGFALPNPQENLPDEFYNDWMTAKHLPDLIESGQLR
hIDO2  MEHHRPNVKTAVPLSLESYHISEEYGFLLPDSLKELPDEFYRPWMEIANKLPQLIDAHQLQ
consensus>50 mepmahnvenavpiSLeSYHIdEEvGFllP#ple#LPDFYndWMMfIAnhLP#LI#agQLq

      60      70      80      90      100     110
hIDO1  ERVEKLNMLSDHLLTDHKSORLARLVLCITMAYVWVGKCHGDVRKVLPRNIAVPYCOLSA
hIDO2  AHVDKMPPLSCQFLKGRERORLAHLVLSFLTMGYVWQEGEAQPAEVLPRNLALPFEVSR
consensus>50 ehV#K$n$LSi#fLkdHkeQRLAhLVLGfiTMaYVWqeGaa#vaeVLPfRNIaVp%v#vSa

      120     130     140     150     160     170
hIDO1  ALELPPILVYADCVLIANWKKKDPNKKPLTYENMDVLFSEFRDGDCKSGFFLVSLIVEIAAAS
hIDO2  NLGLPPILVHSDLVLTNWTKKDPDGFLEIGNLETTIISFPGGESLHGFFLVTALVEKEAVP
consensus>50 nLeLPPILVyaDlVLaNwKkKDP#gflEieN$#viiSFpDg#clhGfILVslLVEieAvp

      180     190     200     210     220     230
hIDO1  AIKVIPTVFKAMQMQRDTLLKALEIASCLEKALQVFHQIHDHVNEPKAFFSVIRIYLSG
hIDO2  GIKALVQATNAILQPNQEAALLQALQRLRLSIQDITKTLGCMHDYVDEDFIYAGTRIFLSG
consensus>50 aIKvIvqvfnAilmq#q#aLLqALLeialci#dilqvlqQiHDyV#PdiF%aviRI%LSG

      240     250     260     270     280     290
hIDO1  WKENPOLSDGLVYEGFWEDPKKEFAGGSAGQSsVFQCFDVLVIGIQQTAGGCHAAQFLQDMR
hIDO2  WKDNPAmpAGLMEYGVSOEPLKYSGGSAAQSTVLFHAFDEELGIRHKSESG...DFLYRMR
consensus>50 WKdNPq$pdGLvYEGvs##Ple%aGGSAAQSSVlqaFDvLVIGIqqsaeGhaa#FLydMR

      300     310     320     330     340     350
hIDO1  RYMPPAHRNFLCSLESNPsvREFVLSKGDAGLREAYDCAVKALVLSRSYHLQIVTKYILI
hIDO2  DYMPPSHKAFIEDIHSAPSIRDYTLSSGQDHLLTAYNQCVCALAE LRSYHITMVKYLIIT
consensus>50 dYMPPaHknFiedieSnPSvR##!LSkG#dgLleAY#qCVqALveLRSYHiqIVTKYIii

      360     370     380     390     400
hIDO1  PASQQP...KENKTSSEDPskLEAKGTGGTDLMNfLkTVRSTTEKSLLEKeg.
hIDO2  AAAKAKHGKPNHLPGPPQALKDRGTGGTAVMSElKsvRDKTLESILHPRG
consensus>50 aAaqqkhgKeNhlpedPqaLedkGTGGTdvMnFLKsvRdkTleSiLhegg

```

FIGURE 2.5: Sequence alignment of hIDO2 with hIDO1 considering a start at M14 for hIDO2, without any tag according to Multialign software [52] with Blosum62 matrix.

From a structural point of view, the structure of hIDO2 is experimentally unknown at present. In some publications, homology models have been carried out but are not freely available for review. [40, 50, 51] These models were built on the basis of a sequence alignment of hIDO1 with hIDO2, which share 43% identity (Figure 2.5). Sequence alignment highlights a non-conserved portion between hIDO1 and hIDO2, namely the N-terminus of the enzyme. The residues of the fragment V180 to H215 also are not preserved. This corresponds to the B and C helices of hIDO1, at the

remote parts of the active site. The general fold of the protein, in these homology models, is preserved (Figure 2.6, Upper right corner). [40]

Concerning the conservation of the active site (conserved at 70% between hIDO1 and hIDO2 [53]), Röhrig *et al.* [50] demonstrated in 2016 that four amino acids in the pocket A were not conserved (Y126, C129, F164, and S167 of hIDO1 are replaced by H130, L133, I168, and T171 for hIDO2, respectively)⁶, inducing a larger (15%) binding pocket than for hIDO1 and a loss of some substrate stabilization (with F164 and C129) (Figure 2.6, main picture). [45, 50] The pocket B is more polar by replacing F227 by Y231 and I356 by T357.⁶ [51] One of the negative points of these models is that they have a rigid vision of the system. Right now, to the best of our knowledge, no study by Molecular Dynamics has been published for hIDO2.

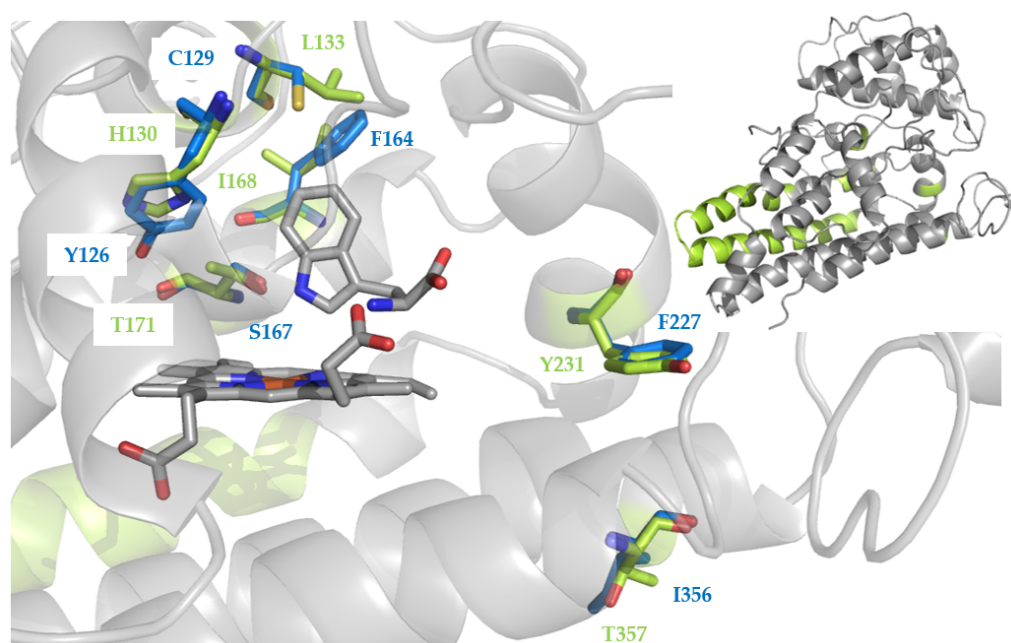


FIGURE 2.6: Main picture: Amino acids differing according to literature between hIDO1 (blue) and hIDO2 (green) in the homology models. In the absence of an available model, the structure of hIDO2 is based on the model made during the thesis. Upper right corner: global fold of hIDO2 and highlighting of the B' and C' loops.

In 2021, a revolutionary program in structural chemistry is released, AlphaFold. The software proposes a machine learned based structural model for hIDO2. [54, 55] However, the program indicates a large inaccuracy for the N-terminal non-conserved

⁶Considering the methionine start as M14.

parts and the JK-loop analog, named in this manuscript JK'. Another known structural information is that two polymorphs of hIDO2 are present in the population, namely R235W and Y346X⁶. [37, 56] The role or reason for the appearance of these polymorphs is still unknown. However, it could be shown that it abolished the activity of the protein even more than for the WT protein (90% for R235W and 100% for Y346X). [56] It is estimated that 25% of the human population has a dysfunctional hIDO2 enzyme. [50]

To summarize, the available information on hIDO2 is very succinct. No data is reported in the literature on its plasticity, the behavior of the JK'-loop or the lability of its heme cofactor. Furthermore, the difficulty in understanding its biological role leads to confusion and contradiction between the different articles in the literature. The race to find the inhibitor makes us forget the study of the protein functioning. This thesis will highlight the importance to study the protein in a fundamental way, before designing inhibitors.

Bibliography

- [1] M. Sono, M. P. Roach, E. D. Coulter, and J. H. Dawson. Heme-containing oxygenases. *Chemical reviews*, 96(7):2841–2888, 1996.
- [2] O. Takikawa. Biochemical and medical aspects of the indoleamine 2, 3-dioxygenase-initiated L-tryptophan metabolism. *Biochemical and Biophysical research communications*, 338(1):12–19, 2005.
- [3] K. Oohora and T. Hayashi. Reconstitution of heme enzymes with artificial metalloporphyrinoids. *Methods in Enzymology*, 580:439–454, 2016.
- [4] V. Fiorito, D. Chiabrando, S. Petrillo, F. Bertino, and E. Tolosano. The multifaceted role of heme in cancer. *Frontiers in oncology*, 9(1540):1–15, 2020.
- [5] B. Wu, Y. Wu, and W. Tang. Heme catabolic pathway in inflammation and immune disorders. *Frontiers in pharmacology*, 10(825):1–15, 2019.
- [6] H.-R. Kim, S. J. Won, C. Fabian, M.-G. Kang, M. Szardenings, and M.-G. Shin. Mitochondrial dna aberrations and pathophysiological implications in hematopoietic diseases, chronic inflammatory diseases, and cancers. *Annals of Laboratory Medicine*, 35(1):1, 2015.

- [7] M. Kondo, N. Hirota, T. Takaoka, and M. Kajiwara. Heme-biosynthetic enzyme activities and porphyrin accumulation in normal liver and hepatoma cell lines of rat. *Cell biology and toxicology*, 9(1):95–105, 1993.
- [8] M. M. H. El-Sharabasy, A. M. El-Waseef, M. M. Hafez, and S. A. Salim. Porphyrin metabolism in some malignant diseases. *British journal of cancer*, 65(3):409–412, 1992.
- [9] J. Basran, E. S. Booth, M. Lee, S. Handa, and E. L. Raven. Analysis of reaction intermediates in tryptophan 2, 3-dioxygenase: a comparison with indoleamine 2, 3-dioxygenase. *Biochemistry*, 55(49):6743–6750, 2016.
- [10] J. Basran, I. Efimov, N. Chauhan, S. J. Thackray, J. L. Krupa, G. Eaton, G. A. Griffith, C. G. Mowat, S. Handa, and E. L. Raven. The mechanism of formation of n-formylkynurenine by heme dioxygenases. *Journal of the American Chemical Society*, 133(40):16251–16257, 2011.
- [11] A. Lewis-Ballester, S. Karkashon, D. Batabyal, T. L. Poulos, and S.-R. Yeh. Inhibition mechanisms of human indoleamine 2, 3 dioxygenase 1. *Journal of the American Chemical Society*, 140(27):8518–8525, 2018.
- [12] I. Efimov, J. Basran, S. J. Thackray, S. Handa, C. G. Mowat, and E. L. Raven. Structure and reaction mechanism in the heme dioxygenases. *Biochemistry*, 50(14):2717–2724, 2011.
- [13] U. F. Röhrig, O. Michielin, and V. Zoete. Structure and plasticity of indoleamine 2, 3-dioxygenase 1 (ido1). *Journal of Medicinal Chemistry*, 64(24):17690–17705, 2021.
- [14] U. F. Röhrig, A. Reynaud, S. R. Majjigapu, P. Vogel, F. Pojer, and V. Zoete. Inhibition mechanisms of indoleamine 2, 3-dioxygenase 1 (ido1). *Journal of Medicinal Chemistry*, 62(19):8784–8795, 2019.
- [15] I. Efimov, J. Basran, X. Sun, N. Chauhan, S. K. Chapman, C. G. Mowat, and E. L. Raven. The mechanism of substrate inhibition in human indoleamine 2, 3-dioxygenase. *Journal of the American Chemical Society*, 134(6):3034–3041, 2012.
- [16] B. Weber, E. Nickel, M. Horn, K. Nienhaus, and G. U. Nienhaus. Substrate inhibition in human indoleamine 2, 3-dioxygenase. *The Journal of Physical Chemistry Letters*, 5(4):756–761, 2014.

- [17] A. O. Kolawole, B. P. Hixon, L. S. Dameron, I. M. Chrisman, and V. V. Smirnov. Catalytic activity of human indoleamine 2, 3-dioxygenase (hido1) at low oxygen. *Archives of Biochemistry and Biophysics*, 570:47–57, 2015.
- [18] G. J. Maghzal, S. R. Thomas, N. H. Hunt, and R. Stocker. Cytochrome b5, not superoxide anion radical, is a major reductant of indoleamine 2, 3-dioxygenase in human cells. *Journal of Biological Chemistry*, 283(18):12014–12025, 2008.
- [19] R. Giovannetti. The use of spectrophotometry uv-vis for the study of porphyrins. *Macro to nano spectroscopy*, pages 87–108, 2012.
- [20] D. Dolphin. The porphyrins v3: Physical chemistry, part a. *Academic press*, 1978.
- [21] M. Gouterman, G. H. Wagnière, and L. C. Snyder. Spectra of porphyrins: Part ii. four orbital model. *Journal of Molecular Spectroscopy*, 11(1-6):108–127, 1963.
- [22] M. R. Dayer, A. A. Moosavi-Movahedi, and M. S. Dayer. Band assignment in hemoglobin porphyrin ring spectrum: using four-orbital model of gouterman. *Protein and peptide letters*, 17(4):473–479, 2010.
- [23] M. Gouterman. Spectra of porphyrins. *Journal of Molecular Spectroscopy*, 6:138–163, 1961.
- [24] M. T. Nelp, P. A. Kates, J. T. Hunt, J. A. Newitt, A. Balog, D. Maley, X. Zhu, L. Abell, A. Allentoff, R. Borzilleri, et al. Immune-modulating enzyme indoleamine 2, 3-dioxygenase is effectively inhibited by targeting its apo-form. *Proceedings of the National Academy of Sciences*, 115(13):3249–3254, 2018.
- [25] H. Sugimoto, S.-i. Oda, T. Otsuki, T. Hino, T. Yoshida, and Y. Shiro. Crystal structure of human indoleamine 2, 3-dioxygenase: catalytic mechanism of o₂ incorporation by a heme-containing dioxygenase. *Proceedings of the National Academy of Sciences*, 103(8):2611–2616, 2006.
- [26] S. Luo, K. Xu, S. Xiang, J. Chen, C. Chen, C. Guo, Y. Tong, and L. Tong. High-resolution structures of inhibitor complexes of human indoleamine 2, 3-dioxygenase 1 in a new crystal form. *Acta Crystallographica Section F: Structural Biology Communications*, 74(11):717–724, 2018.

- [27] G. V. Long, R. Dummer, O. Hamid, T. F. Gajewski, C. Caglevic, S. Dalle, A. Arance, M. S. Carlino, J.-J. Grob, T. M. Kim, et al. Epcadostat plus pembrolizumab versus placebo plus pembrolizumab in patients with unresectable or metastatic melanoma (echo-301/keynote-252): a phase 3, randomised, double-blind study. *The Lancet Oncology*, 20(8):1083–1097, 2019.
- [28] G. Mondanelli, M. Mandarano, M. L. Belladonna, C. Suvieri, C. Pelliccia, G. Bellezza, A. Sidoni, A. Carvalho, U. Grohmann, and C. Volpi. Current challenges for ido2 as target in cancer immunotherapy. *Frontiers in immunology*, 12(679953):1–7, 2021.
- [29] K. Odunsi, F. Qian, A. A. Lugade, H. Yu, M. A. Geller, S. P. Fling, J. C. Kaiser, A. M. Lacroix, L. D’Amico, N. Ramchurren, et al. Metabolic adaptation of ovarian tumors in patients treated with an ido1 inhibitor constrains antitumor immune responses. *Science Translational Medicine*, 14(636):eabg8402, 2022.
- [30] K. N. Pham, A. Lewis-Ballester, and S.-R. Yeh. Structural basis of inhibitor selectivity in human indoleamine 2, 3-dioxygenase 1 and tryptophan dioxygenase. *Journal of the American Chemical Society*, 141(47):18771–18779, 2019.
- [31] L. Capece, M. Arrar, A. E. Roitberg, S.-R. Yeh, M. A. Marti, and D. A. Estrin. Substrate stereo-specificity in tryptophan dioxygenase and indoleamine 2, 3-dioxygenase. *Proteins: Structure, Function, and Bioinformatics*, 78(14):2961–2972, 2010.
- [32] F. A. Greco, E. Albin, A. Coletti, D. Dolciami, A. Carotti, C. Orabona, U. Grohmann, and A. Macchiarulo. Tracking hidden binding pockets along the molecular recognition path of l-trp to indoleamine 2, 3-dioxygenase 1. *ChemMedChem*, 14(24):2084–2092, 2019.
- [33] L. Álvarez, A. Lewis-Ballester, A. Roitberg, D. A. Estrin, S.-R. Yeh, M. A. Marti, and L. Capece. Structural study of a flexible active site loop in human indoleamine 2, 3-dioxygenase and its functional implications. *Biochemistry*, 55(19):2785–2793, 2016.
- [34] R. F. Ortiz-Meoz, L. Wang, R. Matico, A. Rutkowska-Klute, M. De la Rosa, S. Beard, R. Midgett, K. Strohmer, D. Thomson, C. Zhang, et al. Characterization of apo-form selective inhibition of indoleamine 2, 3-dioxygenase. *ChemBioChem*, 22(3):516–522, 2021.

- [35] H. J. Ball, A. Sanchez-Perez, S. Weiser, C. J. D. Austin, F. Astelbauer, J. Miu, J. A. McQuillan, R. Stocker, L. S. Jermini, and N. H. Hunt. Characterization of an indoleamine 2, 3-dioxygenase-like protein found in humans and mice. *Gene*, 396(1):203–213, 2007.
- [36] G. Pantouris, M. Serys, H. J. Yuasa, H. J. Ball, and C. G. Mowat. Human indoleamine 2, 3-dioxygenase-2 has substrate specificity and inhibition characteristics distinct from those of indoleamine 2, 3-dioxygenase-1. *Amino acids*, 46(9):2155–2163, 2014.
- [37] P. Li, W. Xu, F. Liu, H. Zhu, L. Zhang, Z. Ding, H. Liang, and J. Song. The emerging roles of ido2 in cancer and its potential as a therapeutic target. *Biomedicine & Pharmacotherapy*, 137:1–6, 2021.
- [38] M. Mandarano, G. Bellezza, M. L. Belladonna, J. Vannucci, A. Gili, I. Ferri, C. Lupi, V. Ludovini, G. Falabella, G. Metro, et al. Indoleamine 2, 3-dioxygenase 2 immunohistochemical expression in resected human non-small cell lung cancer: a potential new prognostic tool. *Frontiers in Immunology*, 11(839):1–10, 2020.
- [39] M. Chilosi, C. Doglioni, C. Ravaglia, G. Martignoni, G. L. Salvagno, G. Pizzolo, V. Bronte, and V. Poletti. Unbalanced ido1/ido2 endothelial expression and skewed kynurenine pathway in the pathogenesis of covid-19 and post-covid-19 pneumonia. *Biomedicines*, 10(1332):1–24, 2022.
- [40] D. Meininger, L. Zalameda, Y. Liu, L. P. Stepan, L. Borges, J. D. McCarter, and C. L. Sutherland. Purification and kinetic characterization of human indoleamine 2, 3-dioxygenases 1 and 2 (ido1 and ido2) and discovery of selective ido1 inhibitors. *Biochimica et biophysica acta (BBA)-proteins and Proteomics*, 1814(12):1947–1954, 2011.
- [41] H. J. Ball, H. J. Yuasa, C. J. D. Austin, S. Weiser, and N. H. Hunt. Indoleamine 2, 3-dioxygenase-2; a new enzyme in the kynurenine pathway. *The international journal of biochemistry & cell biology*, 41(3):467–471, 2009.
- [42] P. Song, T. Ramprasath, H. Wang, and M.-H. Zou. Abnormal kynurenine pathway of tryptophan catabolism in cardiovascular diseases. *Cellular and Molecular Life Sciences*, 74(16):2899–2916, 2017.

- [43] L. M. F. Merlo, J. B. DuHadaway, J. D. Montgomery, W.-D. Peng, P. J. Murray, G. C. Prendergast, A. J. Caton, A. J. Muller, and L. Mandik-Nayak. Differential roles of ido1 and ido2 in t and b cell inflammatory immune responses. *Frontiers in Immunology*, 11(1861):1–16, 2020.
- [44] R. Metz, C. Smith, J. B. DuHadaway, P. Chandler, B. Baban, L. M. F. Merlo, E. Pigott, M. P. Keough, S. Rust, A. L. Mellor, et al. Ido2 is critical for ido1-mediated t-cell regulation and exerts a non-redundant function in inflammation. *International Immunology*, 26(7):357–367, 2014.
- [45] A. Dolšak, S. Gobec, and M. Sova. Indoleamine and tryptophan 2, 3-dioxygenases as important future therapeutic targets. *Pharmacology & Therapeutics*, 221:107746, 2021.
- [46] H. J. Yuasa and R. Stocker. Methylene blue and ascorbate interfere with the accurate determination of the kinetic properties of ido2. *The FEBS Journal*, 288(16):4892–4904, 2021.
- [47] C. Adrain. Pseudoenzymes: dead enzymes with a lively role in biology. *The FEBS Journal*, 287(19):4102–4105, 2020.
- [48] J. M. Murphy, P. D. Mace, and P. A. Eyers. Live and let die: insights into pseudoenzyme mechanisms from structure. *Current opinion in structural biology*, 47:95–104, 2017.
- [49] Y.-K. Lee, H. B. Lee, D.-M. Shin, M. J. Kang, E. C. Yi, S. Noh, J. Lee, C. Lee, C.-K. Min, and E. Y. Choi. Heme-binding-mediated negative regulation of the tryptophan metabolic enzyme indoleamine 2, 3-dioxygenase 1 (ido1) by ido2. *Experimental & Molecular Medicine*, 46(11):e121–e121, 2014.
- [50] U. F. Röhrig, S. R. Majjigapu, D. Caldelari, N. Dilek, P. Reichenbach, K. Ascencao, M. Irving, G. Coukos, P. Vogel, V. Zoete, et al. 1, 2, 3-triazoles as inhibitors of indoleamine 2, 3-dioxygenase 2 (ido2). *Bioorganic & Medicinal Chemistry Letters*, 26(17):4330–4333, 2016.
- [51] X. He, G. He, Z. Chu, H. Wu, J. Wang, Y. Ge, H. Shen, S. Zhang, J. Shan, K. Peng, et al. Discovery of the first potent ido1/ido2 dual inhibitors: A promising strategy for cancer immunotherapy. *Journal of Medicinal Chemistry*, 64(24):17950–17968, 2021.

- [52] F. Corpet. Multiple sequence alignment with hierarchical clustering. *Nucleic acids research*, 16(22):10881–10890, 1988.
- [53] C. J. D. Austin and L. M. Rendina. Targeting key dioxygenases in tryptophan–kynurenine metabolism for immunomodulation and cancer chemotherapy. *Drug discovery today*, 20(5):609–617, 2015.
- [54] M. Varadi, S. Anyango, M. Deshpande, S. Nair, C. Natassia, G. Yordanova, D. Yuan, O. Stroe, G. Wood, A. Laydon, et al. Alphafold protein structure database: Massively expanding the structural coverage of protein–sequence space with high-accuracy models. *Nucleic acids research*, 50(D1):D439–D444, 2022.
- [55] J. Jumper, R. Evans, A. Pritzel, T. Green, M. Figurnov, O. Ronneberger, K. Tunyasuvunakool, R. Bates, A. Žídek, A. Potapenko, et al. Highly accurate protein structure prediction with alphafold. *Nature*, 596(7873):583–589, 2021.
- [56] A. K. Witkiewicz, C. L. Costantino, R. Metz, A. J. Muller, G. C. Prendergast, C. J. Yeo, and J. R. Brody. Genotyping and expression analysis of *ido2* in human pancreatic cancer: a novel, active target. *Journal of the American College of Surgeons*, 208(5):781–787, 2009.

Chapter 3

Objectives and strategies

3.1 Objectives and strategies

Taking into account this research context, the objective of this work was to deepen the knowledge on human Indoleamine-2,3-dioxygenase 1 (hIDO1) and human Indoleamine-2,3-dioxygenase 2 (hIDO2). On the one hand, this better understanding of these two therapeutic targets was essential to benefit the development of inhibitors and to improve treatments for cancer or COVID-19 disease. On the other hand, the development of multidisciplinary techniques for the study of these proteins brought new methodologies to this field of scientific research. In this vision, the project was articulated around three main axes (Figure 3.1):

- Characterization
- Comprehensive study
- Comparison

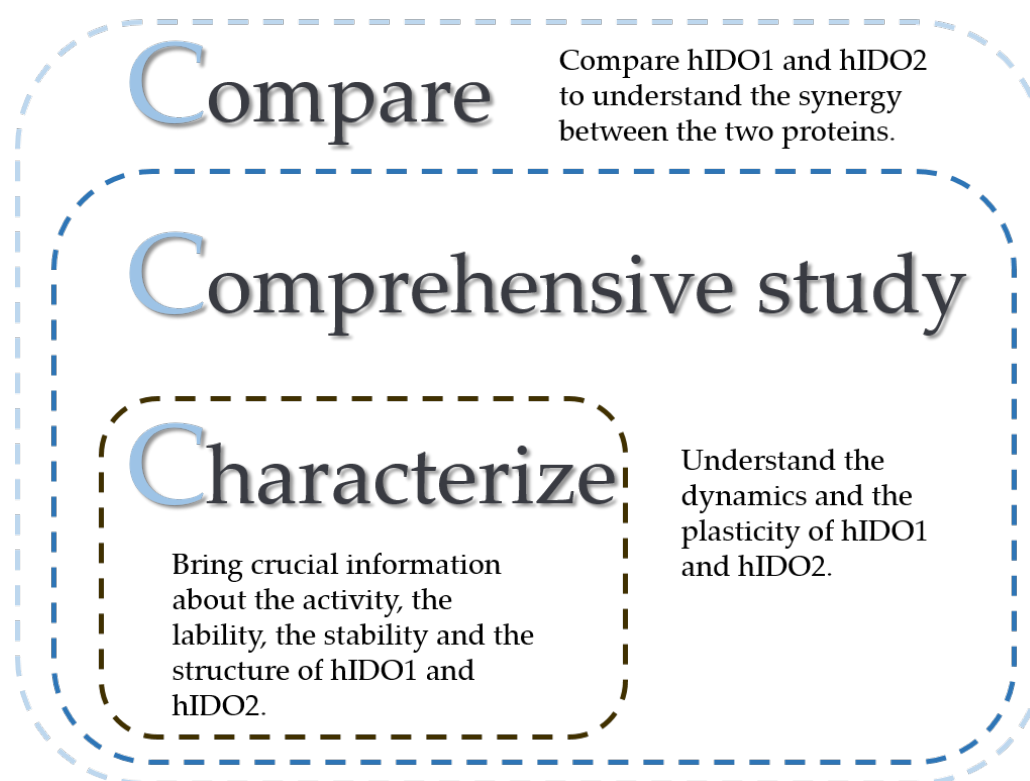


FIGURE 3.1: Summary of the different axes approached during this thesis.

The **characterization axis** allowed to build the basis of the study by providing a detailed characterization of each protein. This characterization was focused in the incorporation of the cofactor and the possible affinity/lability of the latter (performed with UV-Visible absorption spectroscopy analyses of the Soret band), the stability of proteins (using differential scanning fluorimetry (DSF)) and the activity of the protein (followed by enzymatic tests). During the thesis, the study of the structure adopted by proteins in solution as well as in the solid state has also been studied by means of complementary techniques such as X-ray diffraction (XRD) or Molecular Dynamics (MD). However, these techniques will not be detailed since they are the subject of the following chapters.

Once these bases were established, it was possible to look deeper into the areas of misunderstanding of the enzymes. This is the **comprehensive study axis**. Concerning the protein hIDO1, crystallographic studies supplemented by Molecular Dynamics and bioinformatics analyses allowed to study the dynamic JK-loop. The thesis was focused in understanding the conformation adopted by this loop as a function of the presence of the heme cofactor or ligands with which it is in presence. Interest was also shown in the study of the entire plasticity of the active site with a focus on residues G261 to G265. At last, plasticity outside the enzyme was also investigated through the study of an exo-site in the small subunit. Concerning the protein hIDO2, given that the state of the art has highlighted a total lack of structural information, the first part of this study was to optimize the crystallization of the protein. For that, construction optimization efforts were developed to try to improve the chances of crystallization. Unfortunately, the approach did not succeed and a computational approach was needed to collect more information about the structural aspect of hIDO2. The computational approach allowed, by homology modeling, Molecular Dynamics simulations and docking, to analyze the global plasticity of the protein and, especially, the dynamic loop closing the active site. The influences of presence of the heme cofactor, the L-Trp or polymorphism were also addressed in the research.

With all this information in hand, it was possible to undertake a **comparison axis** of the two proteins at the end of the thesis. They are compared according to different aspects such as the physico-chemical properties and the structural features of holo, apo, L-Trp bound forms. With this finite comparison axis, the whole thesis brings new information to enrich the discussion on the design of inhibitors specific to the

particularities of each protein in order to obtain a selective inhibition.

Part II

Physico-chemical characterization of the two targets

*“Cerveau sature comme un train dès qu’y’a un peu d’grèves
Pas d’pauses, même si les pneus crèvent
On papote, on verra c’que nos erreurs créent
Bad boys ne connaissent pas les regrets.”*

Lomepal - Lucy

Chapter 4

Characterization of hIDO1

4.1 Introduction

The present chapter concerns the characterization of hIDO1. Indeed, during the thesis, the protein was first characterized according to different criteria (stability, lability and affinity of the cofactor for the protein, and activity) before starting an in-depth study. This characterization aims at filling information, often missing, in the scientific literature of hIDO1, which is mainly focused on the discovery of new inhibitor molecules.

4.2 Characterization of the cofactor incorporation

Once the protein is purified (methods are described in Appendix A), the first and most accessible characterization is the incorporation of the heme cofactor. This characterization is based on the unique property of hemoproteins to absorb at around 400 nm, and to a lesser extent, around 500 nm and 600 nm. This major band at 400 nm, called the Soret band, reflects the heme present and bound to the protein. The observed maximum for the Soret bands varies as a function of oxidation state of the central iron in the cofactor. The forms at 406 nm and 422 nm are the wavelengths for the oxidized and reduced forms respectively [1], as reported in the literature. These wavelengths are well those observed during the thesis as shown in Figure 4.1 and Table 4.1. The binding of small molecules to the iron ion also causes a shift in the maximum from 412 nm (binding of such as oxygen or carbon dioxide) to 415 nm (binding of L-Trp or analogues).

4.2.1 Definition of the absorbance ratio and relation with the holo protein ratio in solution

Hemoproteins of the kynurenine pathway have a unique feature, namely a labile cofactor. Indeed, in other academically studied hemoproteins, such as hemoglobin or myoglobin, heme is so affine that there is no apo-hemoglobin or apo-myoglobin *in vivo*. In the case of hIDO1, Nelp *et al.* [2] proved in 2018 that lability exists for the oxidized cofactor form. In order to quantify the amount of holo protein in relation to the total amount of protein, the absorbance ratio (A_i) is therefore used (Equation 4.1).

$$A_i = \frac{A_{Soret}(\lambda_{max:400-450nm})}{A(280nm)} \quad (4.1)$$

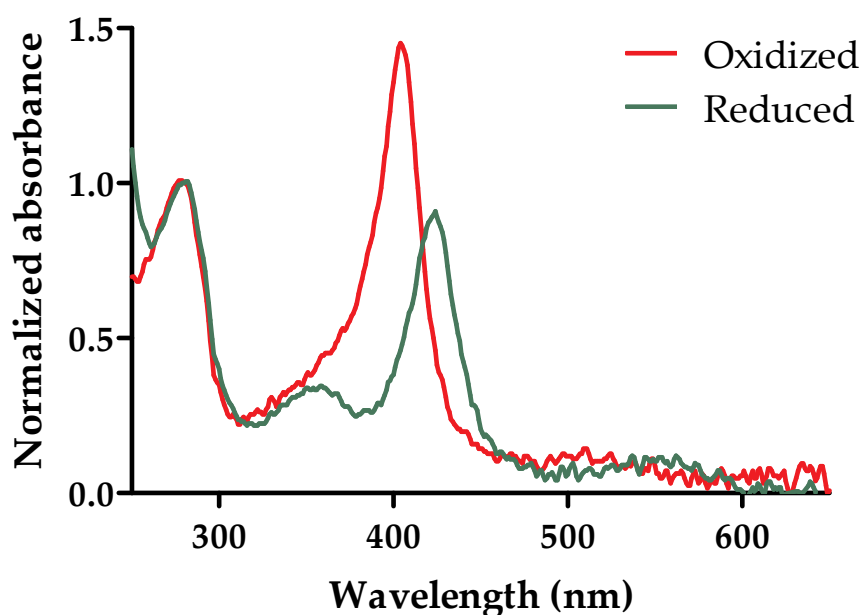


FIGURE 4.1: UV spectrum obtained between 250 nm and 600 nm for hIDO1 in oxidized (50 mM in K_2HPO_4 buffer pH 7.4 and 200 mM NaCl) and reduced (50 mM in K_2HPO_4 buffer pH 7.4 and 200 mM NaCl supplemented with 5 mM of dithiothreitol (DTT)) form for a concentration in proteins of 1.0 mg mL^{-1} . Absorbances are normalized at 280 nm.

The absorbance ratio varies slightly between the different buffers (Table 4.1)¹. However, the variation is more pronounced depending on the presence of oxidant or reductant agents. In the buffers without reductant, the absorbance ratio varies between 1.0-1.5. The change of buffer to buffers with DTT leads to a decrease of the absorbance ratio to reach values around 0.7-1.0. This could be explained by two hypotheses. In the first case, if the molar extinction coefficient of the Soret band caused by the reduced heme bounded is the same as that of the oxidized one, this would indicate a better affinity of the oxidized form. Secondly, it is also possible that this difference in absorbance comes from a difference in the molar extinction coefficients between the two redox forms of the Soret band. The analysis of the intensity between the two forms must therefore be considered with caution.

¹TRIS buffer consists in 50 mM TRIS pH 7.4, PO₄ buffer is composed of 50 mM $\text{K}_2\text{HPO}_4/\text{KH}_2\text{PO}_4$ pH 7.4 and 150 mM of NaCl supplemented with 5% of glycerol and HEPES buffer is made of 5 mM HEPES pH 6.5 supplemented with 200 mM of NaCl. For the reduced buffers, the previous composition is used supplemented with 5 mM of DTT.

TABLE 4.1: Influence of the buffer on the absorbance ratio. * The buffer used directly after Immobilized Metal Affinity Chromatography (IMAC) consist in 50 mM Tris(hydroxymethyl)aminomethane (TRIS), NaCl, 5% Glycerol, 150 mM Imidazole. 4-(2-hydroxyethyl)-1-piperazineethanesulfonic acid is named as HEPES.

Buffer	Composition	Maximum of the Soret peak	Ri A_{Soret} / A_{280}
Oxidized	Directly after IMAC*	412	1.0 - 1.6
	TRIS	406	1.0 - 1.5
	PO4	404	1.4 - 1.5
Reduced	HEPES DTT	422	0.7 - 1.0
	TRIS DTT	422	0.7 - 1.0
	PO4 DTT	422	0.7 - 0.9

This lack of information on the extinction coefficient comes from the ability of the cofactor to be labile. Usually, the method to determine the molar extinction coefficient of Soret band due to the bound heme often requires a measurement of the total heme in solution [3]. In the case of a labile protein, it can be problematic because some of the heme is not necessarily bound to the protein. There is therefore an error made on the measurement. The choice of not converting absorbance ratios without reliable molar extinction coefficient values has therefore been made in this manuscript.

4.2.2 Peak attribution at 360nm

In Figure 4.1, in addition to the Soret band and the absorption band at 280 nm, a band with a maximum at 360 nm is observed, particularly for the reduced state. For the oxidized state, it tends to merge with the Soret peak, which makes the determination of the maximum imprecise. In order to attribute this peak, different buffer changes were performed. This also allowed to study the evolution of the incorporation in relation to these changes. The experiment was done in the presence or absence of 60 μ M hemin in both cases to assure a huge excess in cofactor. The procedure is detailed at Figure 4.2. The protein in KH_2PO_4 buffer without DTT is defined as oxidized (OX) and the protein in KH_2PO_4 buffer with DTT as reduced (RED). Depending on the number of runs per buffer exchange column, the name of the sample is increased (for example: RED1, RED2, RED3).

As mentioned at Figure 4.3, the protein at the IMAC output presents an absorbance of the Soret band with a maximum at 412 nm. This indicates a reduced form, which

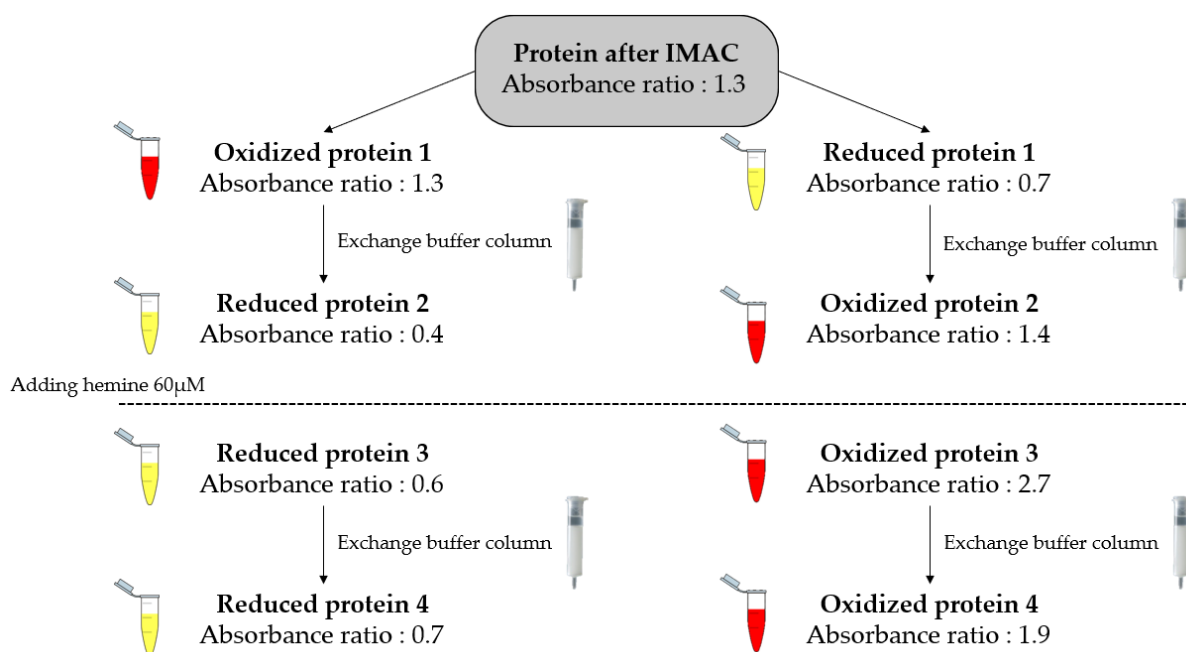


FIGURE 4.2: Reversibility of the heme gain/loss process depending on the buffer in which the protein is found. The analysis is performed at a protein at a starting concentration of 10 μM in hIDO1 and in KH_2PO_4 buffer). Protein was concentrated during the steps to maintain a sufficient concentration to see the Soret band. The amount of hemin added reaches a final value of 60 μM . Hemin and protein are incubated 15min together before the buffer exchange.

has auto-oxidized by binding to an oxygen molecule (shift from 422 nm to 412 nm). A signal is also observed at 360 nm. When changing buffer, the analysis without addition of hemin shows that the change to a reducing buffer induces a shift of maxima at 423 nm (Figure 4.3, A.). The intensity of the absorbance is then decreased. It could be due to 1) a trend to lose its bonded-cofactor when switching the buffer for the reduced form 2) a difference in term of molar extinction coefficient of the Soret band in comparison to the oxidized form. In this reducing buffer, the peak at 360 nm is always observed.

On the contrary, the oxidized form present the maximum of the Soret band absorbance at 404 nm (Figure 4.3, B.). The observed absorbance is increased. This phenomenon can be explained, as for the reduced form, by two hypotheses: 1) a difference of molar extinction coefficient between the two oxidation forms of the Soret band 2) a difference of affinity for the cofactor which indicates that the protein takes

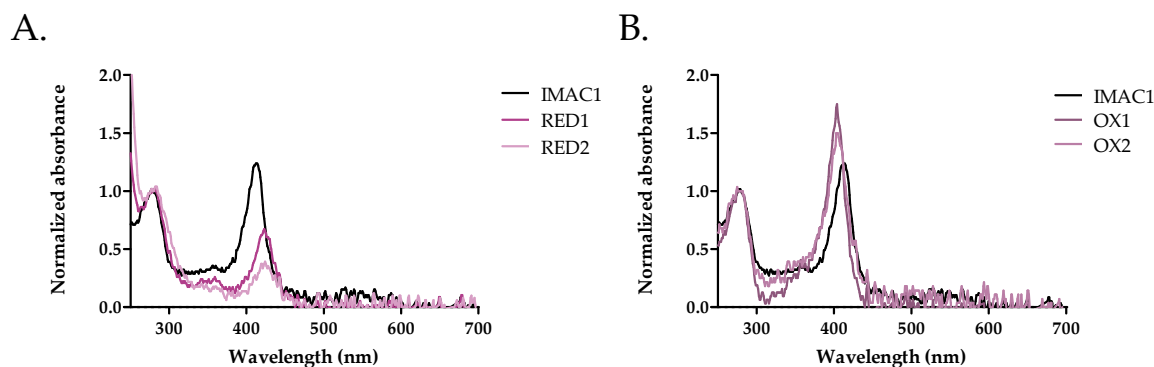


FIGURE 4.3: Reversibility of the heme gain/loss process depending on the buffer in which the protein is found. The analysis is performed at a protein at a starting concentration of $10\ \mu\text{M}$ in phosphate buffer. Absorbances were normalized at 280 nm. A. Results for the reduced form. B. Results for the oxidized form.

up free hemin and re-incorporates its cofactor. Without solid information on the extinction coefficient, it is not possible to decide on this phenomenon at the present time. The absorption band at 360 nm is then no longer observed.

A hypothesis is therefore made on the attribution of this peak as being free heme in solution. By deduction, this state with a free heme is closer to a state where the heme is not covalently bound to the protein but located in the active site rather than a heme randomly present in the solvent. The steric hindrance and the slight different surrounding of the cofactor generated by the protein in the unbounded position would explain the intermediate value of maximum absorbance for the Soret band, slightly different from spectra observed for totally free hemin in solution (Appendix C). Since the analyses are not performed in an oxygen-free environment, it is also possible that this form is the result of a lability of the ferrous heme form with bounded dioxygen. This possible intermediate was already mentioned by Röhrig *et al.* in 2019. [4] This attribution of this peak to a free form of the heme is consistent with the two hypotheses on absorbance. In the case of the molar extinction coefficients of the Soret band in the two oxidative state turn out to be identical, this would justify how the intensity of the Soret band can increase during the transition from a reduced to oxidized state in an inverse manner than the band at 360 nm. The protein can then use this free heme to increase its incorporation. The absence of the band for the oxidized form supports

to the hypothesis of a different affinity for the cofactor exists depending on the oxidative state. If the molar extinction coefficients are not identical, the hypothesis remains valid and shows that the reduced form could be labile if dioxygen is bounded to the cofactor.

To verify this hypothesis, hemin in huge excess was added to both forms of protein (Figure 4.4). After an incubation of 15 min, an exchange is performed using a PD10 column to remove the excess of cofactor. Before exchange, the incorporation of the reduced protein went up to 0.6 (Figure 4.4, A.). This shows that, over a short time and with a high concentration of hemin, the protein can be forced to re-incorporate a small amount of cofactor. Buffer exchange does not change significantly this incorporation. This one is little improved and remains at the value close to 0.7. The observed spectral signature shows a broadly marked signal at 360 nm associated with the migration of hemin along with the protein. This confirms that hIDO1 manages to drag hemin with it during the buffer exchange. The most likely mechanism is that the heme is in this case not covalently bound to the protein and therefore does not absorb the maximum of the known Soret band. For the oxidized protein (Figure 4.4, B.), the behavior is totally different. The absorbance before buffer exchange is boosted by the presence of excess hemin. This is not total since there remains a large signal at 360 nm but an absorbance ratio of 2.7 is observed with the protein. This value is nevertheless questionable by the accuracy of the spectrum. The change of buffer leads to a slight loss of absorbance but the ratio remains relatively high, with a value of 1.9. This highlights lability of the oxidized protein cofactor since it allows to increase the absorbance ratio. A trend towards a greater increase in the band at 360 nm is observed compared to the reduced form. This could be an indication of a better affinity. Oxidative form would attract more hemin with it as it passes through the column. However, an evaluation of the molar extinction coefficients of this intermediate state is also necessary to decide on this information.

In order to study the lability of heme cofactor in hIDO1, the proteins obtained from the first exchange (OX1 and RED1) and the last exchange (OX4 and RED4) were analyzed over time to see if the remaining free hemin tended to continue its incorporation or to be lost (Figures 4.5 and 4.6). The oxidized form without addition of hemin (OX1) remains stable over time with a very high incorporation, above 1.5. The boosted form (OX4) tends to reach this value of 1.5 after 3 days. This analysis corroborates the

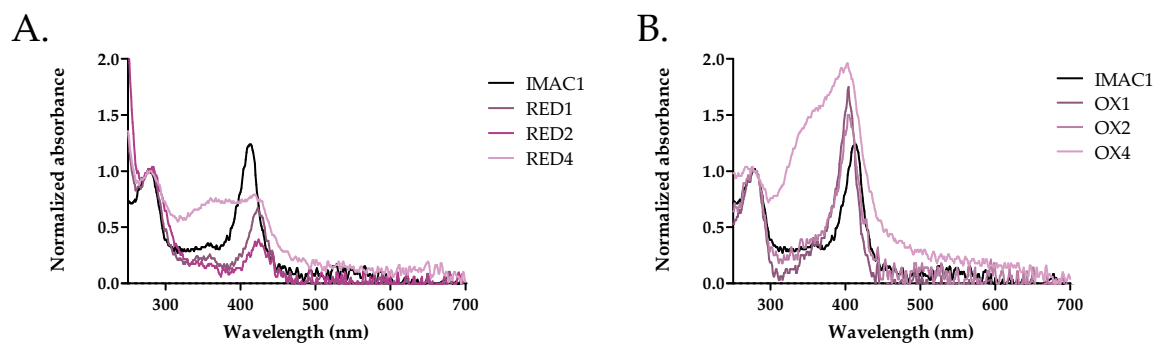


FIGURE 4.4: Reversibility of the heme gain/loss process depending on the buffer in which the protein is found. The analysis is performed at a protein at a starting concentration of $10\ \mu\text{M}$ in phosphate buffer. The amount of hemin added reaches a final value of $60\ \mu\text{M}$. Absorbances were normalized at $280\ \text{nm}$. A. Results for the reduced form. B. Results for the oxidized form.

results showing that the absorbance ratio obtained for the oxidized form after the first buffer exchange is a stable form of hIDO1. The addition of hemin then disrupts the equilibrium momentarily, even though it tends to return to its initial state with time. Concerning the reduced protein (RED1), the absorbances are not normalized to avoid a bias due to the oxidation of DTT. Indeed, with time, the DTT in the reducing buffer oxidizes and passes from a maximum absorbance at $230\ \text{nm}$ to a maximum at $280\ \text{nm}$. This oxidation has the effect of increasing the band at $280\ \text{nm}$. A normalization would decrease, in a random way, the absorbance of the Soret band. In the case of RED1, no loss of absorbance is observed over time at $423\ \text{nm}$. The maximum of the Soret band remains at $423\ \text{nm}$, suggesting that there is still enough reduced DTT in solution after $72\ \text{h}$ to reduce the protein. In consequence, the ratio of 0.6 is the stable ratio of incorporation over time. If the protein has been boosted (RED4) by the addition of hemin, a drop in incorporation is noticed with a precipitation of the free hemin as in the case of the oxidized protein.

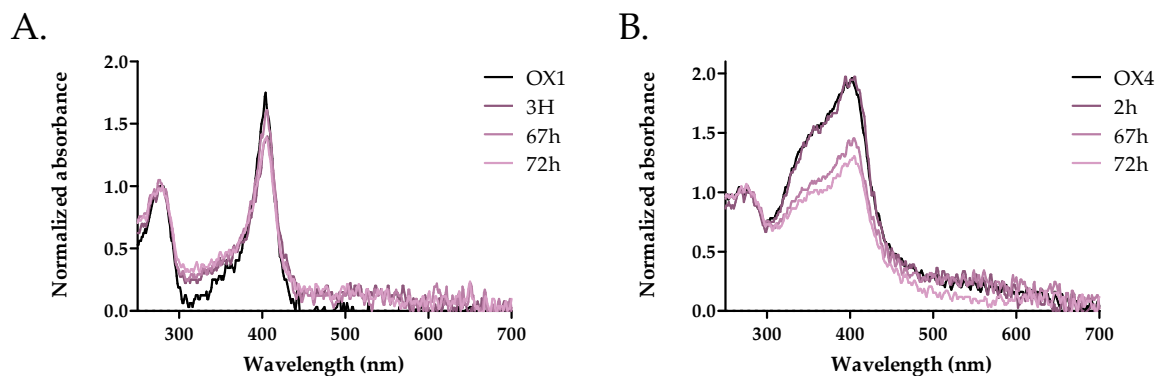


FIGURE 4.5: Reversibility of the heme gain/loss process over time for the oxidized protein. Absorbances were normalized at 280 nm. A. Results for the oxidized form 1. B. Results for the oxidized form 4.

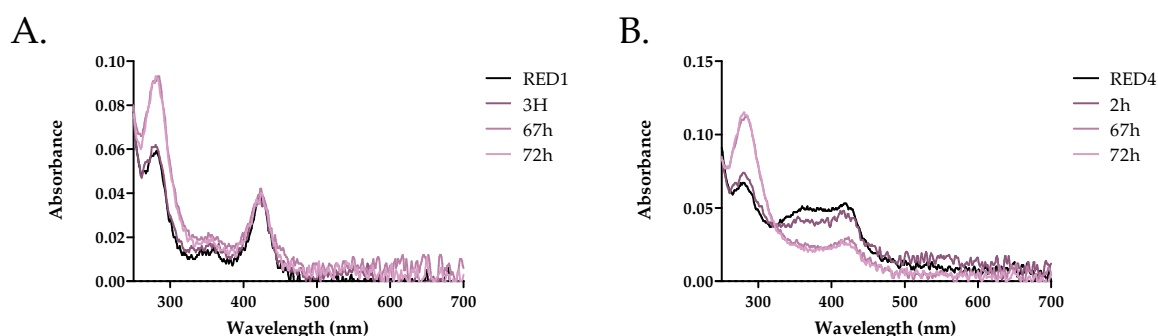


FIGURE 4.6: Reversibility of the heme gain/loss process over time for the reduced protein. A. Results for the reduced form 1 (RED1). B. Results for the reduced form 4 (RED4).

To sum up, these results indicate that, indisputably, the oxidized form (A_i : 1.0-1.5) shows a greater absorbance ratio than the reduced one (A_i : 0.4-0.6). In both cases, these ratios are stable over time at 4 degrees. The protein whose incorporation has been forced over time does not remain stable in this form and returns at values of A_i : 0.4-0.6 (reduced protein) or A_i : 1.0-1.5 (oxidized protein). The reduced form has almost no amplitude of change in incorporation compared to the oxidized form, which indicates a lack of lability of the reduced cofactor. To this lack of lability, the decrease of the absorbance ratio could be related to lower affinity of the protein for reduced heme, showing depleted incorporation. However, this is not the only explanation. It is also possible that the molar extinction coefficients of the two redox

forms of the Soret band are different, thus influencing the intensity of the absorbance band without the effect of affinity. At the present time, the experimental tools do not allow to determine these coefficients and to decide on this information. This study allowed the identification of a possible free unbound heme form at 360 nm. This state would thus be an intermediate state between a holo form and an apo form totally observed in the absence of porphyrins in the active site. This form could also be related to a lability of the ferrous heme if it is bound to oxygen, since the conditions are not made under anaerobic conditions.

4.2.3 Lability/affinity evaluation of hemin cofactor at 25 °C

In order to prove the hypothesis that, in solution, the reduced cofactor of hIDO1 is not as labile as the oxidized one, a UV-Visible absorption spectroscopy analysis was performed at 25 degrees. After producing the protein in apo form, lability tests are performed by UV monitoring of the Soret band upon addition of different hemin concentrations. The addition is performed under reducing² and oxidizing buffer³. An identical protein concentration (25 μM) is used in both cases. In the context of oxidized protein, it is noted that it is possible to increase the ratio of absorbance of the protein over time and as a function of the amount of hemin added (Table 4.2 and in Appendix C, Figure C.4). The maximum of the Soret band does not vary during the lability study and presents a value of 405 nm. For a concentration ratio of 1:1 (25 μM in hemin) or 1:2 (50 μM in hemin) between the protein and the cofactor, the difference in incorporation is hardly visible. From a 1:3 ratio (75 μM in hemin), there is an increase in the intensity of the Soret band over time. This effect is even more pronounced with higher hemin concentrations. Incorporation does not increase linearly as it shows saturation at 1.3-1.4, as was observed in the previous point analyses when 125 μM or 200 μM of hemin are added. Maximum incorporation is reached after 30 minutes.

For the reduced form, a different behavior is observed. No or little increase of incorporation takes place with time (Table 4.3). The Soret band remains at a maximum of 424 nm during the whole analysis and with a ratio of 0.6-0.7, as presented for the spectra recorded in Appendix C, Figure C.3. Therefore, it can be concluded that the reduced cofactor of the protein is not labile at temperatures close to that of the human

²In presence of 5 mM of DTT

³Without DTT

TABLE 4.2: Influence of time and hemin concentration on the absorbance ratio of hIDO1 in oxidizing buffer. The final protein concentration is 25 μ M.

Concentration	0 min	15 min	30 min	45 min	60 min
0 μ M	0.7	0.8	0.8	0.8	0.8
25 μ M	0.9	0.9	1.0	0.9	0.9
50 μ M	0.8	0.8	0.8	0.8	0.8
75 μ M	0.9	1.0	1.1	1.1	1.1
100 μ M	0.9	1.0	1.1	1.2	1.1
125 μ M	1.0	1.3	1.3	1.4	1.4
200 μ M	1.0	1.2	1.3	1.3	1.3

body. In the hypothesis of different molar extinction coefficient between the oxidized form and the reduced form of the Soret band, it could be considered that the reduced form presents a smaller coefficient. Therefore, even if *in vivo* it is proved that the incorporation of heme is not maximal, it could be possible *in vitro* that this absorbance ratio of 0.6-0.7 is the form with heme in all active sites. This would be consistent with the fact that globally this ratio is hardly reducible and that crystallography (without apo inhibitors) only gives structures with heme in all active sites.

TABLE 4.3: Influence of time and hemin concentration on the absorbance ratio of hIDO1 in reducing buffer. The final protein concentration is 25 μ M.

Concentration	0 min	15 min	30 min	45 min	60 min
0 μ M	0.6	0.6	0.6	0.6	0.6
25 μ M	0.6	0.6	0.6	0.6	0.5
75 μ M	0.6	0.7	0.7	0.6	0.7
100 μ M	0.6	0.6	0.7	0.6	0.7
125 μ M	0.6	0.6	0.6	0.7	0.6

4.3 Characterization of the protein stability

During the thesis, the second kind of characterization performed was the protein stability. This is done by means of a Differential Scanning Fluorimetry study using intrinsic fluorescence of the protein. The manipulations were performed in the laboratory of Raphael Frederick, part of the Louvain Drug Research Institute in Brussels.

4.3.1 Principle of Differential Scanning Fluorimetry study

This analysis is based on the fluorescence changes of the tryptophan residues of a protein following structural modifications. Once excited by the LED light at 280 nm, these amino acids will effectively have a fluorescence emission signal at 330 nm (in a hydrophobic environment) or 350 nm (in a polar environment) depending on its environment. During the analysis, the protein is heated from 35 °C to 95 °C degrees. Due to the increase of temperature, unfolding events appear and the hydrophobic parts of the protein are exposed to the solvent. Among these hydrophobic parts are the aromatic residues, in particular represented by the tryptophan side chains, of the protein. Due to this change of surrounding for tryptophans, the fluorescence signal changes. [5] It is therefore possible to follow the unfolding of a protein with increasing temperature and evaluate the stability of a protein, without depending on an external probe. For more accurate results, the ratio of the fluorescence signal at 350 nm/330 nm is recorded. A typical DSF curve and its first derivative are shown in Figure 4.7.

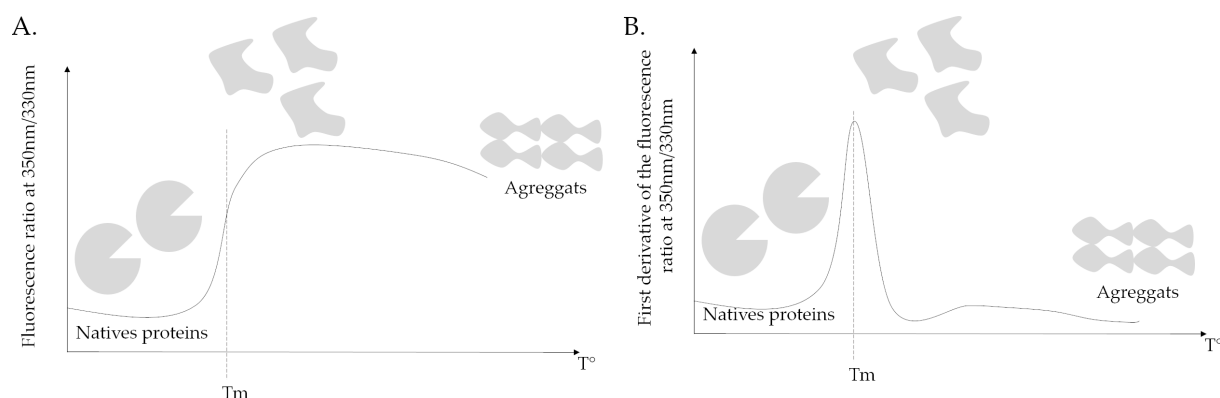


FIGURE 4.7: Characteristic spectral signature obtained during an analysis by Differential Scanning Fluorimetry. A. Fluorescence signal according to the temperature increase. B. First derivative of fluorescence according to the temperature increase.

4.3.2 Effect of the redox environment on the stability

To see if the redox state influenced the stability of hIDO1, the protein was studied in reducing (with 5 mM of DTT) and oxidizing (in the absence of DTT) conditions, in phosphate buffer. All results are summarized in the Table 4.4. The stabilization of the reduced form (melting temperature (T_m): $62.4\text{ °C} \pm 0.1\text{ °C}$) compared to the oxidized form (T_m : $58.1\text{ °C} \pm 0.2\text{ °C}$) is observed (Figure 4.8). This difference of 4 degrees can

be explained by the lability of the two cofactor forms as developed in the previous part. Since only the oxidized cofactor of hIDO1 was labile, the stabilization of the reduced heme can be explained by a support, like a structure for scaffolding, of the protein architecture by the cofactor bound inside the active site.

TABLE 4.4: Overview of the stability values (in °C) of hIDO1 as a function of the additives present during the analysis.

Condition	Concentration in additive if added	Melting temperature (°C) if oxidized	Melting temperature (°C) if reduced
Without additive		58.1 ± 0.2	62.4 ± 0.1
With DTT	5 mM	62.4 ± 0.1	/
With K ₃ FeCN ₆	5mM	/	64.3 ± 0.1
With hemin	30 μM	58.6 ± 0.4	59.7 ± 0.8
	50 μM	58.3 ± 0.3	+ 68.2 ± 0.2
			68.8 ± 0.2

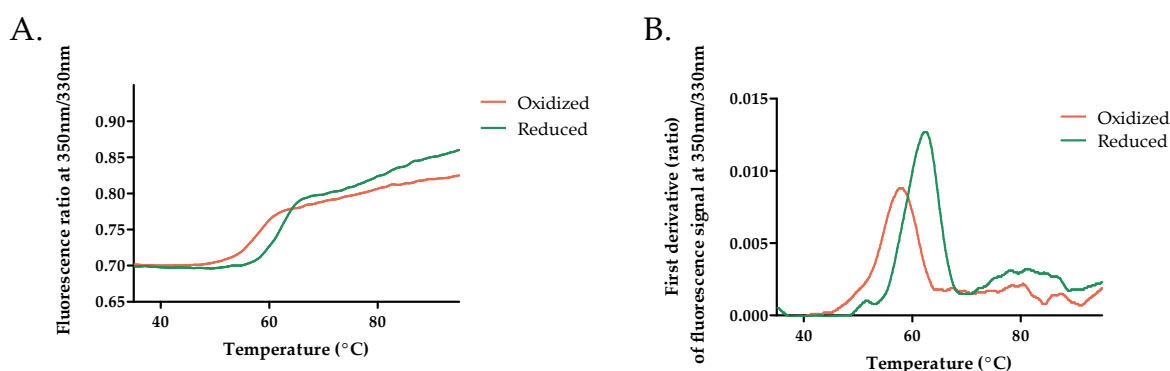


FIGURE 4.8: Stability analyses of holo hIDO1 under oxidized and reduced conditions A. Recorded fluorescence signal according to the temperature B. First derivative of the fluorescence intensity.

In the context of the reduced form (Figure 4.8), it is interesting to highlight a slight maximum at 50 degrees, before the majority transition. This corresponds to the apo protein⁴. As this protein form does not have a bounded cofactor, the architecture is not maintained and denaturation occurs more rapidly. The attribution of this peak

⁴With a lower fluorescence which could be explained by an apo state with free heme in solution in the active site causing fluorescence quenching.

could be verified by DSF measurement of hIDO1 apo (with an incorporation less than 0.4) which shows a T_m of $52.2\text{ }^\circ\text{C} \pm 0.1\text{ }^\circ\text{C}$ (Figure 4.9). This experiment showed that there was no redox effect on the stability of the apo form. This result was expected in view of the low bounded cofactor persistence in the apo protein. However, since the incorporation is not zero, a transition close to 60 degrees co-exists in apo form. The addition of hemin to this apo form makes the 50 degree form disappear and strengthens the 60 degree form. Events at higher temperatures than the main peak are also observable but difficult to attribute. These are, however, more marked for the oxidized form and the apo form.

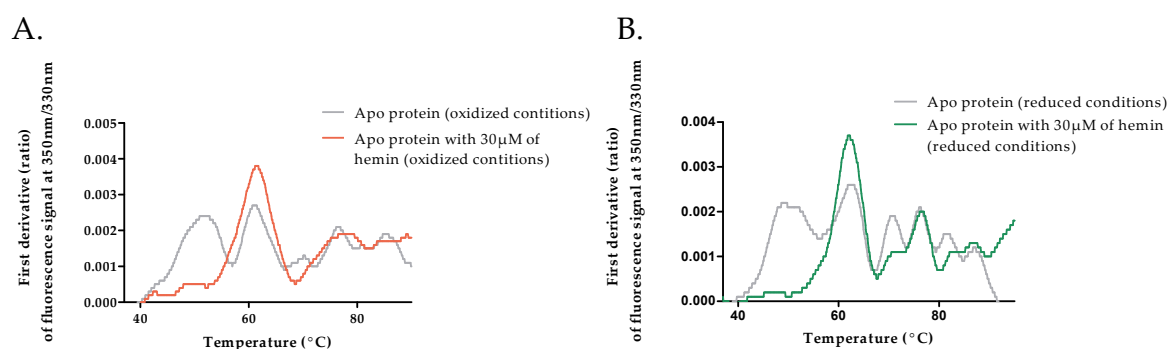


FIGURE 4.9: Stability analyses of apo hIDO1 under oxidized and reduced conditions A. Recorded fluorescence signal according to the temperature B. First derivative of the fluorescence intensity.

To analyze the reversibility of the stability due to redox changes, experiments consisting in adding an oxidizing (K_3FeCN_6 , Figure 4.10) or reducing agent (DTT, Figure 4.11) were performed. The addition of oxidizing agent has the effect of stabilizing the protein by two degrees (T_m : $64.3\text{ }^\circ\text{C} \pm 0.1\text{ }^\circ\text{C}$). The transition of the apo form is not influenced by the addition of the additive. The fact that the oxidized form is not observed can be explained by the presence of a large excess of DTT in the medium.

Addition of reducing agent to an oxidized form (Figure 4.11) leads to the increase of the melting temperature from the reduced protein (T_m : $62.4\text{ }^\circ\text{C} \pm 0.1\text{ }^\circ\text{C}$). This is consistent with the wavelength of the Soret band showing a reduced protein. The addition of oxidant induces a first transition at 50 degrees, sign of the apo form.

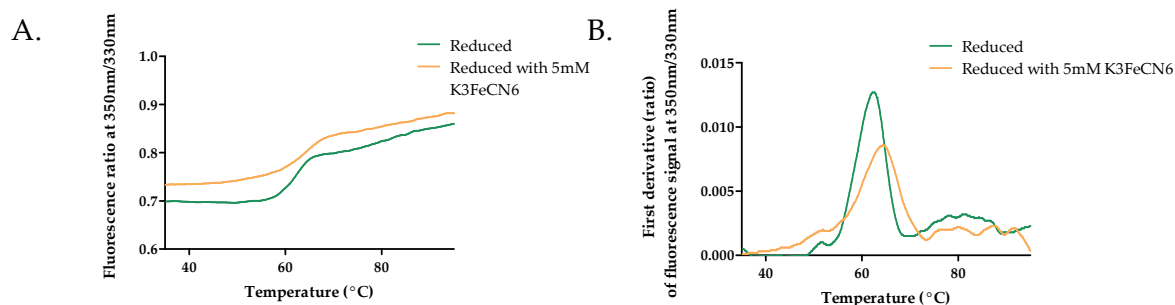


FIGURE 4.10: Stability analyses of hIDO1 under reduced condition where K_3FeCN_6 is added. A. Recorded fluorescence signal according to the temperature B. First derivative of the fluorescence intensity.

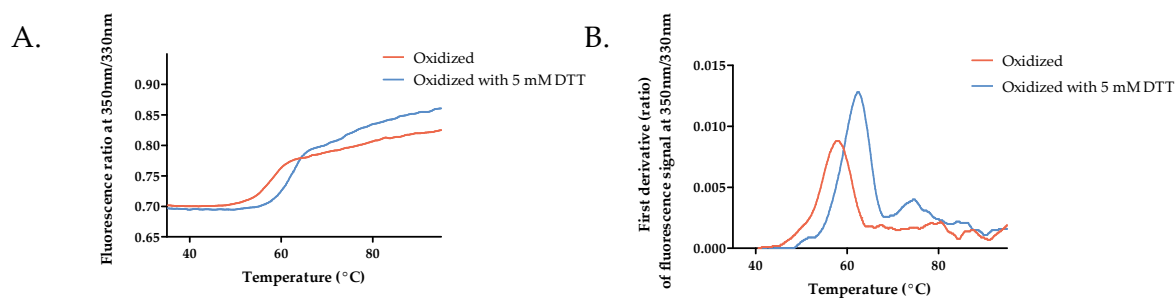


FIGURE 4.11: Stability analyses of hIDO1 under oxidized condition where DTT is added. A. Recorded fluorescence signal according to the temperature B. First derivative of the fluorescence intensity.

4.3.3 Effect of hemin on the stability

The addition of hemin to the protein has a stabilizing effect for the reduced protein (Figure 4.12). This makes a second transition appear at $68.8^\circ\text{C} \pm 0.2^\circ\text{C}$. It is necessary to add $50\ \mu\text{M}$ of the additive for the protein to be fully stabilized. At $30\ \mu\text{M}$ in hemin, the stabilization is partial with two transitions, one at $59.7^\circ\text{C} \pm 0.8^\circ\text{C}$ and one at $68.2^\circ\text{C} \pm 0.2^\circ\text{C}$. This stabilization could be explained either by 1) a forced incorporation of the reduced form following the temperature of analysis and the large concentration of hemin 2) a stabilization action of the heme around the protein.

The addition of hemin to the oxidized form has a different effect. The fluorescence signal tends to decrease with time. This can be explained by the fact that there is free hemin in solution. A fluorescence quenching is thus observed by overlapping the

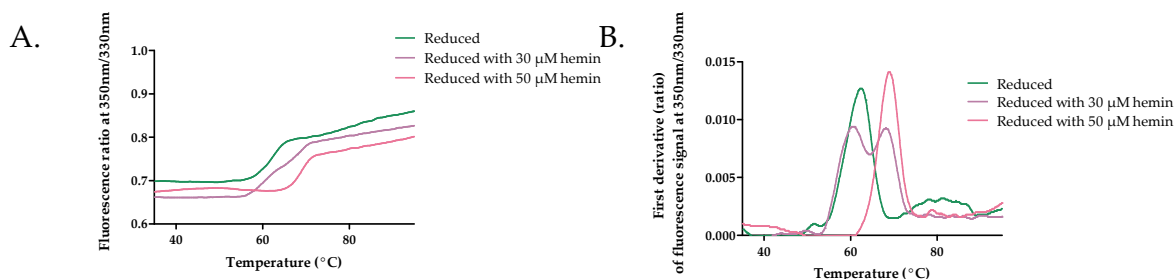


FIGURE 4.12: Stability analyses of hIDO1 under reduced condition where hemin is gradually added. A. Recorded fluorescence signal according to the temperature B. First derivative of the fluorescence intensity.

absorption spectra of free hemin and emission spectra of tryptophan residues. This hemin in solution comes from the fact that it is not possible to reincorporate all the hemin in solution. No stabilization of the main transition is observed. The average value is $58.3\text{ }^{\circ}\text{C} \pm 0.3\text{ }^{\circ}\text{C}$. However, the more hemin is added, the higher temperature events are observed.

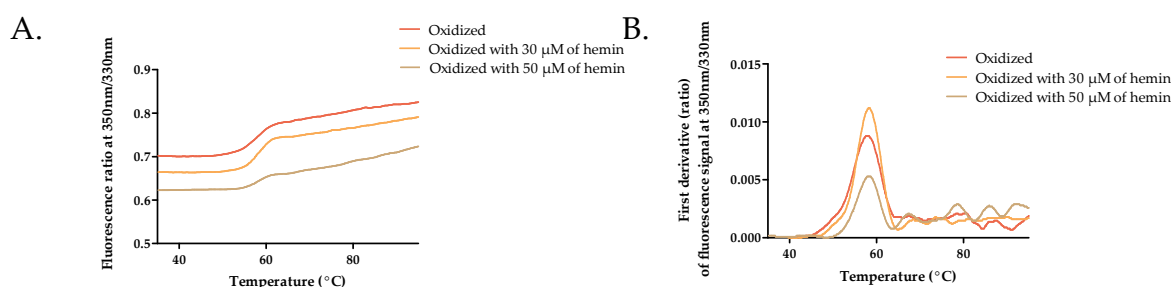


FIGURE 4.13: Stability analyses of hIDO1 under oxidized condition where hemin is gradually added. A. Recorded fluorescence signal according to the temperature B. First derivative of the fluorescence intensity.

4.4 Characterization of the protein activity

The last fundamental characteristic of the protein addressed in this thesis is its ability to perform the indole ring opening reaction of L-Trp. To study this enzymatic reaction, the appearance of the reaction product, N-formylkynurenine, was monitored at 321 nm. The protein is reduced by the association of ascorbic acid and methylene

blue. The Michaelis-Merten curves are presented at Figure 4.14, A.. Catalase at a final concentration of 150 nM is added to the mixture to prevent the harmful action of H_2O_2 on the system. In the literature, it is observed that, often, the presented values of K_m show measurements at a concentration of L-Trp lower than 200 μM . In this case, the K_m value obtained is 39.9 ± 0.7 , consistent with the literature, and follows the typical Michaelis curve. However, the results obtained with higher concentration show a retro-inhibition of the enzyme by its substrate at high concentration. As reported in the literature, the K_m is in the micro-molar range with a value of 141 μM calculated on the basis of a retro-inhibition model⁵. The maximal reaction rate is 0.00101 O.D per minute. The inhibition constant (K_i) due to the retro-inhibition is 138 μM .

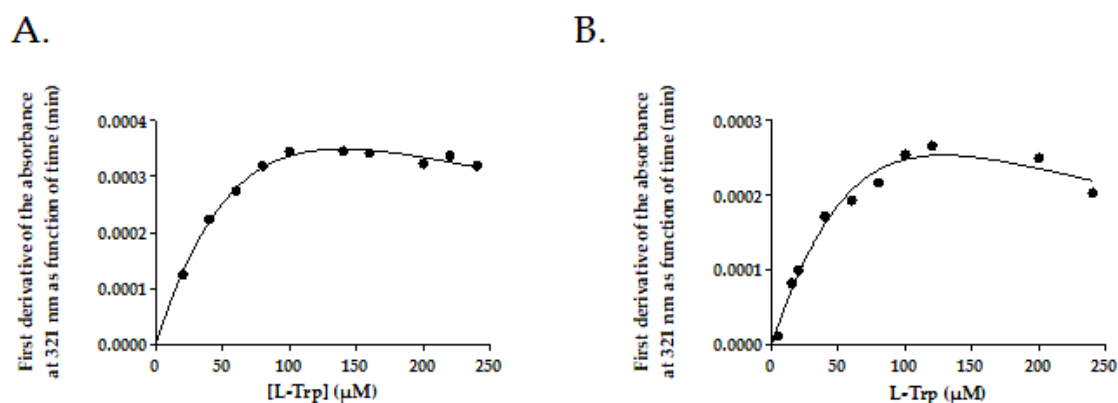


FIGURE 4.14: Michaelis-Merten curve of hIDO1. The reaction rates were obtained from absorbance monitoring at 321nm on a SpectraMax 3i apparatus. The protein is studied at a concentration of 1mg/ml in 50 mM Tris buffer. A. without hemin with the retro-inhibited fit model B ($R^2 = 0.9906$). with 100 μM of hemin with the retro-inhibited fit model ($R^2 = 0.9752$).

The effect of the addition of hemin on the reaction kinetics was studied by adding 100 μM of hemin to the enzyme before reduction by the association of ascorbic acid and methylene blue. The incubation of the hemin with the protein takes place for at least 15 minutes. Depending on the replicates and the protein batch, it could be that the heme has an impact on the inhibition constant (Figure 4.14, B.), on the K_m or on the reaction speed. This could look like an inhibiting effect, due to a second

⁵Experiment in two biological replicates. The replicate presented here has a standard deviation of 37.5 and 0.000211 for K_m and V_{max} , respectively

equilibrium established in competition with the reaction. However, it is difficult to conclude anything because of the difficulty of reproducibility. Further tests, in cell, could be a way to refine the conclusions of the effect of the presence of heme.

4.5 Intermediate conclusions

As a conclusion of this chapter, the physico-chemical study of hIDO1 has allowed to highlight or confirm some characteristics of the enzyme. Firstly, from the point of view of lability of the cofactor for hIDO1, it appears that hIDO1 presents a pronounced lability of the oxidized cofactor. The reduced form can, in some particular cases, increase its incorporation but this is on a small scale and at low temperature. Therefore, this capacity to increase the absorbance ratio for the reduced protein is unlikely to be present in the human body. On the other hand, it is therefore not possible to determine the affinity of the protein for the two forms of cofactors because the molar extinction coefficients of the Soret band according to the different oxidative state are not known.

Concerning the stability of the protein, a greater stability of the reduced form than of the oxidized form is observed, explicable by the lability of the cofactor once more of the two forms. However, with a denaturation temperature of 58.1 and 62.4 degrees for the oxidized and reduced form respectively, we can consider that the protein is stable in solution. The addition of free hemin, reducing or oxidizing agents can influence this stability. Finally, the studied protein is active and presents a K_m consistent with the literature. A retro-inhibition at high concentration of L-Trp is also observed. The addition of hemin during the kinetic analysis has an effect on the kinetic but, at the end of the thesis, it is difficult to define which one and additional testing must be performed to address the issue.

Bibliography

- [1] A. Lewis-Ballester, S. Karkashon, D. Batabyal, T. L Poulos, and S.-R. Yeh. Inhibition mechanisms of human indoleamine 2, 3 dioxygenase 1. *Journal of the American Chemical Society*, 140(27):8518–8525, 2018.

- [2] M. T. Nelp, P. A. Kates, J. T. Hunt, J. A. Newitt, A. Balog, D. Maley, X. Zhu, L. Abell, A. Allentoff, R. Borzilleri, et al. Immune-modulating enzyme indoleamine 2, 3-dioxygenase is effectively inhibited by targeting its apo-form. *Proceedings of the National Academy of Sciences*, 115(13):3249–3254, 2018.
- [3] E. A. Berry and B. L. Trumpower. Simultaneous determination of hemes a, b, and c from pyridine hemochrome spectra. *Analytical biochemistry*, 161(1):1–15, 1987.
- [4] U. F. Röhrig, A. Reynaud, S. R. Majjigapu, P. Vogel, F. Pojer, and V. Zoete. Inhibition mechanisms of indoleamine 2, 3-dioxygenase 1 (ido1). *Journal of medicinal chemistry*, 62(19):8784–8795, 2019.
- [5] J. R. Lakowicz. Protein fluorescence. In *Principles of fluorescence spectroscopy*, pages 341–381. Springer, 1983.

Chapter 5

Characterization of hIDO2

5.1 Introduction

In this second chapter of the characterization part, the characterization of hIDO2 is detailed. This was done using the same methodology as for hIDO1 in order to compare them later. Different characterization criteria were chosen, namely stability, affinity and lability of the cofactor for the protein and activity of the protein.

5.2 Characterization of the cofactor incorporation

In terms of characterization, the UV-Visible absorption spectroscopy analysis allows to determine the maxima of the Soret bands in reducing and oxidizing conditions (Figure 5.1). A maximum at 406 nm is observed for the oxidized form and at 422 nm for the reduced form. The binding to small molecules such as water, O₂ or CO₂, leads to a shift at 412 nm. Absorbance is strongly influenced by redox changes, as highlighted in the Table 5.1. The protein has a higher ratio of absorbance in its oxidized state than in the reduced one. As for hIDO1, without knowledge of the molar extinction coefficients of the Soret band for ferric and ferrous form of the cofactor, it is not possible to discern whether this effect is an affinity effect or an effect due to a difference in these molar extinction coefficient of the Soret band according to the oxidative state of the bounded heme cofactor. The change of buffer shows that the protein tends to slightly better incorporate the cofactor in a phosphate buffer than in TRIS buffer.

TABLE 5.1: Influence of the buffer on the absorbance ratio. * The buffer used directly after IMAC consists in 50 mM TRIS, NaCl, 5% Glycerol, 150 mM Imidazole. The maximum observed at 412 nm can be explained by the binding of small molecules (O₂ or CO₂) during production.

Buffer	Composition	Maximum of the Soret peak	Ratio A_{Soret} / A_{280}
Oxidized	Directly after IMAC*	412	0.4 - 1.0
	TRIS	406	0.7
	PO4	406	0.8 - 1.0
Reduced	HEPES DTT	422	0.6
	TRIS DTT	422	0.4 - 0.6
	PO4 DTT	422	0.4 - 0.6

A specific feature of hIDO2 is the influence of temperature on the solubility of the protein as well as the incorporation of the porphyrin cofactor. Indeed, it was quickly

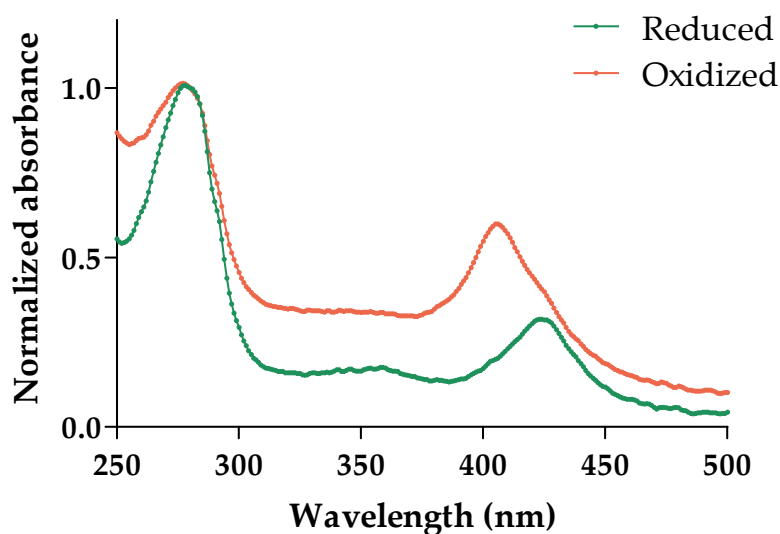


FIGURE 5.1: UV-spectrum recorded between 250 nm and 600 nm for hIDO2 in oxidized (50 mM in K_2HPO_4 buffer pH 7.4 and 200 mM NaCl) and reduced (50 mM in K_2HPO_4 buffer pH 7.4 and 200 mM NaCl supplemented with 5 mM of DTT) forms. Absorbances are normalized at 280 nm.

noticed during the thesis that it was essential to have an induction temperature below 25°C to observe a production of the protein in soluble form. The slightest increase in temperature dramatically affects the yield. This is due to the high surface hydrophobicity observed for the protein. In the same way, it turns out that the cofactor incorporation by hIDO2 protein is very sensitive to temperature. The absorbance ratio can be very low when the protein is produced at temperatures above 20°C .

5.3 Characterization of the lability of the cofactor

Unlike hIDO1, no information for hIDO2 on the lability of its cofactor is available. In order to study the lability of the cofactor, UV-Visible absorption spectroscopy analyses were performed at 25°C with the protein of interest, obtained pure, after purification. The protein used is a so-called "apo" protein. Indeed, after production and purification at a temperature higher than 20°C , the cofactor contained in the obtained protein was low incorporated (A_i : 0.4). Following buffer exchanges, the incorporation of the cofactor was further decreased until it was almost undetectable. The analysis of this "apo" protein by DSF revealed a protein with the same stability and behavior as

the other batches of holo proteins. The enzymological analysis, detailed later, after hemin addition, allows to have an active protein. It is therefore concluded that this protein is sufficiently folded to be used as an apo protein for UV-Visible absorption spectroscopy analysis.

TABLE 5.2: Influence of time and hemin concentration on the absorbance ratio of hIDO2 in oxidizing buffer. The final protein concentration is 20 μM .

Concentration	0 min	15 min	30 min	45 min
0 μM	0.2	0.2	0.3	0.3
25 μM	0.2	0.3	0.2	0.4
50 μM	0.5	1.2	1.3	1.3
75 μM	0.7	1.8	1.6	1.6
100 μM	0.9	1.9	1.9	1.9
125 μM	1.2	1.8	1.8	1.9
200 μM	1.2	2.7	2.5	2.6

The UV-Visible absorption spectroscopy analysis shows several surprising results (Table 5.2 and Table 5.3). Spectra are available in Appendix C at Figure C.5 and C.6. First, regardless of the oxidation state, there is an increase in intensity of the Soret band for hIDO2. This means that both cofactor forms can be labile. Second, this incorporation takes time to initiate. For hIDO2 in the presence of a ferric cofactor (Table 5.2), one must add an amount greater than two equivalents to see a significant increase in the Soret band. Incorporation is also not an instantaneous process, it takes 15 minutes to see an increase in incorporation for a 1:2 protein/cofactor ratio. For higher concentrations, the more hemin is added to the medium, the faster the cofactor binding appears but the stabilization of the signal is always observed after 15 minutes. The addition of 200 μM hemin leads to supremely high absorbance ratios, with a value of $A_i = 2.7$. In general, the absorbance signal of the Soret band is stable after incorporation and does not tend to decrease significantly.

Regarding the evolution of the Soret band upon addition of a ferrous cofactor (Table 5.3), it can be seen that, although timid at the beginning and less marked than for the oxidized state, there is an increase of the absorbance. This requires a larger protein/cofactor ratio (1:3) than for the oxidative state. The addition of a large excess (200 μM) allows the observation of a very important band. Once again, a latent time is linked to this incorporation since it is necessary to wait 15 min before seeing the effect

TABLE 5.3: Influence of time and hemin concentration on the absorbance ratio of hIDO2 in reducing buffer. The final protein concentration is 25 μM .

Concentration	0 min	15 min	30 min	45 min
0 μM	0.1	0.1	0.2	0.2
25 μM	0.1	0.2	0.2	0.2
50 μM	0.1	0.2	0.2	0.2
75 μM	0.2	0.3	0.3	0.3
100 μM	0.3	0.5	0.5	0.5
125 μM	0.3	0.8	0.8	0.7
200 μM	2.0	1.7	1.4	1.3

except at 200 μM . For this concentration, the increase is instantaneous. However, not all the added cofactor is bound since a signal at 350-360 nm is observable. For most of the cofactor concentrations, the absorbance of the Soret band is stable over time, except for the measurement with 125 μM and 200 μM . In these cases, a decrease of the Soret band absorbance is observed at 30 and/or 45 min. This shows that the strong incorporated ferrous state for hIDO2 can be forced but is not stable over time.

5.4 Characterization of the protein stability

The stability of the protein could then be quantified by nanoDSF analysis in collaboration with the laboratory of Raphael Frederick, from the Louvain Drug Research Institute in Brussels. All results are summarized in the Table 5.4. Differential Scanning Fluorimetry studies of the protein show a denaturation temperature of $47.7^\circ\text{C} \pm 0.1^\circ\text{C}$ for the reduced protein and $48.1^\circ\text{C} \pm 0.1^\circ\text{C}$ for the oxidized protein (Figure 5.2). The difference between the two proteins is therefore very small. This result supports that the existence of lability for the two cofactor forms since the cofactor does not help to maintain the structure of one form more than the other. The addition of either oxidizing agent (K_3FeCN_6) or reducing agent (DTT) also has little effect since the melting temperatures observed are respectively $47.7^\circ\text{C} \pm 0.1^\circ\text{C}$ and $47.8^\circ\text{C} \pm 0.1^\circ\text{C}$ (Figure 5.3).

TABLE 5.4: Overview of the stability values (T_m in $^{\circ}\text{C}$) of hIDO2 as a function of the additives present during the analysis.

Condition	Concentration in additive if added	T_m ($^{\circ}\text{C}$) if oxidized	T_m ($^{\circ}\text{C}$) if reduced
Without additive	/	48.1 ± 0.1	47.7 ± 0.1
With DTT	5 mM	47.8 ± 0.1	/
With K_3FeCN_6	5mM	/	47.7 ± 0.1
With hemin	30 μM	57.5 ± 0.9	64.1 ± 0.7
	50 μM	64.4 ± 1.1	68.7 ± 0.0
	70 μM	65.3 ± 1.2	68.8 ± 0.2
	600 μM	71.4 ± 0.3	69.3 ± 0.0

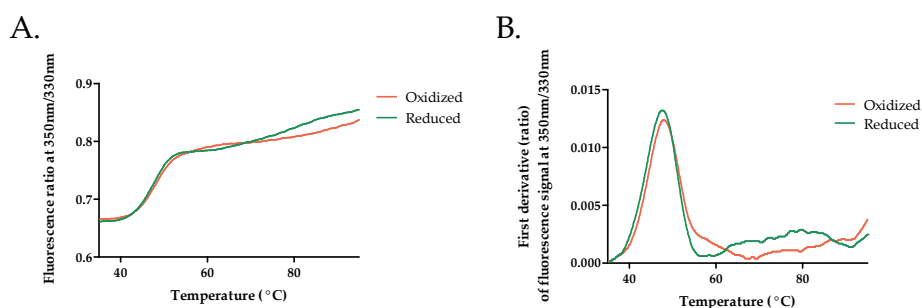


FIGURE 5.2: Stability analyses of hIDO2 under oxidized and reduced conditions A. Recorded fluorescence signal as a function of the temperature B. First derivative of the fluorescence intensity.

In contrast, the addition of hemin to the forms has a dramatic effect as the melting temperature increases significantly. However, the magnitude of this effect is highly dependent on the protein batch analyzed (and the initial absorbance ratio). For example, for a batch with the reduced form and a standard absorbance ratio of 0.6, the temperature observed is $64.1^{\circ}\text{C} \pm 0.7^{\circ}\text{C}$ after the addition of 30 μM of hemin, then $68.7^{\circ}\text{C} \pm 0.0^{\circ}\text{C}$ for 50 μM and stabilizes at $68.8^{\circ}\text{C} \pm 0.0^{\circ}\text{C}$ for 70 μM . The first derivative observed at 30 μM is relatively large, showing the coexistence of several forms in the mixture with different stability. This shows therefore an in-homogeneity in solution. At 50 μM and 70 μM , the peak is better defined even if a maximum around 57 $^{\circ}\text{C}$ is still observed.

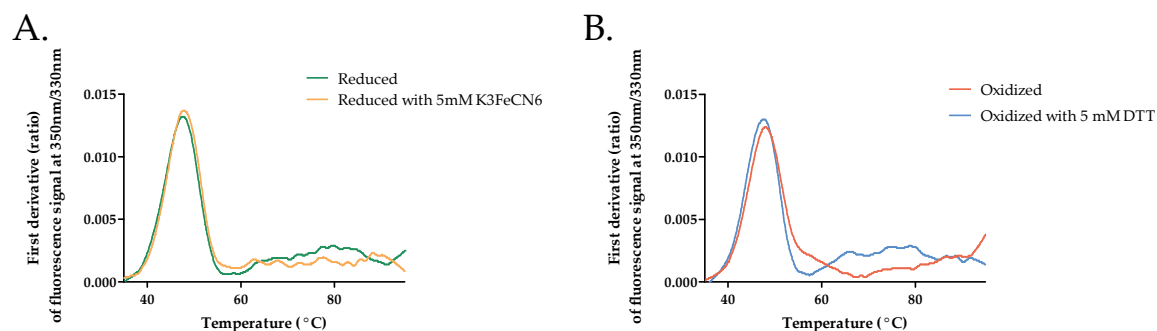


FIGURE 5.3: Stability analyses of hIDO2 under reduced condition where A. K_3FeCN_6 B. DTT is gradually added. First derivative of the fluorescence intensity.

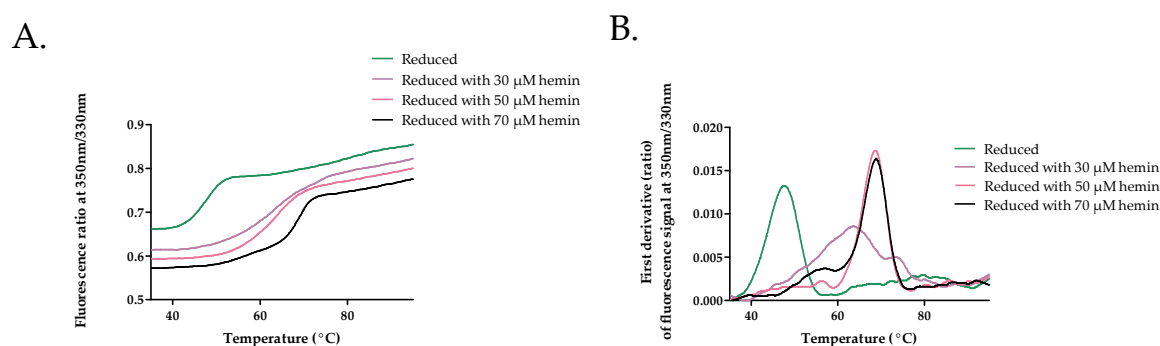


FIGURE 5.4: Stability analyses of hIDO2 under reduced condition where hemin is gradually added. A. Recorded fluorescence signal according to the temperature B. First derivative of the fluorescence intensity.

For the oxidized form with an absorbance ratio of 1.0, the stabilization is initially less strong with a T_m of $57.5^\circ\text{C} \pm 0.9^\circ\text{C}$ after the addition of $30\ \mu\text{M}$ of hemin. This could be due to a greater initial incorporation of the heme in oxidized form. Higher is the addition, the more marked is the stabilization with a T_m of $64.4^\circ\text{C} \pm 1.1^\circ\text{C}$ for $50\ \mu\text{M}$ and 65.3 ± 1.2 for $70\ \mu\text{M}$. As for the reduced form, the width of the DSF peak suggests the coexistence of several denaturation temperatures during the addition of $30\ \mu\text{M}$ and $50\ \mu\text{M}$. This would come from the fact that not all the protein incorporates heme. It can be seen that the measurements on the oxidized protein show a greater variability. It can be assumed that this is due to the ongoing process of incorporation, more marked than in the case of the reduced protein.

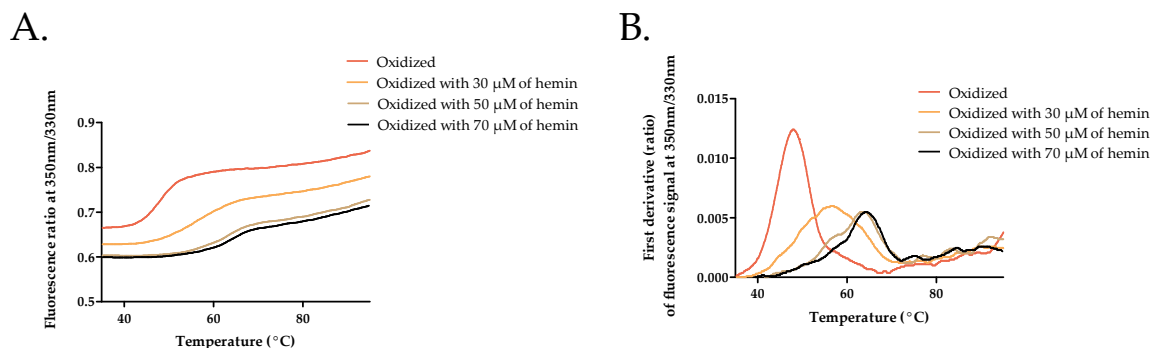


FIGURE 5.5: Stability analyses of hIDO2 under oxidized condition where hemin is gradually added. A. Recorded fluorescence signal according to the temperature B. First derivative of the fluorescence intensity.

For the reduced form, the analysis showed that adding more hemin had little effect because a large excess ($600\ \mu\text{M}$) causes a melting temperature of 69.3 ± 0.0 degrees. In a more noticeable way, the addition of an excess of hemin to the oxidized form ($600\ \mu\text{M}$) results in a stabilization at $71.4\ ^\circ\text{C} \pm 0.3\ ^\circ\text{C}$. A difference in behavior between the oxidized and reduced form is also noticed when adding such a quantity of hemin: the decrease of the fluorescence at low temperature. While this decrease is not very marked for the reduced form, it is almost the majority for the oxidized form at a T_m of $51\ ^\circ\text{C} \pm 0.1\ ^\circ\text{C}$. One hypothesis to explain this effect is the presence of free heme in solution for the oxidized form which can then cause a fluorescence quenching phenomenon on the radiative wave emitted by L-Tryptophan at the same wavelengths. This indicates that the oxidized form has reached its maximum of incorporation since there is hemin in solution.

5.5 Characterization of the protein activity

Evaluation of the kinetic parameters of hIDO2 is difficult. Indeed, despite the addition of a huge amount of substrate (L-Trp), it is very difficult to discern precise evolution of the absorbance at 321 nm, and consequently, an affinity constant. The analysis just proves that there is an amount of NFK created during the reaction and therefore that the enzyme is active. The addition of hemin does not improve the precision of the measurements.

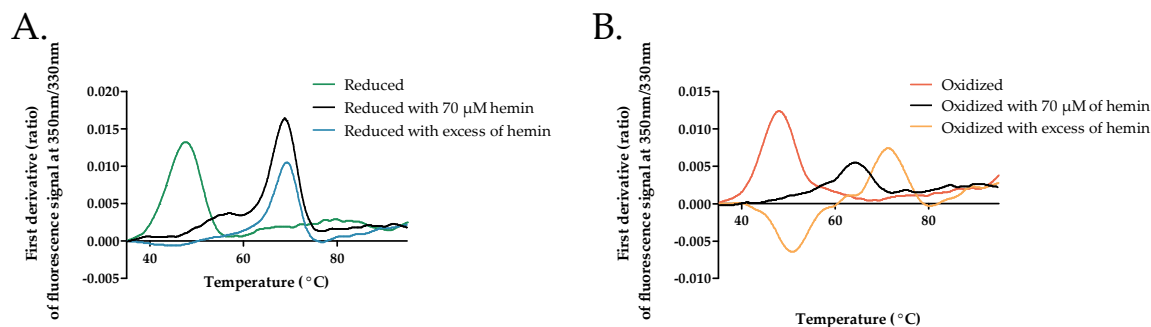


FIGURE 5.6: Stability analyses of hIDO2 under reduced or oxidized conditions where a excess of hemin (600 μM) is gradually added. A. in reduced conditions B. in oxidized conditions.

5.6 Intermediate conclusions

As a conclusion, this chapter allows to learn more about the still unknown characteristics of hIDO2. In particular, a high lability of the cofactor is observed, regardless of the oxidation state of the protein. This lability results in the two forms (oxidized or reduced) of the enzyme having the same stability. Their stabilities are thus not influenced by the addition of oxidizing or reducing agent but see their value being strongly modified by the addition of hemin. Lastly, the hIDO2 protein studied is active. Due to the accuracy of the calculated reaction rates, it is not possible to give a precise K_m value. However, it is clear that hIDO2 is much less active than hIDO1, with a difference of at least an order of magnitude.

Part III

Comprehensive study of hIDO1 plasticity

*“Les doutes d’une incroyante
Se perdent dans la nuit
Et tout s’est décidé
Je ne vis que d’idéaux (HIDO)”*

Coeur de Pirate - Somnambule

Chapter 6

The JK-loop plasticity study by means of crystallographic snapshots

6.1 Introduction

Among the areas of poor understanding of the hIDO1 protein are the conformation of the JK-loop and its molecular mechanism of refolding. Given the involvement of this loop in the activity of the enzyme, it seems essential to understand its role. In this part of the manuscript, the different advances in the understanding of the functioning of this dynamic loop that have been collected during this thesis are detailed. For this purpose, this chapter details different crystallographic structures obtained for hIDO1 with or without ligands in the active site. The aim of this study was to collect experimental information on the conformation of the loop, partially or totally refined, in order to serve for a further study of it by Molecular Dynamics (Chapter 7). All the results detailed in this chapter were awarded the "Young Medicinal Chemist Award in Belgium (SRC)" at the 3rd FNRS Med Chem Symposium. It was also honored with a presentation at the international conference "EFMC-YMCS 2022 ; 8th EFMC Young Medicinal Chemists' Symposium" in September 2022.

6.2 JK-loop behavior without ligand in the active site

This part was written on the basis of the article "Influence of the presence of the heme cofactor on the JK-loop structure in indoleamine-2,3-dioxygenase-1" published in 2020 by M. Mirgaux in *Acta. D. Crystallography*. [1] From this article is derived a structure filed in the PDB under the code 7a62. For the fluidity of the reading, only the essential information is included in the present manuscript without modification of structure or content from the original literature. Any additional information concerning the methods can be found in the associated literature. This work has been presented at several conferences and workshops, including the ReNaForBis training week in Oleron (2020).

6.2.1 Contextualizing the results

During the early part of the thesis, efforts were made to determine the conformation of the JK dynamic loop in the absence of ligand. For this purpose, the crystallization conditions of hIDO1 were optimized in order to find new polymorphs and to establish other crystal interfaces. The goal of this research was to modify the crystal packing to stabilize and allow the refinement of the JK-loop. At the end of this work, a structure

of ferrous hIDO1 at a medium resolution level (2.44 Å) was obtained. The structure consists of a heme-linked hIDO1 enzyme with a complete JK-loop.

6.2.2 Quality of the refined structure

The hIDO1 crystals obtained with the hanging-drop vapor method belong to the $P2_12_12$ space group, and the unit cell parameters are $a=80.96$ Å, $b=117.95$ Å and $c=216.41$ Å. The heme-bound hIDO1 crystal structure is composed of four monomers (A, B, C, D) with missing atoms at the extremities or in the JK-loop (residues 360 to 380) for monomer A, B and D. The JK-loop of monomer C is fully refined, leading to a complete structure of the loop ever reported. The heme-bound hIDO1 structure is solved and refined at a resolution of 2.44 Å, with R_{work} and R_{free} equal to 0.2118 and 0.2579 respectively. Seven glycerol molecules and two chloride ions are also present in the structure. The Ramachandran plot, obtained using MolProbability [2], shows that 96 % of the residues adopt allowed Φ - Ψ values, and only 0.33 % are reported as outliers in the structure. Rotamers outliers amount to 1.3 %. Since most of these outliers are located in the JK-loop, their conformation variability highlights a greater flexibility. Statistics for the refined model (bond lengths and bond angles r.m.s.d values) stress a good quality of the structure. The crystal structure has an overall B-factor of 39.83 Å². Particularly, residues Q360 to G380 are characterized by the largest B values in each monomer (Figure 6.1). It reflects the enhanced dynamics of the protein residues around the JK-loop. Entire statistical and collection data are in Appendix D, Table D.1.

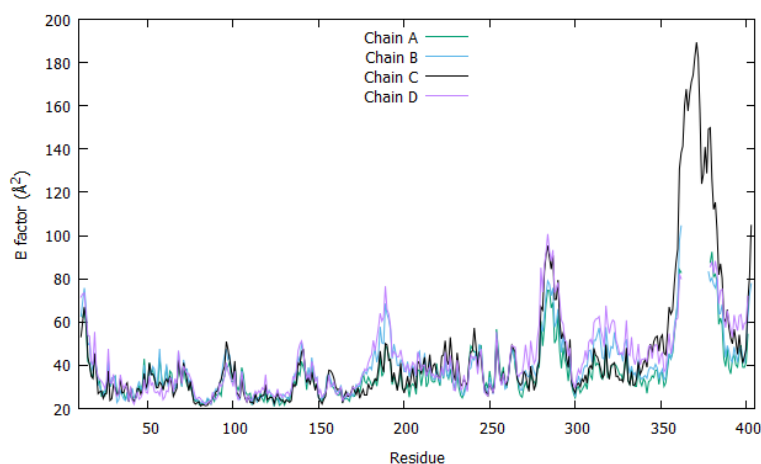


FIGURE 6.1: B-factor (Å²) profile of the residues main chain for each monomer.

6.2.3 Description of the dimerization interface

While hIDO1 functions as a monomer in the biological state, the hIDO1 unit cell of the crystal structures in the PDB contains more than one molecule per asymmetric unit. In the crystal structures described in the literature, dimeric interfaces stabilize the JK-loop, the C-terminal part being involved in more interactions than the N-terminal part of the loop. These interfaces involve the J- and K- α -helices, the H45-S52 α -helix (Figure 6.2, (a)), and the Q54-K61 α -helix (Figure 6.2, (b)) from the next asymmetric unit. Weak interactions contribute to the organization of the N-terminal part of the loop, in particular hydrogen bonds involving Q348/R58, T351, and water molecules, as well as close contacts between F41/S359 and L49/I356. In contrast, amino acids of the K α -helix are involved in strong electrostatic interactions (D48/K389, E51/R392, E51/K397, R56/E401 and K94/E396) and contribute to a dense hydrogen bond network (S52 /R392/K94/water and R56/E401/water), and a chalcogen bond interactions¹ between oxygen and sulfur atom of D48 and M385. Resulting from these interfaces, the C-terminal part of the JK-loop is more stable leading to better refinement of this extremity in contrast to the N-terminal part that remains unclear.

In the present crystal structure, the four hIDO1 molecules of an asymmetric unit are interconnected and can be considered as a dimer of dimers. Translation and inversion operations appear between the dimers A/D and B/C. Alignment of the two dimers results in a r.m.s.d of 0.26 Å. Such a crystal packing results in multiple monomer/monomer interfaces in both the small and large domains of the protein (Appendix D, Tables D.3 and D.5). Especially, pre- α -helix D, and the BC- and HI-loops are involved in dimerization in the crystal structure. These interactions at the interfaces are detailed in the associated article. [1] Consequently to this packing, an empty space is generated through the crystal packing close to the C-terminal part of the JK-loop allowing a less constrained conformation (Figure 6.3). Nevertheless, in the same way as observed for the C-terminal extremity in other structures of hIDO1, the stabilization of the pre- α -helix D close to the N-terminal part of the JK-loop facilitates the refinement of this part of the loop. Differences in crystal packings thus allow the observation of distinct structural features on the protein surface. It highlights the importance of analyzing polymorphism during protein refinement and justifies the

¹IUPAC definition: net attractive interaction between an electrophilic region associated with a chalcogen atom in a molecular entity and a nucleophilic region in another, or the same, molecular entity. [3]

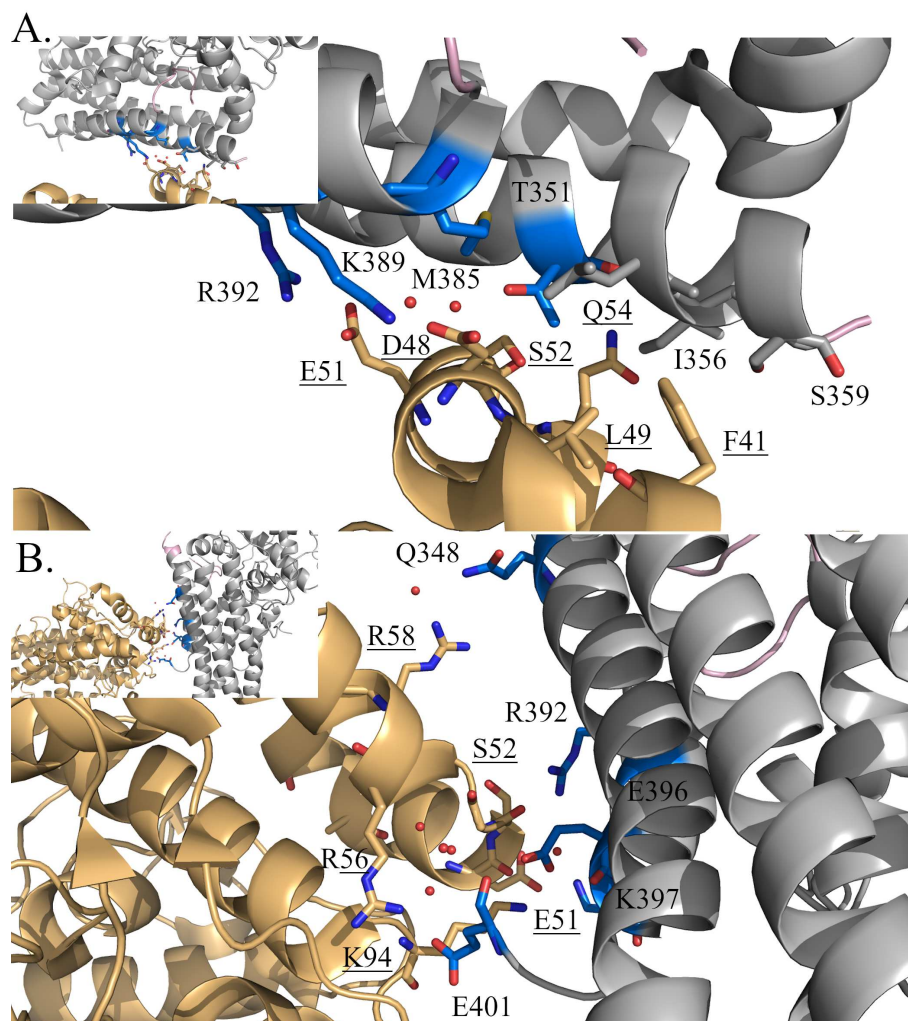


FIGURE 6.2: Dimerization interfaces in 5whr around the JK-loop. A. Interface with the α -helix H45-S52. B. Interface with the α -helix Q54-K61.

study of alternative crystal forms to provide a more detailed structural picture of a protein.

6.2.4 Conformation of JK-loop

In the crystal structure reported here, a fully refined JK-loop is obtained for the monomer C. Quality of the electron density for that region of the protein is still poor but all heavy atoms of the main chain of the JK-loop could be traced and refined for the first time. The N-terminal end of the loop (residues Q360-L374) is still very flexible, as confirmed by very high B factors (Figure 6.4, (a)) and the electron density distribution remains unclear for some lateral chains and for residue S372. However,

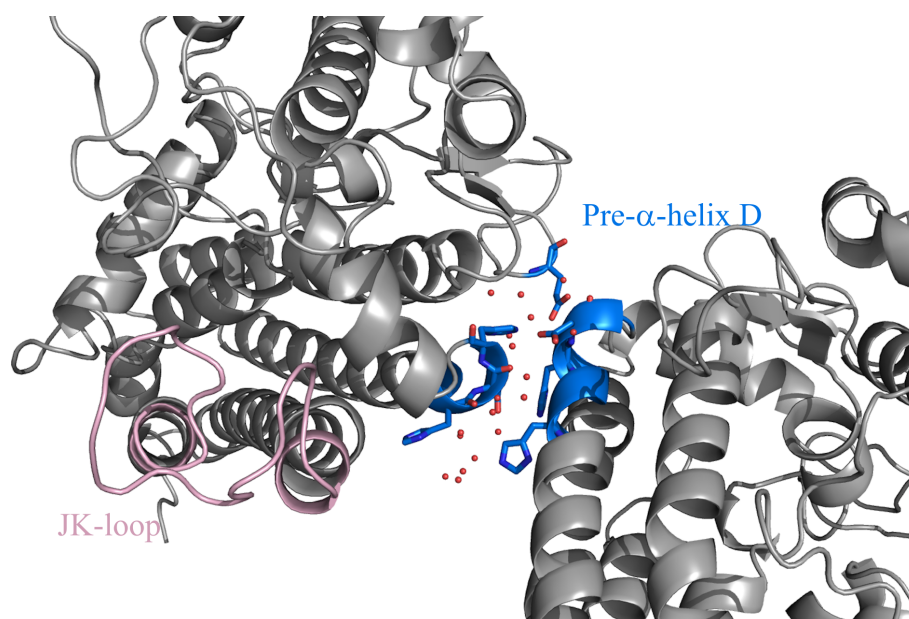


FIGURE 6.3: Dimerization interface of the α -helix D (in blue) in relation to the JK-loop (in pink).

overall, the electron density distribution for most of the main chain of the loop is defined. Most residues of the C-terminal part of the JK-loop (E375-G380) are defined (Figure 6.4, (a) and (b)) except for A376.

The refined JK-loop adopts a conformation between the intermediate and the fully extended ones. The C-terminal part of the loop interacts with the heme moiety through electrostatic interactions with K377 (Figure 6.4, (b)) at 4.3 Å and 5.1 Å between the residue and the carboxylate of the cofactor. Compared to what is observed in other available crystal structures, the conformation of the JK-loop presented here is new although close to the one reported by Luo *et al.*². [4] In the present crystal structure, the JK-loop completes the α -helix K with a supplementary turn. This conformation of the JK-loop prevents the orientation of T379 and G380 into the active site, while residue K377 interacts with the heme cofactor. Consequently, the C-terminal part is oriented towards the active site, in an opposite way to the opened conformations of Luo *et al.* Because of this overall conformation, the pocket A is not open in the crystal structure due to a movement of residues 262-265, as there is no ligand. The same can be observed in other published IDO1 X-ray structures. The pocket B is formed within the free space between the DE-fragment and the JK-loop

²6e41, 6e42, 6e44 and 6e45

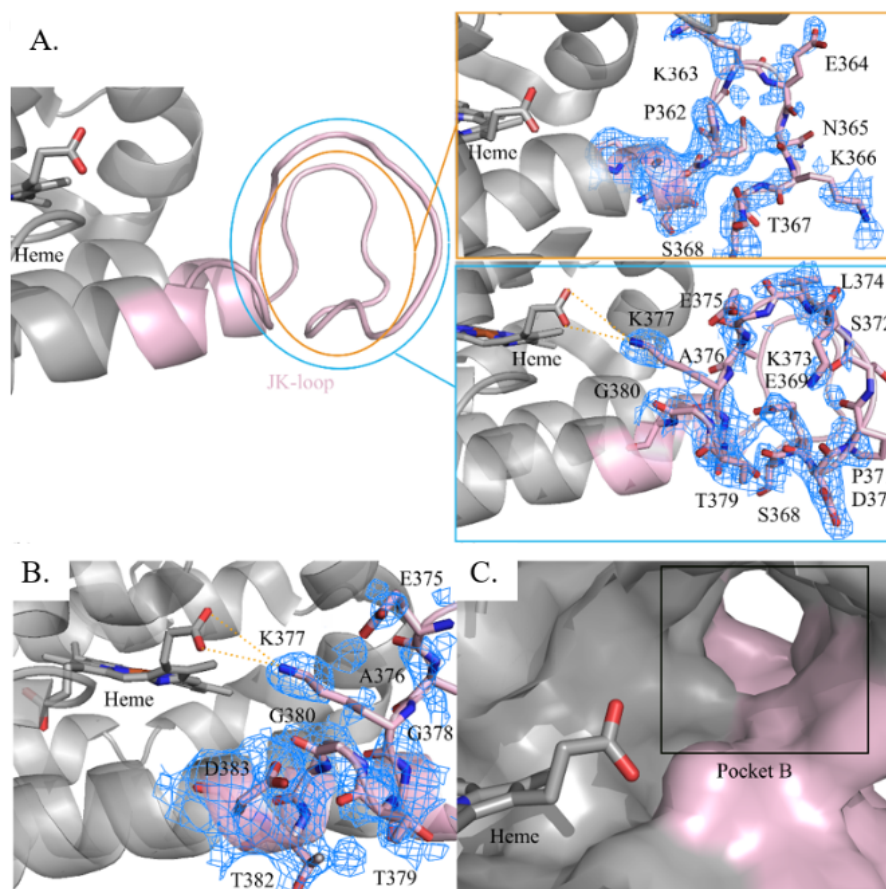


FIGURE 6.4: Conformation of the JK-loop in crystal structure. The 2Fo-Fc map around the residues is represented at 0.5σ (blue mesh), only density of interest in drawn for clarity. A. Density around N-terminal part (residues Q360 to L374) represented in two levels: amino acid from Q360 to S368 in orange and amino acid from S368 to L374 in blue. B. Density around the JK-loop in the C-terminal part. Interaction of K377 with the carboxylate function of heme moiety in orange. C. Pocket B resulting in the active site.

(Figure 6.4, (c)) and allows the entrance of a L-Trp into the enzyme (volume of 249 \AA^3 , as calculated with POCASA 1.1 server, Appendix D, Figure D.1). [5] As previously mentioned, the JK-loop may play a role in the regulation of the enzyme activity. Indeed, the conformation of this loop may help the protein to regulate the entrance of L-Trp into the active site and thus its degradation, while maintaining the heme moiety inside the active site through interactions with residue K377.³

³At the end of the thesis, by analyzing all the structures obtained, it is also possible to reconstruct the loop in some empty monomer A or C of the asymmetric unit, with a slight increase of quality for

6.2.5 In summary

The hIDO1 crystal structure reported here contains four monomers in the asymmetric unit. The hIDO1 structure was refined at a resolution of 2.44 Å and the R_{work} and R_{free} are equal to 0.2118 and 0.2579, respectively with reasonable statistics (Ramachandran plot, rotamer analysis and r.m.s deviation values). The structure, which is mainly composed of two domains consisting of α and 3_{10} helices, is involved in multiple dimerization interfaces between the monomers within the asymmetric unit.

For the first time, a fully refined JK-loop was determined in one of the monomers. The refined conformation of the JK-loop adopts a new conformation between the reported intermediate and the fully extended ones. Lysine K377, located at the C-terminal part of the loop, is involved in an electrostatic interaction with the heme cofactor. The N-terminal part of the loop is very flexible, this segment being associated with high B-factors values. As a result of the intermediate conformation of the loop, the active site of the enzyme forms a "pocket B" with a volume of 249 Å³. In the absence of a ligand, the JK-loop intermediate conformation of hIDO1, is seen to play a crucial role in the regulation of the activity on the enzyme and/or the stable binding of the heme cofactor into the active site. Given the low accuracy of the density maps around the side chains of the JK-loop in this structure, a Molecular Dynamics analysis is needed to complement this study and assess the behavior of the loop in solution (Chapter 7).

6.3 JK-loop behavior in the presence of L-Trp in the active site

This part was written on the basis of the article "Temporary Intermediates of L-Trp Along the Reaction Pathway of Human Indoleamine 2,3-Dioxygenase 1 and Identification of an Exo Site" published in 2021 by M. Mirgoux in *International Journal of Tryptophan Research*. [6] For the fluidity of the reading, only the essential information is included in the present manuscript without modification of structure or content from the original literature. Any additional information concerning the methods can be found in the associated literature. From this article are derived three structures the density around the residues. In this case, the loop is in an intermediate position, with K377/Heme interaction. There is still a lack of refinement for S372 and some side chains.

filed in the PDB under the code 7nge, 7p0n, 7p0r. This work was presented at the Belgian Crystallography Symposium in March 2021.

6.3.1 Contextualizing the results

At this stage of understanding the dynamic loop, the complete JK-loop was refined for the first time in the absence of ligand. [1] Even if the quality of the density map around the loop remains poor, the structure shows an intermediate position of the JK-loop in hIDO1. In this free-ligand bond structure, the heme cofactor located inside the enzyme interacts by an electrostatic interaction with the residue K377 of the loop. This lysine could thus have a role in the lability of the cofactor. Since the information on the conformation of the loop is recent, the folding mechanism in presence or absence of substrate remains still unclear. To clarify the latter, it would be necessary to obtain the conformation of the JK-loop according to several intermediate positions of L-Trp when it enters the active site. The presence of substrate could also stabilize the loop and improve its refinement. Although several reaction snapshots showing the protein in the presence of L-Trp were recently generated by Molecular Dynamics [7], the first intermediate position of L-Trp by crystallography was obtained by Pham *et al.* [8] in 2021. However, the dynamic loop was still only partially refined in their structure. Thus, the study of L-Trp along the reaction pathway characterized by the fully refined JK-loop was the next step to improve the understanding of the refolding mechanism of the JK-loop and help to the design of new drugs.

In the present study, three new crystal structures of hIDO1 (resolution values of 2.30 Å, 2.50 Å, and 2.50 Å) were refined in ferrous state with L-Trp inside the active site. L-Trp is observed in different positions allowing to trace its entry in the active site as well as the evolution of the dynamic loop during this process. In order to characterize the influence of the conformation of the dynamic loop on the affinity of heme and/or L-Trp, MM-GBSA calculations were performed. Entire statistical and collection data are in Appendix D, Table D.6.

6.3.2 Positions of L-Trp inside the active site

After the analysis of a large amount of hIDO1/L-Trp co-crystals in ferrous condition using synchrotron radiation and the refinement of the data, three crystal structures, presenting different L-Trp positions in the active site, were obtained (7nge, 7p0n,

7p0r). For the clarity of the following manuscript, the structures will be renamed hIDO1-closed, hIDO1-intermediate, and hIDO1-opened, respectively. The structures present hIDO1 as a dimer of dimer, as mentioned in the literature [1]. The protein crystallizes in a holo form, with a heme group in each monomer of the asymmetric unit. Molecules of L-Trp are observed around the protein and inside the active site of three monomers, one for each structure. Since crystallization takes place under reducing conditions, it is also possible to observe the product of the reaction between hIDO1 and L-Trp, N-formylkynurenine (NFK), outside the enzyme.

The position of the L-Trp in the three active sites relative to the heme cofactor is shown in Figure 6.5. In the structure hIDO1-closed (Figure 6.5, A.), L-Trp (occupancies = 68%) is located in the so-called reactive position of the monomer A. As previously mentioned in the literature (Appendix D, Figure D.2) [9], the aromatic part of L-Trp occupies the pocket A of the active site. The indole moiety is stabilized by the hydrophobic core involving Y126, F163, F226, L234, G262, and A264. S263 forms a hydrogen bond with the nitrogen atom of the indole ring. The polar part of L-Trp is positioned in the pocket B of the active site. The residues R231, K373, and K377 bring positive charges and stabilize the carboxylate part of L-Trp. To allow this interaction, the JK-loop is closed, as detailed later. The protonated amine group of the substrate directly interacts with one carboxylate group of the heme cofactor.

In the structure hIDO1-intermediate (Figure 6.5, B.), the substrate is located in the monomer B (occupancies = 86%), in a position that is close to the one recently described by Pham *et al.* (Appendix D, Figure D.3). [8] However, unlike Pham *et al.*, no photochemical intermediate is observed in the present case. The currently observed position is thus a temporary position⁴ showing the entry of L-Trp into the active site. It mainly occupies pocket B, opened by the intermediate conformation of the JK-loop. The heme cofactor interacts with the nitrogen atom of the indole group and participates to the stabilization of the polar part of L-Trp by means of a hydrogen bond with a water molecule in interaction with the protonated amine. The carboxylate part of L-Trp is stabilized by the main chain of G236 and K238. In this case, K373 and K377 are not directly involved in the stabilization of the polar part.

⁴This term refers to the isolation in the crystallographic structure of a positioning intermediate of L-Trp in the active site.

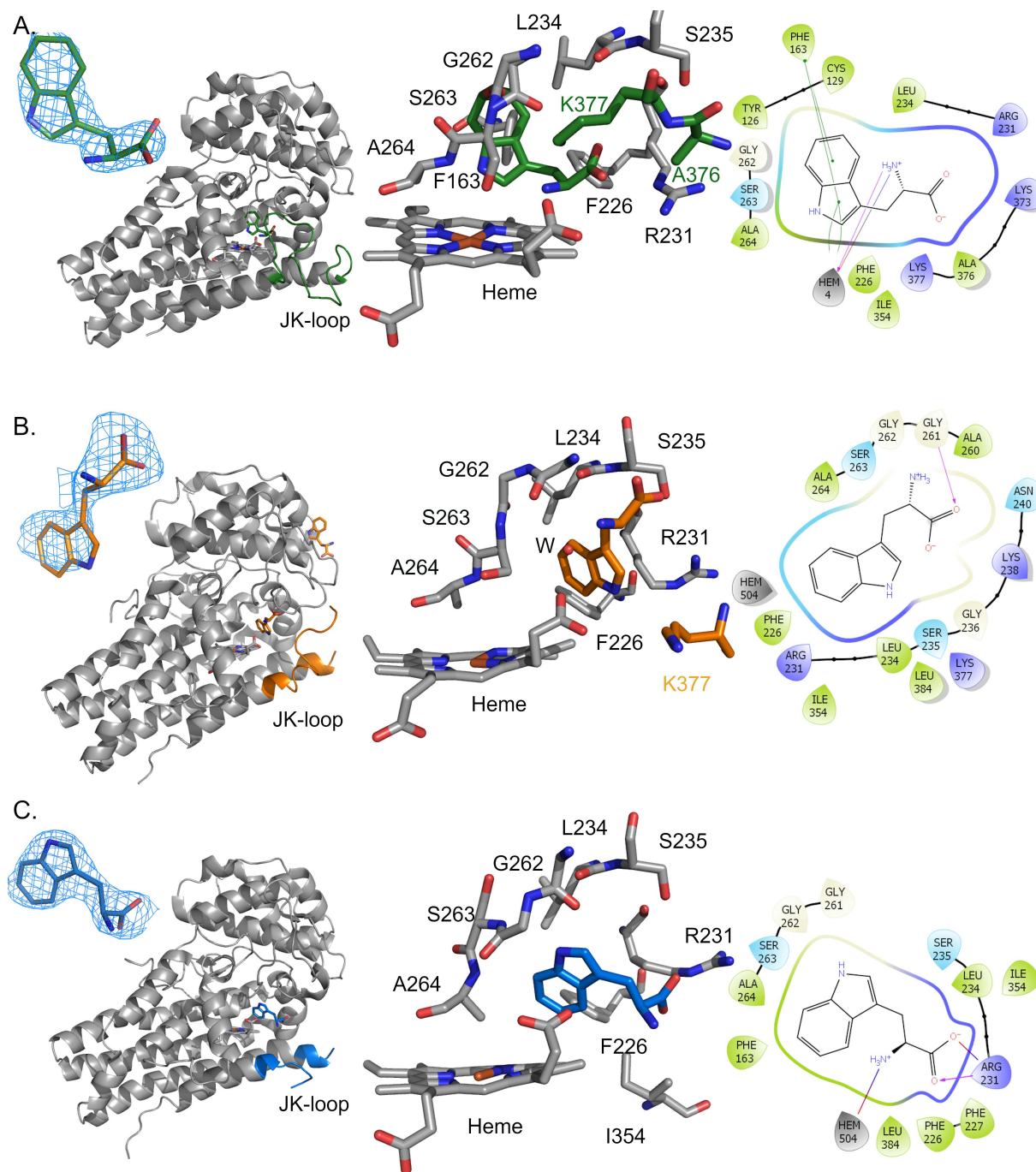


FIGURE 6.5: General view and zoom on the position of the residues in the active site with respect to L-Trp in structure A. hIDO1-closed ($\sigma = 1.0$, carve = 1.4) B. hIDO1-intermediate ($\sigma = 0.8$, carve = 1.8) C. hIDO1-opened ($\sigma = 1.0$, carve = 1.6). All interaction maps were obtained using the program Maestro.

The structure hIDO1-opened (Figure 6.5, C.) contains L-Trp in monomer C with an occupancies of 87%. The molecule is not positioned in a reactive position but in another intermediate position which is less well oriented position with respect to the active site. This position has never been reported in any other crystal structure but is very close to the metastable positions resulting from the MD analysis of Greco *et al.* [7] Consequently, L-Trp lies in pockets B and C and does not have access to pocket A. The stabilization of the indole ring of L-Trp is mainly achieved by the heme cofactor. Concerning the polar part, the heme cofactor interacts directly with the protonated amine while R231 is involved in an electrostatic interaction with the carboxylate function. In the present case, the JK-loop is located too far from the active site to contribute to an interaction with the substrate or the cofactor.

On the whole, the heme conformation is not totally planar in order to interact with the ligand in the case of the two temporary intermediate positions. Such a distortion is known for other hemoproteins but has never been highlighted for hIDO1 [10].

6.3.3 Conformation of the JK-loop according to the L-Trp position

Depending on the relative position of L-Trp with respect to the active site and the heme cofactor, the dynamic loop adopts different conformations. In the case of the hIDO1-closed structure (Figure 6.6, A.), a closed loop is observed with very little surface opening (Figure 6.6, B.). The mean B-factor for the loop in a closed position in presence of L-Trp amounts to 94 \AA^2 . This value is 16 \AA^2 lower than the ligand-free structure (PDB code: 7a62, 110 \AA^2), and is totally acceptable in comparison to the average of B-factor on the whole structure (56.5 \AA^2). It suggests that the presence of L-Trp in the reaction position and the closure of the loop lead to a large stabilization of the loop compared to the previously published ligand-free structure. [1]

In such a closed conformation of the C-terminal part of the loop, K377 adopts two distinct conformations according to the location of L-Trp (Figure 6.6, C.). When L-Trp is inside the active site, K377 is oriented toward the substrate (K377 (A) in green with an occupancies of 83%) which is stabilized. The distances between the nitrogen atom of K377 and the two oxygen atoms belonging to the carboxylate group of L-Trp amount to 3.0 \AA and 3.6 \AA . In this position, K377 brings a positive charge near the carboxylate of the cofactor. The distances between the nitrogen atoms of K377 and

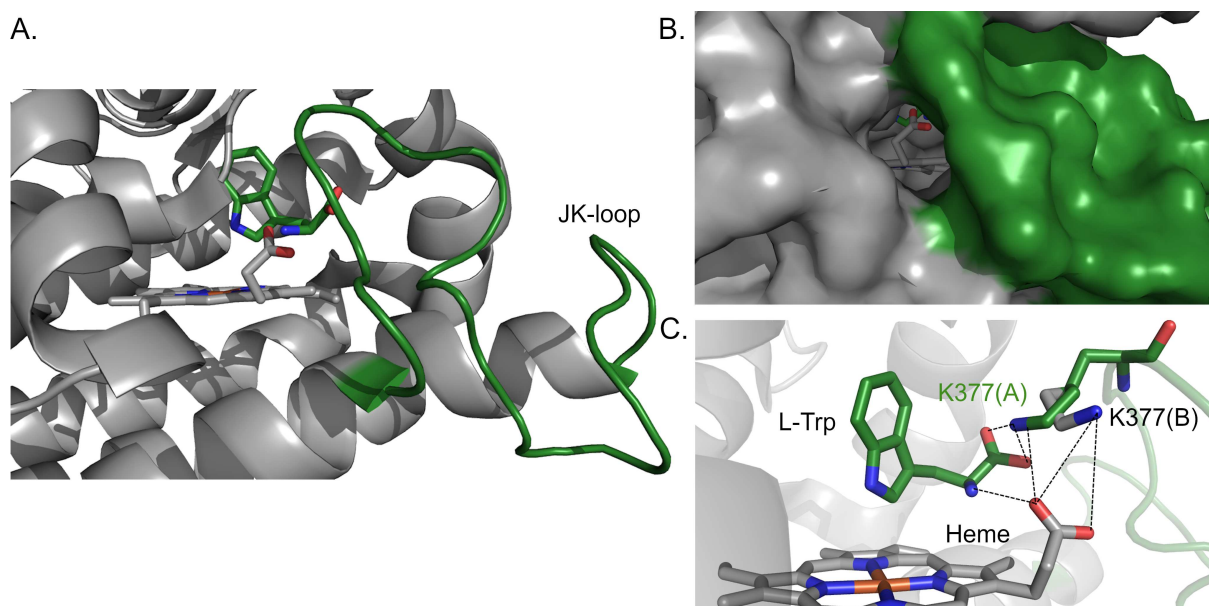


FIGURE 6.6: JK-loop in monomer A of hIDO1-closed structure A. Relative conformation of the loop with respect to the active site B. Surface of the protein with the closure of the loop C. Alternative conformations of K377 with an interaction between K377(A) (green) and L-Trp or an interaction between K377(B) (grey) and the heme cofactor.

the oxygens from the carboxylate of the heme cofactor amount to 3.1 Å and 4.8 Å. Otherwise, K377 (K377 (B) in grey with an occupancies of 17%) interacts only with the cofactor at distances between the nitrogen atom and the two oxygens of 4.0 Å and 4.7 Å, as observed in the case of the substrate-free structure. Thus, the loop has a dual role, both stabilizing the substrate and the cofactor.

In the temporary intermediate positions (Figure 6.7, A., I), a first possible conformation shows that the loop is no longer closed but is partially open, as already described by Pham *et al.* [8] It is explained by the position of the ligand which has not yet fully entered the active site. The loop has not yet fully closed. Consequently, the flexibility of the loop increases due to its partial opening. The presence of the ligand in a temporary intermediate position leads to a less stable JK-loop with a mean B-factor of 114 \AA^2 for the refined C-terminal part. The C-terminal part remains close to the active site, allowing the electrostatic interaction of the protonated amine from K377 with the carboxylate group of the cofactor, at a distance of 5.2 Å (Figure 6.7, A., II). As already mentioned in the case of the structure without ligand [1], this interaction confirms the role of lysine K377 to maintain the cofactor in its pocket during the

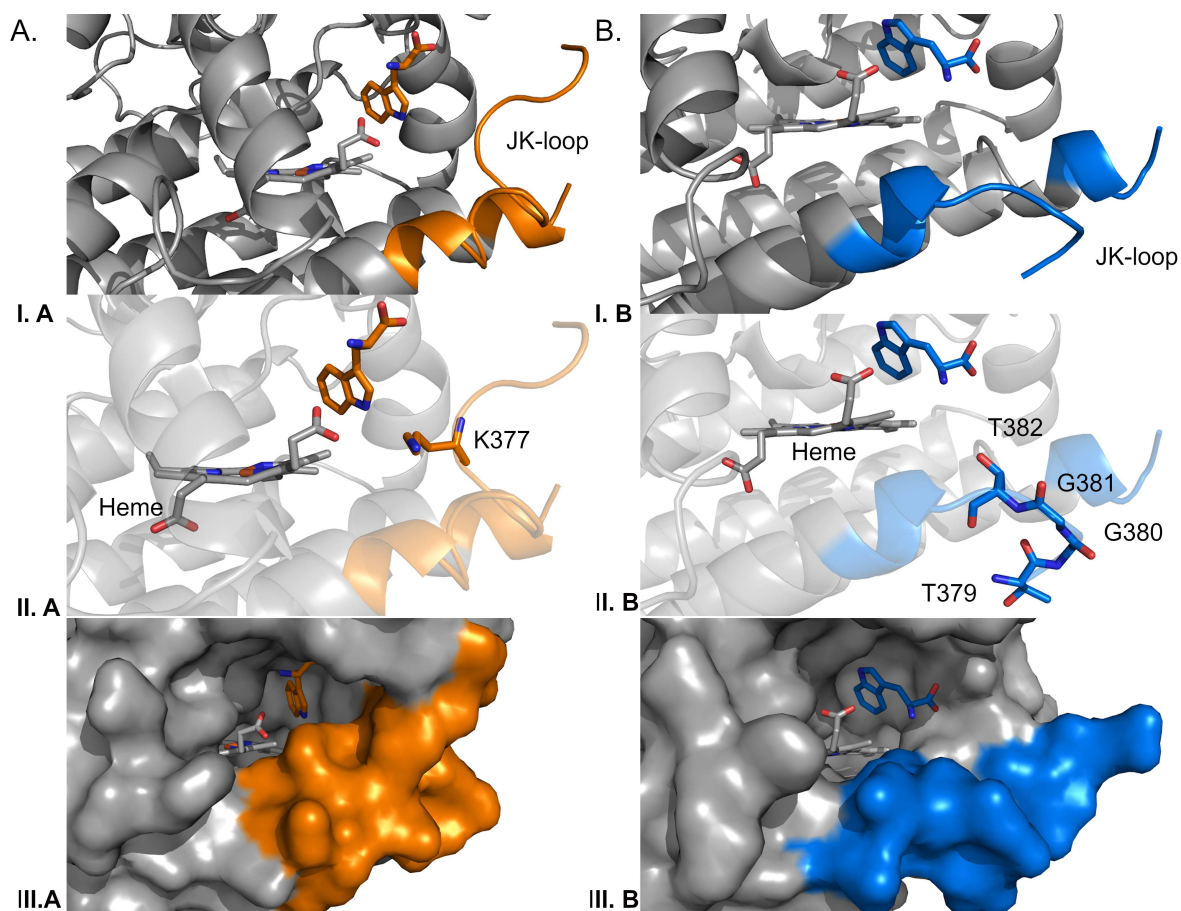


FIGURE 6.7: Conformation of the JK-loop in different states of the active site. **A. I.** Conformation of the JK-loop in hIDO1-intermediate structure according to the ligand position. **II.** Role of K377 for the interaction with the heme cofactor. **III.** van der Waals surface resulting of the partial opening of the JK-loop. **B. I.** Conformation of the JK-loop in hIDO1-opened according to the ligand position. **II.** Positioning of the C-terminal part away from the ligand. The refined fragment is from T379 to G380. **III.** Van der Waals surface resulting from the total opening of the JK-loop.

positioning of the substrate and to avoid lability of the latter. Therefore, the loop does not have any longer a role in stabilizing the substrate. In this case, due to a larger flexibility, the N-terminal part is too disordered to be refined. It may be caused by the rapid positioning of L-Trp, resulting in a fast rearrangement of the loop at the N-terminus. As a consequence, the protein surface is much more open than in the case of hIDO-closed (Figure 6.7, A., III). In the second possible conformation (Figure 6.7, B., I), the less well oriented position of L-Trp leads to a fully opened JK-loop as indicated by the fragment composed of residues T379 to T382 (Figure 6.7, B., II). Since

the ligand is not well positioned in the active site, the loop is not well refined, even at the C-terminus. The surface formed by the C-terminal part is widely open (Figure 6.7, B., III) and the A-site is hardly accessible to the ligand.

6.3.4 Influence of the JK-loop conformations on the cofactor affinity

All the above results indicate the occurrence of a strong interaction between the heme cofactor and the C-terminal part of the JK-loop. In order to evaluate the resulting affinity, MM-GBSA calculations were performed (Table 6.1). Concerning the holo protein/substrate complexes, the results highlight the same order of affinity for the different crystal positions of L-Trp with respect to the holo protein. In all cases, these negative values for the binding ΔG for the three structures support the possible observation of these temporary intermediates by crystallography. It suggests that the influence of the conformation of the loop on the substrate affinity is moderate when the orientation of L-Trp can lead to a (future) placement in a reaction position. Contrarily, the affinity of the heme for the protein is strongly influenced by the conformation of the loop. In the open-loop situation, the binding ΔG is positive, showing no affinity of the heme for the enzyme. Thus, such a conformation state favors the apo versus the holo form. When the loop is in an intermediate position (hIDO1-ligand free and hIDO1-intermediate with L-Trp), the binding ΔG for the cofactor presents a negative value which favours the holo rather than the apo form. It can be explained by the electrostatic interaction observed between K377 and the cofactor. The closure of the enzyme drastically decreases the ΔG by a factor of 10, leading to an increase of the heme affinity and, consequently, a decrease of the heme lability. This analysis supports the role of the JK-loop on the modulation of cofactor lability.

6.3.5 In summary

The dynamic loop of hIDO1 has long been a poorly understood area in the enzyme. To shed light on the reaction pathway of the protein, results obtained through X-ray diffraction experiments and MM-GBSA calculations are presented. In particular, three new crystal structures highlight three possible conformations of the JK-loop. These conformations can be related to both 1) the entry and position of the ligand in the active site, and 2) the binding of the cofactor inside the enzyme pocket involving the residue K377. Together with the MM-GBSA results, it is now clear that the conformation of the JK-loop has a fundamental role in the lability of the heme cofactor.

TABLE 6.1: MM-GBSA calculations of the different PDB structures with a partially or totally refined JK-loop. Influence of the JK-loop conformation on the affinity for L-Trp or heme cofactor. The affinity for L-Trp or heme cofactor is calculated on the basis of the position as observed in the corresponding crystal structure. In the case of the affinity of the heme cofactor, the substrate is removed from the active site during the calculation. Values of ΔG are in kcal/mol.

Structures	PDB code	ΔG between holo protein and L-Trp	ΔG between apo protein and heme
Ligand-free	7a62	/	-2.1
Closed with L-Trp	7nge	-40.6	-33.2
Intermediate with L-Trp	7p0r	-43.8	-3.9
Opened with L-Trp	7p0n	-29.8	0.7

6.4 JK-loop behavior in the presence of L-Kynurenine in the active site

6.4.1 Contextualizing the results

At this stage of the thesis, the structures of several preliminary intermediates for the reaction are known. However, no information on the exit of the product from the active site is available. As the product of the reaction has an excessive tendency to hydrolyse at room temperature and is consequently not stable, it was therefore interesting to co-crystallize hIDO1 with an analogue of the product, namely L-Kynurenine (Figure 6.8). The structure presented in this work (PDB: 7z2l) was obtained at a resolution of 2.56 Å. Entire statistical and collection data are in Appendix D, Table D.7.

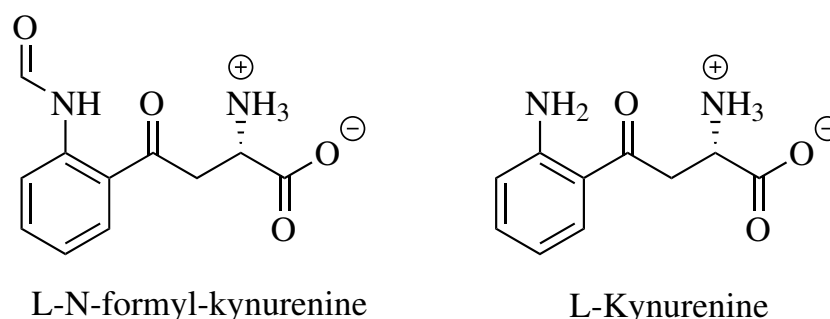


FIGURE 6.8: Structure of NFK in comparison with the structure of the product analogue (L-Kynurenine) used in the crystallographic study.

6.4.2 Overall characterization

After co-crystallization and diffraction experiments, structure with L-Kynurenine was refined and presents four molecules of L-Kynurenine around the four monomers composing the asymmetric unit. Although they are mainly located at the dimeric interfaces, one of them (Real-space correlation of 0.83) is found in the pocket B of an active site (Figure 6.9, A. and B., monomer B). This active site is also occupied by a dioxygen molecule. In this position, L-Kynurenine has an affinity of -20.0 kcal/mol calculated by MM-GBSA method.

For the molecule in the active site, the aromatic ring of L-Kynurenine can adopt two distinct positions (Figure 6.9, A.). The first (occupancies: 82%) is oriented with the aniline upward and performs interaction mainly by means of weak hydrogen bonds (distance between 3.4 Å and 3.8 Å for angles of 130°-165° from the nitrogen atom of the aniline ring) with the residues L234, S235, water and glycerol molecules (Figure 6.9, C.). For the second one (Figure 6.9, D.), less frequent (occupancies: 18%), the aniline points toward the cofactor. The ligand interacts by hydrogen bonds with the heme cofactor (2.7 Å and 159°, between N(aniline-KYN)-O1(carboxylate-Heme) atoms) and the dioxygen molecule (3.3 Å and 150°, between N(aniline-KYN)-O(O₂) atoms). To consolidate the position of the ligand in the active site, hydrogen bonds network between alcohol moiety of T379 (2.4 Å and 160°), water molecules (2.7 Å and 136°) and the carboxylate part of L-Kynurenine is established. This is strengthened by electrostatic interactions (4.0 Å) between the carboxylate functions and R231.

A molecule of dioxygen is observed in coordination with the heme cofactor. This molecule is in a position already observed for water molecules in the PDB⁵. However, it seems more likely, given the density, that it is a O₂ molecule. The presence of the dioxygen molecule leads to the induced fit of residues G262, S263 and A264 (Figure 6.9, D.). The plasticity of this fragment will be detailed in a later chapter (Chapter 8). Despite the presence of a ligand in the active site, pocket A is completely closed which prevents the evolution of L-Kynurenine closer to the heme cofactor and the fragment G262-G265.

⁵6mq6/A and 6dpq/A

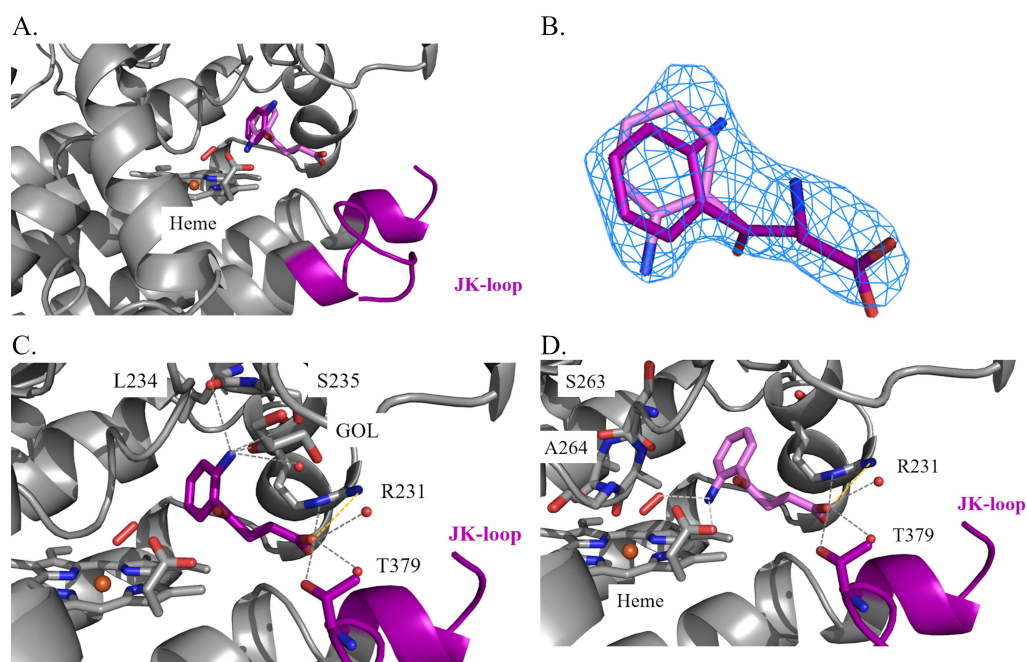


FIGURE 6.9: Binding mode of L-Kynurenine in the active site. Dynamic JK-loop and L-Kynurenine are represented in purple. Two conformations are observed for the aniline part. Conformation 1 (occupancies: 82%) is in dark purple while conformation 2 (occupancies: 18%) is in light purple. H-bonds are represented as grey dotted lines while electrostatic interactions are observed as orange dotted lines. A. Overall position of L-Kynurenine in the active site. B. Polder density map around the L-Kynurenine, represented in blue ($\sigma = 3.0$, carve = 1.6). C. Residues in interactions with L-Kynurenine in conformation 1. D. Residues in interactions with L-Kynurenine in conformation 2.

6.4.3 Influence on the dynamic loop on presence of L-Kynurenine

The position adopted by the aniline part in 82% of the cases is close to that observed by the indole group in the 7p0n structure (Figure 6.10, A.). As it had been shown by Molecular Dynamics that the ligand in 7p0n could not be positioned in the active site and had to leave the protein for better orientation [6] (detailed later in Chapter 7), this position of L-Kynurenine could therefore indicate an upcoming release of the ligand. In this mechanism, the change in orientation of the aromatic ring is an indicator for the protein of ligand exit from the active site. However, it should be kept in mind that in the case of NFK, the aniline group is replaced by a N-formyl group, which has the effect of changing the possible interactions with the protein. To verify that this observation is transposable to NFK, computational studies using Molecular Dynamics

simulations were performed.

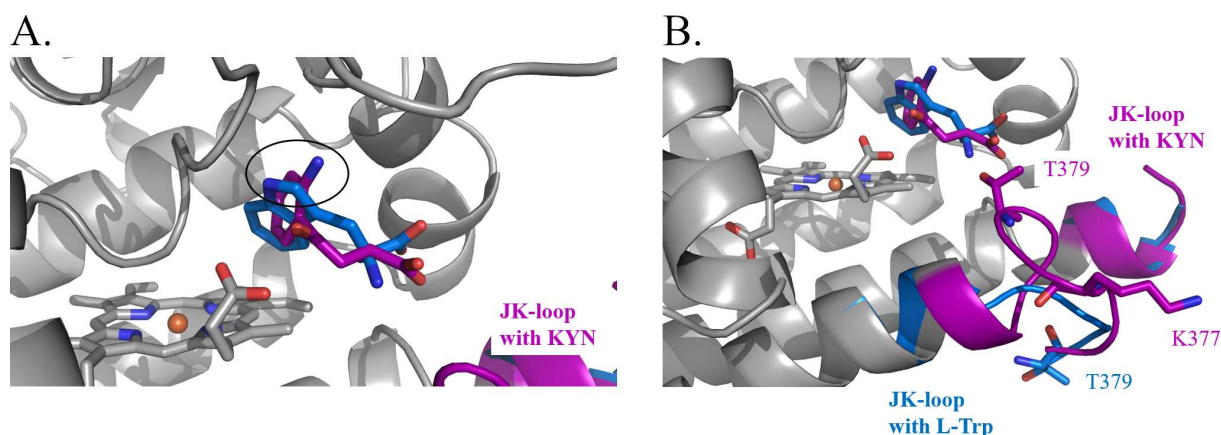


FIGURE 6.10: A. Position of aniline part of L-Kynurenine (in purple, 82% of occupancies) in comparison to the L-Trp observed in the pocket C (in blue, PDB code: 7p0n). B. Intermediate JK-loop conformation observed in presence of L-Kynurenine (in purple) in comparison of the open conformation in presence of L-Trp in the pocket C (in blue, PDB code: 7p0n).

In contrast to the two ligands, comparison of dynamic loop conformation in the 7p0n structure with one in the structure with L-Kynurenine shows a totally different behavior (Figure 6.10, B.). In the presence of L-Trp in the less well oriented position with respect to the active site, the loop is completely open and T379 points outwards. Conversely, in the presence of L-Kynurenine, the loop is in an intermediate position at the C-terminus. This results in an orientation of T379 towards the ligand. The loop is less agitated (with a mean B-factor of 104 \AA^2 for the refined C-terminal part) than in the case of 7p0n structure or 7p0R structure (with a mean B-factor of 114 \AA^2 for the refined C-terminal part). This justifies the entire refinement of the C-terminal part of the loop (L374-G380). Moreover, it is notable that K377 is not oriented towards the active site as is the case for other structures with L-Trp. In this case, the stabilization of the carboxylate part of the ligand by this amino acid is replaced by a hydrogen bridge with T379. This intermediate orientation is very similar to those observed in the literature for structures with inhibitors.

6.4.4 In summary

To sum up, for the first time, L-Kynurenine is refined in the active site of hIDO1. The ligand is observed mainly in pocket B, while pocket A is completely closed. The position of the ligand highlights two possible conformations for the aniline ring. The

first one is stabilized by weak H-bonds with the solvent, S235 and a glycerol molecule while the other one interacts with the cofactor. These two possible orientations for the aromatic part of the ligand can be used as a ratchet to open the loop. The polar part of the ligand is stabilized by R231 and T379. Concerning the JK-loop, this new structure with a product analogue highlights a novel folding of the dynamic loop. Although the refinement of the loop is partial (L374-G380), an organization in intermediary conformation is observed for the C-terminal part. However, this conformation differs from the previously described intermediate positions because it no longer involves stabilization between the cofactor and K377. The residue T379 is observed to stabilize the ligand for the first time. The observed conformation is reminiscent of that observed for the pattern with inhibitors in PDB.

6.5 Intermediate conclusions

This chapter has highlighted different structures collected during the thesis. Taken together, these results present several temporary intermediates of substrate and product positioning. These structures report conformational changes at the JK-loop due to the binding of the substrate (L-Trp) or the product analog (L-Kynurenine) in the active site compared to the structure without ligand. Thanks to this study, a first range of conformations of the JK-loop can be observed. The binding of the ligand leads to a progressive closure of the loop according to the position of the ligand. Residues K373, K377 and T379 seem to be very important in this mechanism.

However, the dynamic loops in these ligand structures of hIDO1 are not refined in all cases. Mostly, the information provided shows the C-terminal end except when L-Trp is in the reactive position or with the empty active site. In this case, a stabilization effect occurs, mixed with the favorable crystal packing, and the loop is fully refined. To complete the information of this chapter and to have a vision of the behavior of dynamic JK-loop in solution, a computational approach has been developed and is detailed in the next chapter.

Bibliography

- [1] M. Mirgaux, L. Leherte, and J. Wouters. Influence of the presence of the heme cofactor on the JK-loop structure in indoleamine 2,3-dioxygenase 1. *Acta Crystallographica Section D: Structural Biology*, 76:1211–1221, 2020.
- [2] V. B. Chen, W. B. Arendall, J. J. Headd, D. A. Keedy, R. M. Immormino, G. J. Kapral, L. W. Murray, J. S. Richardson, and D. C. Richardson. Molprobity: all-atom structure validation for macromolecular crystallography. *Acta Crystallographica Section D: Biological Crystallography*, 66(1):12–21, 2010.
- [3] C. B. Aakeroy, D. L. Bryce, G. R. Desiraju, A. Frontera, A. C. Legon, F. Nicotra, K. Rissanen, S. Scheiner, G. Terraneo, P. Metrangolo, et al. Definition of the chalcogen bond (iupac recommendations 2019). *Pure and Applied Chemistry*, 91(11):1889–1892, 2019.
- [4] S. Luo, K. Xu, S. Xiang, J. Chen, C. Chen, C. Guo, Y. Tong, and L. Tong. High-resolution structures of inhibitor complexes of human indoleamine 2, 3-dioxygenase 1 in a new crystal form. *Acta Crystallographica Section F: Structural Biology Communications*, 74(11):717–724, 2018.
- [5] J. Yu, Y. Zhou, I. Tanaka, and M. Yao. Roll: A new algorithm for the detection of protein pockets and cavities with a rolling probe sphere. *Bioinformatics*, 26(1):46–52, 2010.
- [6] M. Mirgaux, L. Leherte, and J. Wouters. Temporary intermediates of l-trp along the reaction pathway of human indoleamine 2, 3-dioxygenase 1 and identification of an exo site. *International Journal of Tryptophan Research*, 14:1–11, 2021.
- [7] F. A. Greco, E. Albin, A. Coletti, D. Dolciami, A. Carotti, C. Orabona, U. Grohmann, and A. Macchiarulo. Tracking Hidden Binding Pockets Along the Molecular Recognition Path of l-Trp to Indoleamine 2,3-Dioxygenase 1. *ChemMedChem*, 14(24):2084–2092, 2019.
- [8] K. N. Pham, A. Lewis-Ballester, and S.-R. Yeh. Conformational plasticity in human heme-based dioxygenases. *Journal of the American Chemical Society*, 143(4):1836–1845, 2020.

- [9] A. Lewis-Ballester, K. N. Pham, D. Batabyal, S. Karkashon, J. B. Bonanno, T. L. Poulos, and S.-R. Yeh. Structural insights into substrate and inhibitor binding sites in human indoleamine 2, 3-dioxygenase 1. *Nature communications*, 8(1):1–8, 2017.
- [10] S. Neya, M. Suzuki, T. Hoshino, H. Ode, K. Imai, T. Komatsu, A. Ikezaki, M. Nakamura, Y. Furutani, and H. Kandori. Molecular insight into intrinsic heme distortion in ligand binding in hemoprotein. *Biochemistry*, 49(27):5642–5650, 2010.

Chapter 7

The JK-loop plasticity study by Molecular Dynamics from crystallography snapshots

7.1 Introduction

For several reasons, the structural characterization of the JK-loop by crystallography is not sufficient. Indeed, although the C-terminal part can be refined in all cases, some ligands make the loop so agitated that it is no longer possible to refine the N-terminus. On the other hand, the low quality of some diffraction maps (PDB: 7a62) requires support by other methods of observation. Concerning the structures with ligands, a structure was obtained with an analog of the product (L-Kynurenine) since the product (NFK) is not commercially available. However, there is currently no evidence that the protein behaves similarly in solution in the presence of both ligands. Finally, crystallography gives a solid state version, rigidified by packing, of the system. One could ask if the conformation observed by crystallography for the structures without ligand (PDB: 7a62) or with L-Trp in reaction position (PDB: 7nge) are close to the behavior in solution. To address these questions, the crystallographic analysis was complemented by Molecular Dynamics analyses.

7.2 JK-loop behavior without ligand in the active site

This part was written on the basis of the article "Influence of the presence of the heme cofactor on the JK-loop structure in indoleamine-2,3-dioxygenase-1" published in 2020 by M. Mirgaux in *Acta. D. Crystallography*. [1] As already mentioned, the part included in the present manuscript is presented without modification of structure or content from the original literature. Any additional information concerning the methods can be found in the associated literature.

7.2.1 Structural comparison of the holo and apo forms

The first step of the work, after the methodological considerations (detailed in Appendix B), was to characterize the JK-loop in the absence of ligand on the basis of the structure respectively obtained under the same conditions by crystallography. Since the density maps obtained by crystallography are not defined around lateral chains, it allows to bring weight to the crystallography study and to compare the solvated systems obtained by MD with the structure in the solid state. In order to investigate the dependence of the JK-loop conformation on the heme group, MD simulations were performed with and without the cofactor. In the simulation with the cofactor,

this latter remains free to move in order to be consistent with its reported lability. [2, 3] In this way, the covalent bond was not rigidly established between histidine and the ferrous ion. However, the orientation of H346 in relation to the heme cofactor remains mostly well oriented during the dynamics, with a more relaxed distance of $3.6 \pm 0.4 \text{ \AA}$ (more information in Appendix B). During the production stage, the simulations illustrate the independence in conformations of the C-terminal extremity of the JK-loop in relation to the N-terminal extremity.

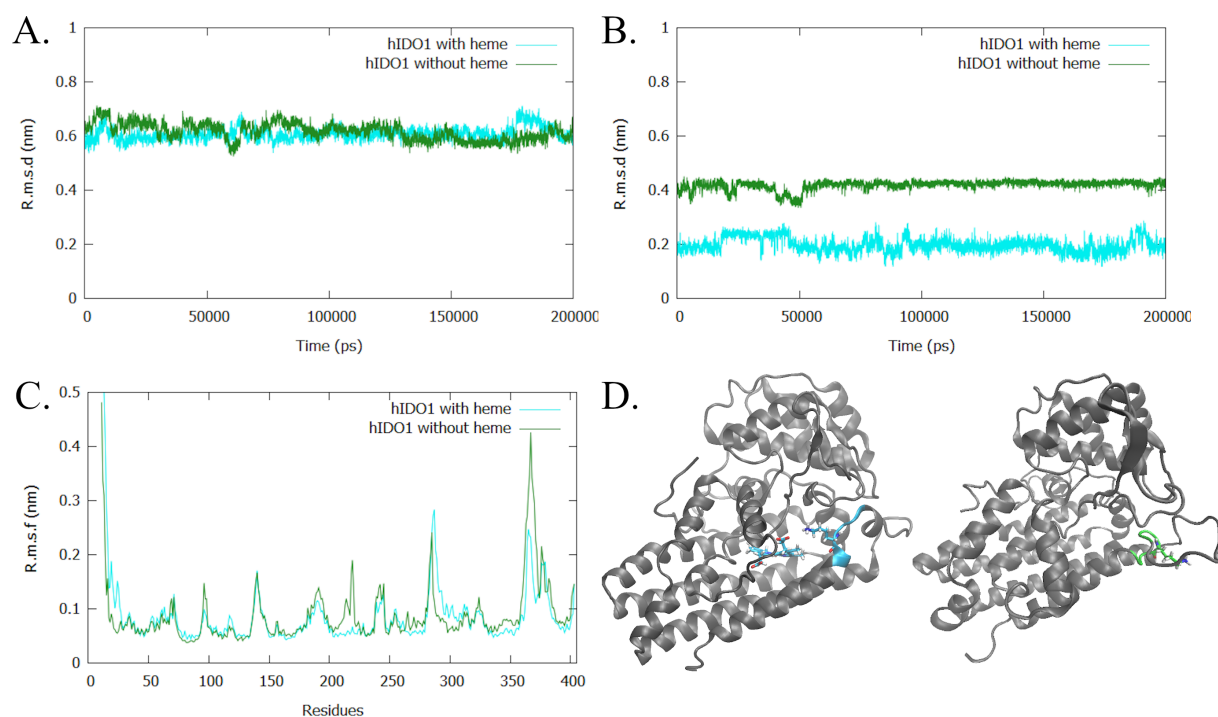


FIGURE 7.1: Impact of the heme cofactor on the JK-loop conformation (with the cofactor (cyan), without the cofactor (green)). A. R.m.s.d analysis of the JK-loop according to the cofactor occupancy in comparison to the starting conformation. B. R.m.s.d of the C-terminal part of the JK-loop according to the cofactor occupancy in comparison to the starting conformation. C. R.m.s.f analysis of the residues of the protein. D. Conformation of the JK-loop on the C-terminal part according to the presence of the heme cofactor. The opening of the JK-loop is illustrated with the heme (left) and without the heme (right) as obtained from 200 ns of MD simulation at 310 K and 1 bar.

For simulation with the cofactor, the simulated conformations present only slight differences at the level of the C-terminal part of the loop compared to the crystallographic structure (Figure 7.1, B. and Appendix D, Figure D.4). Without the cofactor, the differences between the simulations and the crystallographic structure are more significant in terms of Root Mean Square Displacement (r.m.s.d) deviation (Figure 7.1, B. and Appendix D, Figure D.4). The N-terminal part changes its conformations during the MD simulations (Figure 7.2, A.) as observed with high r.m.s.d values.

The Root Mean Square Fluctuation (r.m.s.f) and r.m.s.d profiles (Figure 7.1, A., B. and C.) confirms that the JK-loop has a significant dynamical character as recorded in experimental structures. The conformation of the C-terminal part of the loop (considered between E375 and G380) is linked to the presence of the heme cofactor. In presence of the heme cofactor, lysine K377 is oriented towards the active site (Appendix D, Figure D.5). The average distance between K377 and the carboxylate of the heme cofactor amounts to $6.8 \text{ \AA} \pm 2.4 \text{ \AA}$ and $6.9 \text{ \AA} \pm 2.4 \text{ \AA}$. To characterize the JK-loop opening as a function of the presence of the cofactor, the distance between K377 and A264, located above the heme moiety, is chosen as a criterion. In the simulated structure with the heme cofactor, the mean distance between the atoms CB of A264 and NZ of K377 amounts to $12.5 \text{ \AA} \pm 2.3 \text{ \AA}$. The standard deviation highlights a variability in the location of the lysine K377. In comparison to previous results reported in the literature by Alvarez and coworkers [4], the most recurrent conformation of the JK-loop in the C-terminal extremity can be considered as intermediate conformation, between closed and open, (Figure 7.1, D. and Appendix D, Figure D.5). In the absence of the heme cofactor, K377 is oriented towards the solvent with the amine group pointing towards the outside of the enzyme (Appendix D, Figure D.5). Without the heme moiety, the distance between the atoms CB of A264 and NZ of K377 considerably increases to $25.5 \text{ \AA} \pm 1.3 \text{ \AA}$. Thus, this displacement of K377 is seen as a stage that initiates the opening of the JK-loop (Figure 7.1, D.).

Regarding the N-terminal part (Q360-L374), the MD simulations support the high flexibility of this part of the loop as illustrated by the larger r.m.s.d values than for the C-terminal part (Figure 7.2, A.). Conformational differences are detected between the crystallographic structure and the MD structures. In the presence of the heme cofactor, the conformation of the N-terminal part is close to the α -helix D, leading to a more compact protein (Figure 7.2, C.). Hydrogen bonds (1.3 ± 1.0) are established

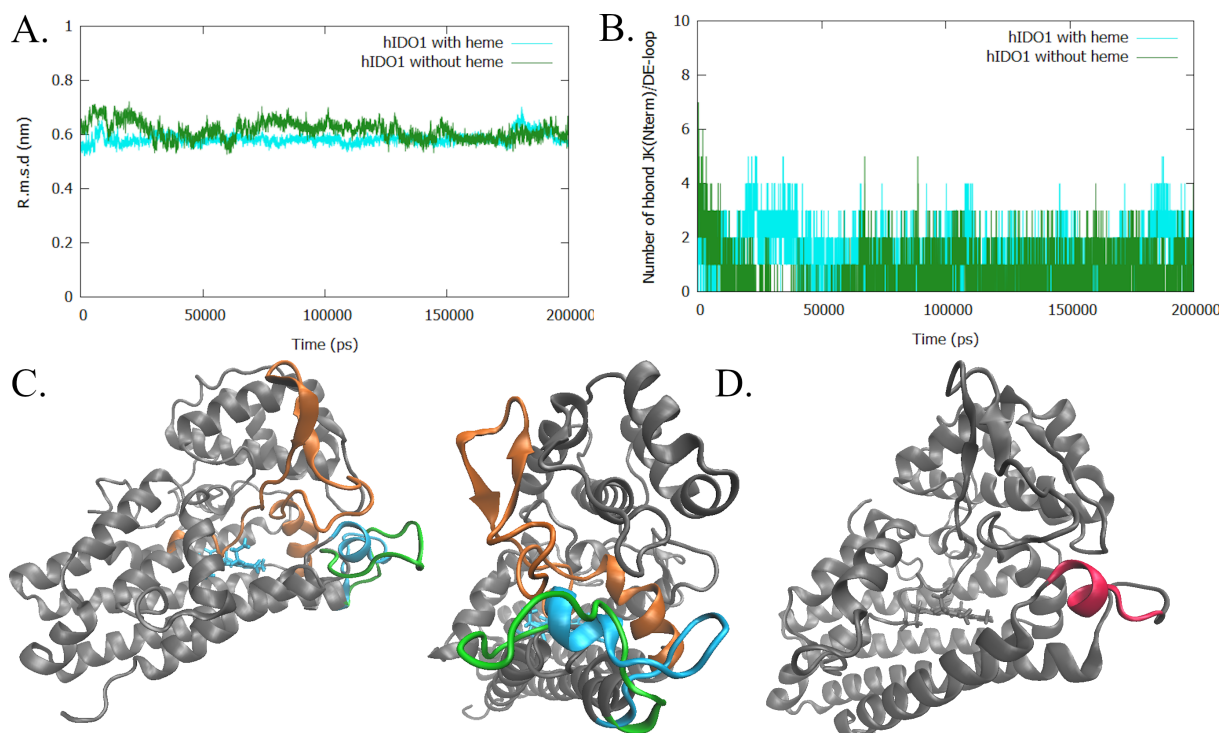


FIGURE 7.2: Impact of the heme cofactor on the JK-loop conformation on the N-terminal part (with the cofactor (cyan), without the cofactor (green), DE-fragment is coloured in orange). A. R.m.s.d profiles of the N-terminal part (Q360-L374) of the JK-loop according to the cofactor occupancy in comparison to the starting structure. B. Hydrogen bonds pairs (cut-off value of 3.5 Å and angle of 30 degrees between the hydrogen, the donor and the acceptor) analyses for residues Q360 to L374, per frame of 20 ps. C. Conformation of N-terminal extremity according to the presence of heme cofactor with frontal view (left) and lateral view (right) as obtained from 200 ns of MD simulation at 310 K and 1bar. D. Conformation of helix between S369 to E375 (red) in simulation with heme cofactor as obtained from 200 ns of MD simulation at 310 K and 1 bar.

between the two fragments (Q360-L374 for the JK-loop and K224-V269 for the α -helix D, Figure 7.2, B.). Consequently to this compact conformation, few hydrogen bonds are observed between the N-terminal fragment and the solvent (45.5 ± 4.8). Contrarily, in the simulated apo-enzyme, the loop extends from the enzyme into the solvent (Figure 7.2, C.). Thus, few hydrogen bonds (0.7 ± 0.9) are observed between the N-terminal extremity and the DE-fragment (Figure 7.2, B.) but more hydrogen bonds are established between the solvent and this part of the JK-loop (55.5 ± 4.2). Conformation variability of the N-terminal extremity may be essential for the protein. With this simultaneous opening of the C-terminal and the N-terminal extremities in

absence of the cofactor, the protein pocket B is open and allows a free heme cofactor to enter in the active site. Consequently, the N-terminal part of the loop regulates hIDO1 activity. Similar hypothesis is consistent with the heme lability and the incorporation of a L-Trp in the inhibitor site in absence of the heme cofactor. At last, independently from the presence or the absence of the cofactor, the N-terminal extremity involves the folding of residues E369 to E375 into a short helix stabilized by an increased number of hydrogen bonds (Figure 7.2, D.). This folding (Figure 7.2, D.) indicates the possible structural organization of the segment despite its flexibility.

7.2.2 Contribution of MD simulation to the structural study

Through the analysis of Molecular Dynamic (MD) trajectories, the flexibility of the JK-loop was quantified by r.m.s.d and r.m.s.f profile analyses. Simulation with a potentially labile heme cofactor leads to a structure consistent with the crystal structure, the heme remaining stabilized in its position by interactions with lysine K377. The lack of a heme cofactor induces (1) an opening of the C-terminal extremity of the JK-loop, starting at K377 as indicated by the increase by a factor of 2 of the distance between A264 and K377 (2) a transfer of hydrogen bonds from the DE-fragment to the solvent molecules at the level of the N-terminal extremity. Regarding the N-terminal part of the JK-loop, a helix-type folding of residues E369 to E375, stabilised by an increased number of hydrogen bonds is observed, independently from the presence or the absence of the cofactor.

7.3 JK-loop behavior with L-Trp in the active site

This part was written on the basis of the article "Temporary Intermediates of L-Trp Along the Reaction Pathway of Human Indoleamine 2,3-Dioxygenase 1 and Identification of an Exo Site" published in 2021 by M. Mirgoux in *International Journal of Tryptophan Research* [5]. For the fluidity of the reading, only the essential information is included in the present manuscript without modification of structure or content of the original literature. Any additional information concerning the methods can be found in the associated literature.

7.3.1 Structural comparison of the different snapshots

Following the different structures obtained with temporary intermediates of L-Trp in the active site, MD simulations were carried out to study the behavior of the solvated dynamic loop depending on different ligand positions in these crystal structures. The MD simulations were run for the three crystal structures obtained with L-Trp in the previous chapter over 300 ns, at 310 K and 1 bar. The structure with L-Trp in the reactive position with a fully refined closed loop (7nqe) was studied on the basis of crystallographic coordinates. In the two crystal structures with intermediate positions for the L-Trp (7p0n and 7p0r), the loop was not completely refined. Thus, the protein structure was first reconstructed by homology.

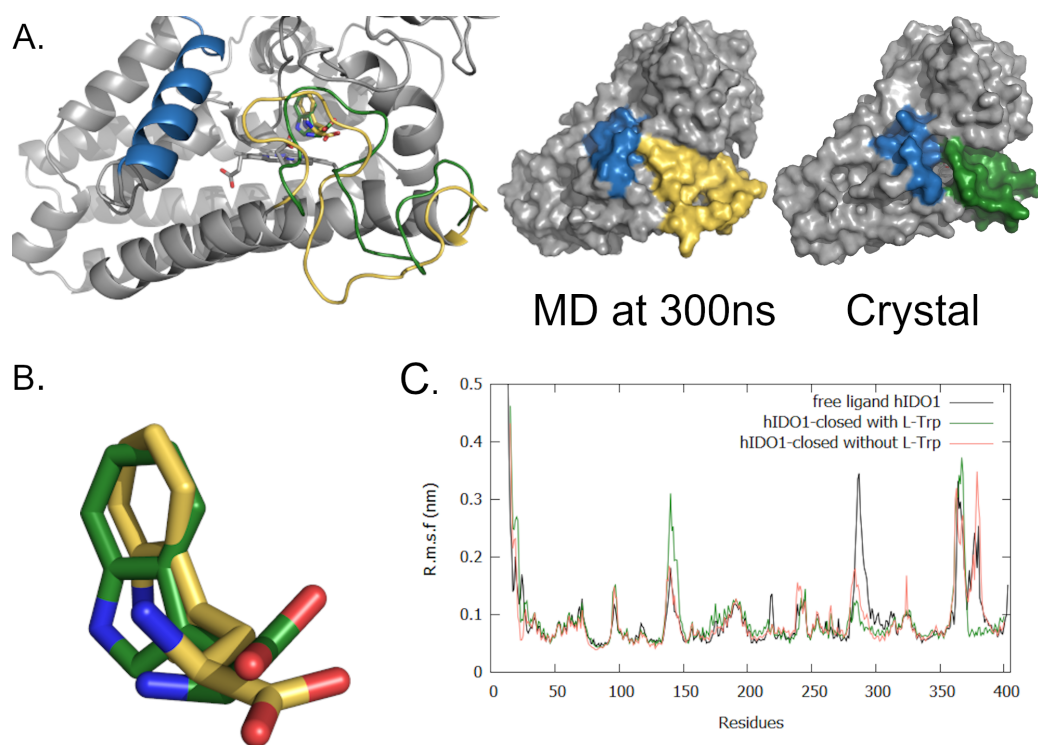


FIGURE 7.3: Molecular Dynamics studies of hIDO1-closed as obtained from 300 ns simulation at 310 K and 1 bar. A. Final conformation of the JK-loop compared to the hIDO1-closed crystal structure. Induced fit of the JK-loop in hIDO1-closed during the MD production stage in comparison to the crystal structure, respectively in green and yellow while the helix F is in blue. B. Superposition of the L-Trp conformation in the hIDO1-closed crystal structure (in green) and as obtained from 300 ns of MD simulation (in yellow). C. R.m.s.f analyses of hIDO1-closed (with and without ligand) in comparison to free-ligand hIDO1 MD studies [1].

The analysis of the 300 ns hIDO1-closed MD trajectory highlights that L-Trp does not significantly move during the simulations (Figure 7.3, A. and B.). Consequently, the distance between the protonated amine of L-Trp and the carboxylate group of the cofactor amounts to 3.6 ± 1.0 Å. This is close to the distance of 3.0 Å observed experimentally by crystallography. The conformation of the loop observed from a 300 ns-MD trajectory with L-Trp is consistent with the starting closed-structure resulting from crystallographic experiments. Nevertheless, a slight induced fit is observed (Figure 7.3, A.) wherein the last turn of the K helix is deconstructed in contrast to the experimental structure. It leads to a complete closure of the protein surface by bringing the JK-loop closer to the helix F (residues 286 to 300). Residue T379 directly interacts with residue D394 in the helix F (Figure 7.4). The MD simulation confirms the presence of an interaction, described by Greco *et al.*, between the JK-loop and the helix F. [6] Due to the complete closure, the K377/ heme interaction is lost at 300 ns. However, it is hypothesized that the closure preserves enough heme inside the active site to avoid the need of the stabilizing K377/heme interaction. During the MD simulation, K377 moves to assist the stabilization of the substrate. Particularly, the distance between the two oxygen atoms of L-Trp and K377 varies over the 300 ns, with an average of 4.1 ± 1.1 Å for O1 and 5.8 ± 1.2 Å for O2 from L-Trp, in comparison to the 3.0 Å and 3.6 Å observed in the crystal structure. On the whole, the results of the simulations confirm the stabilization of the C-terminal part for the loop as observed in crystallography. Indeed, the r.m.s.f analysis of the C α atoms (Figure 7.4, C., green) of the protein shows a stable and non-agitated loop for the C-terminal part compared to the results already published for the protein without ligand (Figure 7.4, C., black). [1] When a MD simulation is performed without L-Trp but with the same starting closed conformation for the loop, the flexibility of the C-terminal part is recovered (Figure 7.4, C., pink). This mobility increase comes from a reopening of the enzyme, leading to an intermediate conformation of the JK-loop in the absence of ligands (data not shown). It thus suggests that the ligand is essential for a stabilization of the JK-loop.

In the same way as the 300 ns-MD simulation with L-Trp in the closed conformation, two other 300 ns-MD simulations were performed with structures with the JK-loop in intermediate and opened conformations as starting points. First, the 300 ns-MD trajectory for hIDO1 with the JK-loop in the intermediate conformation shows a total reorganization of the loop and ligand position, leading to a drastic increase

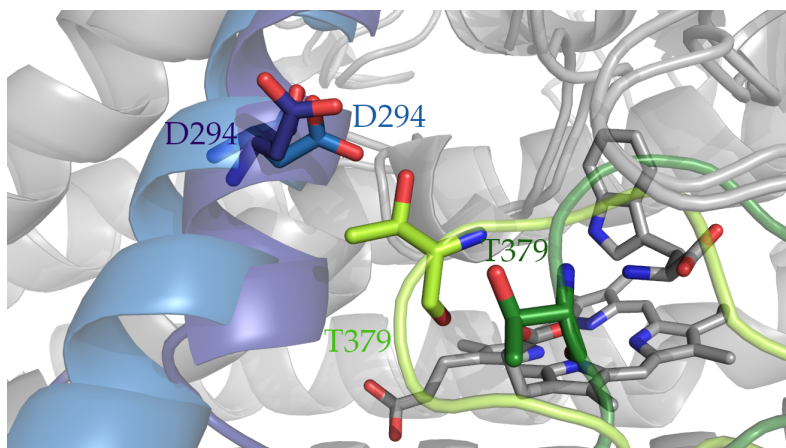


FIGURE 7.4: Interaction between T379 and D294 resulting from the induced fit during the 300 ns MD simulation at 310 K and 1 bar. The green position of T379 is the position observed by crystallography while the lemon/yellow position is the final position after 300 ns of MD simulation. Helix F are represented in blue.

of the r.m.s.f values for the C-terminal part of the loop (Figure 7.5, A.). The L-Trp stays relatively mobile until it finds its definite position within the active site (Figure 7.5, B. and C.). The position closest to the reactive state position in the active site is considered as an additional intermediate position of L-Trp (Figure 7.5, C., in yellow). This position is stabilized after 200 ns until the end of the simulation. During its migration, the distance between the protonated amine of L-Trp and the heme cofactor varies with an average of $3.8 \pm 1.3 \text{ \AA}$. The displacement of L-Trp leads to the displacement of the JK-loop. The access to the active site of the protein gradually closes. In this intermediate conformation of the JK-loop, K377 points outwards the enzyme. However, the cofactor is maintained in the active site due to the establishment of an interaction between K373 and the substrate acting as a network between the JK-loop, the substrate and the heme (Figure 7.5, C., left). The simulation starting from the reconstructed hIDO1-opened structure does not show the same displacement trend due to the fact that L-Trp does not undergo a full 180° rotation around its initial position. The improper orientation of the indole ring with respect to the heme cofactor and the closure of the pocket A prevent the displacement of L-Trp in the active site. Consequently, L-Trp remains in its position and the JK-loop is still open. In a biological context, it is hypothesized that L-Trp would potentially slightly exit the enzyme to rotate and to re-enter in the correct orientation.

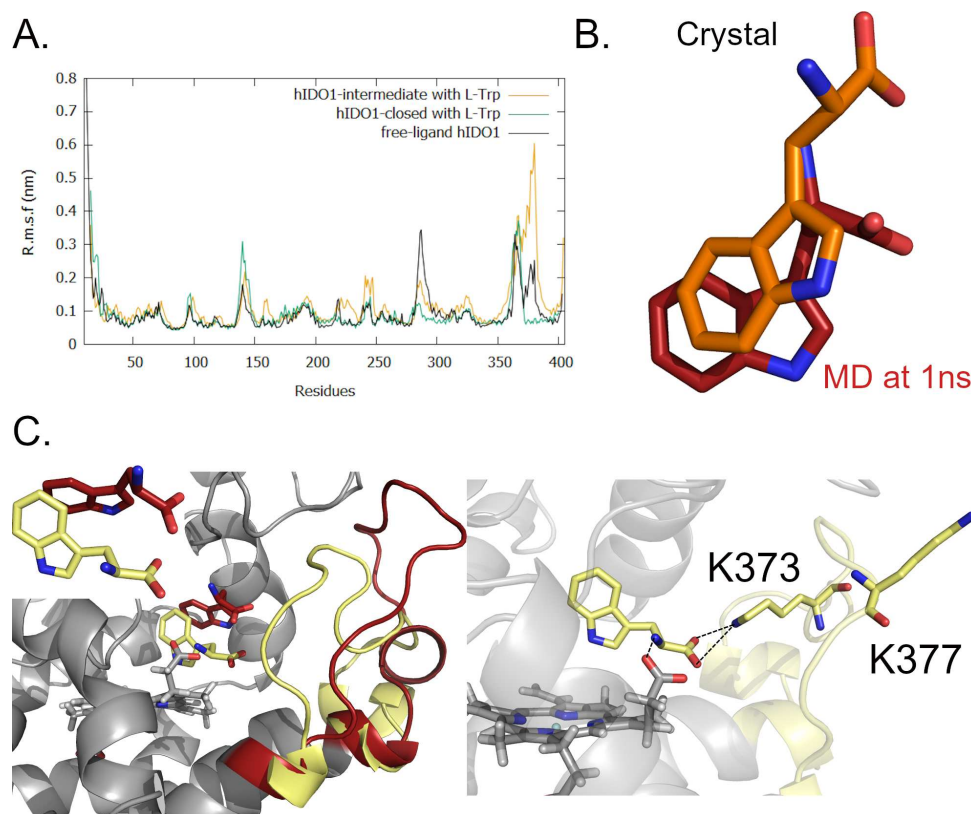


FIGURE 7.5: MD snapshots as obtained from a 300 ns MD simulation at 310 K and 1 bar with hIDO1-intermediate as the starting point. A. R.m.s.f analyses of hIDO1-intermediate in comparison to the free-ligand hIDO1 and hIDO1-closed simulations. B. Position of L-Trp at 1ns of production (in red) in comparison to the position observed in the crystal structure (in orange). C. Left - Two MD snapshots of the displacement for the JK-loop during the production stage after 1 ns (in red) and after 300 ns (in yellow). Right - Interaction between L-Trp and K373 after 300 ns in yellow. Loss of contact between the heme and K377.

7.3.2 Contribution of MD simulation to the structural study

A comparison of the three crystal structures, superimposed to the MD conformations illustrating transient intermediate positions of L-Trp allows to propose a possible re-folding trajectory for the JK-loop. When L-Trp enters in the active site of hIDO1, the loop is first open (Figure 7.6, A., I.). L-Trp adopts a temporary intermediate position which corresponds to position 1 or position 2 (Figure 7.6, B.) in crystallography. In the case of position 1, it must first perform a 180° rotation to allow a better anchoring of the substrate in the active site to shift in the A-pocket. As a result, the loop changes

from an open to an intermediate conformation (Figure 7.6, A., II and III). This conformation is close to the conformation of the loop in the ligand-free structure. Stabilizing interactions are likely established between the loop, L-Trp and the cofactor to allow the confinement of the heme and the substrate into the active site (Figure 7.6, C.). The substrate is displaced into pocket A, through a movement from position 2 to position 3 and then 4 (Figure 7.6, B.) through favorable hydrophobic stabilizations. The stabilization of the L-Trp in this final position allows the closure of the active site (Figure 7.6, A., IV.).

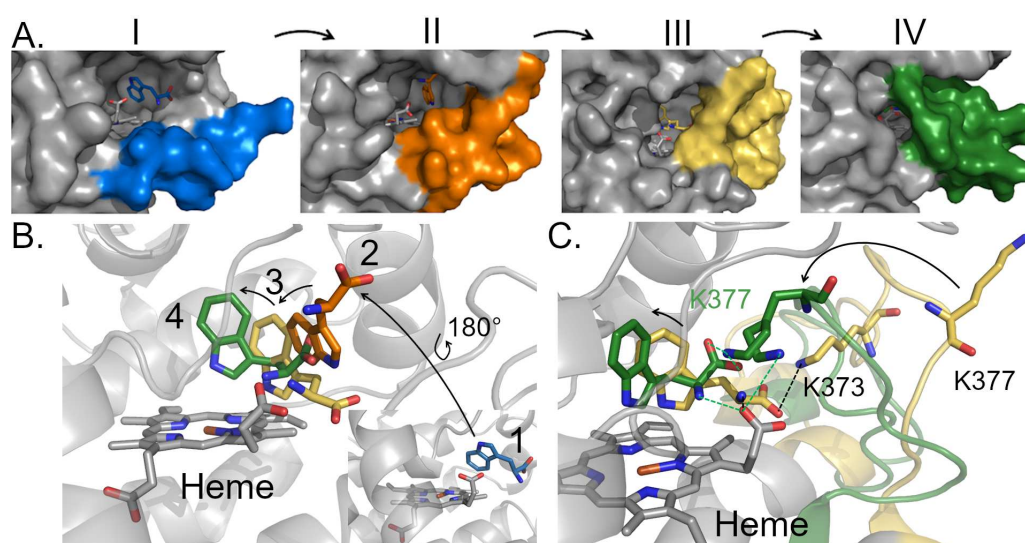


FIGURE 7.6: Superposition of the different conformations for the JK-loop in the three PDB structures and the MD simulations. The structure hIDO1-closed is in green, hIDO1-intermediate in orange and hIDO1-opened in blue. Structures from MD simulation after 300 ns are in yellow. A. JK-loop opening according to the different structures. B. Trajectory of L-Trp in the different structures. C. Interactions network between the JK-loop, the substrate and the heme to maintain the cofactor in the active site in the MD simulation and in hIDO1-closed structure.

If a dioxygen molecule is previously bound to the iron ion under the right oxidation-redox conditions, the reaction can take place. After reaction, it is suggested that less favourable interactions with the product of the reaction lead to the opening of the loop and the release of the product. To conclude, in this study, MD trajectories have supported the existence of these conformations of the JK-loop in solution and revealed additional snapshots at the three temporary intermediates observed in crystallography. The set of these five positions allowed a better understanding of the dynamics of the JK-loop during substrate positioning.

7.4 JK-loop behavior with L-Kynurenine or NFK in the active site

The previous section allowed to trace the displacement of the substrate in the active site. Based on this analysis, it seems important to know the behavior after the reaction for the product release. In this purpose, the dynamic loop in the structure with L-Kynurenine was completed for the missing residues, by means of a homology modeling, and a 300 ns MD simulation was performed. At first, this allows to check the validity of the crystallographic structure in solution. This also allows the comparison of the behavior between N-formyl-kynurenine and L-Kynurenine by placing an NFK molecule in the same position as the L-kynurenine molecule observed by crystallography. The MD runs were performed, for both simulations, in triplicates. Results are presented at Figures 7.7 and 7.8.

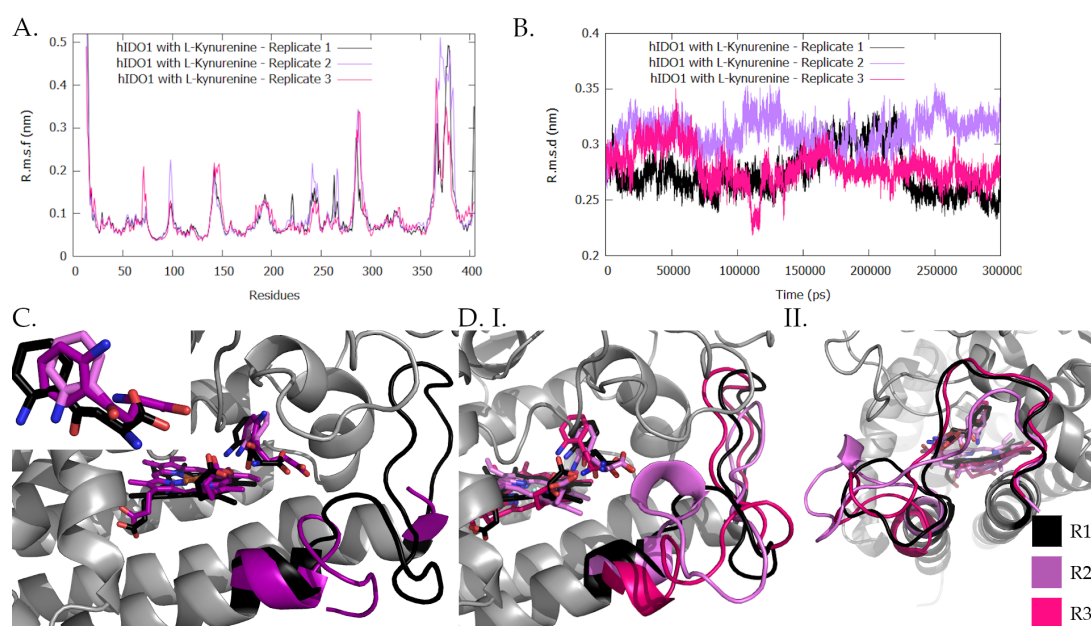


FIGURE 7.7: Molecular Dynamics studies on hIDO1 in presence of L-Kynurenine as obtained from 300 ns of MD simulation at 310 K and 1 bar for three replicates (R1 = black, R2 = violet, R3 = pink). A. R.m.s.f profiles of residues fluctuation for each replicate. B. R.m.s.d profiles in comparison to the starting conformation for each replicate. C. Final 300 ns-MD position for replicate 1 and comparison with crystal structure (in purple). Focus on the position of L-Kynurenine and the conformation of the JK-loop. D. Conformation of the JK-loop in the different replicates after 300 ns of simulation. I. Focus on the C-terminal extremity. II. Focus on the N-terminal extremity.

For the simulation with L-Kynurenine, it can be seen that the replicates are consistent with each other. The values of r.m.s.f are close, with slight differences in the flexibility of the JK-loop (Figure 7.7, A.). The divergence from the initial structure (r.m.s.d) is also of the same order of magnitude (Figure 7.7, B.). In all three simulations, the position of the ligand is similar after 300 ns (Figure 7.7, C. and D.) to the observed position B in crystallography. Although starting from position A with the aniline pointing to L234 and S235, the aromatic part of the ligand quickly its changes position to adopt position B in a stable and durable manner. The mean interaction energy of protein-ligand complexes (calculated with short-range coulomb and Lennard-Jones energies) are strongly negative with values around -240 kJ mol^{-1} with small standard deviations (R1 = $-228.7 \text{ kJ mol}^{-1} \pm 32.8 \text{ kJ mol}^{-1}$, R2 = $-254.6 \text{ kJ mol}^{-1} \pm 37.1 \text{ kJ mol}^{-1}$, R3 = $-239.6 \text{ kJ mol}^{-1} \pm 18.0 \text{ kJ mol}^{-1}$). The dynamic loop presents an intermediate conformation in the C-terminal part (Figure 7.7, D. I.). The high mobility of this part no longer shows stabilization as in the case of L-Trp. The order of magnitude of the r.m.s.f is even greater than for an empty active site (Figure 7.7, A.). Consequently, this conformation of C-terminal part fluctuates with time and replicate. In the present cases, T379 does not interact with the ligand during the simulation with an average distance of $9.3 \text{ \AA} \pm 1.1 \text{ \AA}$ between the carboxylate of the ligand and the residue and $8.9 \text{ \AA} \pm 0.9 \text{ \AA}$ between the amine of the ligand and the residue. This interaction is therefore not essential to maintain L-Kynurenine in the active site. The flexibility and the conformation of the N-terminal part is not affected by the ligand (Figure 7.7, A.) as it remains close to the DE-loop and adopts a globular folding (Figure 7.7, D. II.). Finally, the heme changes its position during the dynamics (Figure 7.7, D. I.), which was not observed in the presence of L-Trp. This indicates a possible loss of affinity and an increase in lability once the enzymatic reaction is completed.

As the L-Kynurenine remains a product analogue, simulations were performed with NFK to check if the behavior is identical. The results show that the replicates are consistent with each other in terms of overall protein folding (Figure 7.8, A. and B.). However, discrepancies may exist in the mobility of the JK-loop at the C-terminal extremity (Figure 7.8, A.). The different flexibility is explained by the variable positioning of the NFK molecule in the active site (Figure 7.8, D.). In the three simulations performed, two possible conformations are observed for the aromatic part, as was the

case in crystallography. These correspond to two possible minima for the protein-ligand complex. In the first minimum (replicate 1 with an mean ligand/protein interaction energy of $-294.0 \text{ kJ mol}^{-1} \pm 33.3 \text{ kJ mol}^{-1}$), the C=O bond of the aldehyde is oriented towards the cofactor and the G261-G265 fragment. It then performs a H-bonds stabilization with the main chain of A264 ($3.1 \text{ \AA} \pm 0.3$). On the contrary, in the second minimum, observed in replicates 2 (mean ligand/protein interaction energy of $-247.8 \text{ kJ mol}^{-1} \pm 42.8 \text{ kJ mol}^{-1}$) and 3 (mean ligand/protein interaction energy of $-196.1 \text{ kJ mol}^{-1} \pm 70.8 \text{ kJ mol}^{-1}$), the aldehyde part points to the residues L234 and S235 but do not interact with these amino acids. Stabilization of the ligand occurs by intra-interactions with the carboxylate part or amide group. The first conformation (minimum 1) with more interactions is more stable than the second one.

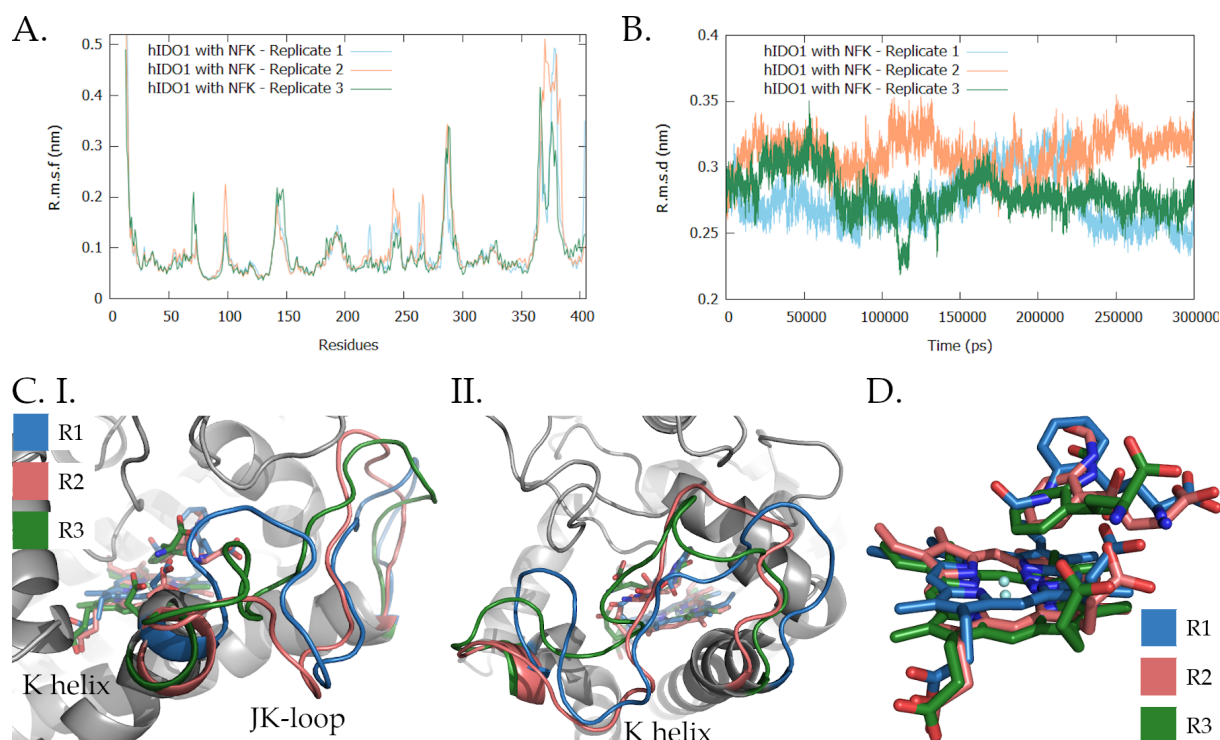


FIGURE 7.8: MD studies of hIDO1 in presence of N-formyl-kynurenine as obtained from triplicates of 300 ns of MD simulation at 310 K and 1 bar (R1 = skyblue, R2 = salmon, R3 = green). A. R.m.s.f analyses of residues fluctuation for each replicate. B. R.m.s.d analyses in comparison to the starting conformation for each replicate. C. Conformation of the JK-loop in the different replicates after 300 ns of simulation. I. Focus on the C-terminal extremity. II. Focus on the N-terminal extremity. D. Final 300 ns MD position of NFK in the different replicates according to the position of heme cofactor.

It is observed that the C-terminal end of the JK-loop is no longer shifted with the K-helix and is advanced towards the solvent (Figure 7.8, C., I. and II.). This is typical of this type of simulation. In this new organization, K377 and T379 are too far away to interact with the ligand or cofactor (Figure 7.9, A. and Appendix D, Table D.8). The stabilization of the product is then assumed by K373 (Figure 7.9, B.), whose distances are shown in Table 7.1. The N-terminus of the JK-loop is not affected by the presence of NFK and adopts a globular conformation (Figure 7.8, C., II.).

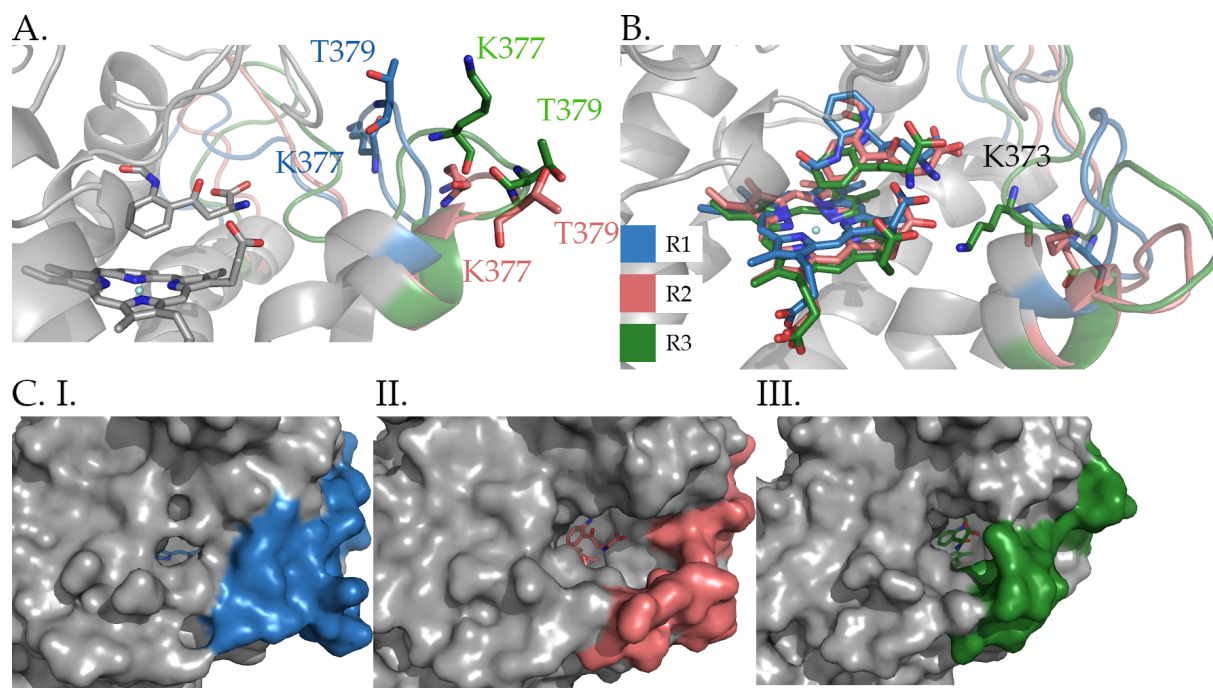


FIGURE 7.9: MD studies of hIDO1 in presence of N-formyl-kynurenine as obtained from triplicate of 300 ns at 310 K and 1 bar (R1 = skyblue, R2 = salmon, R3 = green). A. Positioning of K377 and T379 according to each replicate and the position of the cofactor/ligand. B. Positioning of K373 according to each replicate and the position of the cofactor/ligand. C. Surface opening into the different replicates.

TABLE 7.1: Mean distances and standard deviations (in Å) between K373 and the ligand. The analysis was performed on the 300 ns of simulations at 310 K and 1 bar, for each replicate.

Distances	Replicate 1	Replicate 2	Replicate 3
K373 (N) - NFK (O1)	5.4 ± 2.2	5.8 ± 1.9	5.7 ± 1.3
K373 (N) - NFK (O2)	7.4 ± 2.2	7.4 ± 1.9	5.9 ± 1.4

This movement of the C-terminal loop has the effect of opening the surface of the protein wide enough to allow the exit of the product (Figure 7.9, C.). The observed surfaces are similar over the whole dynamic range for each replicate. The degree of opening is intimately linked to the positioning of the NFK molecule. When the aldehyde is oriented towards the cofactor, the active site is closed. The conformation switch of this organic group initiates the opening, with a gradual move away from K377 and T379 (Appendix D). As replicate 2 is more open than replicate 3, chronologically, it is therefore likely to have the sequence "replicate 1 > replicate 3 > replicate 2" when the product is released. The "in-between" character of replicate 3 may explain the greater deviation of the latter in terms of ligand/protein interaction energy. Finally, the opening of the surface can be related to the motion of the JK-loop at the C-terminal extremity since the larger the opening, the more flexible the loop is.

7.4.1 Structural comparison of the NFK and the L-kynurenine

In order to compare the simulations with NFK and with L-Kynurenine, replicate 1 with L-Kynurenine was chosen as well as replicates 1 and 2 with NFK. The choice of replicate 1 is justified for L-Kynurenine by the fact that all replicates are similar. For NFK, the first two replicates are chosen in order to have a sampling of the two possible conformations for the ligand (with an mean ligand/protein interaction energy that deviates less in standard deviation). First, as far the ligands are concerned, the simulation with L-Kynurenine adopts a similar conformation to replicate 1, and thus the first minimum, with NFK (Figure 7.10, A.). This minimum is the most stable minimum adopted by the protein-complex for the study of the two different ligands. However, it is less stable for simulations with L-Kynurenine than with NFK. In the simulation with L-Kynurenine, the other minimum was not isolated during MD. It could be that this second conformation is therefore less stable than the first one but more stable in NFK. It appears by crystallography through the rigidity of the system and the presence of glycerol close to the molecule inducing new interactions.

Into the two type of simulations, the general folding of the protein is conserved except for the JK-loop and the K helix (Figure 7.10, B.). In the case of the structure with L-Kynurenine, the JK-loop follows the extension of the K-helix at the C-terminal end whereas, in the presence of NFK, the C-terminal part is shifted towards the solvent. The opening of the active site differs between the type of simulation. While the loop

is closed in the presence of NFK in the minimum 1 (Figure 7.9, C. II.) and open for the minimum 2 (Figure 7.9, C. I.), an intermediate position in the presence of L-Kynurenine is observed (Figure 7.10, D.). The nature of ligand greatly influences the flexibility of this loop, which is strongly increased in the presence of L-Kynurenine in minimum 1 (Figure 7.10 C.) while it is not the case for replicate 1 with NFK with the same conformation. Lastly, in the case of the simulations with NFK, K373 participates in the stabilization of the product. This is no longer the case in the presence of L-Kynurenine, with distances greater than 12 Å between the ligand and the residue (11.9 ± 2.2 and 12.1 ± 0.3). In both cases, T379 and K377 never interact with the ligand or cofactor. The observed interaction with T379 could therefore be an artefact of crystal packing. An MD simulation starting from an X-ray structure with NFK where this interaction is observed could be done to confirm/reject this hypothesis.

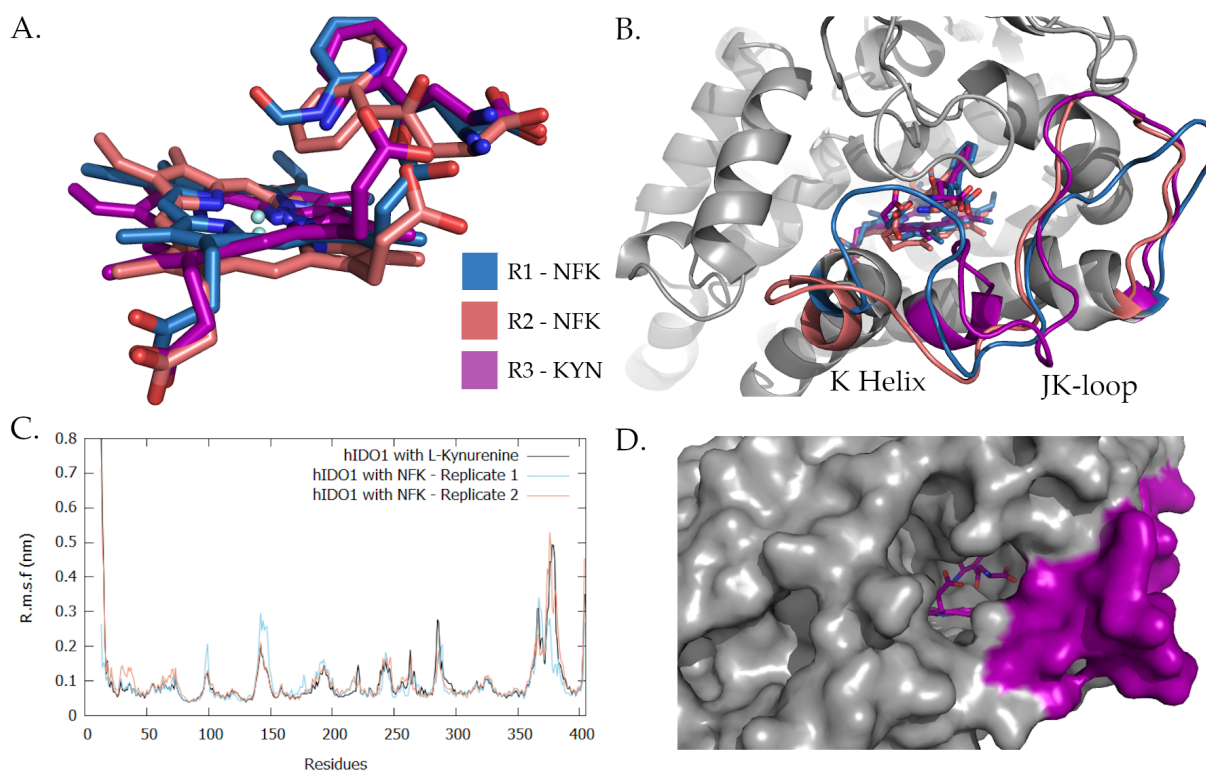


FIGURE 7.10: Comparison of the MD simulations at 310 K and 1 bar with L-Kynurenine (R1 in purple) and NFK (R1 in blue, R2 in salmon). A. Alignment of cofactor and ligand in the active site. B. Conformation of the JK-loop in the different simulations. C. R.m.s.f analyses for protein residues. D. van der Waals surface opening in presence of L-Kynurenine.

7.4.2 Contribution of MD simulation to the structural study

Thanks to this computational study, the positioning of L-kynurenine in the active site of hIDO1 was validated. It was also shown that L-Kynurenine is a good product analogue in terms of its active site position. However, as far as the dynamic loop is concerned, the behavior is different between the two molecules. It is therefore necessary to have a multidisciplinary approach to study the behavior of the JK-loop based on a similar position of NFK relative to L-Kynurenine. While NFK can adopt a second conformation for its aldehyde group resulting in an opening of the dynamic loop, this is not the case for L-Kynurenine. Consequently, the loop in the presence of L-Kynurenine remains in an intermediate position.

7.5 Intermediate conclusions

In regards to the questions mentioned in the introduction to this chapter (lack of refinement for the N-terminal part of the JK-loop, consistency of ligand positioning, difference between solution and solid state behavior), the present chapter has allowed to bring keys supporting and completing the results of crystallography. Together, these experimental and MD results [1, 5] stress the importance of the JK-loop on the protein dynamics that occurs during catalysis and the importance of the conformation of the JK-loop in the absence of an other ligand to maintain a labile heme into the active site. Taken as a whole, it is then possible to propose a final folding mechanism for the JK-loop (Figure 7.11). First, the conformations of the ligands observed by crystallography were in most cases verified by MD. This indicates that solid state structures of hIDO1 can be considered as a good starting system to generate ligand conformations in solution in the active site of hIDO1. There is also little difference between the solution behavior of the JK-loop and the one observed by crystallography for the fully resolved loops. Nevertheless, MD allows to complete the information often missing when the loop is not solved in order to have a global vision of the system. In the course of the MD simulations and with the crystal structures, the importance of residues K373 and K377 could be related to the different folding stages of the loop. The role of these two residues differs. The residue K373 allows to bring the substrate to the final position or to take the product out of the active site. The role of K377 is to maintain the cofactor in the absence of ligand in the active site and to stabilize L-Trp in the reactive position.

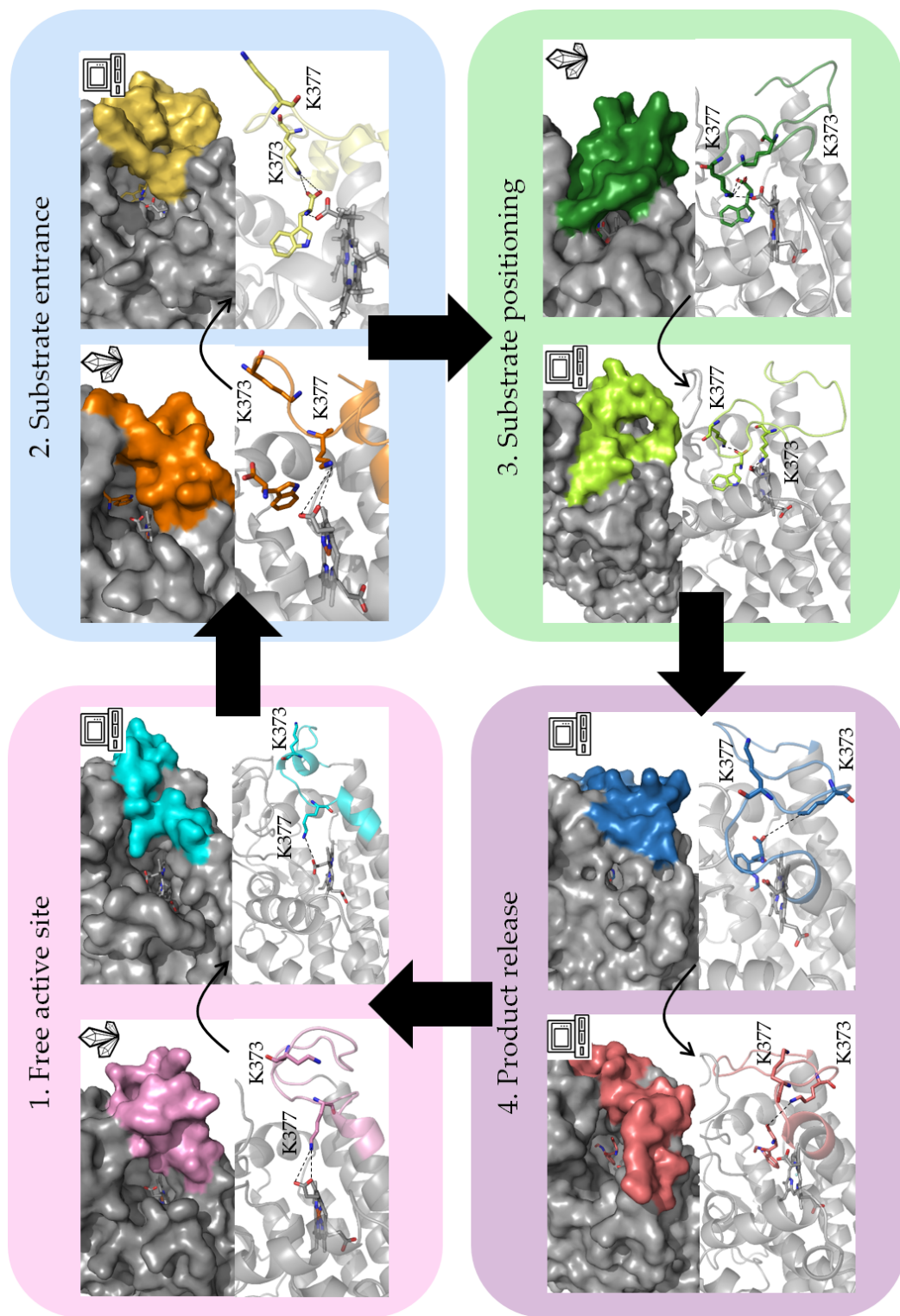


FIGURE 7.11: Final refolding mechanism for the JK-loop as established based on the contribution of the experimental (symbolized by a crystal) and MD results (symbolized by a computer).

The ability of the F-helix to interact with T379 at the C-terminal JK-loop when L-Trp is well oriented in the active site has also been demonstrated. The different conformations adopted by the dynamic loop could also be related to different motion values (B factor or r.m.s.f) for the C-terminal part, depending on the folding steps. The flexibility of this C-terminal part surpasses that of the N-terminal part when it is reorganized to close the active site. This demonstrates that, although the N-terminal part has often been judged to be more agitated than the C-terminal part because it is not resolved in crystallographic structures, this is not always the case depending on the observed temporary intermediate. This mobility is therefore essential to carry out the positioning the substrate.

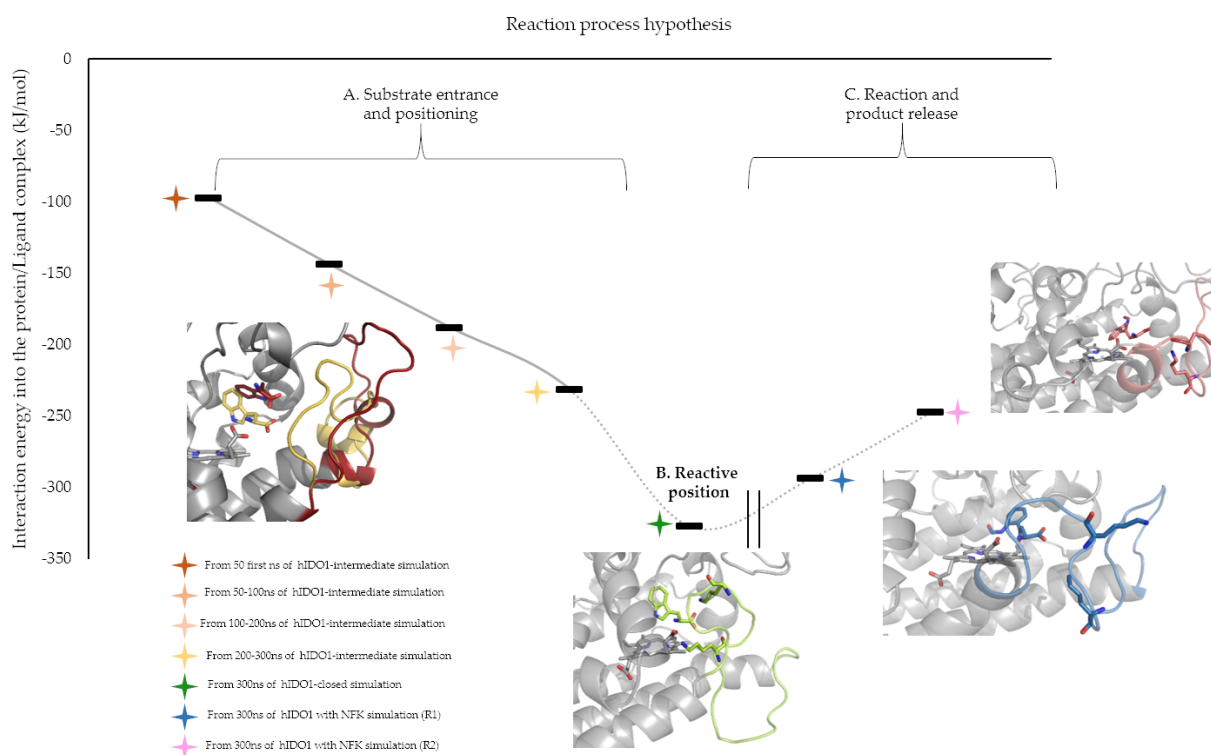


FIGURE 7.12: Mean short-range (Coulomb and Lennard-Jones) interaction energies diagram for the different protein/ligand complexes studied. A. Substrate positioning interaction energies evaluated from different range of time of the MD simulation starting from hIDO1-intermediate structure. B. Interaction energy between L-Trp and hIDO1 when the L-Trp is in the reactive position resulting from the MD results with hIDO1-closed as starting point (analyses on the all 300 ns of simulation). C. Product release interaction energies evaluated from the two replicates with NFK (analyses on the all 300 ns of simulation in each case).

Figure 7.11 shows that, although the flexibility of the C-terminal JK-loop increases upon positioning of the L-Trp in the active site, closure and positioning leads to stabilization of the enzyme/substrate complex. Once in the correct reactive position, the JK-loop is strongly stabilized. After reaction, the product obtained is less stabilized by the enzyme. The opening of the loop by changing the orientation of the NFK aldehyde leads to a re-increase in its flexibility and allows the product release. Modulation of the JK-loop mobility could therefore be a point of action for future drugs. These could either block the loop in an intermediate or open conformational state or stabilize it so that it cannot be reopened.

The N-terminal part of the JK-loop adopts, in the presence of a ligand in the active site, a globular structure, close to the DE-fragment. The only conformational change observed is in the absence of cofactor. In this case, the flexibility of the N-terminal part is significant, showing a high flexibility. The protein adopts a more extended conformation at the level of the N-terminal part, allowing in conjunction with an open C-terminal part to bind a free cofactor in the solvent. This might explain the role of the N-terminal of the JK-loop for the enzyme regulation.

Bibliography

- [1] M. Mirgaux, L. Leherte, and J. Wouters. Influence of the presence of the heme cofactor on the JK-loop structure in indoleamine 2,3-dioxygenase 1. *Acta Crystallographica Section D: Structural Biology*, 76:1211–1221, 2020.
- [2] M. T. Nelp, P. A. Kates, J. T. Hunt, J. A. Newitt, A. Balog, D. Maley, X. Zhu, L. Abell, A. Allentoff, R. Borzilleri, et al. Immune-modulating enzyme indoleamine 2, 3-dioxygenase is effectively inhibited by targeting its apo-form. *Proceedings of the National Academy of Sciences*, 115(13):3249–3254, 2018.
- [3] K. N. Pham, A. Lewis-Ballester, and S.-R. Yeh. Structural basis of inhibitor selectivity in human indoleamine 2, 3-dioxygenase 1 and tryptophan dioxygenase. *Journal of the American Chemical Society*, 2019.
- [4] L. Álvarez, A. Lewis-Ballester, A. Roitberg, D. A. Estrin, S.-R. Yeh, M. A. Marti, and L. Capece. Structural study of a flexible active site loop in human indoleamine 2, 3-dioxygenase and its functional implications. *Biochemistry*, 55(19):2785–2793, 2016.

- [5] M. Mirgaux, L. Leherte, and J. Wouters. Temporary intermediates of l-trp along the reaction pathway of human indoleamine 2, 3-dioxygenase 1 and identification of an exo site. *International Journal of Tryptophan Research*, 14:1–11, 2021.
- [6] F. A. Greco, E. Albini, A. Coletti, D. Dolciami, A. Carotti, C. Orabona, U. Grohmann, and A. Macchiarulo. Tracking Hidden Binding Pockets Along the Molecular Recognition Path of l-Trp to Indoleamine 2,3-Dioxygenase 1. *ChemMedChem*, 14(24):2084–2092, 2019.

Chapter 8

G261 to G265 as sensor of ligand entrance

8.1 Introduction

The dynamic loop of hIDO1 has always been recognized as an area of poor understanding of the enzyme. However, it is not the only one. More unnoticed in the literature, a plasticity in the active site of hIDO1 and, particularly of the fragment formed from residues 261 to 265, exists. The latter was usually presented in the conformation detailed in Figure 8.1, A., in the presence of L-Trp or inhibitor. In this "L-Trp bound" conformation, S263 is oriented towards the ligand, allowing, in some cases, H-bonds stabilization with the protonated amine. The indole ring nitrogen is stabilized by hydrogen bonds with water molecules and the aromatic part of the ligand is sequestered between A264 and F163. For the remainder of the chapter, this type of conformation for the two amino acids will be called "S263 in the forward plane" and "A264 in the reverse plane".

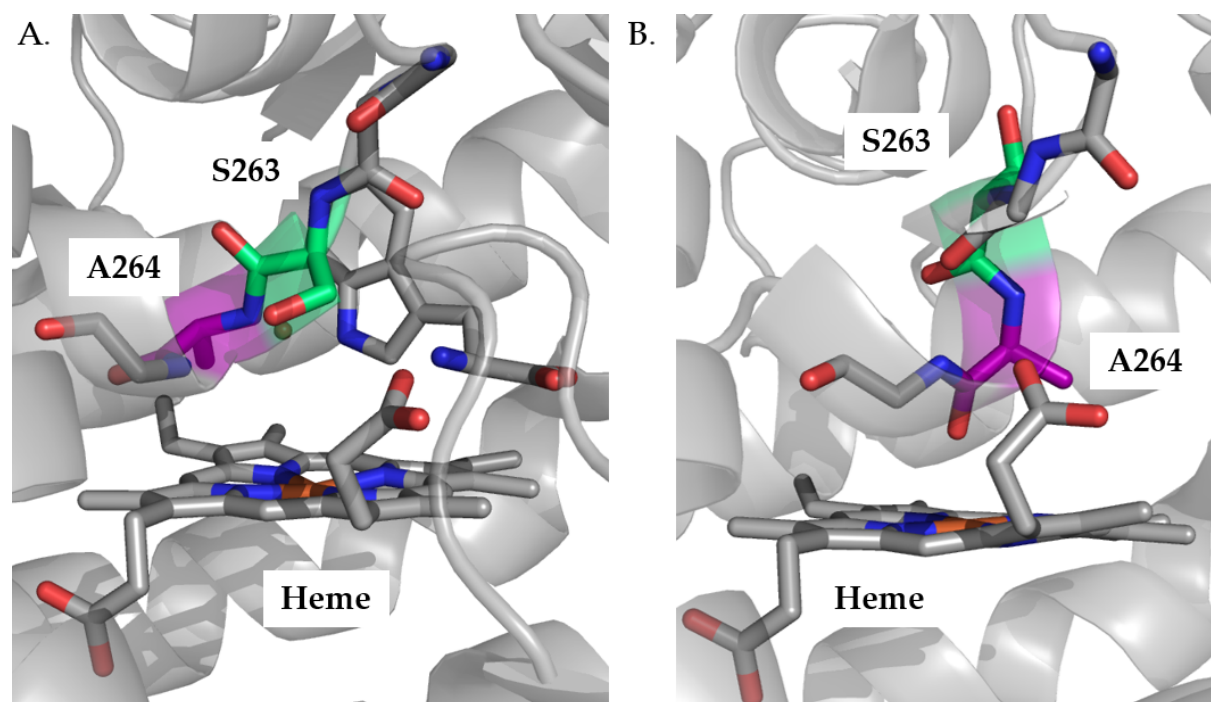


FIGURE 8.1: Conformation of the fragment G261 to G265 A. Adopted in presence of L-Trp in the active site (PDB: 6e46). S263 (in light green) is in the forward plane and A264 (in purple) is in the reverse plane. B. Adopted in some monomers with ferric heme cofactor (PDB: 6e44). S263 (in light green) is in the reverse plane and A264 (in purple) is in the forward plane.

In 2021, Röhrig *et al.* [1] has sparked some interest on this fragment plasticity and established another conformation for this fragment (Figure 8.1, B.), particularly for S263 and A264. According to the Author, this conformation is observed in almost 50% of the free ferric enzyme. In this second conformation, the orientation of S263 is named as "in the reverse plane" and A264 as "in the forward plane". The carbonyl of A264 coordinates the heme cofactor. This kind of arrangement has never been detailed in the literature before. As this conformation only appears in the case of ferric active sites, but not in all cases, it was concluded that it may be due to a redox effect. However, this conclusion may be due to insufficient sampling of the ferrous iron form of the protein. In fact, at the time of the article published by [1], only three structures under ferrous iron conditions were available in the PDB. Two of them were deposited without ligands in the active site (7a62, 6e45, 4 molecules in the asymmetric unit each) while the last contained a L-Trp molecule (6e46, with four monomers in the asymmetric unit). Röhrig *et al.* [1] states that the conformations without ligand and with a reduced cofactor are similar to that with L-Trp. The article also states that there is no significant structural difference between the structure with a ligand in the active site with ferric or ferrous cofactor. In this context, the crystallographic studies detailed in Chapter 6 were not only useful to determine new conformations of the JK-loop. In the set of active sites obtained, a significant sampling of the different conformations adopted by the G261 to G265 fragment in presence of ferrous cofactor could be obtained. In this chapter, the plasticity of the active site according to presence of the ligand is detailed.

8.2 Highlighting of the different conformations collected

During the thesis, six crystallographic structures of hIDO1, with or without ligand, were deposited in the PDB (7a62, 7nge, 7p0n, 7p0r, 7yxt, and 7zl2). Articles reporting these structures have mainly focused on the monomers occupied by a ligand or the dynamic loop. However, if we look at the other monomers, three main types of conformations for the G261 to G265 fragment are observed. In many cases, most density maps show a positive or negative residual $F_o - F_c$ density, possibly indicating mobility of this fragment. In this manuscript, the mean correlation coefficients (CC) between the density map and the PDB model for the residues of the G261-G265 fragment are reported for each monomer to reflect the quality of the model. These have been calculated with Phenix software, an Model-map correlations tool. [2]

Type I conformation: S263 reverse/A264 forward The type I conformation corresponds to the new conformation described by Röhrig *et al.* [1], with S263 in the reverse plane and A264 is in forward of the plane. However, in this present study, this conformation is not only conferred to the protein whose cofactor is in the oxidized state. Indeed, obtaining several crystallographic structures with different intermediates in the active site highlight that this conformation is obtained in many structures obtained under reducing conditions (Figure 8.2) ¹.

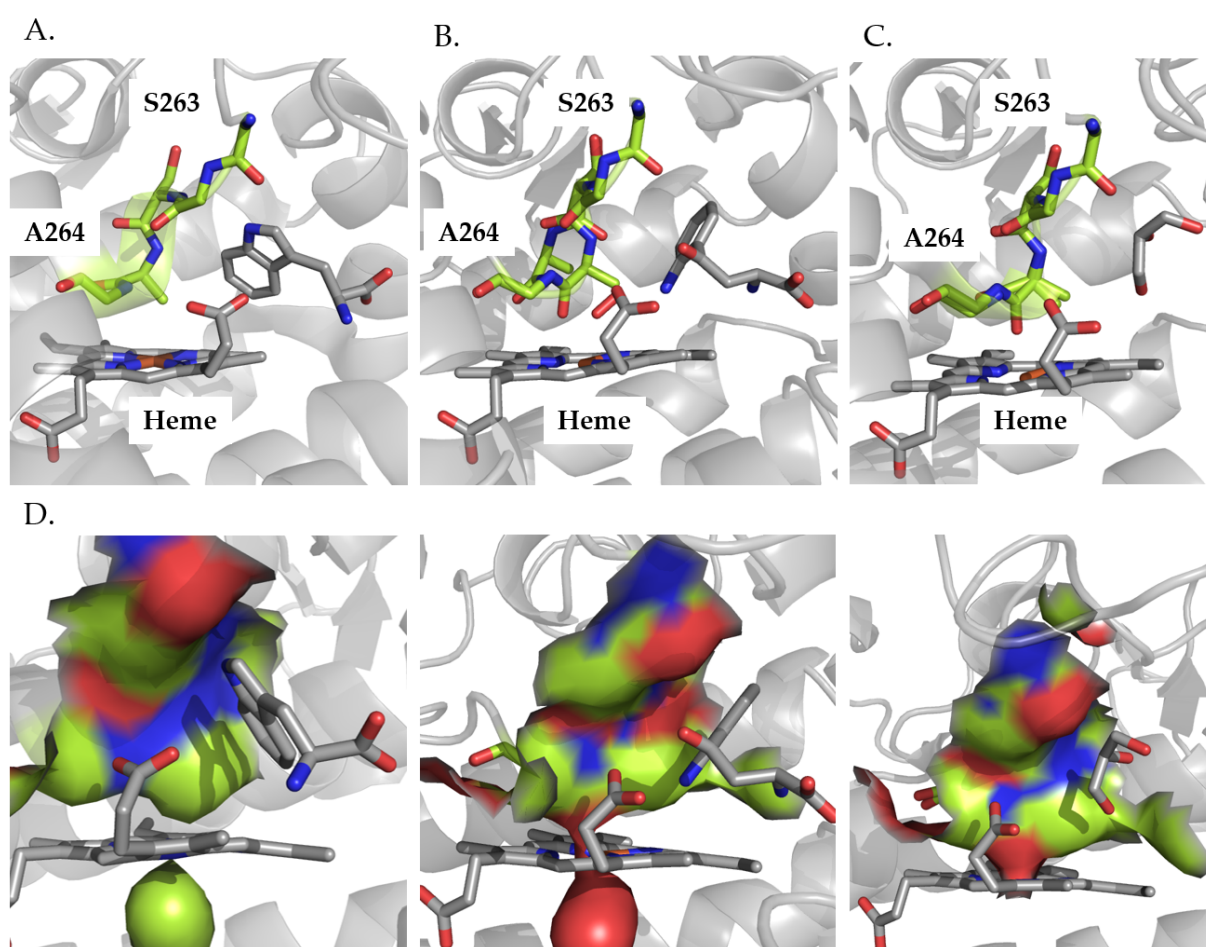


FIGURE 8.2: Type I conformation (in green) of the fragment G261 to G265 in the different monomers. A. In presence of less well oriented L-Trp with respect to the active site (7p0n/C(CC: 0.86 ± 0.05)). B. In presence of L-Kynurenine (7z2l/B(CC: 0.85 ± 0.06)). C. In presence of glycerol (7yxt/B(CC: 0.80 ± 0.1)). D. Surface representations and closure of the pocket A in presence of L-Trp, L-Kynurenine and glycerol respectively.

¹7nge/B(CC: 0.86 ± 0.03)/C(CC: 0.88 ± 0.02)/D(CC: 0.80 ± 0.03), 7yxt/B(CC: 0.80 ± 0.1)/D(CC: 0.82 ± 0.06), 7z2l/A(CC: 0.87 ± 0.02)/B(CC: 0.85 ± 0.06)/C(CC: 0.91 ± 0.03), 7p0n/C(CC: 0.86 ± 0.05)

The common point between these conformations is the presence in most cases of 1) a ligand upstream the pocket A but which is not specific to the protein or not well oriented or 2) an auto-oxidation of the cofactor or 3) a possible molecule of O₂ not coordinated to the heme cofactor. For example, this category includes the monomer with the L-Trp temporary intermediate in the less well orientation with respect to the active site (Figure 8.2, A., 7p0n/C(CC: 0.85 ± 0.05)), glycerol molecules (Figure 8.2, C., in 3 monomers out of 9) or the monomer with L-Kynurenine inside (Figure 8.2, B., 7z2l/B(CC: 0.85 ± 0.06)). In presence of non-specific ligands, it is usual to find the carbonyl of the main chain of A264 in two possible orientations: either behind the plane or coordinated to the iron atom of the heme. This latter can be due to an auto-oxidation of the cofactor during the crystallization process. In result, the oxidative state changes and can be considered as ferric. To sum up, the first use of this conformation would be to block the access to the active site. Indeed, if the plasticity of the protein allows to adopt this conformation in case of foreign bodies in the active site or incorrect oxidation state, the A pocket is totally closed and the reaction is blocked (Figure 8.2, D.).

The second possible use of this conformation is the delivery of O₂. As a matter of fact, in three active sites, monomers are empty in this conformation (7z2l/A(CC: 0.87 ± 0.02), 7nge/B(CC: 0.86 ± 0.03) and 7nge/D(CC: 0.80 ± 0.03)) without coordination between the carbonyl from A264 and the cofactor. This position cannot be linked to a bad oxidation state or to the presence of an intruder ligand. There is also a monomer with an approaching dioxygen molecule and the presence of both a type I and type II conformation (7yxt/D(CC: 0.82 ± 0.06)). For the empty active sites, the density that is currently occupied by water could also be assigned to dioxygen molecules as for the case of monomer D in 7yxt (Figure 8.3). This type I conformation could be related to the placement of the O₂ even if the mechanism involving with the water/solvent channel is not yet understood. S263 could thus serve as a hub in the delivery of the substrate in the active site from the channel. This could justify that the approach of this substrate, leads to the change of conformation of the fragment.

Type II conformation: S263 forward/A264 forward As mentioned, a transition is possible between type I and type II (Figure 8.3). For this, there is an inversion of the position of S263 which passes from the reverse plane to the forward plane. A264 remains in the forward plane. Mostly, the type II conformation includes all the empty

active sites (with a cofactor in ferrous conditions²) and all the active sites with a substrate molecule (O_2 (7p0n/A(CC: 0.88 ± 0.01)/B(CC: 0.88 ± 0.03)/D(CC: 0.87 ± 0.03)) or L-Trp (7p0r/B(CC: 0.88 ± 0.02))) in approach, into a good orientation. The conformational change between type I and II could thus be the result of ligand recognition by the active site. This organization in space is the preliminary step to type III but also allows a stabilization of an incoming dioxygen molecule through hydrogen bonds with S263. In the case of type II conformations, the carbonyl is always in a planar orientation with respect to the methyl of the lateral chain, without coordination of the central iron of the heme (Figure 8.3, C.). Consequently, compared to type I, the presence in the front plane of the side chain is less pronounced, this is mainly due to this orientation of the carbonyl. Generally, the dihedral angle between the lateral chain and the carbonyl adopts values between -65° and -85° (Figure 8.3, B. - Upper corner).

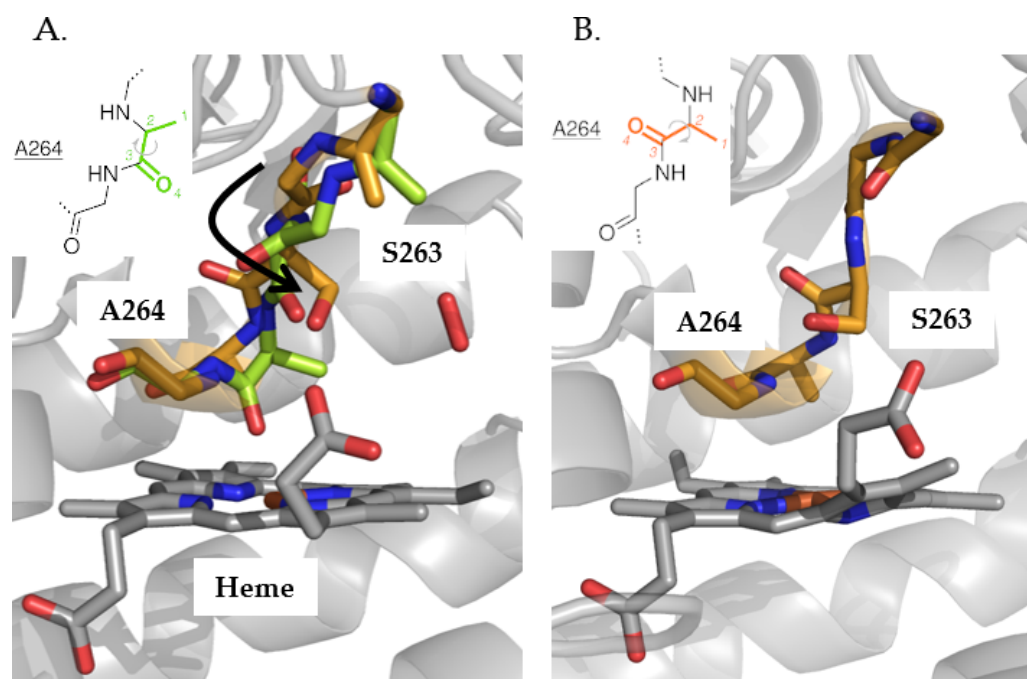


FIGURE 8.3: Type II conformation (in orange) of the fragment G261 to G265 in the different monomers. A. Co-existence of conformation I (in green) and II (in orange) in presence of O_2 molecule in monomer D of 7yxt (CC: 0.82 ± 0.06). B. Conformation II in empty active site of monomer A from 7a62 (CC: 0.90 ± 0.02).

²7a62/A(CC: 0.90 ± 0.02)/B(CC: 0.90 ± 0.02)/C(CC: 0.90 ± 0.01)/D(CC: 0.89 ± 0.02), 7yxt/A(CC: 0.88 ± 0.03)/C(CC: 0.91 ± 0.03), 7z2l/D(CC: 0.89 ± 0.02), 7p0r/A(CC: 0.89 ± 0.02)/C(CC: 0.87 ± 0.05)/D(CC: 0.89 ± 0.02)

For the same reasons, this type **II** conformation, although assimilated to type **III** in the literature, is not totally identical. Indeed, this orientation of the side chain of A264 is important for the closure of pocket A and the binding of substrates. However, the passage through the conformation **II** allows the junction between conformation **I** and **III**. This explains why the side chain of A264 is often less well defined in this conformation.

Type III conformation: S263 forward/A264 reverse The last conformation (Figure 8.4) is only observed in the presence of L-Trp in the active site (7nqe/A(CC: 0.82 ± 0.05)). It is equivalent to that detailed in the literature. In this case, S263 stabilizes the substrate and presents a forward conformation. The residues A264 is oriented in the reverse plan, with a dihedral angle of -55° between the lateral chain and the carbonyl. There is no coordination between the carbonyl of A264 and the central atom of the porphyrin in the type **III** conformation. This conformation is characterized by an induced-fit of the fragment G261-G265 (Figure 8.4, B.) in comparison to the previous conformations to open pocket A to bind the ligand (Figure 8.4, C.). This pocket opening allows sequestration of the L-Trp aromatic ring between the side chain of A264 and F163. In the monomer A from 7nqe, G262 adopts two different conformations depending on the presence of the ligand to avoid steric clash with the aromatic rings. This opening is essential because, without it, the L-Trp cannot position itself correctly to react. The different conformations detailed in this section could be analyzed during MD with and without ligands. It turns out that, in all cases, the fragment keeps the conformation observed by crystallography. For the MD study with the temporary intermediate in the right orientation, the displacement of the ligand is linked with the initiation of the pocket A opening.

8.3 What's observed in other PDB structures?

After this complete analysis of the crystal structure of monomers obtained during the thesis, it is interesting to see if this is also observed in the other structures of the literature. To do so, the problem is separated in two blocks, first the analysis of the other ferrous structures and then the analysis of all the ferric structures. The structures are classified in their respective categories according to the conditions of crystallization and cryo-protection involving sodium dithionite and thus allowing the reduction of the metal ion.

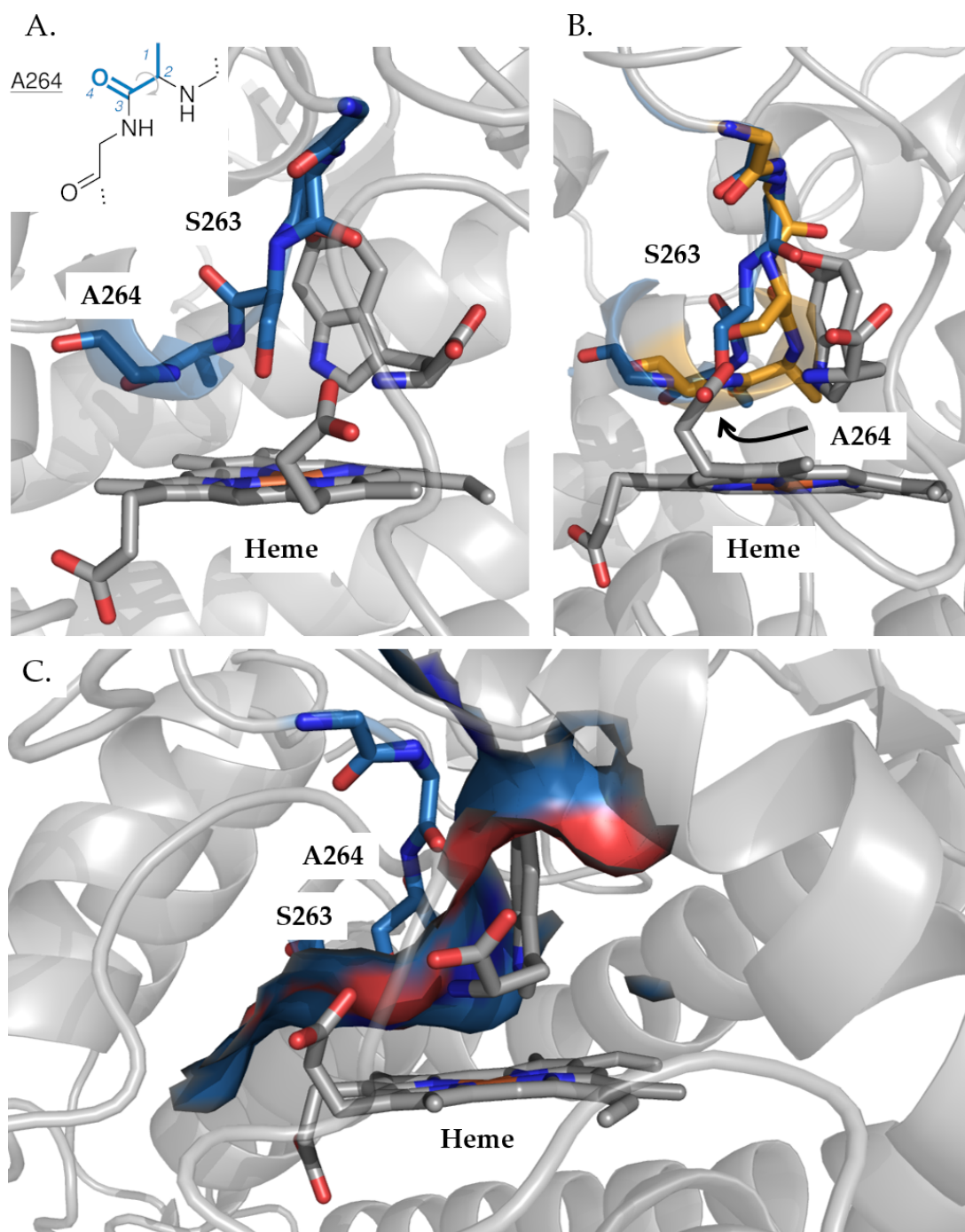


FIGURE 8.4: Type III conformation (in blue) of the fragment G261 to G265 in the different monomers. A. In presence of reactive L-Trp (7nge/A(CC: 0.82 ± 0.05)). B. Induced fit observed between conformation II and III (7a62/A(CC: 0.90 ± 0.02)). D. Surface representation and opening of pocket A in conformation III.

8.3.1 Conformations for other ferrous proteins in the PDB

Regarding the other structure without ligand in ferrous condition (pdb:6e45 [3]³), conformation **II** is always adopted in the four monomers, with a dihedral angle ranging from -72° to -73° . It is intriguing to note that, while the presence of glycerol resulted in a type **I** conformation in the previously developed structures, this is not the case for monomer A and D of 6e45 which also has such a ligand. However, this can be explained by an unassigned residual density blob (Figure 8.5) in the 4 monomers of 6e45. This blob could be attributed to oxygen, justifying the type **II** conformation.

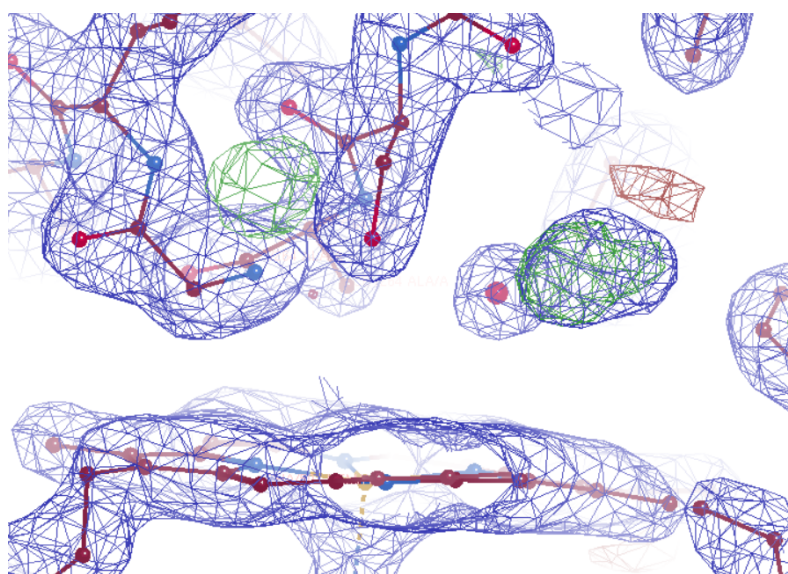


FIGURE 8.5: Residual density blob observed in the ferrous structure without ligand from Luo *et al.* (pdb: 6e45). [3]

Concerning the ferrous structure in presence of L-Trp (pdb:6e46 [3]⁴), an identical type **III** conformation of monomers with L-Trp is observed in all monomers from the structure 6e46 with a dihedral angle of -55° between the lateral chain and the carbonyl (Figure 8.6). With a redundancy of 5 monomers, this confirms this conformation and this value for the dihedral angle as probably the closest to the biological reaction state.

³A(CC: 0.95 ± 0.009), B(CC: 0.95 ± 0.005), C(CC: 0.97 ± 0.005), D(CC: 0.96 ± 0.00)

⁴A(CC: 0.94 ± 0.02), B(CC: 0.95 ± 0.005), C(CC: 0.94 ± 0.01), D(CC: 0.92 ± 0.01)

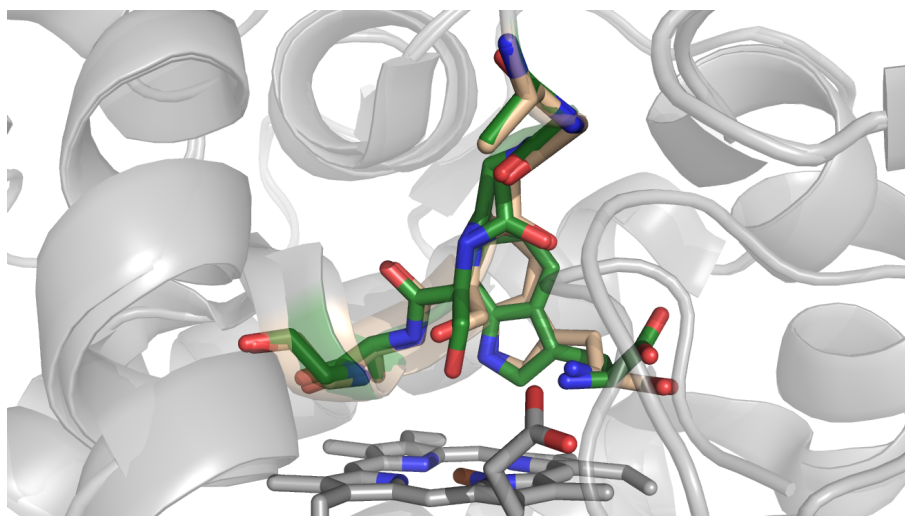


FIGURE 8.6: Conformation of fragment G261 to G265 in the structure from Luo *et al.* (pdb: 6e46, in wheat) in comparison the the monomer A from 7nge (in green). [3]

8.3.2 Conformations for other ferric proteins in the PDB

Structural analysis of hIDO1 with an ferric cofactor is very rich. Indeed, with more than 54 structures, i.e. 128 monomers, the conformational sampling in the presence of multiple ligands is very important. It is possible to differentiate the structures into several subgroups in the presence of the ligand type. To report the quality of the fit on the data, a summary table of the correlation coefficient between the map and the PDB model for the fragment residues is included in the Appendices D, Tables D.9, D.10, D.11 and D.12, with an average for each monomer. In general, the analysis of the averages shows that the values are qualitative, with mean CC values between the density map and the PDB model for the residues of the G261-G265 fragment above 0.8.

Structures without ligands These structures (6e40, 6e44 and 6azu), mentioned by Röhrig *et al.* [1], concern 9 monomers. Voluntarily, the monomers 6mq6/A, 6dpr/A and 6dpq/A are removed from this group compared to the analysis of Röhrig *et al.* [1] The reason of this removal is detailed in the next paragraph. In the structures without ligand (Figure 8.7), either type I or type II conformations are observed. Type I conformations are observed when the carbonyl of A264 coordinates the heme (6e44/A/C and 6azu/A/B/C/D). In this case, the dihedral angle between the side chain of A264

and the carbonyl has a value between -55° and -65° (Table 8.1).

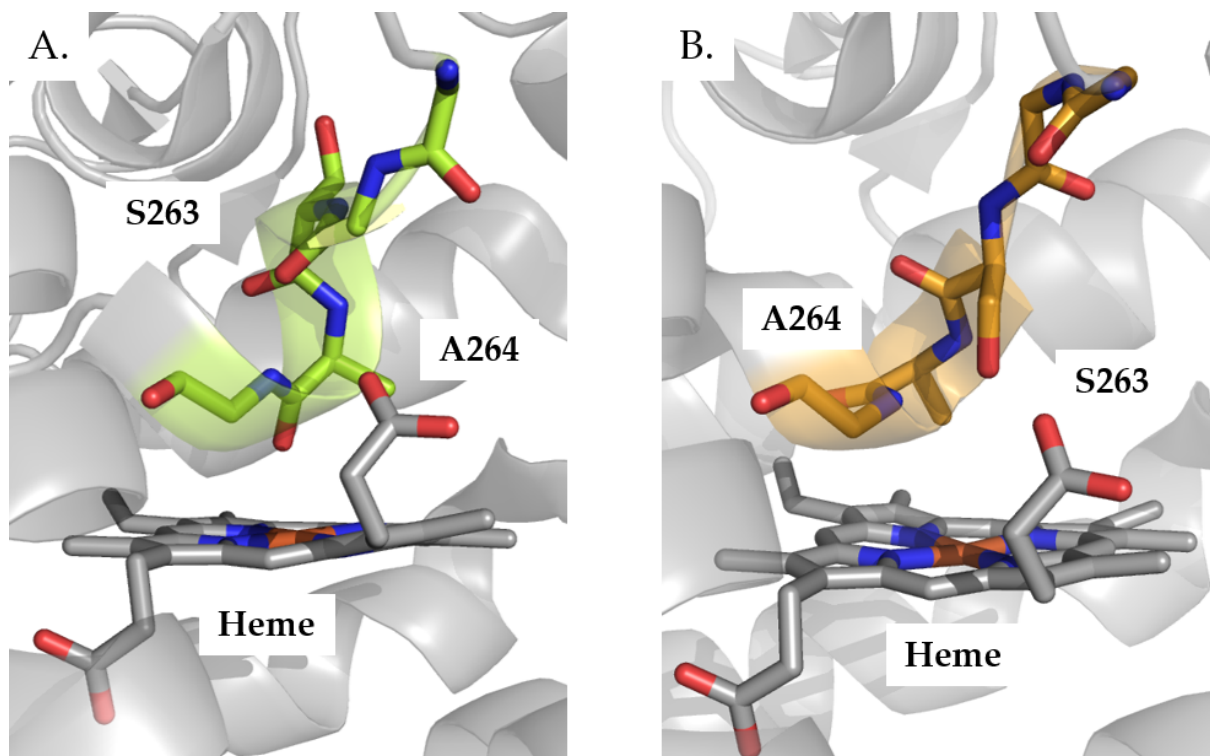


FIGURE 8.7: Conformation of fragment G261 to G265 in the ferric structures on the PDB without ligands. A. Monomer A form 6e44 B. Monomer B from 6e44.

It is interesting to note that in the 6azu structure, S263 is mutated to alanine. However, no mutation is indicated on the PDB and residue is mentioned as a serine in the sequence. Therefore, it is likely that this is a modeling error. For type II conformations, they are adopted when the carbonyl does not coordinate the heme and has dihedral angles ranging from -45° to -85° (Table 8.1). This confirms the hypothesis that type I conformations of an empty active site appear when coordination between the heme and the carbonyl is present, and therefore the binding of a substrate is potentially prevented.

Structures with substrates For hIDO1, two types of substrate can be distinguished, namely either dioxygen or L-Trp. Concerning the structures with dioxygen, none is mentioned as such in the literature. Nevertheless, for the 6mq6/A and 6dpq/A structures (Figure 8.8, A. and B.), careful observation of the density maps reveals

TABLE 8.1: Ligand observed in ferric active site and associated conformation type for the G261-G265 fragment and A264 dihedral angle. ¹ = Coordination C=O/Heme, ² = mutation S263A, ³ = glycerol in the active site, ⁴ = Upstream position

Kind of ligands	PDB code	Resolution (Å)	Ligand	Number of monomers	Monomers concerned	Type	Angle [°]
No ligand	6e44 ¹	1.9 [3]	no	2	A, C	I	-59, -65
		1.9 [3]	no	2	B, D	II	-82, -75
	6e40	2.7 [3]	no	1	C	II	-45
	6azu ^{1,2}	2.8 [4]	no	4	A, B, C, D	I I	-58, -58, -55, -60
O ₂	6mq6 ³	3.1 [5]	O ₂	1	A	II	-62
	6dpq ³	2.9 [5]	O ₂	1	A	II	-65
	2d0u	2.3 [6]	CN	2	A, B	II	-69, -73
TRP	6ubp ⁴	3.0 [7]	L-Trp + CO	2	A, B	II	-65, -70
	6e35	2.8	L-Trp + CN	2	A, B	III	-63, -57
	6cxv ⁵	2.6 [8]	L-Trp + CN	2	A, B	III	-74, -58
	6cxu ⁵	2.5 [8]	L-Trp + CN	2	A, B	III	-66, -62
	5wmx	2.7 [9]	L-Trp + CN	2	A, B	III	-52, -53
	5wmw	3.0 [9]	L-Trp + CN	2	A, B	III	-56, -49
	5wmv	2.6 [9]	L-Trp + CN	2	A, B	III	-55, -55
	5wmu	2.4 [9]	L-Trp + CN	2	A, B	III	-54, -59

that a water molecule coordinated to the central atom of porphyrins is also observed. The density around this water molecule is also consistent with a potential molecule of dioxygen. This is supported by the exact alignment of the oxygen atoms when aligning the monomers with monomer B of 7z2l, which has a coordinated dioxygen molecule. Consequently, these monomers cannot be considered as empty since, in addition, there is the presence of a molecule of glycerol in the active site. The conformation observed for these two monomers is consistent with a type **II** conformation and a dihedral angle of -62° and -65° respectively for each monomer (Table 8.1). This is irrefutably reminiscent of what is observed for the A and D monomers of the ferric structure 6e45 and, therefore, justifies the hypothesis of O₂ binding in this active site to explain the type **II** conformation in presence of glycerol molecules. An active site with an O₂ analogue (CN in presence of NHE molecule, in 2d0u) gives the same result.

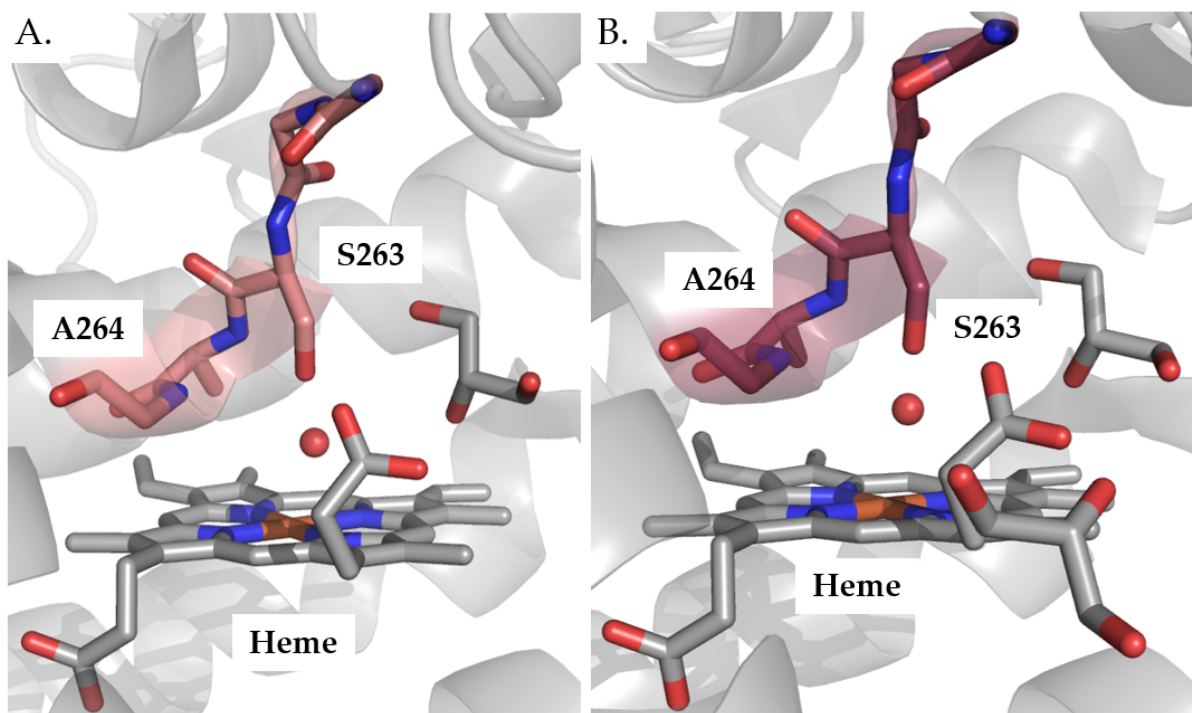


FIGURE 8.8: Conformation of fragment G261 to G265 in the ferric structures on the PDB with dioxygen as substrate. A. Monomer A from 6m6q
B. Monomer A from 6dpq.

The other, better-known substrate, is L-Trp. In this case, eight structures⁵, or 16 monomers, present this ligand in the active site with a ferric cofactor. In these structures, seven of them present L-Trp in the reactive position and in the presence of cyanide (Figure 8.9, A.). The conformation of the G261 to G265 fragment is a type **III** conformation with a dihedral angle ranging from -49° to -63° (Table 8.1). In the ferric state, the type **III** conformation is therefore somewhat more relaxed, with a dihedral angle less than -60° . The mutation of S167A (structure 6cxv and 6cxu) causes an increase of this dihedral angle (from -58° to -74° , Table 8.1), which is more like a type **II** conformation. The position of the indole ring of L-Trp is slightly more distant from fragment G261-G265 in case of a ferric rather than a ferrous structure, as mentioned by Röhrig *et al.* [1] As with the type **III** conformation in ferrous structures, carbonyl coordination in ferric structures is not observed in either case. However, this is prevented in all cases by the presence of the cyanide. It could be interesting to obtain a ferric structure, in the absence of cyanide, for comparison. The eighth ferric structure with L-Trp presents the ligand as a temporary intermediate (Figure

⁵6ubp, 6e35, 6cxv, 6cxu, 5wmx, 5wmw, 5wmv, 5wmu

8.9, B.). In this case, as it was the case of the intermediate in ferrous condition, the fragment adopts a type II conformation with a dihedral angle of -65° and -70° in each monomer (Table 8.1).

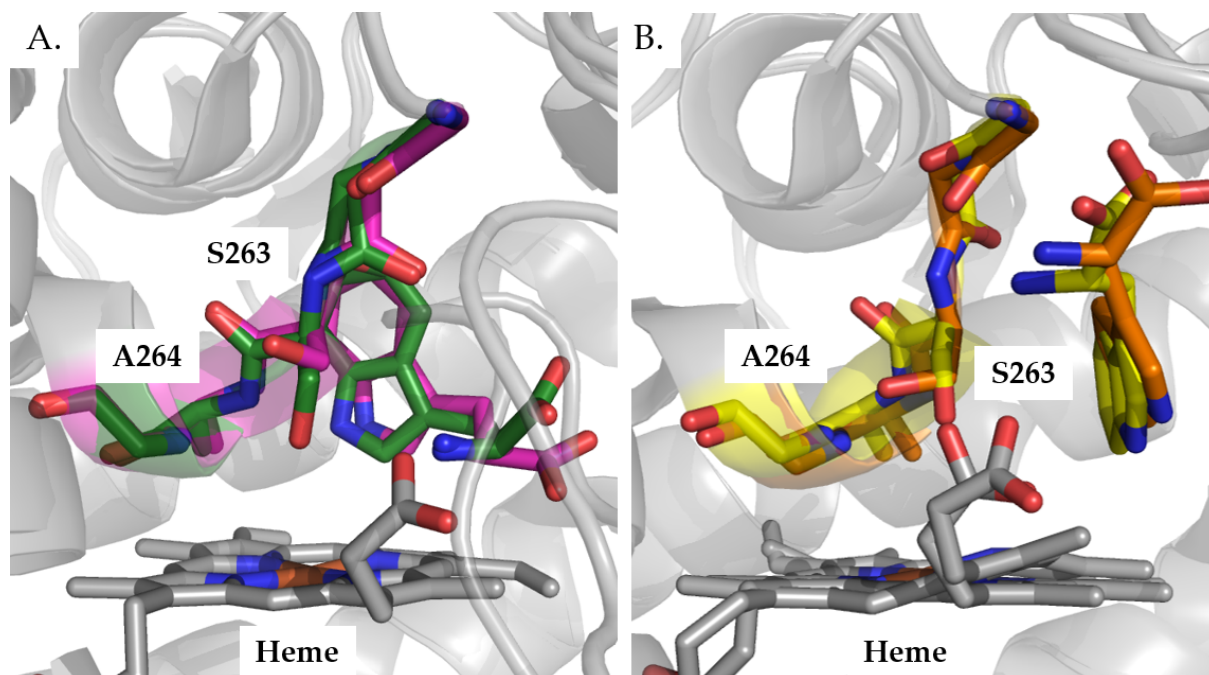


FIGURE 8.9: Conformation of fragment G261 to G265 in the ferric structures on the PDB with L-Trp as substrate. A. Superimposition of monomer B from ferric 5wmx structure (in purple) with monomer A from 7nge ferrous structure (in green). B. Superimposition of monomer A from 6ubp (in yellow) with monomer B from 7p0R ferrous structure (in orange).

Structures with inhibitors For structures with hIDO1 inhibitors, a distinction is made between apo and holo inhibitors as mentioned in the introduction (in Figures 1.5 and 1.6). Apo inhibitors are defined as inhibitors that position themselves at the original position of the heme cofactor or are in competition with the cofactor for the binding. The holo inhibitors are positioned in active sites in the presence of the cofactor. These inhibitors are in competition with O_2 or L-Trp. The development of apo inhibitors is quite recent. The first structure of hIDO1 in complex with apo inhibitors on PDB dates from 2018. There are currently 14 structures with apo inhibitors, distributed 30 monomers. Regarding these structures (Figure 8.10, A.), the conformation found in all cases is a type II conformation with large dihedral angles, whose value is greater than -60° (value ranging from -60° to -100° (Table 8.2), depending on the

inhibitor).

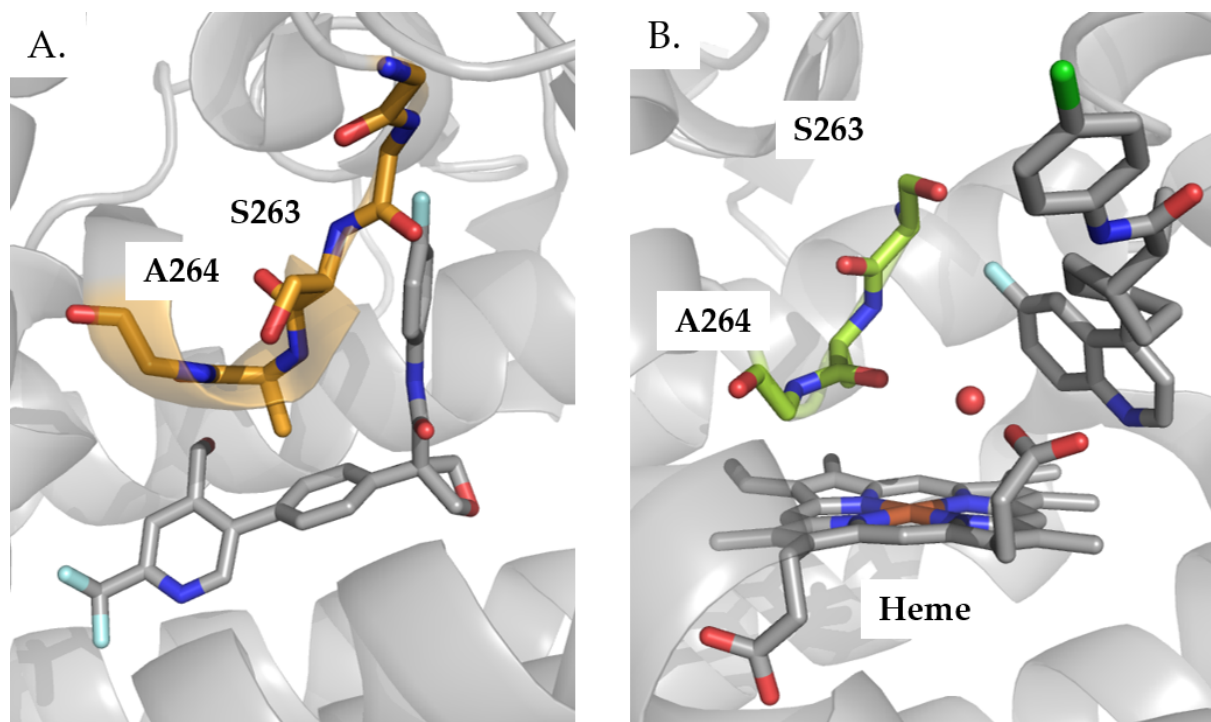


FIGURE 8.10: Conformation of fragment G261 to G265 in the ferric structures on the PDB with apo inhibitors. A. Type II conformation in ferric 7rrc structure (in orange). B. type I or type II conformation in ferric 6dqr structure (in limon).

No relationship is noticed between the inhibitory capacity of the inhibitor and the dihedral angle of A264. There are also, for some inhibitors such as BMS-986205, studies of trajectories of this positioning of the latter. In these studies, monomers with heme and inhibitor, even if BMS-986205 is an apo inhibitor, is presented as the inhibitor is not in the binding site (Figure 8.10, B., monomer A of 6pqr). For this monomer of 6dpr, it is unclear whether the structure adopts a type I or type II conformation as a result of the lack of refinement of residues G246-G262 and the abruptness of the density around residue S263. Nevertheless, given the rather high position of S263, this looks more like a type I conformation.

In a general way, a significant difference between the two types of inhibitors (apo/holo) at the level of the dihedral angle between the lateral chain of A264 and the main chain is noticed. This is due to the absence of the cofactor, allowing a greater

TABLE 8.2: Ligand census for apo inhibitors, based on conformation type for the G261-G265 fragment and A264 dihedral angles in ferric structures for hIDO1. The structure of the ligands can be found on the PDB website from their ligand code (<https://www.ebi.ac.uk/pdbe/>). ¹ = No refinement of G246-G262. NP: Not provided

PDB code	Resolution (Å)	Ligand code	IC50 (nM)	Number of monomers	Monomers concerned	Type	Angle [°]
7rrc	2.2 [10]	6RI	2	2	A, B	II	-100, -87
7rrb	2.7 [10]	6ZI	6.3	2	A, B	II	-86, -81
7b1o	2.6 [11]	SLW	1.6	2	A, B	II	-86, -84
7m63	3.1 [11]	YRP	0.69	2	A, B	II	-77, -78
6x5y	2.7	URJ	NP	2	A, B	II	-90, -93
6wpe	2.4 [12]	UG6	9	2	A, B	II	-86, -88
6wjy	1.9 [13]	U41	9.2	2	A, B	II	-86, -85
6v52	1.8 [14]	QPV	3.1	2	A, B	II	-80, -82
6e43	1.7 [3]	HQM	NP	4	A, B, C, D	II II	-82, -85, -83, -83
6mq6	3.1 [5]	H7P	0.5	1	B	I	-92
6dpr ¹	3.2 [5]	H7P	NP	1	B	II	-98
6dpq	2.9 [5]	GOL	/	1	A	I	-85
6dpq	2.9 [5]	H7P	NP	1	B	II	-95
6azw	2.8 [4]	C51	NP	2	A, B	II	-86, -84
6azv	2.8 [4]	C4V	4.2	4	A, B, C, D	II II	-76, -81, -66, -62

twist of the fragment without steric hindrance. For the holo inhibitors, there is a great variety of structures, for a total number of 73 monomers. However, based on the definition of type **III** as a conformation with an angle smaller than -60° in the ferric state, the conformations observed are either type **II** or type **III** depending on the inhibitors. Indeed, the kind of ligand affects on the dihedral angle between the side chain of A264 and the carbonyl of the main chain. This angle value varies from -42° to -73° (Table 8.3). Into the six large families of inhibitors detailed in the Figure 1.5 of the introduction (Chapter 1), the type 2 present a dihedral angle closest to the one observed in the presence of L-Trp. NLG-919 (LKP) and close crystallized analogues (YRM, 5PF, 5PJ include in type 3 inhibitors) with high inhibition constants also exhibit such a low dihedral angle (-52° to -65°). Concerning the type 4 inhibitor (MMG-0752 family), an angle close to the one observed with L-Trp is observed but not for all analogues (RCW, RCQ and RCN). Finally, the Amg-1 family of inhibitors (type 6) is associated with inhibitors causing a type **III** conformation.

TABLE 8.3: Ligand census for holo inhibitors, based on G261-G265 fragment conformation type and A264 dihedral angles in ferric structures for hIDO1. ¹ = Not linked to the heme, ² = G262A mutant, ³ = A260G mutant. NP: Not provided

Ligand type	PDB code	Resolution (Å)	Ligand code	IC50 (μM)	Number of monomers	Monomers concerned	Type	Angle [°]
1	6pz1 ¹	2.7 [15]	AOJ	0.41	2	A, B	II	-67, -72
	5whr ¹	2.3 [16]	AOJ	0.41	2	A, B	II	-58, -61
2	6pu7	2.4 [17]	OY4	0.035	2	A, B	III	-63, -55
	6e41	2.3 [3]	HQS	NP	4	A, B, C, D	III	-49, -52, -56, -60
	6e40	2.7 [3]	BBJ	0.073	3	A, B, D	III	-47, -55, -57
	5wn8	2.5 [9]	BBJ	0.073	2	A, B	III	-54, -57
	5xe1	3.2 [18]	IUU	0.067	2	A, B	III	-52, -51
3	7m7d	2.6 [11]	YRM	0.024	2	A, B	III	-59, -59
	7e0u	2.3 [19]	HUC	0.29	2	A, B	II	-69, -60
	7e0t	2.3 [19]	HU9	1.23	2	A, B	II	-58, -64
	7e0s	2.7 [19]	HU6	0.64	2	A, B	II	-61, -67
	7e0q	2.5 [19]	HU3	2.9	2	A, B	II	-72, -66
	7e0p	2.6 [19]	HU0	5.6	2	A, B	II	-73, -66
	7e0o	3.3 [19]	HS0	9.5	2	A, B	II	-67, -70
	6o3i	2.7 [20]	LKP	0.028	2	A, B	III	-52, -60
	6e42	2.1 [3]	HQJ	2.6	4	A, B, C, D	II	-73, -71, -72, -72
						A, B	II	-65, -60
	5etw	2.7 [21]	XNL	NP	2	A, B	III	-57, -57
	5ek4	2.2 [21]	5PF	0.019	2	A, B	II	-65, -66
	5ek3	2.7 [21]	5PK	0.28	2	A, B	III	-52, -56
	5ek2	2.3	5PJ	48	2	A, B	II	-65, -65
	4u74 ²	2.0	PIM	48	2	A, B	II	-62, -62
4u72 ³	3.4 [6]	PIM	48	2	A, B	II	-65, -65	
4	7ah6	3.0 [22]	RCW	0.024	2	A, B	II	-73, -70
	7ah5	2.9 [22]	RCQ	0.035	2	A, B	II	-71, -73
	7ah4	2.4 [22]	RCN	1.5	2	A, B	II	-73, -76
	6r63	2.9 [23]	JTB	0.059	2	A, B	III	-56, -46
	6f0a	2.3 [24]	C82	11.3	2	A, B	III	-56, -42
6	6kw7	3.0 [25]	DYC	0.38	2	A, B	III	-53, -55
	6kps	2.3 [25]	DU6	0.1	2	A, B	III	-65, -61
	6kof	2.3 [25]	D09	0.016	2	A, B	III	-61, -55
	4pk6	2.8 [26]	PKL	1.9	2	A, B	III	-55, -51
	4pk5	3.5 [26]	PKJ	3	2	A, B	III	-55, -62

In general, the angle of dihedral of A264 is a good indicator of the inhibition capacity of an inhibitor. Indeed, with the exception of RCW (from 7ah6), RCQ (from 7ah5) and 5PK (from 5ek3) which are good inhibitors but present a type **II** conformation, all the most affine inhibitors (with an $IC_{50} < \text{than } 0.1 \mu\text{M}$) are inhibitors that present a type **III** conformation. However, this tool is not infallible because some false positive inhibitors are also observed such as PKJ (from 4pk5), PKL (from 4pk6) and C82 (from 6f0a). For the 4pk5 and 4pk6 ligands, this judgment error comes from the intrinsic quality of the structures, which are of low resolution and therefore not very precise in terms of coordinates. It is therefore important to keep in mind the quality of the dataset and the accuracy of the map in this region if we use the A264 dihedral angle as a marker of inhibitory capacity for holo ligands. In summary, whether holo or apo, active sites with inhibitors never adopt type **I** conformations. This is because they are good dupes for the protein, affine for the active site.

8.4 Intermediate conclusions

In the literature [1], two types of conformations are mentioned for fragment S263-G265. In the first conformation, residue S263 faces the heme cofactor and interacts with a possible L-Trp while A264 is oriented toward the pocket A to sandwich the substrate with F163. The second conformation is observed in empty ferric monomer and presents an inverted conformation. However, little information exists on this organization and its study is poorly done throughout the crystallographic literature. In this chapter, the analysis of the different conformations observed, in the ferrous state, for the six crystallographic structures obtained during the thesis, has been performed as well as a review study of the ferric conformation reported in the PDB. This allowed to highlight three possible conformations for the G261-G265 fragment.

The first conformation (type **I**) is a so-called "S263 reverse/A264 forward" conformation. This one is obtained 1) under the conditions of an empty active site where the carbonyl of A264 coordinates the heme 2) in the case of active sites filled by "foreign" molecules not having a good affinity for the active site (glycerol, products of the kynurenine pathway, etc.) 3) dioxygen molecules provided that the fragment is in conformational rearrangement. The second conformation (type **II**) presents an organization called "S263 forward/ A264 forward". In this case, the heme is never coordinated by the carbonyl of A264. This conformation is observed 1) when a substrate

(O₂ or L-Trp) is entering the active site, regardless of the oxidation state 2) in the case of holo inhibitors of hIDO1 with less affinity or apo inhibitor of the enzyme. The last conformation (type **III**) is called "S263 forward/A264 reverse". This conformation is strictly observed with L-Trp in the reactive conformation or for some very affine inhibitors of the protein (Epacadostat, NLG-919, Amg-1 or MMG-0358 and analogs). This conformation is associated with an induced-fit of the fragment in order to allow the opening of the A pocket.

To conclude, this chapter highlights a too often forgotten plasticity of hIDO1 active site which is nevertheless crucial for the reaction. It is possible that this plasticity, associated with the reorganization of the JK-loop, is at the origin of the positioning of the substrate in the A pocket. This positioning is only possible by a digital recognition of the latter by the fragment and its reorganization.

Bibliography

- [1] U. F. Röhrig, O. Michielin, and V. Zoete. Structure and plasticity of indoleamine 2, 3-dioxygenase 1 (ido1). *Journal of Medicinal Chemistry*, 64(24):17690–17705, 2021.
- [2] P. D. Adams, P. V. Afonine, G. Bunkóczi, V. B. Chen, I. W. Davis, N. Echols, J. J. Headd, L-W Hung, G. J. Kapral, R. W. Grosse-Kunstleve, et al. Phenix: a comprehensive python-based system for macromolecular structure solution. *Acta Crystallographica Section D: Biological Crystallography*, 66(2):213–221, 2010.
- [3] S. Luo, K. Xu, S. Xiang, J. Chen, C. Chen, C. Guo, Y. Tong, and L. Tong. High-resolution structures of inhibitor complexes of human indoleamine 2, 3-dioxygenase 1 in a new crystal form. *Acta Crystallographica Section F: Structural Biology Communications*, 74(11):717–724, 2018.
- [4] M. T. Nelp, P. A. Kates, J. T. Hunt, J. A. Newitt, A. Balog, D. Maley, X. Zhu, L. Abell, A. Allentoff, R. Borzilleri, et al. Immune-modulating enzyme indoleamine 2, 3-dioxygenase is effectively inhibited by targeting its apo-form. *Proceedings of the National Academy of Sciences*, 115(13):3249–3254, 2018.
- [5] K. N. Pham and S.-R. Yeh. Mapping the binding trajectory of a suicide inhibitor in human indoleamine 2, 3-dioxygenase 1. *Journal of the American Chemical Society*, 140(44):14538–14541, 2018.

- [6] H. Sugimoto, S.-i. Oda, T. Otsuki, T. Hino, T. Yoshida, and Y. Shiro. Crystal structure of human indoleamine 2, 3-dioxygenase: catalytic mechanism of o₂ incorporation by a heme-containing dioxygenase. *Proceedings of the National Academy of Sciences*, 103(8):2611–2616, 2006.
- [7] K. N. Pham, A. Lewis-Ballester, and S.-R. Yeh. Conformational plasticity in human heme-based dioxygenases. *Journal of the American Chemical Society*, 143(4):1836–1845, 2020.
- [8] A. Lewis-Ballester, S. Karkashon, D. Batabyal, T. L. Poulos, and S.-R. Yeh. Inhibition mechanisms of human indoleamine 2, 3 dioxygenase 1. *Journal of the American Chemical Society*, 140(27):8518–8525, 2018.
- [9] A. Lewis-Ballester, K. N. Pham, D. Batabyal, S. Karkashon, J. B. Bonanno, T. L. Poulos, and S.-R. Yeh. Structural insights into substrate and inhibitor binding sites in human indoleamine 2, 3-dioxygenase 1. *Nature communications*, 8(1):1–8, 2017.
- [10] D. Li, D. L. Sloman, A. Achab, H. Zhou, M. A. McGowan, C. White, C. Gibeau, H. Zhang, Q. Pu, I. Bharathan, et al. Oxetane promise delivered: Discovery of long-acting ido1 inhibitors suitable for q3w oral or parenteral dosing. *Journal of Medicinal Chemistry*, 2022.
- [11] M. M. Hamilton, F. Mseeh, T. J. McAfoos, P. G. Leonard, N. J. Reyna, A. L. Harris, A. Xu, M. Han, M. J. Soth, B. Czako, et al. Discovery of iacs-9779 and iacs-70465 as potent inhibitors targeting indoleamine 2, 3-dioxygenase 1 (ido1) apoenzyme. *Journal of Medicinal Chemistry*, 64(15):11302–11329, 2021.
- [12] D. Li, Y. Deng, A. Achab, I. Bharathan, B. A. Hopkins, W. Yu, H. Zhang, S. Sanyal, Q. Pu, H. Zhou, et al. Carbamate and n-pyrimidine mitigate amide hydrolysis: structure-based drug design of tetrahydroquinoline ido1 inhibitors. *ACS Medicinal Chemistry Letters*, 12(3):389–396, 2021.
- [13] Q. Pu, H. Zhang, L. Guo, M. Cheng, A. C. Doty, H. Ferguson, X. Fradera, C. A. Lesburg, M. A. McGowan, J. R. Miller, et al. Discovery of potent and orally available bicyclo [1.1. 1] pentane-derived indoleamine-2, 3-dioxygenase 1 (ido1) inhibitors. *ACS Medicinal Chemistry Letters*, 11(8):1548–1554, 2020.

- [14] C. White, M. A. McGowan, H. Zhou, N. Sciammetta, X. Fradera, J. Lim, E. M. Joshi, C. Andrews, E. B. Nickbarg, P. Cowley, et al. Strategic incorporation of polarity in heme-displacing inhibitors of indoleamine-2, 3-dioxygenase-1 (ido1). *ACS medicinal chemistry letters*, 11(4):550–557, 2020.
- [15] K. N. Pham, A. Lewis-Ballester, and S.-R. Yeh. Structural basis of inhibitor selectivity in human indoleamine 2, 3-dioxygenase 1 and tryptophan dioxygenase. *Journal of the American Chemical Society*, 141(47):18771–18779, 2019.
- [16] S. Crosignani, P. Bingham, P. Botteman, H. Cannelle, S. Cauwenberghs, M. Cordonnier, D. Dalvie, F. Deroose, J. L. Feng, B. Gomes, et al. Discovery of a novel and selective indoleamine 2, 3-dioxygenase (ido-1) inhibitor 3-(5-fluoro-1 h-indol-3-yl) pyrrolidine-2, 5-dione (eos200271/pf-06840003) and its characterization as a potential clinical candidate. *Journal of Medicinal Chemistry*, 60(23):9617–9629, 2017.
- [17] H. Zhang, K. Liu, Q. Pu, A. Achab, M. J. Ardolino, M. Cheng, Y. Deng, A. C. Doty, H. Ferguson, X. Fradera, et al. Discovery of amino-cyclobutane-derived indoleamine-2, 3-dioxygenase 1 (ido1) inhibitors for cancer immunotherapy. *ACS medicinal chemistry letters*, 10(11):1530–1536, 2019.
- [18] Y. Wu, T. Xu, J. Liu, K. Ding, and J. Xu. Structural insights into the binding mechanism of ido1 with hydroxylamide based inhibitor incb14943. *Biochemical and Biophysical Research Communications*, 487(2):339–343, 2017.
- [19] X.-L. Ning, Y.-Z. Li, C. Huo, J. Deng, C. Gao, K.-R. Zhu, M. Wang, Y.-X. Wu, J.-L. Yu, Y.-L. Ren, et al. X-ray structure-guided discovery of a potent, orally bioavailable, dual human indoleamine/tryptophan 2, 3-dioxygenase (hido/htdo) inhibitor that shows activity in a mouse model of parkinson's disease. *Journal of Medicinal Chemistry*, 64(12):8303–8332, 2021.
- [20] S. Kumar, J. P. Waldo, F. A. Jaipuri, A. Marcinowicz, C. Van Allen, J. Adams, T. Kesharwani, X. Zhang, R. Metz, A. J. Oh, et al. Discovery of clinical candidate (1 r, 4 r)-4-((r)-2-((s)-6-fluoro-5 h-imidazo [5, 1-a] isoindol-5-yl)-1-hydroxyethyl) cyclohexan-1-ol (navoximod), a potent and selective inhibitor of indoleamine 2, 3-dioxygenase 1. *Journal of Medicinal Chemistry*, 62(14):6705–6733, 2019.
- [21] Y.-H. Peng, S.-H. Ueng, C.-T. Tseng, M.-S. Hung, J.-S. Song, J.-S. Wu, F.-Y. Liao, Y.-S. Fan, M.-H. Wu, W.-C. Hsiao, et al. Important hydrogen bond networks in

- indoleamine 2, 3-dioxygenase 1 (ido1) inhibitor design revealed by crystal structures of imidazoleisoindole derivatives with ido1. *Journal of medicinal chemistry*, 59(1):282–293, 2016.
- [22] U. F. Röhrig, S. R. Majjigapu, A. Reynaud, F. Pojer, N. Dilek, P. Reichenbach, K. Ascencao, M. Irving, G. Coukos, P. Vogel, et al. Azole-based indoleamine 2, 3-dioxygenase 1 (ido1) inhibitors. *Journal of Medicinal Chemistry*, 64(4):2205–2227, 2021.
- [23] U. F. Röhrig, A. Reynaud, S. R. Majjigapu, P. Vogel, F. Pojer, and V. Zoete. Inhibition mechanisms of indoleamine 2, 3-dioxygenase 1 (ido1). *Journal of medicinal chemistry*, 62(19):8784–8795, 2019.
- [24] J. A. C. Alexandre, M. K. Swan, M. J. Latchem, D. Boyall, J. R. Pollard, S. W. Hughes, and J. Westcott. New 4-amino-1, 2, 3-triazole inhibitors of indoleamine 2, 3-dioxygenase form a long-lived complex with the enzyme and display exquisite cellular potency. *ChemBioChem*, 19(6):552–561, 2018.
- [25] Y.-H. Peng, F.-Y. Liao, C.-T. Tseng, R. Kuppusamy, A.-S. Li, C.-H. Chen, Y.-S. Fan, S.-Y. Wang, M.-H. Wu, C.-C. Hsueh, et al. Unique sulfur–aromatic interactions contribute to the binding of potent imidazothiazole indoleamine 2, 3-dioxygenase inhibitors. *Journal of Medicinal Chemistry*, 63(4):1642–1659, 2020.
- [26] S. Tojo, T. Kohno, T. Tanaka, S. Kamioka, Y. Ota, T. Ishii, K. Kamimoto, S. Asano, and Y. Isobe. Crystal structures and structure–activity relationships of imidazothiazole derivatives as ido1 inhibitors. *ACS medicinal chemistry letters*, 5(10):1119–1123, 2014.

Chapter 9

Plasticity outside the protein: discovery of an exo site

9.1 Introduction

After this complete study of the active site, the question is to know how the plasticity of hIDO1 is conferred at the active site only. In 2019, Greco *et al.* [1] highlighted the experimental existence of such an exo-site, located somewhere other than at the active site, without structural information on its location. In crystallographic structures, it is not unusual to find ligands outside the active site. This is mostly due to stabilization between crystal interfaces. As part of this research, and to learn more about the plasticity of hIDO1 outside its active site, ligands outside the protein were systematically studied. The present chapter deals with these results which enrich the knowledge on the functioning of the enzyme. This chapter, regarding the analysis in structures with L-Trp, is part of the article "Temporary Intermediates of L-Trp Along the Reaction Pathway of Human Indoleamine 2,3-Dioxygenase 1 and Identification of an Exo Site" published in 2021 by M. Mirgaux in *International Journal of Tryptophan Research*. [2]

9.1.1 Questioning the existence of an exo site in hIDO1

The questioning of the existence of an exo site in hIDO1 was first performed on the basis of structures with L-Trp obtained in the first chapter of this part (7nqe, 7p0r and 7p0N, Chapter 6). In the three crystal structures, it is possible to observe L-Trp or NFK molecules outside the enzyme, mostly at the interface between monomers in the crystal packing. However, in some monomers of these three crystal structures, L-Trp and NFK molecules are observed with no other monomer less than 10 Å away by crystal symmetry. Such a location site, called exo site, is located in the small subunit around residues I50 to R56 and W92 to R100. Within the structure hIDO1-closed, L-Trp is found in monomer B. In hIDO1-intermediate, two monomers (B and C) contain L-Trp and NFK, respectively. The hIDO1-open structure contains an NFK molecule in monomer A.

L-Trp and NFK are not in the same orientation in the different monomers, as illustrated in Figure 9.1. It is explained by the amount of electrically charged residues of the exo site, which stabilize the polar groups of the molecules. Nevertheless, the common aromatic moiety of the ligands occupies a pocket (pocket I, in green, Figure 9.1, A.) composed of residues L49, I50, G53, and L55. The stabilization of the polar part of the ligands can be achieved with two other pockets (II and III). Pocket II (Figure 9.1,

A., I., in blue) is composed of the residues R100, E57, and/or E60, while the pocket III (Figure 9.1, A., II., in pink) includes the main chain of residues K94 and G93, as well as the lateral chain of D98. The contribution of R56 appears in both polar pockets. The interaction maps (Figure 9.1, B.) highlight that the positioning does not matter what type of ligand it is. Indeed, the position of L-Trp in the hIDO1-closed structure (Figure 9.1, B., I.) is close to that of NFK in monomer C of hIDO1-intermediate (Figure 9.1, B., III.). In contrast, the polar part of L-Trp in the monomer B of hIDO1-intermediate (Figure 9.1, (d), II.) is closer to the position of NFK in hIDO1-opened (Figure 9.1, B., IV.).

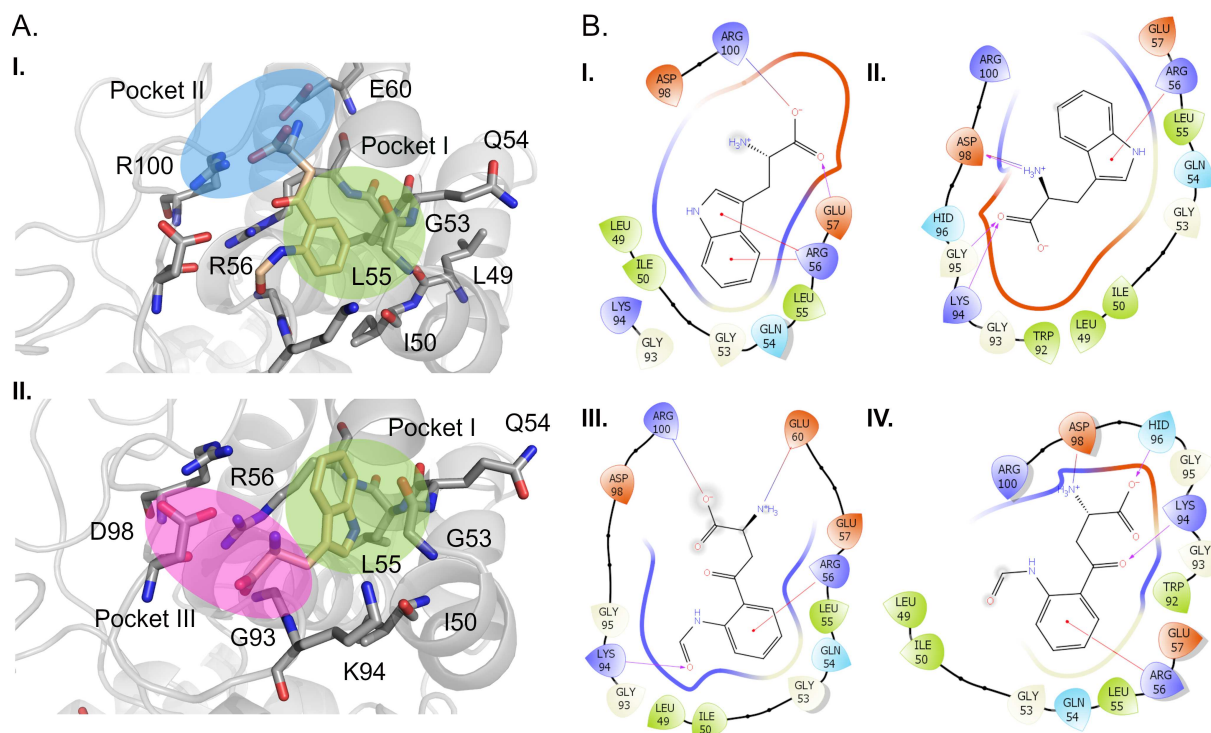


FIGURE 9.1: L-Trp and NFK binding in the exo site of the small subunit of hIDO1. Pocket I is in green while pocket II and III are respectively in blue and in pink. A. I. NFK in monomer C of hIDO1-intermediate as positioned in the pockets I and II. II. L-Trp in monomer B of hIDO1-intermediate as positioned in the pocket I and III. B. Interaction maps of L-Trp or NFK in the exo site of the different monomers (I. = Monomer B of hIDO1-closed, II. = Monomer B of hIDO1-intermediate, III. = Monomer C of hIDO1-intermediate, IV. = Monomer A of hIDO1-opened).

Beside the crystallography results, a computational study was performed using Maestro [3] to determine the possible binding sites at the protein surface. The calculations were carried out using the SiteMap tool on monomers with or without a ligand in the exo site. Although the known active site of hIDO1 is recognized as the best site with a site score higher than 1.0 [3], the program also finds the site of the small subunit with a lower score of 0.6-0.7 (Table 9.1). The volume of the active site is lower in the case of monomer A in hIDO1-closed due to the closed conformation of the JK-loop. In the two other monomers, it is bigger due to the absence of refinement of the JK-loop (free space caused by the lack of residues refinement). According to this approach, the exo site has an overall size between 45 \AA^3 and 90 \AA^3 (Table 9.1). This shows some variability of the pocket depending on the monomer. Surprisingly, the hIDO1-intermediate structure is characterized by narrower binding sites. So far, it is not possible to establish a link between the position of the loop and the size of the exo site. The observation of the site surface interacting with L-Trp or NFK inside shows that this exo site is indeed able to accommodate an NFK as well as a L-Trp molecule. All these results support the recent study performed by Greco *et al.* [1] who suggested that an exo site may be present in hIDO1. The study of the role for this site is an interesting track to follow in the near future.

TABLE 9.1: SiteMap analyses for the different monomers with ligand in the exo-site or in the active site in the three hIDO1 crystal structures.

Structure	Monomer	Molecule in exo site	Active site Site score	Volume (\AA^3)	Exo site Site score	Volume (\AA^3)
Closed	A	/	1.074	119.4	0.646	69.4
	B	L-Trp	1.036	460.4	0.718	81.6
Intermediate	B	L-Trp	1.023	621.9	0.611	51.2
	C	NFK	1.018	535.7	0.573	45.5
Opened	A	/	1.029	446.4	0.745	89.4
	C	NKF	1.064	376.0	0.729	71.0

The structure with L-Kynurenine underwent the same analysis. However, despite the presence of L-Kynurenine outside the active site, no molecule is found in the new exo site. This site could therefore be specific to L-Trp and NFK. It is interesting to note that this pocket can also be occupied by a glycerol molecule in the structures.

9.2 Occupancy of the exo site in the other PDB structures

To study the occupancy of the exo site in other PDB structures, the structures on the PDB containing L-Trp in the active site have been analyzed as well as their electron density map. These structures can be grouped in two groups according to the type of crystal assembly, namely 1) those with two molecules in the asymmetric unit (6dpq, 6e35, 6cxu, 5wmx, 5wmw, 5wmv, 5wmu and 6ubp) 2) those with four molecules in the asymmetric unit (6e40, 6e44 and 6azu). For the situation with two molecules in the asymmetric unit¹, the observations are systematically identical. Monomer A present no residual density in the potential exo site. This is justified by the crystal packing which leads to an interface at this place. The molecule are too close in this crystal packing to allow the binding of a molecule of L-Trp in the pocket. The site is not very refined at the level of the side chains in most of the monomers. This is mainly due to the relatively high motion of these residues (bfactor larger than 135 \AA^2). On the other hand, for monomer B, these chains are very clearly refined. There is an unresolved residual electron density in most structures exactly at the potential location of an L-Trp molecule, as highlighted by the Figure 9.2. This density overhang is not satisfied by the positioning of water molecules (as in 5wmv) since residual density is still visible. It is then possible to position a glycerol (like in 6dpq and potentially in 6ubp and 5wmu) or L-Trp (potentially in 5wmx, 5wmw, 5wmv and 6cxu).

During the thesis, this analysis has been done for the different structures based on the maps available on the PDB. For example, monomer B of structure 5wmx (Figure 9.2, A.) shows a residual density in the supposed exo-site before addition of the ligand. Using the program Coot, a search for L-Trp present in the structure with a cut-off of 1.0 for the $2F_o - F_c$ density map is performed. The ligand is directly found in monomer B. The new refinement proposal, with this new exo ligand, is submitted to two cycles of refinement by Phenix (with removal of the ligand in the inhibitor pocket since it does not seem to be realistic). The result is shown in Figure 9.2, B. The new density map fits the ligand, with no extra residual density (Figure 9.2, B. and C.). The results could undoubtedly be further improved by varying the ligand occupancy. The real-space correlation score is then 0.78. The alignment of this new monomer with monomer B of hIDO1-closed structure (Figure 9.2, D.), also contain a L-Trp in the exo site, shows a similar positioning of the two ligands, despite a different occupancy of

¹except for 6e35.

the pockets, as mentioned in the previous section. The aromatic part is in pocket I, composed of I50, G53 and L55. The polar part is stabilized in pocket II, as it was the case in monomer B of the hIDO1-closed structure with interactions including R100 and lateral chain of G53.

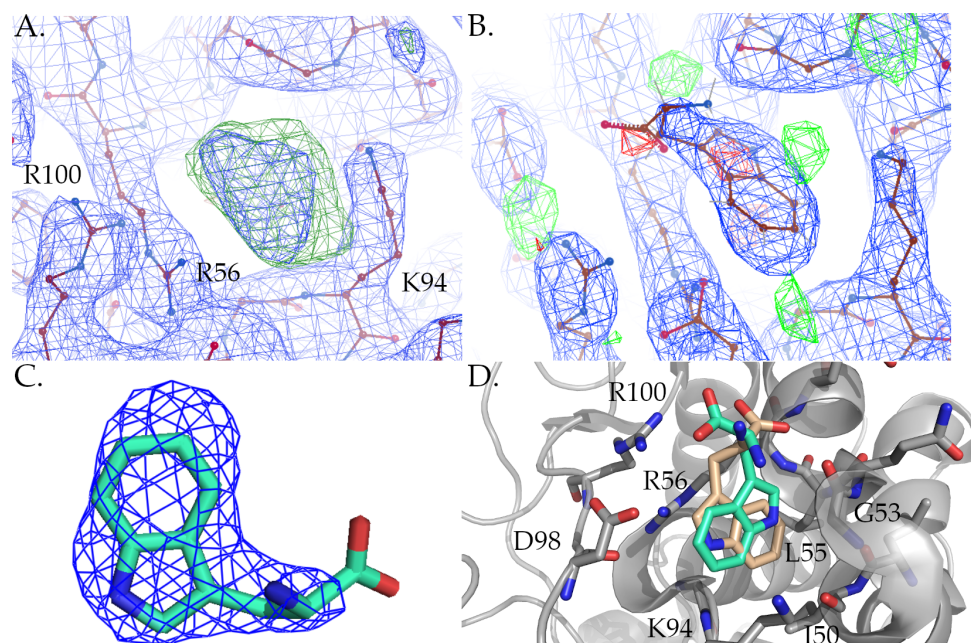


FIGURE 9.2: Possibility of occupying the exo site in monomer B by L-Trp for the 5mwx structure. A. Residual density around the exo site residues. B. Possibility of L-Trp position obtained by Coot program and refinement by Phenix. C. Density around the added L-Trp in the exo site after two refinement cycles ($\sigma = 1.0$, carve = 1.9) D. Alignment with monomer B from the hIDO1-closed structure (7nge).

This methodology was also applied to other structures with L-Trp (6dpq, 6e35, 6cxu, 5wmw, 5wmv, 5wmu and 6ubp) which potentially also containing L-Trp in the exo-site. In each case, repositioning of a substrate molecule in the exo site is possible, with good consistency of the density maps. However, the occupancy of pockets II and III can differ. This might indicate that this site does not necessarily have a specific type of binding but a great plasticity that can favor the ligands binding. For example, in the case of structure 5wmw, monomer B has an L-Trp molecule with the aromatic part in pocket I and the polar part in pocket III. Thus, the carboxylate is stabilized by K94 while the amine part is interacting with D98 (Figure 9.3). In structures with four molecules in the asymmetric unit (6e44, 6e40), no ligands are observed in the exo-pocket except for a lot of water and small buffer molecules (phosphate, glycerol). This is partly explained by the crystal packing. In conclusion, the packing has a great

influence on the presence of a molecule in the exo site. In case of steric hindrance, the site is completely missed. Combined with the lack of research/refinement of the small subunit parts and the rather recent discovery of Greco *et al.*, it justifies the lack of previous research about this exo site. Thus, the new crystal packing identified to premise a refinement of the JK-loop is then also essential to observe the exo site bound to ligand molecules.

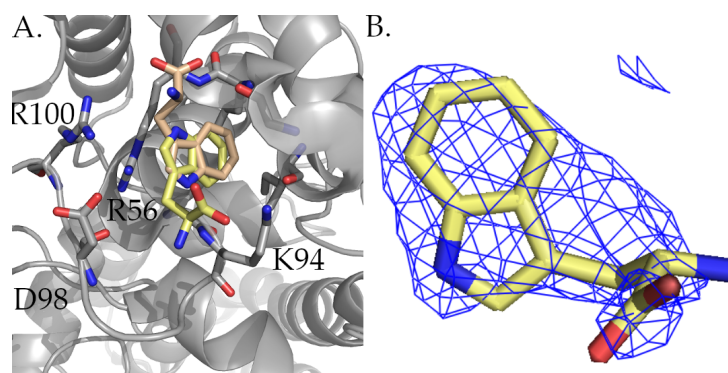


FIGURE 9.3: Possibility of occupying the exo site in monomer B by L-Trp for the 5wmw structure. A. Alignment of monomer B from 5wmw with monomer B from the hIDO1-closed structure (7nge). B. Density around the added L-Trp in the exo site after two refinement cycles ($\sigma = 0.8$, carve = 2.0).

9.3 Investigation of the exo site by Molecular Dynamics

To deepen the understanding of the exo site, MD simulations were carried out. For this purpose, different simulations were performed with a L-Trp or a NFK molecule left free to move near the hIDO1 monomer. The ligand position was chosen to be similar to a NFK position observed outside the enzyme, at a dimeric interface, due to the crystal stacking. Without the interactions caused by the packing, it can be assumed that the ligand is free to move where it wishes and can end up in the sites where it has the highest affinity. The protein presents a closed conformation of the JK-loop (PDB: 7nge). Simulations with L-Trp were performed with and without L-Trp in the active site. To summarize, three kinds of simulations were performed, one with L-Trp outside the active site, one with L-Trp outside and inside the active site and one with NFK outside the active site. Each kind of simulations is run in triplicates (R1, R2 and R3).

9.3.1 Simulation with a L-Trp molecule

For the case of simulations with a L-Trp outside the protein, Figure 9.4, A. reports the r.m.s.d deviations of the three replicates in comparison to the initial structure. The deviation trend is of the same order of magnitude. Contrarily, the r.m.s.f profiles report that R1 and R3 lead to a highly agitated N-terminal part of the JK-loop, specially for P370 residue, in comparison to R2 (Figure 9.4, B.). The r.m.s.f values for the whole JK-loop are high in comparison to the simulations without any ligand, as simulations with L-Trp in the active site. This high flexibility of the JK-loop in the MD replicate R1 and R3 vs. the R2 is due to the displacement of an external L-Trp ligand and the binding of this latter close to the loop. Indeed, in the case of R2, the substrate molecule does not bind to a binding site during the 300 ns of simulation. It rotates around the macromolecule and does not stabilize in pockets for long period of time. The presence of the ligand does not influence the motion of the loop since it does not position itself nearby. For R1 and R3, the ligand stabilizes in a binding pocket formed by the N-terminal part of the JK-loop (NJK, Figure 9.4, C.). This binding, observed for almost 150 ns in R1 and 100 ns in R3, causes a conformational change in the JK-loop and justifies this flexibility. To sum up, despite the same starting point and a convergence of the global protein structure, the displacement of the ligand differs between replicates.

At 50 ns, the ligand in R3 (Figure 9.5) initiates an approach to enter in the pocket formed by the N-terminal JK-loop (called the NJK site), close to residues 218 to 222 and lysine K352 upstream of the N-terminal part of the loop. At the beginning of this binding (≈ 60 ns), the protein structure is considered to be closed at the C-terminal part, with no opening of the JK-loop (Figure 9.5, C.). The N-terminal part is globular and completes the closure of the enzyme. The L-Trp molecule remains in this site for a period of 100 ns. Unrelated to this movement, the loop simultaneously organizes itself to form an alpha helix folding for residues P370 to E375 at 100 ns, as already observed in the simulations without ligands (Figure 9.5, A. and C., II.). This arrangement should be taken with caution, due to the known artifact of CHARMM27. [4, 5] The structure observed by this conformational change at 100 ns shows a partial opening of the N-terminal extremity of the JK-loop towards the active site. After 100 ns, the movement of the JK-loop is still active, especially at the N-terminal part, leading to a wide opening of the enzyme towards the active site at 180 ns (Figure 9.5, C.).

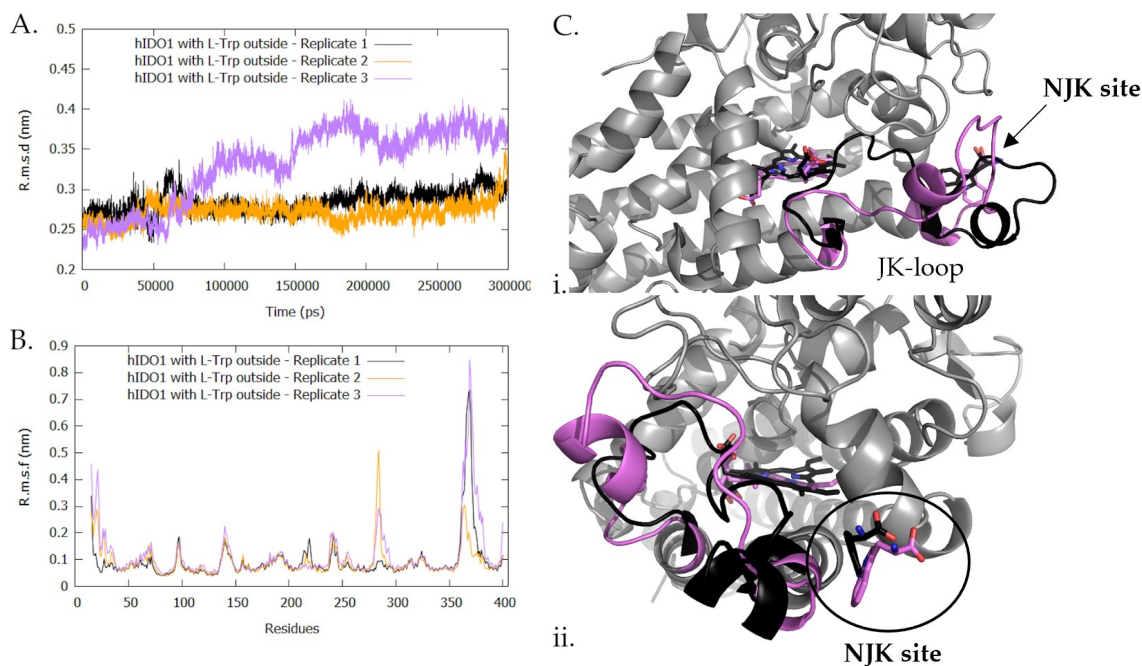


FIGURE 9.4: Replicate reproducibility for 300 ns simulation at 310 K and 1 bar with closed JK-loop hIDO1 and a L-Trp molecule outside the enzyme. A. R.m.s.d profiles of the protein residues in comparison to the starting conformation. B. R.m.s.f profiles of the protein residues. C. Two perpendicular views (i. and ii.) of the JK-loop conformation observed for R1 (black) and R3 (purple) at 190 ns.

After 200 ns, the loop at the N-terminal end is open and the substrate moves to the C-terminal part of the JK-loop. Unfortunately, the strong interaction between K377 and the cofactor prevents the full opening of the active site and thus the entry of the substrate. It is assumed that its opening requires either 1) more time or 2) factors involving O_2 binding or 3) the consideration of electronic effects. This may explain why it is not observed in classical MD simulations.

Further measurements (Figure 9.6) have shown that this prevention of loop opening at the C- and N- terminus is even more pronounced when an L-Trp molecule is already in the active site. The MD simulations with an L-Trp inside the active site and an L-Trp outside were performed in triplicate. All triplicates are consistent, with similar values of r.m.s.d and r.m.s.f (Figure 9.6, A. and B.). The external L-Trp molecule binds close to the loop only but does not lead to its opening. The loop remains stable conformationally, which is consistent with the ligand stabilizing effect on the loop, as already mentioned in the previous chapter (Figure 9.6, C.). Moreover, there is no

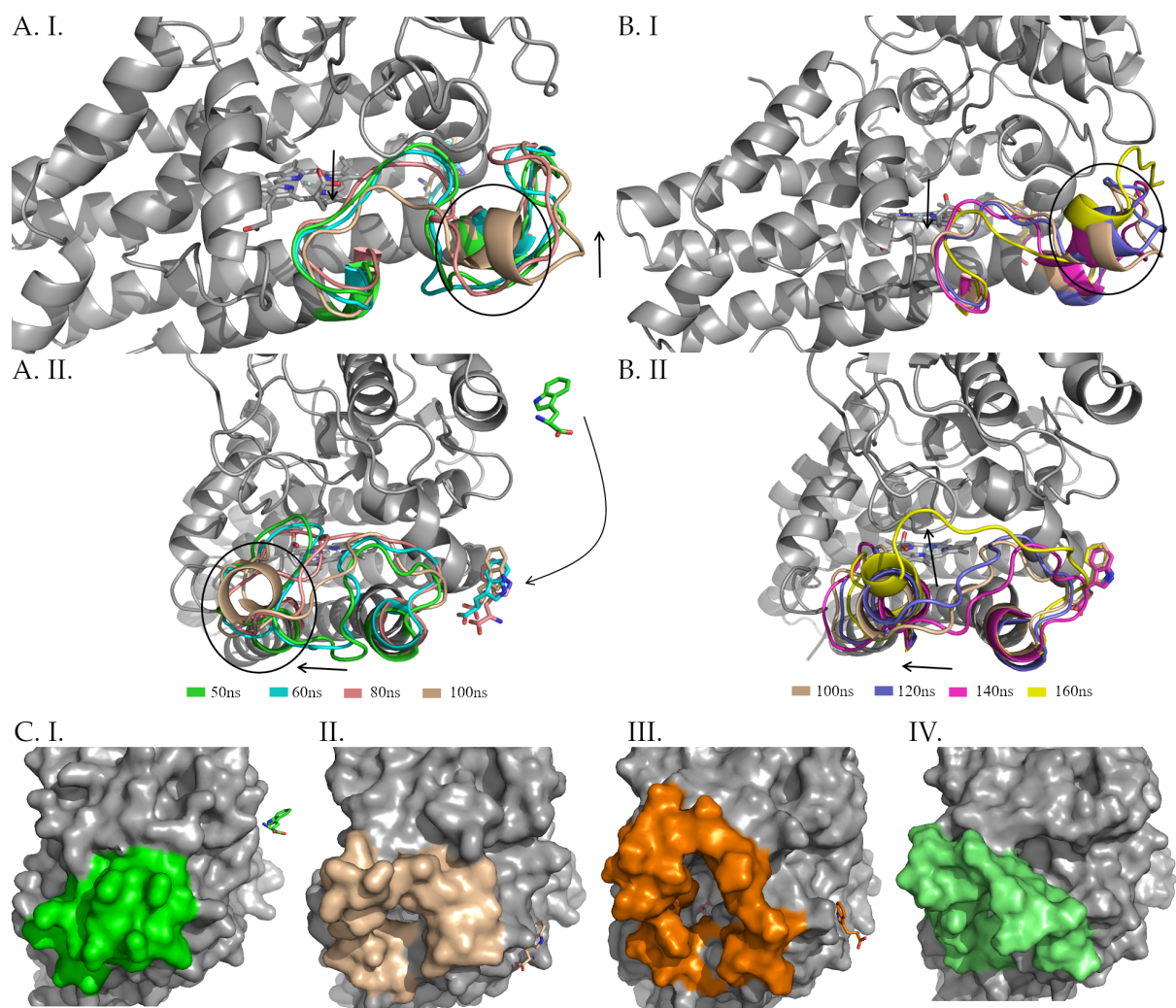


FIGURE 9.5: Displacement of the JK-loop during the unrestrained MD simulation at 310 K and 1 bar. A. Two perpendicular views (I. and II.) of the conformational changes in the JK-loop during the first 100 ns of simulation. B. Two perpendicular views (I. and II.) of the conformational changes in the JK-loop during the 100 ns and 160 ns of simulation. C. Surface change of the protein during the simulation at I. 50 ns, II. 100 ns, III. 180 ns and IV. 200 ns.

point here in opening the loop if the reaction has not yet taken place and L-Trp, the substrate, is still in the active site. Consequently, the decrease of the r.m.s.f values of the JK-loop is of a factor 2 in comparison to the simulations with an external L-Trp without L-Trp in the active site. The r.m.s.f values of the N-terminus are then of the same order as for the simulations without ligand or with a single L-Trp in the active site. The r.m.s.f values for the C-terminus remain slightly higher.

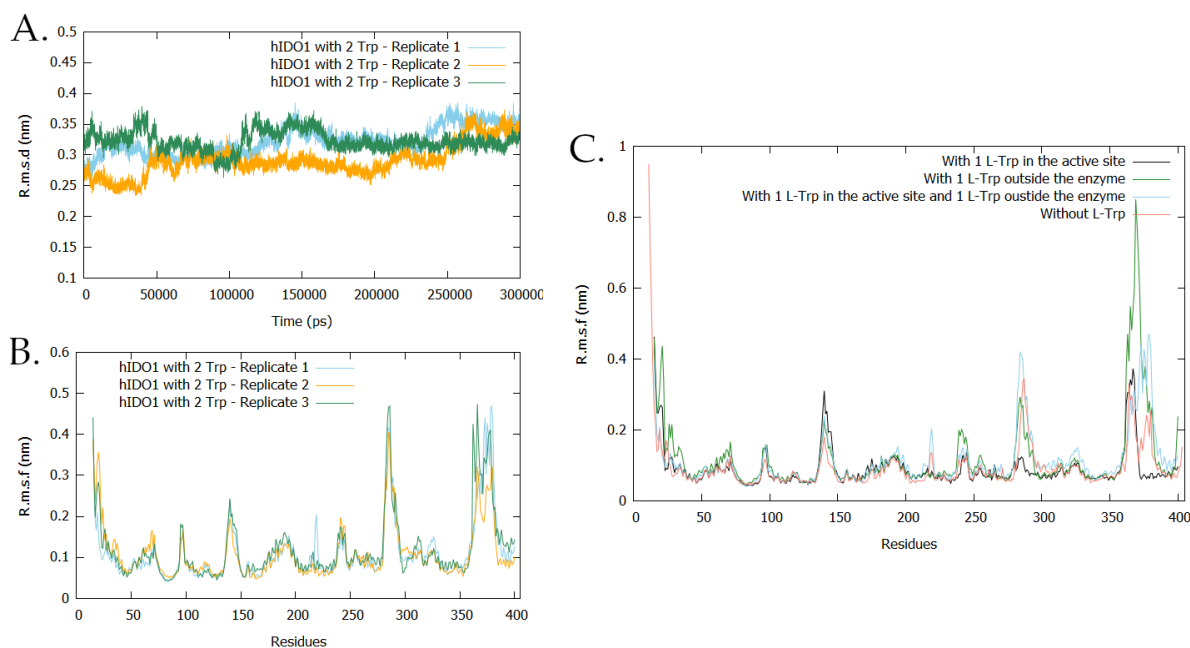


FIGURE 9.6: Replicate reproducibility for 300 ns simulation at 310 K and 1 bar with closed JK-loop hIDO1 and a L-Trp molecule outside the enzyme and a L-Trp molecule in the active site. A. R.m.s.d profiles of the protein residues in comparison to the starting conformation. B. R.m.s.f profiles of the protein residues along the 300 ns. C. Comparison of r.m.s.f profiles from 300 ns MD simulations at 310 K and 1 bar for hIDO1 with L-Trp inside or outside the protein. R3 is considered for the simulations with one L-Trp molecule outside the enzyme and R1 is used for the simulations with two L-Trp molecule (one inside and one outside).

To conclude, even if the characterization of a ligand motion around a protein is a multiple solution problem, the MD simulations carried out in the present work provides significant information. Firstly, the presence of the substrate near the dynamic loop leads to an flexibility increase of that loop. As a consequence, it is considered to initiate its opening at both the C- and N-terminal part. Secondly, even if there are other binding sites on the surface, it is possible that L-Trp has a tendency to bind near the loop, in a site called NJK. This site is located between the N-terminus and the exo site. It enhances the loop flexibility effect and could, in the long run, help the substrate to enter the active site. Lately, this phenomenon of increased mobility is no longer visible when L-Trp is already in the site. It is explained by a stabilization of the loop by the internal L-Trp, and the loop remains closed until the reaction has takes place.

9.3.2 Simulation with a NFK molecule

The same type of simulations were run with the NFK molecule. From the point of view of the deviation from the initial structure, the r.m.s.d profiles of the protein varies in a similar way between the three replicates. R.m.s.f values are also of the same order of magnitude in the triplicates, although a difference is observed for the dynamic parts (F-helix and JK-loop) as a function of the replicates. This can be attributed to the displacement of the product during the simulations. Indeed, in all the MD simulations, the molecule moves around the protein. However, it does not always fit in the exo site. There is only one simulation where such a displacement is observed. In the two other cases, it interacts with the N and C-terminus extremities of the protein. The NFK molecule is also occasionally observed at the F-helix and EF-loop in the simulations. In the rest of this chapter, an in-depth analysis of the MD simulation where it is located in the exo site (R1) is performed.

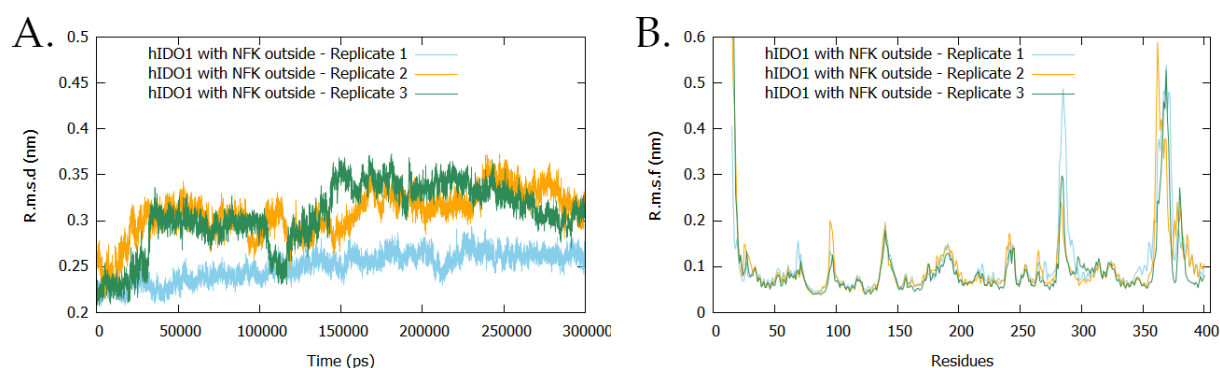


FIGURE 9.7: R.m.s.d and r.m.s.f profiles obtained from the 300 ns of MD simulations at 1 bar and 310 K. R.m.s.d deviations are calculated in comparison to the starting structure of the three replicates.

During the production stage, the displacement of the free-NFK molecule around the protein is observed (Figure 9.8). After remaining for a short time in circulation around the enzyme, the molecule binds to the NFK site. The position is maintained for a time period range of about 50 ns (from 150 to 190 ns). After that, the NFK molecule progressively moves towards the exo-site, goes through an intermediate site (named the IS site, at 190 ns and 200 ns), and eventually binds to the exo site (named the ES site, from 210 ns to 290 ns). NFK then adopts different positions in this exo site (from 230 ns to 290 ns) and leaves the exo site at the end of the dynamics (300 ns) (Figure 9.8). The positions between 230 ns and 290 ns are close to the position IV, described in Figure 9.1 as observed by crystallography. Interactions with R100, D94 and R56

are observed. The main chain of K94 helps to the stabilization of the NFK molecule (Figure 9.8). To verify the affinity of the observed positions, a MM-GBSA calculation was performed for each of them. The values are reported in Table 9.2. An affinity of NFK is observed regardless of the binding site. However, values are better for the NJK site. Probably, the departure of NFK from the NJK site comes from a steric clash induced by the conformational change and not from a lack of affinity for the binding site.

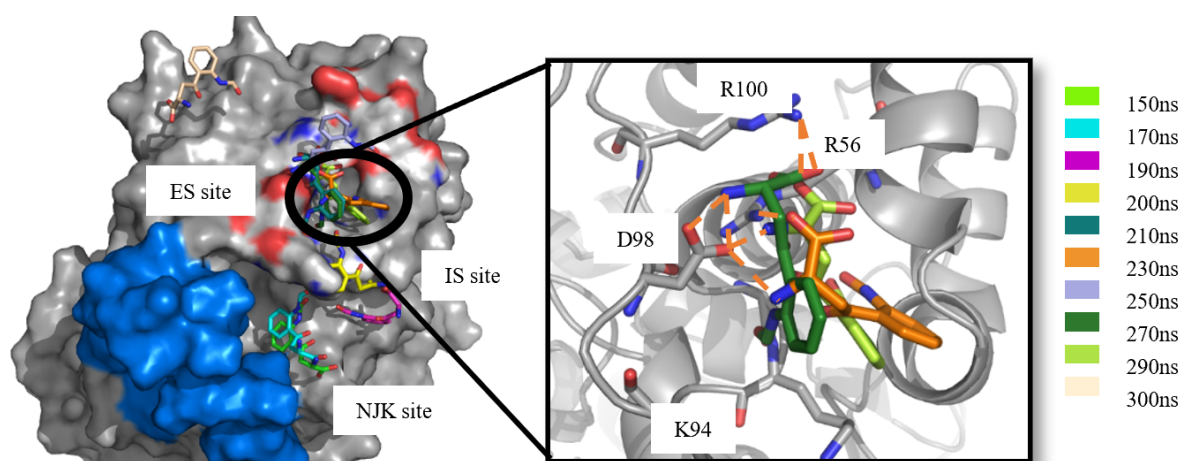


FIGURE 9.8: Left - Displacement of NFK snapshots observed at 150 ns and 300 ns around the protein as obtained during 300 ns of unrestrained MD simulation at 310 K and 1 bar. The surface of the protein appear in grey and the JK-loop in blue. The exo site is highlighted with the dark circle and the oxygen and nitrogen atoms of the amino acid side chains composing the exo site are highlighted in red and blue respectively. Right - Interaction of NFK snapshot at 230 ns, 270 ns and 290 ns with the exo pocket.

To understand what triggers the movement of the NFK molecule, the observed conformations of the JK-loop according the different snapshots of the simulation were analyzed (Figure 9.9). The results show that the conformation of C-terminal part of the loop is not affected by the displacement of the NFK around the protein. Regarding the N-terminal part of the loop, the closer it is the snapshots are to the exo site, the more open it is. It is therefore possible that it is this movement of the N-terminal part of the JK-loop that is responsible for the displacement of the NFK molecule. The displacement of the NFK molecule seems to be caused by a cascade of side chain rearrangements in the protein. During the NFK displacement, the JK-loop interacts with the DE-loop which, in turn, interacts with the V91-V102 fragment of the small

TABLE 9.2: MM-GBSA (ΔG_{bind}) of different snapshots of NFK as observed during the MD simulations at 300 K and 1 bar. The calculations are performed using Maestro. [3]

MD Time (ns)	Site occupied by NFK	ΔG_{bind} (kcal/mol)
150	NJK	-36.0
170	NJK	-35.9
190	IS	-17.3
200	IS	-18.2
230	Down to the exo site (ES)	-22.3
270	ES	-19.1
290	ES	-19.7
250	Up to the exo site (ES)	-11.2
300	Outside	-14.9

subunit (Figure 9.10). It is therefore possible that the exo site is a binding step of the product before leaving the active site, and acts as a molecular arm.

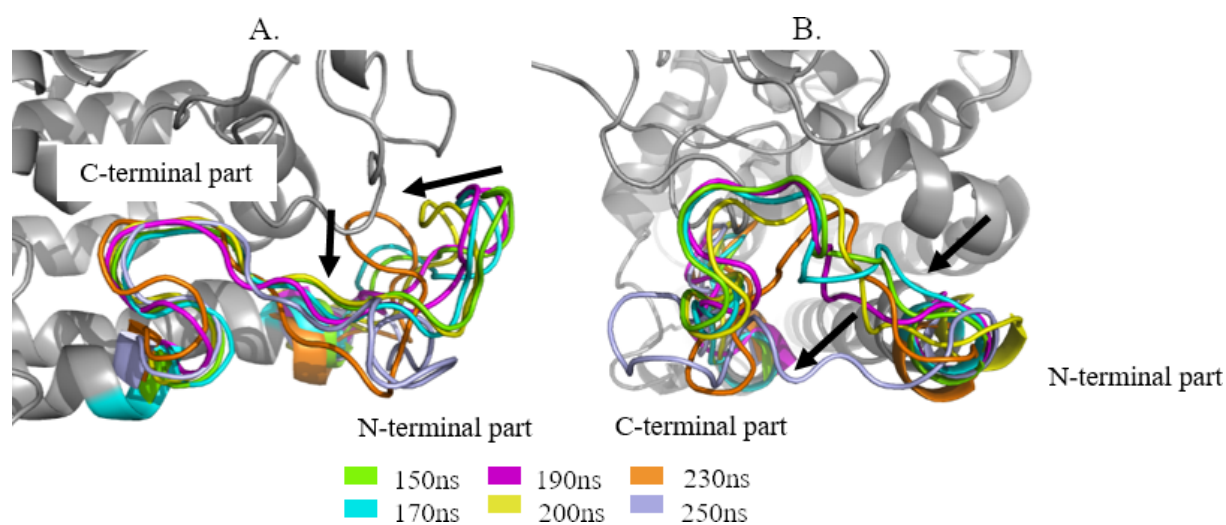


FIGURE 9.9: Two perpendicular views (A. and B.) of the displacement of the JK-loop during 300 ns of unrestrained MD simulation at 310 K and 1 bar.

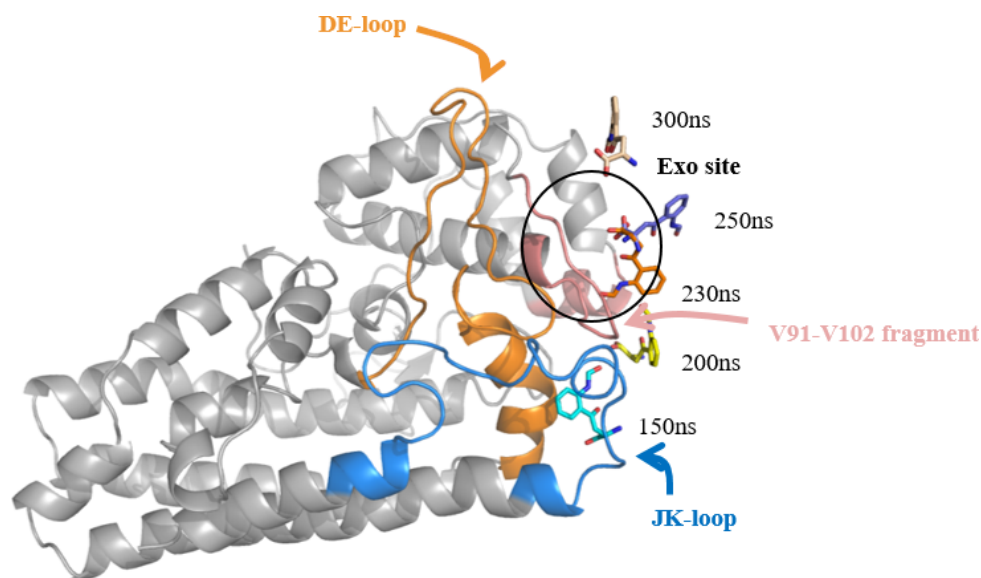


FIGURE 9.10: Summary of the loops and residue fragments involved in NFK exit from the active site. JK-loop appears in blue, DE-loop in orange and V91-V102 fragment in pink.

9.4 Intermediate conclusions

Experimental evidence has demonstrated the presence of an exo site in hIDO1. Although its role is still unknown, its location was discovered using the L-Trp-hIDO1 structures refined during this thesis. The site is located at the level of the small subunit, close to amino acids R100, D94, E56, and G53. It is composed of a binding pocket for the apolar part (pocket I) and two possible pockets for the polar part (pocket II and III). As the occupancy of these two pockets differs according to the monomers studied, it is suggested that the exo site is characterized by a great plasticity of this site. Analyses of density maps of PDB other structures in the presence of L-Trp highlighted that the occupancy of the site is also possible in other structures. The occupancy depends on the crystal packing arrangement.

A MD study was then performed to understand the role of the exo site in the dynamics of the protein. It turns out that the JK-loop is strongly influenced, in terms of flexibility, by the presence of L-Trp at the surface of the enzyme. In this case, an opening of the loop is initiated, where the ligand pass through an external site of the loop in the N-terminal part, named NJK. This site could be linked to the exo site by studying the protein in the presence of NFK. It seems that there is a pathway between

the exo site, the NJK site and the loop, possibly allowing the entry of the substrate or the exit of the products. However, this discovery should be taken with caution as it is not reproducible in terms of MD replicates. A deeper knowledge of this site, possibly for a regulation of the protein, is an interesting perspective.

Bibliography

- [1] F. A. Greco, E. Albin, A. Coletti, D. Dolciami, A. Carotti, C. Orabona, U. Grohmann, and A. Macchiarulo. Tracking Hidden Binding Pockets Along the Molecular Recognition Path of l-Trp to Indoleamine 2,3-Dioxygenase 1. *ChemMedChem*, 14(24):2084–2092, 2019.
- [2] M. Mirgaux, L. Leherte, and J. Wouters. Temporary intermediates of l-trp along the reaction pathway of human indoleamine 2, 3-dioxygenase 1 and identification of an exo site. *International Journal of Tryptophan Research*, 14:1–11, 2021.
- [3] Schrodinger. Schrodinger release 2021-2. SiteMap. LLC, New-York, NY, 2021.
- [4] M. Feig, A. D. MacKerell, and C. L. Brooks. Force field influence on the observation of π -helical protein structures in molecular dynamics simulations. *The Journal of Physical Chemistry B*, 107(12):2831–2836, 2003.
- [5] M. D. Smith, J. S. Rao, E. Segelken, and L. Cruz. Force-field induced bias in the structure of $\alpha\beta 21-30$: A comparison of opls, amber, charmm, and gromos force fields. *Journal of Chemical Information and Modeling*, 55(12):2587–2595, 2015.

Part IV

Comprehensive study of hIDO2 plasticity

*“Ouais, et c’est jamais, jamais vraiment la même
Et ça, moi j’en suis persuadée
Si j’me l’suis pas vraiment promis à moi-même
Que cette fois c’est sûr, ça va aller”*

Angèle - Pensées positives

Chapter 10

Crystallization tests and construction optimization for hIDO2

10.1 Introduction

At this time, no experimental structural information is currently available for the hIDO2 protein. The few information are models by homology, or recently, the contribution of AlfaFold. [1, 2] In this chapter, the crystallization tests performed on hIDO2 are detailed. The aim was to obtain the first crystallographic structure of the enzyme. This part was achieved with the precious help of two students under my supervision: Berta Vall and Robin Zanelli.

10.2 Crystallization assays of hIDO2 WT

After optimization of the protein production and purification, a pure sample of hIDO2 is submitted to various tests. For this purpose, the PACT, JCSG+ and BCS crystallization kits were investigated with a protein concentration of 20 mg mL^{-1} . [3, 4]

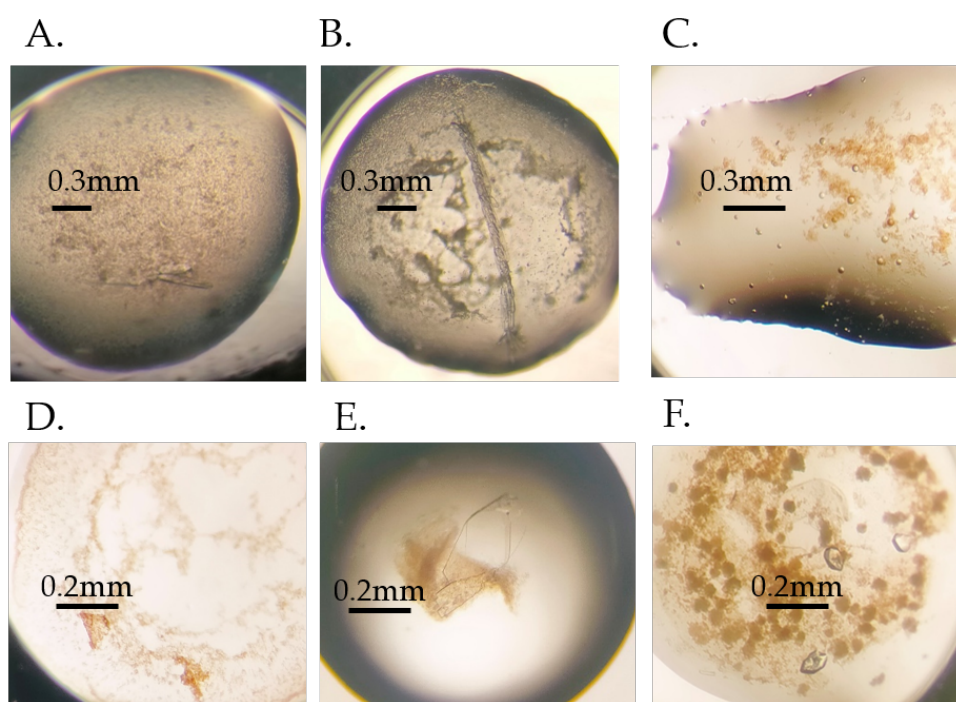


FIGURE 10.1: Crystallization hits of hIDO2. All hits are obtained in phosphate-based buffer A. Salt (BCS kit) B. Salt (BCS kit) C. No diffraction (JCSG+ kit) D. Amorphous (JCSG+ kit) E. No diffraction (PACT kit) F. Salt (PACT kit).

For each kit, the crystallization of the protein is studied in different buffers such as a phosphate-based buffer, a HEPES-based buffer or a TRIS-based buffer. Lastly, the protein is studied in buffer with or without DTT in order to evaluate the influence of the oxido-reductive state of the cofactor but also of the cysteine on the surface on the crystallization. Since the heme cofactor of the protein is known to be low incorporated, it is expected to have both red (protein with cofactor) or apo (protein without cofactor) crystals. Several crystallization hits, mainly transparent crystal, could be obtained (Figure 10.1). Unfortunately, the synchrotron analysis showed that they were salt crystals or amorphous solids without diffraction spots. Around all these hits, the presence of a reddish precipitate, which can be associated with the protein, is observed. The causes of this failure of crystallization can be diverse. The crystallization of a protein is an event that occurs when several conditions are met (Figure 10.2). To crystallize, the sample needs a protein stability. This includes compositional stability (homogeneity of the mixture, proteolysis and stability over the time) but also conformational stability (absence of disordered region). [5] It is logical that a protein with more disordered parts will have more difficulties to organize itself in the solid state in crystalline form. However, stability is not the only element deciding crystallization. In addition, there are thermodynamic effects (which take into account the conditions of crystallization) and kinetic effects (which determine the time that the process will take). [5] If any of these parameters is missing, crystals are unlikely to be obtained.

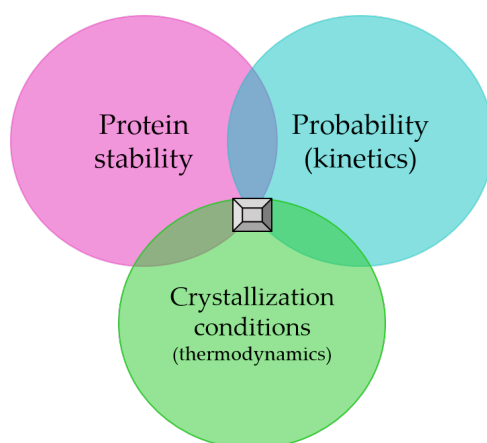


FIGURE 10.2: Conditions necessary for protein crystallization. Image inspired by Deller *et al.* [5]

Within these conditions to crystallize are several known gaps in hIDO2. These gaps concern the protein stability (compositional and conformational). First, as the

heme incorporation is low, an inhomogeneity is present in the mixture, leading to two populations of proteins (apo or holo). Since crystallization is the repeated arrangement in long range space of an identical motif, inhomogeneity is a non-negligible obstacle. Due to this reason, for the rest of the optimization, the phosphate buffer was preferred for the crystallization of the protein. Indeed, as mentioned in chapter 5, the latter allows a better absorbance ratio of the cofactor. Secondly, the hIDO2 WT protein is not very stable (T_m of 47.7 degrees, see chapter 5). Stability being a primary criterion for structural biology, this low melting temperature could be one of the causes of failure. It would therefore be necessary to try to increase the stability of the protein, in particular by adding additives. In the present case, hemin could show a good stabilization effect on the protein. Another fact is that the crystallization analysis by prediction algorithms [6, 7] of the protein also predicts a high surface hydrophobicity, reducing the chances of success. Reminiscent of membrane proteins, this hydrophobicity is a real challenge for the crystallization of hIDO2. The prevention of protein aggregation is thus achieved by the glycerol included in the protein buffer. [8, 9] At last, prediction models [6] have revealed a long disordered chain at the N-terminus of the protein, an additional detriment to crystallization. All these parameters facilitate the precipitation of the protein rather than the formation of a metastable state allowing the appearance of a nucleation point.

10.3 Plasmid design to aid crystallization

Faced with this failure, a plasmid optimization strategy was implemented in order to improve the compositional stability (homogeneity and stability of the protein) and the conformational stability (presence of disorder regions). The first possible modification of the protein construct is the presence of the purification tag at the N-terminus extremity of the protein (Figure 10.3, blue rectangle). Although tags are not supposed to interfere with protein, there is a growing body of evidence in the literature to the contrary. [10–14] In particular, literature mentions their importance in the production and expression of proteins, like membrane proteins. [15] Experimentally, this effect was observed with hIDO2 where the position of the tag was important for the expression of the protein.

crystallization. [5, 10, 14, 17] There are also examples of other hemoproteins where the presence of the poly-histidine tail influences the conformational movements of the protein and its dynamics. [18] In this context, an optimization of the cleavage of N-terminal his-tag in hIDO2 was therefore carried out. This takes place by a cleavage with the trombin which recognizes a binding site (LVPR|GS) between the protein and the tag (Figure 10.3, yellow rectangle). The cleavage occurs between arginine and glycine. After cleavage, crystallization tests were performed.

Secondly, based on the sequence alignment of hIDO1 with hIDO2 (Figure 10.3), it is noted that a region in the N-terminal part of the hIDO2 protein is not present in the sequence used for the crystallization of hIDO1 (Figure 10.3, purple rectangle). The analyses using AlphaFold and CrystalPred servers [1, 2, 6, 7] predict that this part is disordered. It was therefore decided to truncate this N-terminal part to increase the chances of crystallization. This truncation strategy is recognized in the scientific community for having proven itself. [19, 20] This truncated form having a poly-histidine tail, a cleavage of the latter is also studied to allow its purification. Thus, three new forms of proteins are studied: cleaved hIDO2 WT, truncated hIDO2 and cleaved truncated hIDO2.

10.3.1 Physico-chemical characterisations of new constructions

As mentioned in the previous point, it would possible that what is lacking in crystallization is the stability of the sample. As cleavages and truncation are supposed to decrease conformational instability, physico-chemical characterizations have focused on criteria influencing constitutional instability. First of all, to ensure purity, two types of staining were performed (staining with Coomassie blue and silver nitrate). The SDS-PAGE analysis, with blue Coomassie staining, of the samples showed a high purity of the four constructs and an absence of proteolysis (Figure 10.4). This result was then confirmed by silver nitrate staining. This absence of proteolysis is already a first information on the constitutional stability. With the help of the ladder, it can be seen that the observed molecular weights correspond well to the expected molecular weights for the different constructs (hIDO2 WT=47.6 kDa, hIDO2 cleaved= 45.7 kDa, hIDO2 truncated= 46.2 kDa, hIDO2 truncated and cleaved= 44.3 kDa).

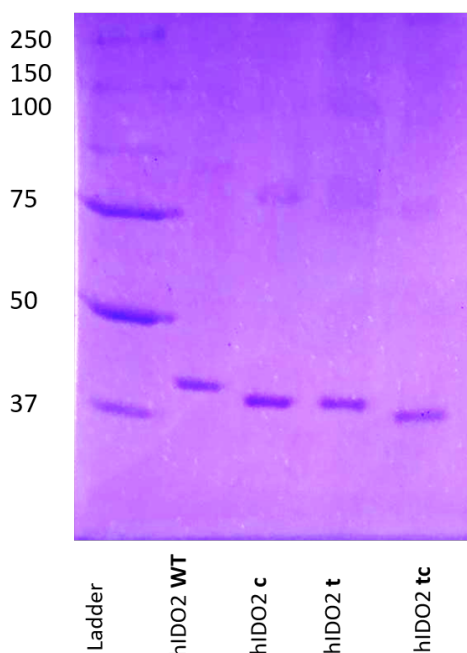


FIGURE 10.4: SDS-PAGE gel (12%) of the different constructs after the purification process. Each well contains 1 μ g of protein. the revelation of the protein occurs with Blue Coomassie staining.

TABLE 10.1: Influence of construction and hemin addition (at a final concentration of 50 μ M) on protein stability. – : Measurement not performed due to lack of protein.

Construction	T _m (°C)	T _m if adding hemin (°C)
hIDO2 WT (oxidized form)	48.1 \pm 0.1	49.6 \pm 0.1
hIDO2 cleaved (oxidized form)	47.6 \pm 0.1	47.9 \pm 0.2
hIDO2 truncated (oxidized form)	–	–
hIDO2 truncated and cleaved (oxidized form)	46.4 \pm 0.3	47.1 \pm 0.4
hIDO2 WT (reduced form)	47.7 \pm 0.1	48.7 \pm 0.1
hIDO2 cleaved (reduced form)	47.1 \pm 0.5	48.2 \pm 0.6
hIDO2 truncated (reduced form)	45.8 \pm 0.2	–
hIDO2 truncated and cleaved (reduced form)	46.1 \pm 0.3	46.6 \pm 0.3

The constitutional stability could be studied by DSF and UV-Visible absorption spectroscopy analysis. The DSF analyses give access to the stability of the protein by means of its melting temperature. The kind of analysis (Table 10.1) does not show any stabilization effect of the samples when the truncations are modified. A destabilization of the truncated form is even observed. Both oxidized and reduced forms have

the same order of magnitude of melting temperature, regardless of the construction. Hemin still has a stabilizing effect since the addition of 50 μM (ratio 2:1) causes an average stabilization of the proteins lower than 2 degrees. The addition of an excess of hemin to the protein therefore could be an interesting strategy for crystallization. Lastly, the protein absorbance ratio is a good indication of the homogeneity of a sample. The values of the latter are shown in the Table 10.2, for each construction and each redox condition. As can be seen, the modifications of the constructs did not strongly improve the incorporation and thus the homogeneity of the sample in a clear way. A slight increase is noticeable for the truncated and cleaved protein.

TABLE 10.2: Influence of construction and hemin addition (at a final concentration of 50 μM) on protein stability. – : Measurement not performed due to lack of protein.

Construction	Ratio A_{Soret} / A_{280} if oxidized form	Ratio A_{Soret} / A_{280} if reduced form
hIDO2 WT	0.8-1.0	0.4-0.6
hIDO2 cleaved	0.7	0.4
hIDO2 truncated	0.9	0.5
hIDO2 truncated and cleaved	1.0-1.2	–

10.3.2 Crystallization assays on cleaved hIDO2 WT, truncated hIDO2 and truncated-cleaved hIDO2

For the crystallization tests, the different constructs are studied under their reduced or oxidized forms, with and without addition of excess hemin (1.2mM) conditions. The protein buffer is composed of 50mM phosphate, 150mM NaCl and 5% glycerol. Different commercial kits are tested (PACT, JCSG+, BCS) as well as the crystallization conditions of hIDO1. In many cases, several solids are observed in the wells (Figure 10.5). A redundancy of certain conditions can be observed. In particular, the pH of the hits is mainly situated between 5.5 and 7. Knowing that a protein is more likely to crystallize at a pH close to its pI and that the pI of hIDO2 is 6.6, this is encouraging. [21–23]

The protein also shows the need for a high concentration of precipitating agent (more than 20%) to arrange itself in solid form. Specifically, the preferred agents are high molecular weight PEG (3500 or 6000) or MDP. These promising crystals were

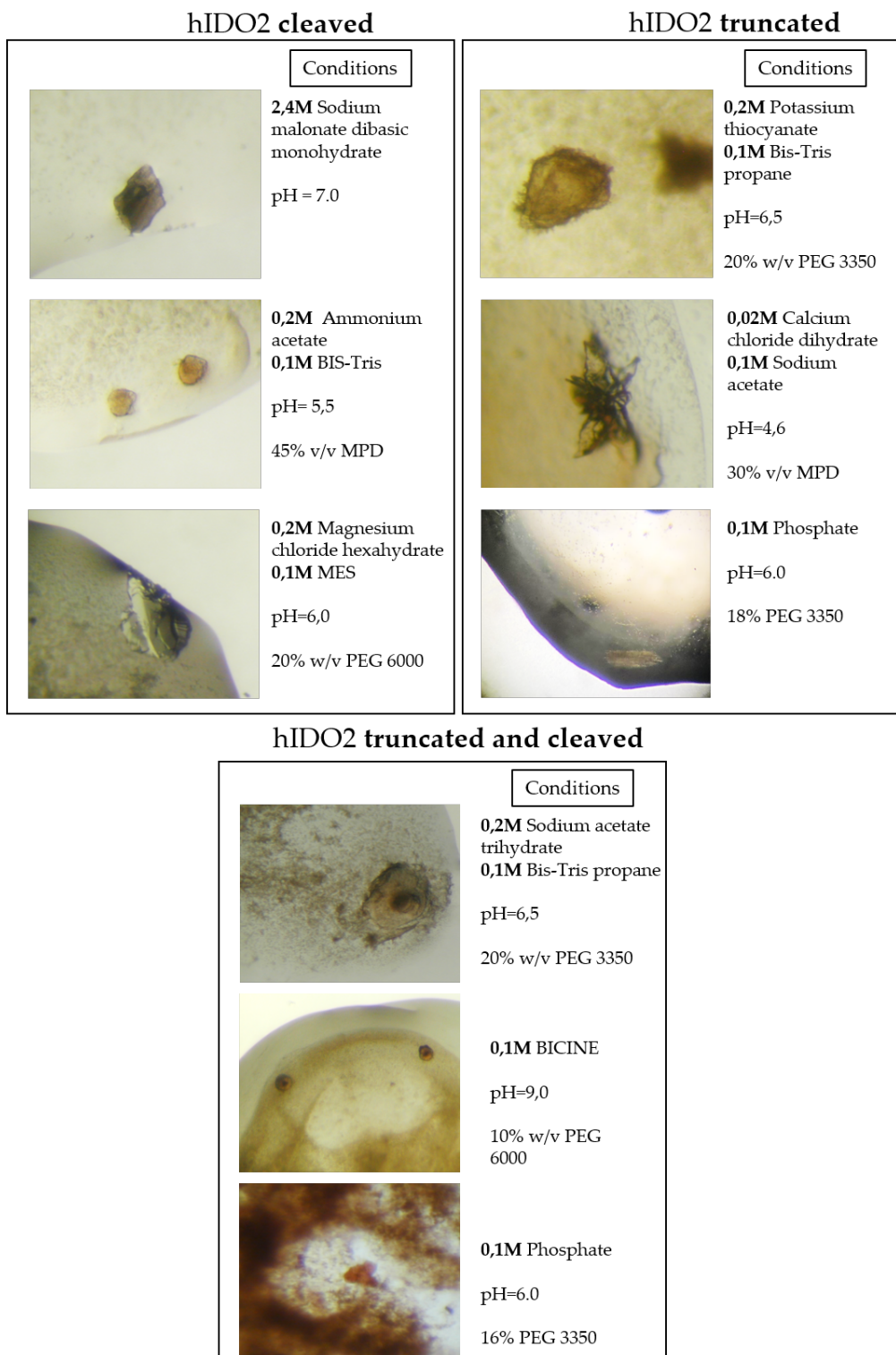


FIGURE 10.5: Promising conditions obtained in the crystallization tests of hIDO2, according to the different constructions.

cryo-protected in order to be sent to the synchrotron (with 30% glycerol in most cases). The solids withstood cryo-protection relatively well and few ice was observable when the loop was mounted for crystallographic analysis. However, the characterization of the different shapes obtained showed no diffraction spots. The collected solids were thus neither salt nor protein crystals but this indicates that the solid phase organization is more of an amorphous organization. The optimization, in 24 wells, of these conditions did not allow more success. Surface mutations have also been studied (data not shown) on the different constructions, without conclusive results. Indeed, the mutations caused a precipitation of the protein in the form of inclusion bodies in the pellet.

10.3.3 What can you learn from this study?

All these failures can mean several things. First, in the three main sinequanone conditions (stability, probability and thermodynamics, see figure 1), two out of three seem to be fulfilled. Indeed, the reaction kinetics seems to be correct: solids appear in a reasonable time range. The range of favorable crystallization conditions (thermodynamics) has been largely investigated and leads well to the obtention of solids. However, the lack of crystallizability of these solids seems to come from the stability of the samples. Although truncations probably improve the conformational stability, the compositional stability of the mixture remains a limiting factor for the crystal organization. It was seen that mutants did not improve incorporation, and thus homogeneity in solution, nor stability. From this, the hIDO2 protein, despite the optimization of construction, is not a good candidate for crystallization.

10.4 Intermediate conclusions

In conclusion of this chapter, crystallization tests were performed on hIDO2 WT but also on a cleaved, truncated and truncated-cleaved form of the enzyme. For this purpose, several crystallization kits were tested. It turns out that hIDO2, whatever the construction studied, does not crystallize. This can be attributed to a constitutional instability of the protein which makes it a poor client for crystallization. Other perspectives could be studied to get the structure of hIDO2. First, the folding in solution should be investigated by methods such as Small-angle X-ray scattering (SAXS) or C^{13}/N^{15} -Nuclear Magnetic Resonance (NMR). In terms of structural determination,

SAXS studies would already allow to learn more about the protein and could allow the comparison of the experimental curve with theoretical models obtained by homology or Molecular Dynamics (Chapter 11). Given the size of the system, NMR and Cryogenic Electron Microscopy (cryo-EM) with the protein alone are not feasible to obtain a molecular structure of hIDO2. The size of the system could be increased by using antibodies to perform cryo-EM. Crystallization using an ordered fusion protein as a chaperone or by focusing on domains could also be two interesting prospects. [5, 24] Lately, the use of TbXo4 to help the assembly of the crystal packing could be an interesting way of study. [25]

Bibliography

- [1] M. Varadi, S. Anyango, M. Deshpande, S. Nair, C. Natassia, G. Yordanova, D. Yuan, O. Stroe, G. Wood, A. Laydon, et al. Alphafold protein structure database: Massively expanding the structural coverage of protein-sequence space with high-accuracy models. *Nucleic acids research*, 50(D1):D439–D444, 2022.
- [2] J. Jumper, R. Evans, A. Pritzel, T. Green, M. Figurnov, O. Ronneberger, K. Tunyasuvunakool, R. Bates, A. Židek, A. Potapenko, et al. Highly accurate protein structure prediction with alphafold. *Nature*, 596(7873):583–589, 2021.
- [3] J. Newman, D. Egan, T. S. Walter, R. Meged, I. Berry, M. Ben Jelloul, J. L. Sussman, D. I. Stuart, and A. Perrakis. Towards rationalization of crystallization screening for small-to medium-sized academic laboratories: the pact/jcsg+ strategy. *Acta Crystallographica Section D: Biological Crystallography*, 61(10):1426–1431, 2005.
- [4] A. Chaikuad, S. Knapp, and F. von Delft. Defined peg smears as an alternative approach to enhance the search for crystallization conditions and crystal-quality improvement in reduced screens. *Acta Crystallographica Section D: Biological Crystallography*, 71(8):1627–1639, 2015.
- [5] M. C. Deller, L. Kong, and B. Rupp. Protein stability: a crystallographer’s perspective. *Acta Crystallographica Section F: Structural Biology Communications*, 72(2):72–95, 2016.
- [6] L. Slabinski, L. Jaroszewski, L. Rychlewski, I. A. Wilson, S. A. Lesley, and A. Godzik. Xtalpred: a web server for prediction of protein crystallizability. *Bioinformatics*, 23(24):3403–3405, 2007.

- [7] S. Jahandideh, L. Jaroszewski, and A. Godzik. Improving the chances of successful protein structure determination with a random forest classifier. *Acta Crystallographica Section D: Biological Crystallography*, 70(3):627–635, 2014.
- [8] V. Vagenende, M. G. S. Yap, and B. L. Trout. Mechanisms of protein stabilization and prevention of protein aggregation by glycerol. *Biochemistry*, 48(46):11084–11096, 2009.
- [9] K. Gekko and S. N. Timasheff. Mechanism of protein stabilization by glycerol: preferential hydration in glycerol-water mixtures. *Biochemistry*, 20(16):4667–4676, 1981.
- [10] P. Ledent, C. Duez, M. Vanhove, A. Lejeune, E. Fonzé, P. Charlier, F. Rhazi-Filali, I. Thamm, G. Guillaume, B. Samyn, et al. Unexpected influence of a c-terminal-fused his-tag on the processing of an enzyme and on the kinetic and folding parameters. *FEBS letters*, 413(2):194–196, 1997.
- [11] K. A. Majorek, M. L. Kuhn, M. Chruszcz, W. F. Anderson, and W. Minor. Double trouble—buffer selection and his-tag presence may be responsible for nonreproducibility of biomedical experiments. *protein science*, 23(10):1359–1368, 2014.
- [12] A. Panek, O. Pietrow, P. Filipkowski, and J. Synowiecki. Effects of the polyhistidine tag on kinetics and other properties of trehalose synthase from *deinococcus geothermalis*. *Acta Biochimica Polonica*, 60(2), 2013.
- [13] A. Araújo, G. Oliva, F. Henrique-Silva, R. C. Garratt, O. Cáceres, and L. M. Beltramini. Influence of the histidine tail on the structure and activity of recombinant chlorocatechol 1, 2-dioxygenase. *Biochemical and biophysical research communications*, 272(2):480–484, 2000.
- [14] M. Carson, D. H. Johnson, H. McDonald, C. Brouillette, and L. J. DeLucas. His-tag impact on structure. *Acta Crystallographica Section D: Biological Crystallography*, 63(3):295–301, 2007.
- [15] A. K. Mohanty and M. C. Wiener. Membrane protein expression and production: effects of polyhistidine tag length and position. *Protein expression and purification*, 33(2):311–325, 2004.
- [16] F. Corpet. Multiple sequence alignment with hierarchical clustering. *Nucleic acids research*, 16(22):10881–10890, 1988.

- [17] W. T. Booth, C. R. Schlachter, S. Pote, N. Ussin, N. J. Mank, V. Klapper, L. R. Offermann, C. Tang, B. K. Hurlburt, and M. Chruszcz. Impact of an n-terminal polyhistidine tag on protein thermal stability. *ACS omega*, 3(1):760–768, 2018.
- [18] M. C. Thielges, J. K. Chung, J. Y. Axup, and Michael D. Fayer. Influence of histidine tag attachment on picosecond protein dynamics. *Biochemistry*, 50(25):5799–5805, 2011.
- [19] Z. S. Derewenda. The use of recombinant methods and molecular engineering in protein crystallization. *Methods*, 34(3):354–363, 2004.
- [20] A. Yamashita. Current pivotal strategies leading a difficult target protein to a sample suitable for crystallographic analysis. *Biochemical Society Transactions*, 48(4):1661–1673, 2020.
- [21] M. Abdalla, W. A. Eltayb, A. Samad, S. Elshareef, and T. Dafaalla. Important factors influencing protein crystallization. *Global Journal of Biotechnology and Bio-material Science*, 2(1):025–028, 2016.
- [22] J. Kirkwood, D. Hargreaves, S. O’Keefe, and J. Wilson. Using isoelectric point to determine the ph for initial protein crystallization trials. *Bioinformatics*, 31(9):1444–1451, 2015.
- [23] K. A. Kantardjieff and B. Rupp. Protein isoelectric point as a predictor for increased crystallization screening efficiency. *Bioinformatics*, 20(14):2162–2168, 2004.
- [24] E. A. Stura, M. J. Taussig, B. J. Sutton, S. Duquerroy, S. Bressanelli, A. C. Minson, and F. A. Rey. Scaffolds for protein crystallisation. *Acta Crystallographica Section D: Biological Crystallography*, 58(10):1715–1721, 2002.
- [25] S. Engilberge, T. Wagner, G. Santoni, C. Breyton, S. Shima, B. Franzetti, F. Riobé, O. Maury, and E. Girard. Protein crystal structure determination with the crystallophore, a nucleating and phasing agent. *Journal of Applied Crystallography*, 52(4):722–731, 2019.

Chapter 11

Investigation of the hIDO2 structure by Molecular Dynamic and homology modeling

11.1 Introduction

The lack of structural knowledge of hIDO2 is an obstacle to the understanding of its role in diseases and to the design of inhibitors. Additionally, it is difficult to understand why an enzyme with more than 40% of sequence similarity to hIDO1 does not catalyze the same reaction as does its cousin. To provide more information on this protein, the present chapter reports a computational analysis of the structure of hIDO2 by means of multidisciplinary approach mixing homology models and Molecular Dynamics (MD) simulations.

11.2 Design of a homology model

To propose a structure for hIDO2, the first step of the research focused on designing a model by homology. To do this, the sequence of the protein given on Uniprot [1] is used as a starting point, as well as the C monomer of the structure 7a62 of hIDO1 where the JK dynamic loop is fully refined (43.7% sequence identity). Since it could be shown in the literature that the starting methionine of hIDO2 is the second one (position 14 of the Uniprot sequence), the sequence was started from this amino acid, considered as M1 in the present study.

The model is generated using the SwissModel program. In the alignment of hIDO2 (named "Model") and hIDO1 (named "Template") at Figure 11.1, A., the conserved residues between the two proteins are marked in black while the non-conserved residues are in gray. The conservation of the secondary structure elements is highlighted by the arrows (beta sheets) or the box (helix) that surrounds the residues. At first sight, most of the secondary structure elements present in hIDO1 are conserved in hIDO2. The alignment shows differences localized in three places of the protein, namely residues in the N-terminal part (M1 to L16 of hIDO2, not present in hIDO1), the EF loop (R284 to E288 of hIDO2, shorter than in hIDO1) and the JK-loop (A360 to G383 of hIDO2, longer than in hIDO1), resulting in a lower accuracy of these parts in the final model (shown in orange). For the sake of understanding, these parts will be named EF' and JK' when the manuscript refers to these loops in hIDO2 while the EF and JK nomenclature will continue to reference the loops in hIDO1.

The results (Figure 11.1, B, C. and D.) report GMQE (Global Model Quality Estimate) values of 0.76 [2], which estimates the accuracy of the tertiary structure of the resulting model. It indicates that the model is of global good accuracy. The QMEAN4 score [3], a deprecated value which nevertheless allows a comparison (based on 4 criteria) of the structure obtained against the same size structures available in the PDB, is equal to -2.28. It shows that the structure is not of poor quality but is rather far from the native structures of the PDB. The local quality estimate score profile [4] reports the quality of the structure for each residue. As expected, the imprecision is more marked at the level of the EF' and JK' loops. There is also an imprecision at residue 80 and at the N-terminus of the protein. The Ramachandran plot indicates that most of the residues are in favorable zones, in spite of some outliers.

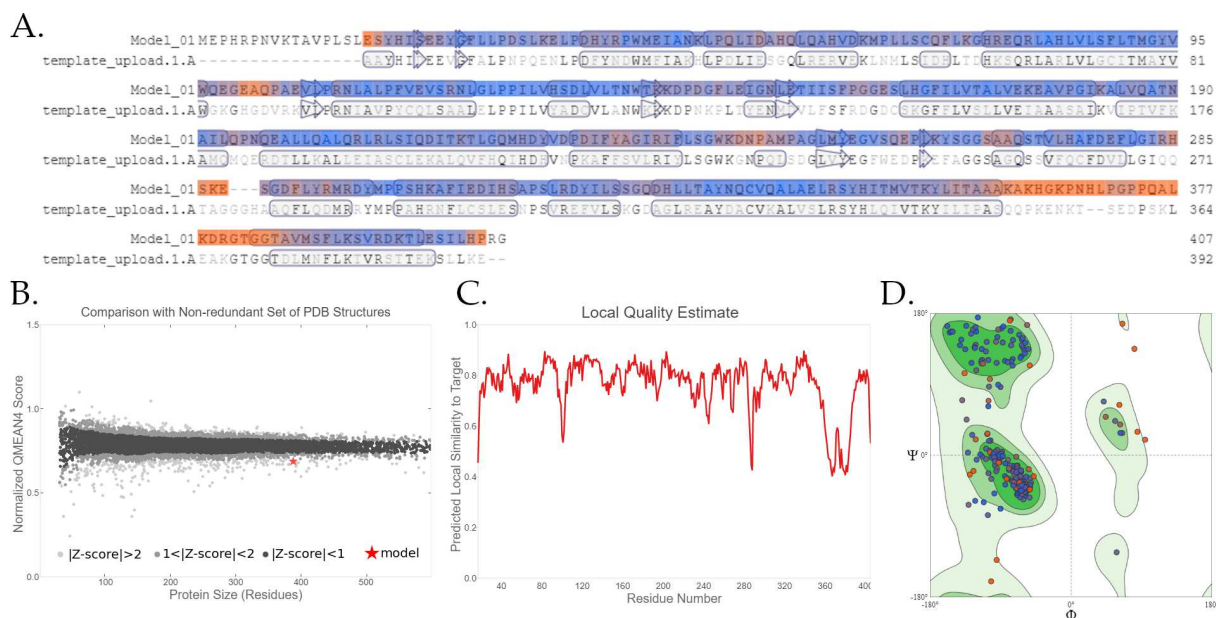


FIGURE 11.1: Homology modelling of the structure of hIDO2. A. Local model quality evaluation. B. QMEAN4 score C. Local Quality Estimation D. Ramachandran plot.

The resulting homology model is shown in Figure 11.2, A.. This model only starts at residue 17 of the protein due to the lack of information on the N-terminal fragment. The heme cofactor was added to be in the homology model of hIDO2 by aligning the structure of hIDO2 with that of hIDO1 (monomer C of 7A62, rmsd of 0.09Å). As expected, the protein has one small and one large subunit. The helices of the large subunit are named in increasing alphabetical order from A' to K'.

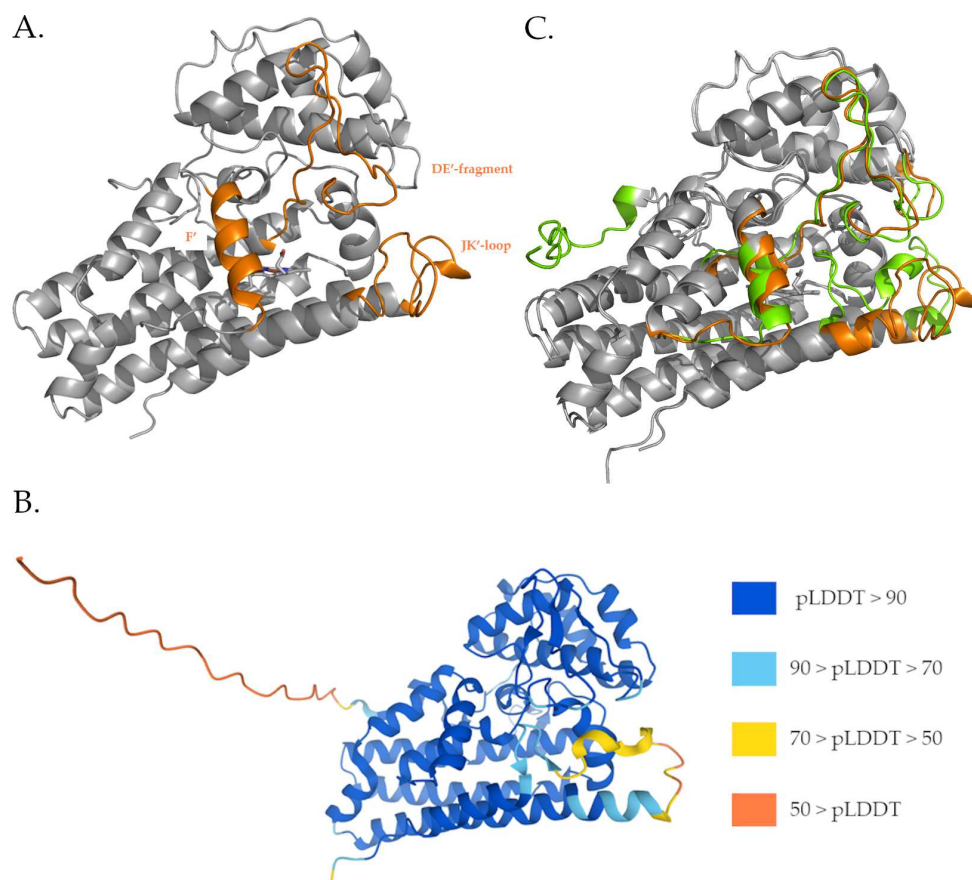


FIGURE 11.2: A. Homology model obtained by SwissModel of hIDO2 B. AlphaFold model available on the server. [5, 6] C. Superimposition of the two models. The divergent areas in the tertiary structure between AlphaFold and the SwissModel homology model are highlighted, respectively, in green for AlphaFold and orange for the SwissModel.

The alignment with the structure retrieved from the AlphaFold server [5, 6] (Figure 11.2, C.) presents a rmsd of 1.0 Å. The AlphaFold machine learning model has the same weaknesses as the homology model with an inaccuracy of the N-terminal part of the protein (very low confidence interval (per-residue confidence score (pLDDT) < 50)) and the JK'-loop (low confidence interval ((70 > pLDDT > 50)). Areas of inaccuracy are also noticed in the DE'-fragment. Logically, these are the areas that differ between the two representations. This is due to the lack of data in the literature for these very disordered parts. The AlphaFold model yields a complete N-terminal part, and includes the two possible start methionines of hIDO2. Like mentioned in the introduction, as the start methionine is the second one (position 14 of the Uniprot sequence), the structure is slightly shorter on the disordered end.

11.3 Study of the JK-loop of hIDO2 with the heme cofactor

To have a less rigid model closer to the structure in solution, a MD study was performed starting from the homology model. MD simulations were run for 300 ns, in triplicates (R1, R2 and R3), by GROMACS. [7] Since the experimental results showed that the cofactor is labile in hIDO2, H347 and the cofactor are not covalently bonded (see details in Appendix B). The three replicates converge towards the same folding (r.m.s.d value of $2.5 \text{ \AA} \pm 0.1 \text{ \AA}$). The parts that diverge along the replicates (Figure 11.4) are also those that diverge from the model obtained by homology (r.m.s.d value of $2.5 \text{ \AA} \pm 0.5 \text{ \AA}$), due to the a great flexibility of these fragments. The main differences are located in the helix F', the heme binding site, the DE'-fragment, and the JK'-loop (Figure 11.4).

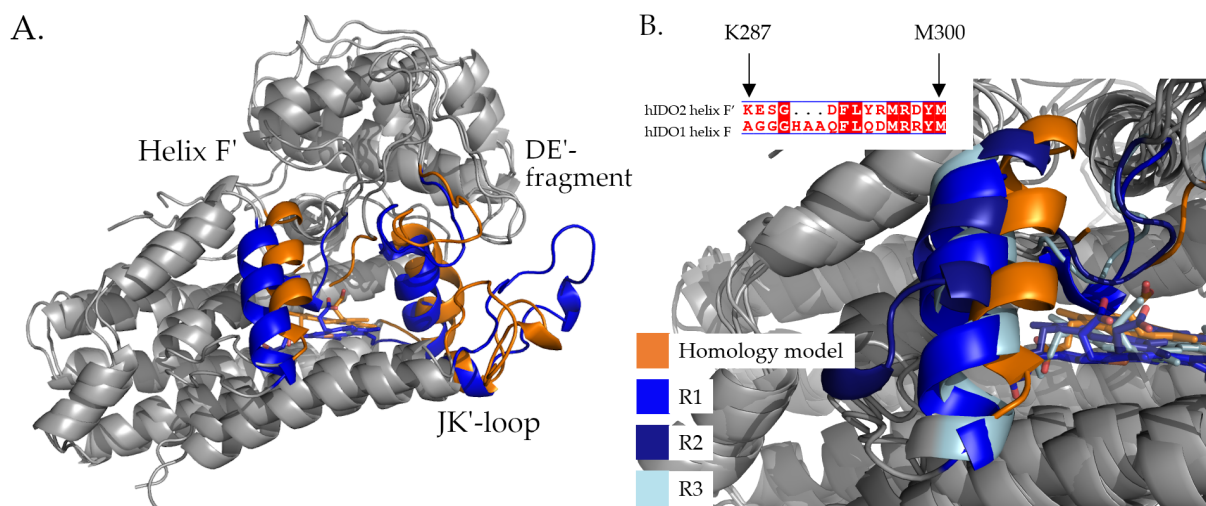


FIGURE 11.3: Structural differences between the homology model (in orange) and the MD replicates after 300 ns of MD simulations at 310 K and 1 bar (in different shades of blue: R1 = medium blue, R2 = dark blue, and R3 = light blue). A. Differences highlighted between the homology model and R1. B. Helix F' in the homology model in comparison to all replicates.

In the hIDO2 homology model, the fold of the helix F' is biased by the structure of hIDO1 whereas, in hIDO2, its length is reduced due to GGHA gap after K287 and E288 (Figure 11.3, B.). Due to the relaxation of the system, the helix F' reorganizes and initiate the formation of a helix turn earlier in the sequence. This loop is likely to be rather flexible since its conformation slightly varies between MD replicates. The

conformation observed in R2 differs from that of R1 and R3 (Figures 11.3, B. and 11.4). Indeed, the beginning of the loop is not ideally folded in R2, for no apparent reason. This less well-folded loop causes a drastic increase in the motion of residues K287 and E288. The role of this flexibility cannot be explained by the model. However, mutagenesis studies have shown that a dual mutation of K287 and E288 results in an inability to produce a cofactor-related protein. It is thus possible that this part of the protein is involved in the retention of the heme in the active site but this assumption requires further investigations.

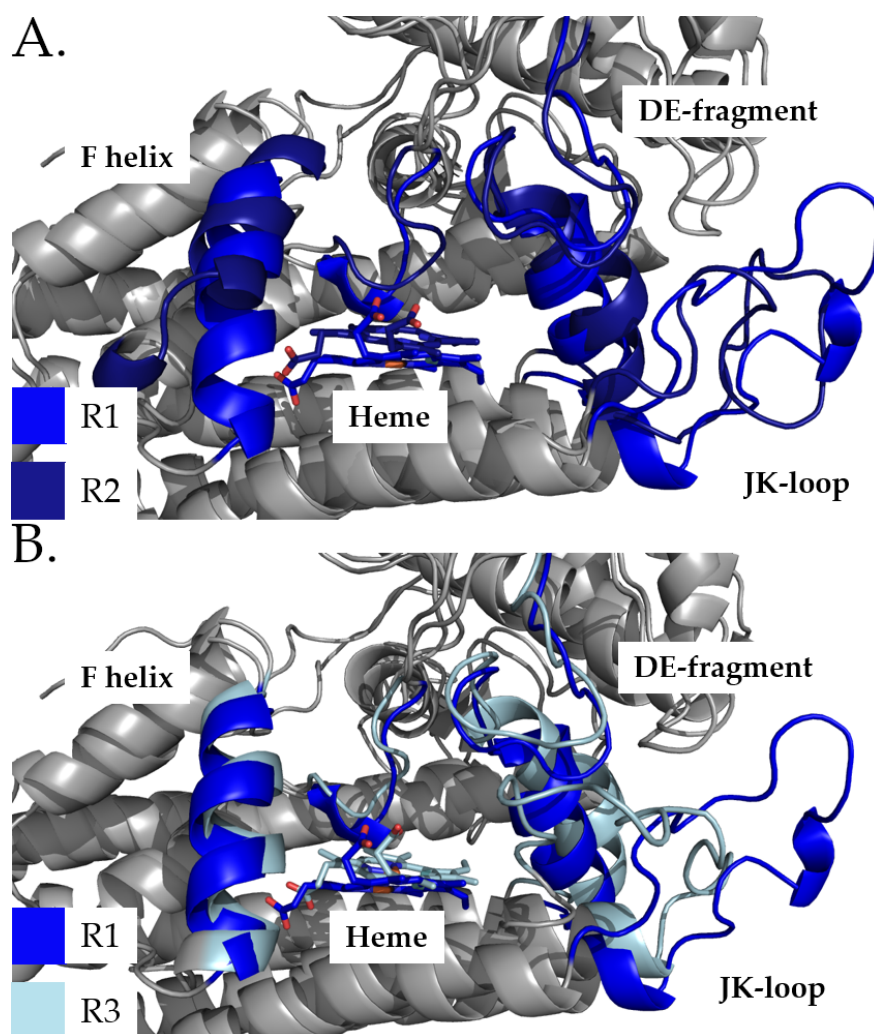


FIGURE 11.4: Structural differences (highlighted in colors) between the replicates after 300 ns at 310 K and 1 bar (in different shades of blue: R1 = medium blue, R2 = dark blue, and R3 = light blue). A. Between R1 and R2 (mainly localized at the helix F' and heme binding site). B. Between R1 and R3 (mainly localized at the JK'- and DE'-fragment).

As for the F' helix, the heme binding site is also an area of divergence between the homology model and MD structures (Figure 11.5). The folding of the heme binding site demonstrates a change in the position of the cofactor in its pocket in comparison with the homology model (in orange, Figure 11.5). This reorganization occurs very quickly upon equilibration of the protein. In particular, this can be explained by a rearrangement of the amino acids of the I' helix (G325 to T352). Notably, the H347 that coordinates the heme cofactor reorients and loses its stabilizing role (Figure 11.5, A.).

As a result, during the production phase, the cofactor is not coordinated to the protein and is much more mobile. This non-coordination is observable in all replicates. Despite this rearrangement, the heme is stable in its new position during the production phase, as shown by r.m.s.d. analysis relative to the initial position (Figure 11.5, B.). The G265-Q270 fragment defining the pocket A of the active site is also impacted by the reorganization, and its conformation varies in comparison to the homology model (Figure 11.5, C.). More precisely, the fragment G265-Q270 adopts two possible conformations during simulations, with S267 oriented toward the heme cofactor and A268 varying in position (analogue to type II and type III conformation in hIDO1). The motion of these residues is moderate during the production phase with an average of $0.10 \text{ nm} \pm 0.02 \text{ nm}$ (Figure 11.5, D.), which is similar to the average for the entire protein ($0.10 \text{ nm} \pm 0.01 \text{ nm}$). That demonstrates a stability of these MD conformations. The r.m.s.d analysis of the G265-Q270 fragment is consistent with this observation (Appendix E, Figure E.1).

From the MD studies, the flexibility of the JK'-loop is highlighted. After relaxation, the loop appears between residues A358 and R380. It is composed of a large number of proline, alanine and lysine residues (four of each type (18%)). These large proportions are intriguing knowing that in the whole protein these amino acids have an occurrence frequency of 7.0%, 7.5%, and 4.9%, respectively. Due to the three large amounts, an alternations of polar and apolar parts is observed (Figure 11.6, A.). The loop can be separated into two parts, an N-terminal part from A358 to P374 and a C-terminal part from Q375 to R380. Concerning the N-terminal part, it could be further subdivided into two parts, i.e., N1 from 358 to 368 and N2 from 369 to 374. The N1 part is polar and, in some frames, presents an alpha helix folding between residues K366 and N368 that increases the fluctuation of the residues (R1). The N2 part is

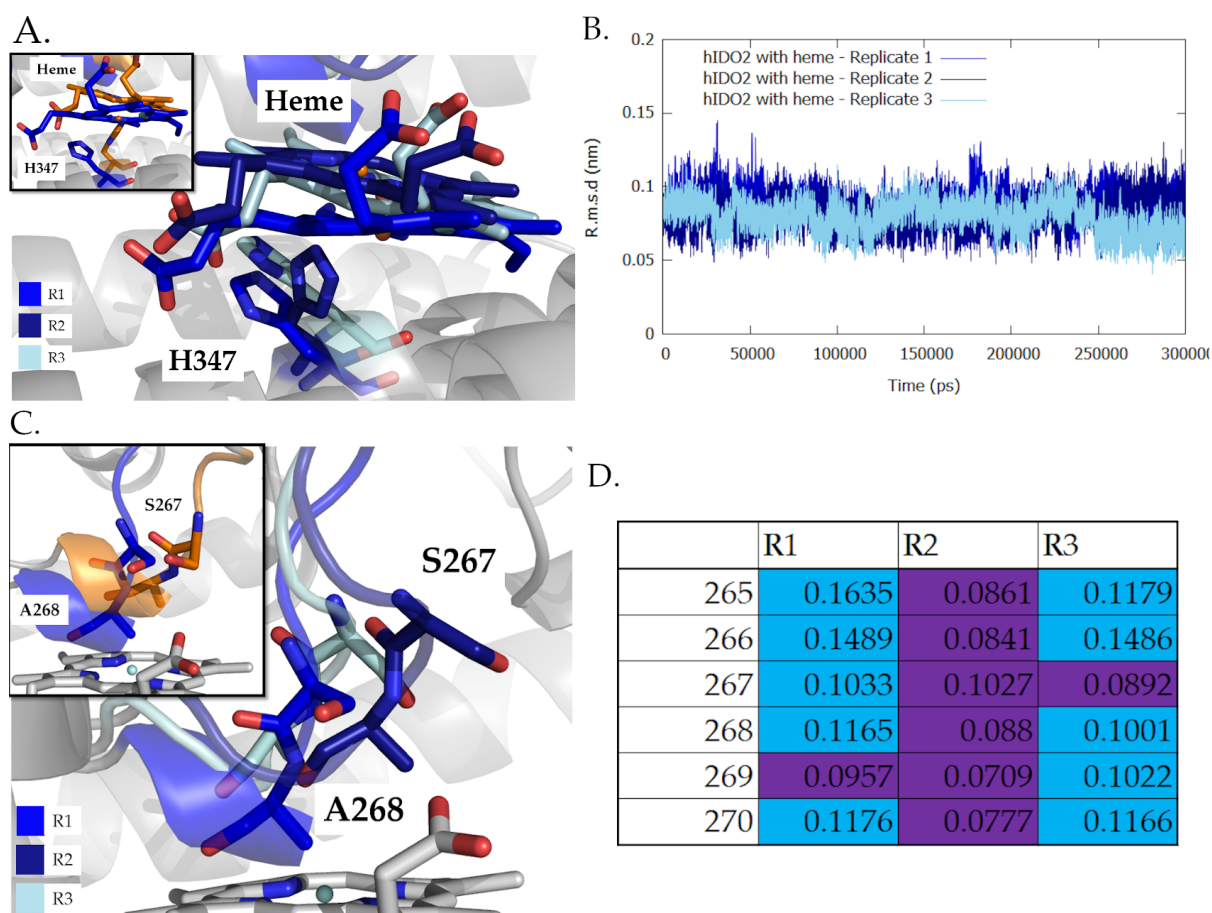


FIGURE 11.5: Comparison of the homology model (in orange) and the MD replicates after 300 ns at 310 K and 1 bar (in different shades of blue: R1 = medium blue, R2 = dark blue and R3 = light blue). A. Positions adopted by the heme and the H347 fragment in the MD replicates (main figure) and the homology-based model (up corner). B. R.m.s.d profile of the heme group during the simulation in comparison to the starting position. C. Positions adopted by the G265-Q270 fragment in the MD replicates (main figure) and the homology-based model (up corner). D. Map of the r.m.s.f values for the G265-Q270 fragment. Purple = lower than 0.1, Blue = between 0.1 and 0.2.

mainly apolar, and is more agitated than N1 and the C-terminal part. The flexibility of the C-terminal part is much less than that of the N2 part but, larger than the N1 part. The mean fluctuation of the JK'-loop is $0.30 \text{ nm} \pm 0.01 \text{ nm}$, i.e. a threefold increase factor in comparison to the mean total fluctuation of the protein (Figure 11.6, B. and C.). The stabilization of the C-terminal part depends on the conformation adopted by the loop and in the interactions. Actually, the C-terminal part of the JK'-loop is characterized by large position differences and a high flexibility (Figure 11.7,

A.). Each of the MD replicates reports variations of the loop conformations as presented in Figure 11.7, B. These percentages are based on the distance values between A268 (CB) and R380 (NH1) considering a closed structure if the distance is less than 10 Å, intermediate between 10Å and 16 Å and open beyond 16 Å. On the whole, there is a slight advantage for the open or intermediate conformation.

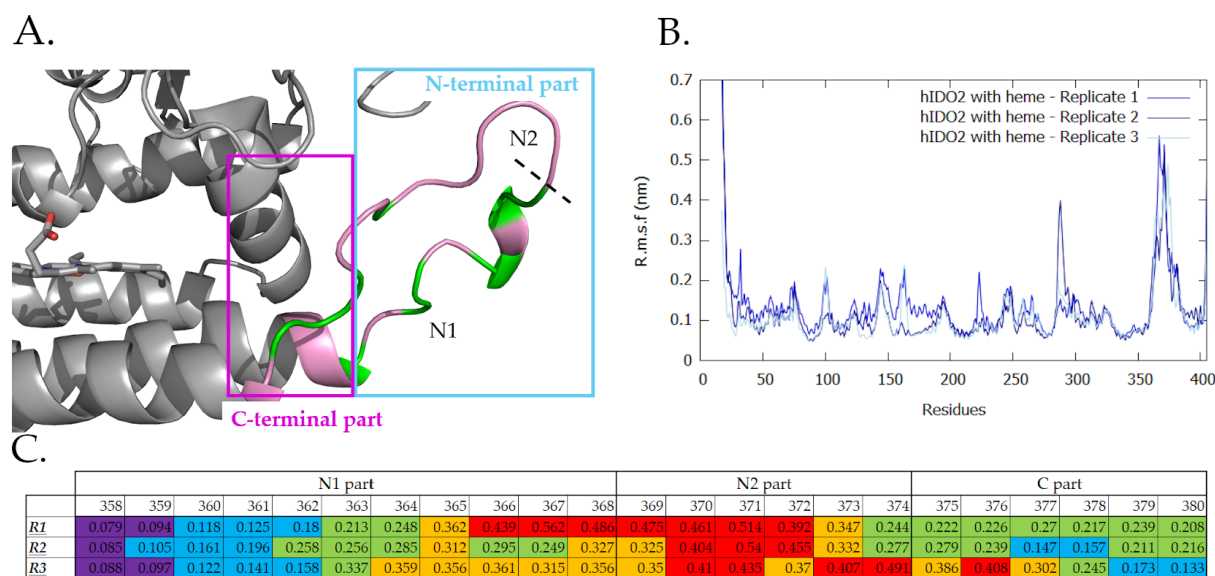


FIGURE 11.6: Characterization of the structure obtained after 300 ns MD simulation at 310 K and 1 bar for holo hIDO2. A. Conformation of the JK-loop. Proportion of polar residues (green) and apolar residues (pink) around the N-terminal and the C-terminal part. B. R.m.s.f profiles for the three replicates. C. Mapping of r.m.s.f values for residues of the JK'-loop. The more the square tends towards warm colours, higher is the fluctuation.

The closed conformation (as in R3, Figure 11.7, A. III.) presents an interaction between R380 and the heme cofactor (mean value of $3.2 \text{ \AA} \pm 0.2 \text{ \AA}$, Figure 11.7, C.), bringing the C-terminal part closer to the heme cofactor than in R1 and R2. The folding has one less helix turn at the C-terminal part. In R1 and R2, R380 does not necessarily stabilize the cofactor. Consequently, R380 is very far from the cofactor with average distance of $10.3 \text{ \AA} \pm 0.1 \text{ \AA}$ and $12.2 \text{ \AA} \pm 1.1 \text{ \AA}$, respectively. In all, K378 is rarely oriented towards the heme pocket as it has an average distance between the carboxylate oxygens and the residue nitrogen of $22.2 \text{ \AA} \pm 0.07 \text{ \AA}$, $21.8 \text{ \AA} \pm 0.3 \text{ \AA}$, and $15.4 \text{ \AA} \pm 0.1 \text{ \AA}$, for R1, R2 and R3 respectively.

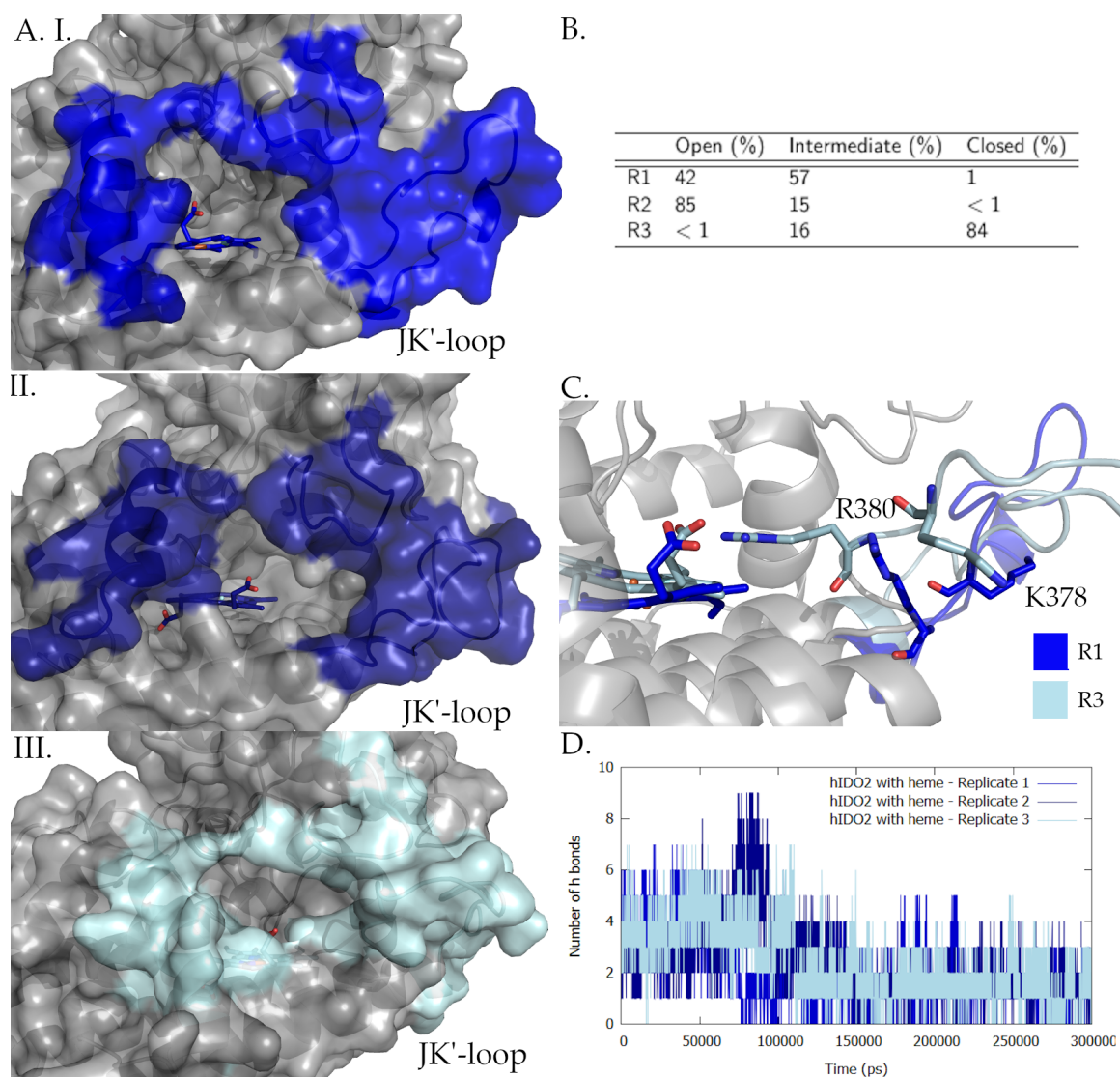


FIGURE 11.7: Characterization of the structure obtained after 300 ns MD simulations at 310 K and 1 bar for holo hIDO2. A. van der Waals surfaces around the heme cofactor and conformations adopted by the JK'-loop in MD replicates (R1 = I, R2 = II, R3 = III). B. Percentage of open, intermediate and closed conformations in MD replicates. C. Hydrogen-bonds (cut-off values of 3.5 Å and 30°) between the JK'-loop and the DE'-loop (V227 to G250) per 20 ps frame. D. Relative position of K378 and R380 with respect to the heme cofactor in R1 (medium blue) and R3 (light blue).

K378 does not participate in the stabilization of the cofactor. Despite the more extended conformation toward the solvent adopted by R3 for N2 and C- parts, the number of H-bonds with the DE'-fragment (defined from V227 to G250, Figure 11.7,

D.) varies only slightly between replicates ($R1 = 1.8$, $R2 = 2.2$, $R3 = 2.2$). This explains why the DE'-loop can also vary slightly in position: it adapts to the change in the JK'-loop position so as to avoid gaps between the JK'- and DE'-loops on the enzyme surface. There is also no more H-bonds with the solvent. To summarize, the enhanced flexibility of the protein, the unfolding of the F' helix, the lack of interaction between H347 and the cofactor and the open loop are elements that decrease the constrain of the cofactor in the active site and increase the chances of lability. In all cases, the heme does not leave the protein but moves in the active site.

11.3.1 Influence of M350 on heme lability

To investigate the absence of coordination for the heme cofactor to H347 in the active site of hIDO2, a mutagenesis study was performed based on the sequence alignment of hIDO1. Indeed, the sequence alignment of helix I' shows two major changes in the H347 environment for hIDO2 (Figure 11.8, A.). In the case of the paralog, residue 349 is a threonine instead of a glutamine while residue 350 is a methionine and not an isoleucine. However, M350 will be of particular interest because its orientation is below the heme cofactor in the WT protein, which is not the case for T349 (Figure 11.8, B.). In order to evaluate if this non-conserved residue is the cause of the loss of coordination of H347, triplicate MD simulations were performed on hIDO2 with an M350I mutant. The simulations are run for 300 ns, at 1 bar and 310 K. The results obtained are presented in the Table 11.1 and in Figure 11.8. The three replicates are consistent with each other in terms of global folding, average fluctuation, and convergence (Appendix E, Figure E.2).

TABLE 11.1: Distances (in Å) between H347 (NE) and the central iron of the heme cofactor. The analysis was performed on the 300 ns of MD simulations at 310 K and 1 bar, for each replicate.

Residue 350	Replicate 1	Replicate 2	Replicate 3
Methionine	5.8 ± 1.5	6.4 ± 1.4	6.9 ± 0.5
Isoleucine	9.0 ± 0.7	5.5 ± 1.4	9.2 ± 0.8

In the hIDO2 WT simulation, M350 is close to H347. One of the working hypothesis was that this proximity accentuated the motion of H347 and caused a loss of coordination between H347 and the cofactor. This loss of coordination could be responsible for the displacement of the heme in the active site. However, it is found

with the M350I simulations that this hypothesis is not valid. Indeed, the protein motion is identical (Figure 11.8, C.), with or without mutation, and particularly stable for residues H347-M350. The MD results show that I350 is placed in a similar way to M350 in hIDO2 (Figure 11.8, D.). Also, the mutation has no effect on the JK'-loop, which remains in open configuration, with high flexibility according to the replicates. Contrary to what would have been imagined, the mutation applied to mimic the hIDO1 sequence unfavors the binding of the heme. While H347 and I350 are oriented in the same way in the replicates (Appendix E, Figure E.2), the heme moves more or less into the different replicates, inducing variable distances between H347 and the iron atom. The H347(NE)-iron distance values increase drastically in R1 and R3 (Table 11.1). It is concluded that the M350 does not unfavor the binding of the heme to hIDO2. Additionally, M350 helps to keep the heme inside the active site. Consequently, the loss of the coordination between the heme and H347 and the cofactor displacement is caused by the conformational change of the F' helix and the G265-Q270 fragment.

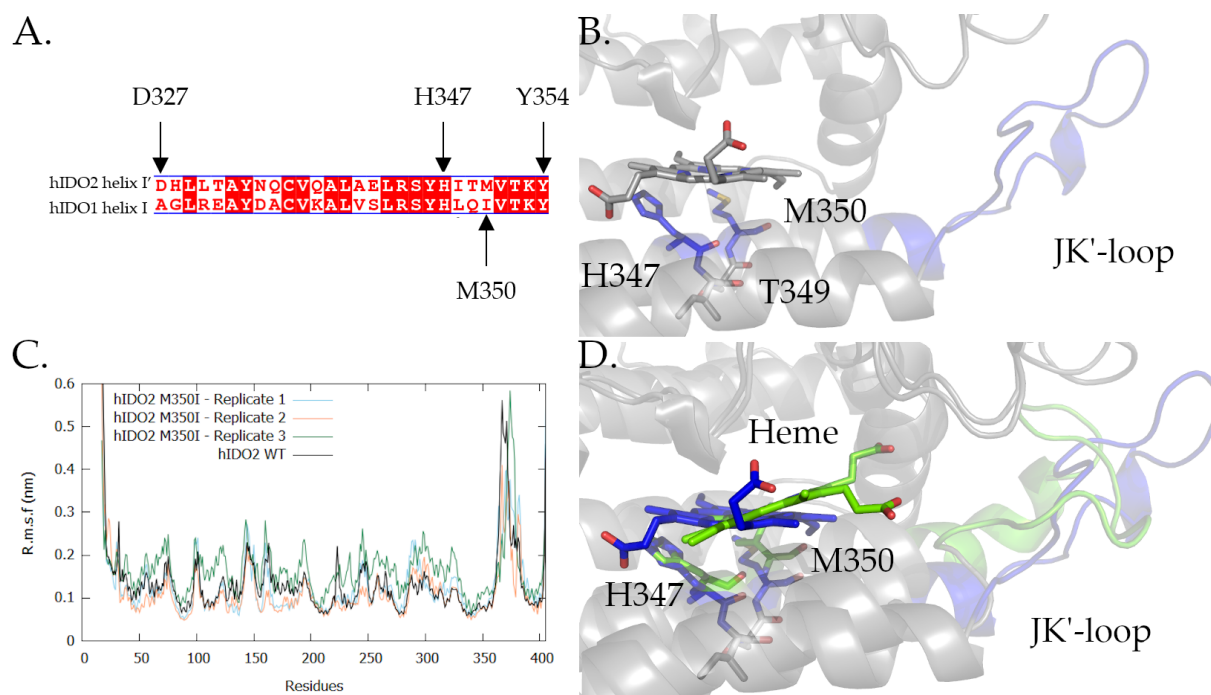


FIGURE 11.8: Effect of the M350I mutation on the position of the heme in the active site. A. Sequence alignment for helix I in hIDO1 with I' in hIDO2. B. Active site of WT hIDO2. C. R.m.s.f. profiles of hIDO2 with or without the M350I mutation. D. Relative positioning of H347, I350, and cofactor in simulations with the mutant protein (R1) compared to the WT protein.

11.3.2 Comparison of the holo and the apo form of hIDO2

Since it has been observed in the simulations that the cofactor of hIDO2 is not maintained in the active site by H347, the study of the plasticity of the apo form of hIDO2 was performed by triplicate Molecular Dynamics simulations (Figure 11.9). It makes sense in view of the high lability of the cofactor demonstrated experimentally (Chapter 5). The holo form of hIDO2 could be in equilibrium with the apo form. The three simulations showed a convergence towards the same folding during the production stage, and the r.m.s.f profiles as well on the r.m.s.d profiles are similar (Figure 11.9, A. and B.).

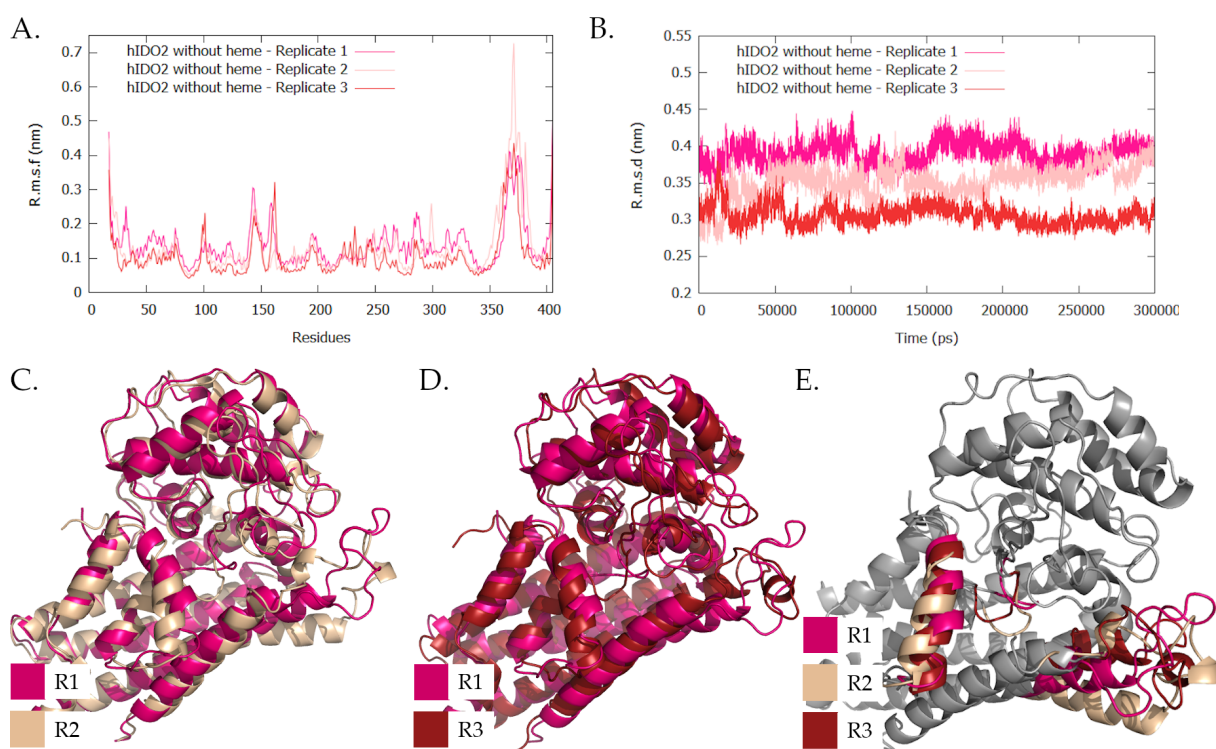


FIGURE 11.9: Structural differences (highlighted in colors) between the MD replicates after 300 ns at 310 K and 1 bar (in different shade of red: R1 = dark pink, r2 = wheat and R3 = red). A. R.m.s.f profiles of hIDO2. B. R.m.s.d profiles of each replicate in comparison to the starting structure. C. Comparison of the folding between R1 and R2. D. Comparison of the folding between R1 and R3. E. Comparison of the folding for the three replicates.

From a quantitative point of view, the observation of the structure changes along

the MD trajectories highlights that the main differences occur at the level of the fragment G265-Q270, the helix F', as well as the helix I' (Figure 11.9, C., D. and E.). Such differences can be explained by an exacerbated plasticity of these parts without marked increase of the flexibility. This is due to the absence of the cofactor in the active site which had a restrain effect on the protein architecture. For example, the G265-Q270 fragment adopts multiple of conformations within replicates along the trajectories (type I, type II or type III). Since these conformations were stable for the holo form, the absence of heme allows an easier transition into the three conformations. In view of the consistency between the replicates, the results are reported for the R1 only. The comparison of the final snapshot of the apo and holo forms highlights that the absence of the cofactor causes large-scale changes in the relative positioning of the G265-Q270 fragment and F', G', K' helices of the protein (Figure 11.10, A.). This supports the already mentioned importance of these helices in the cofactor lability in hIDO2.

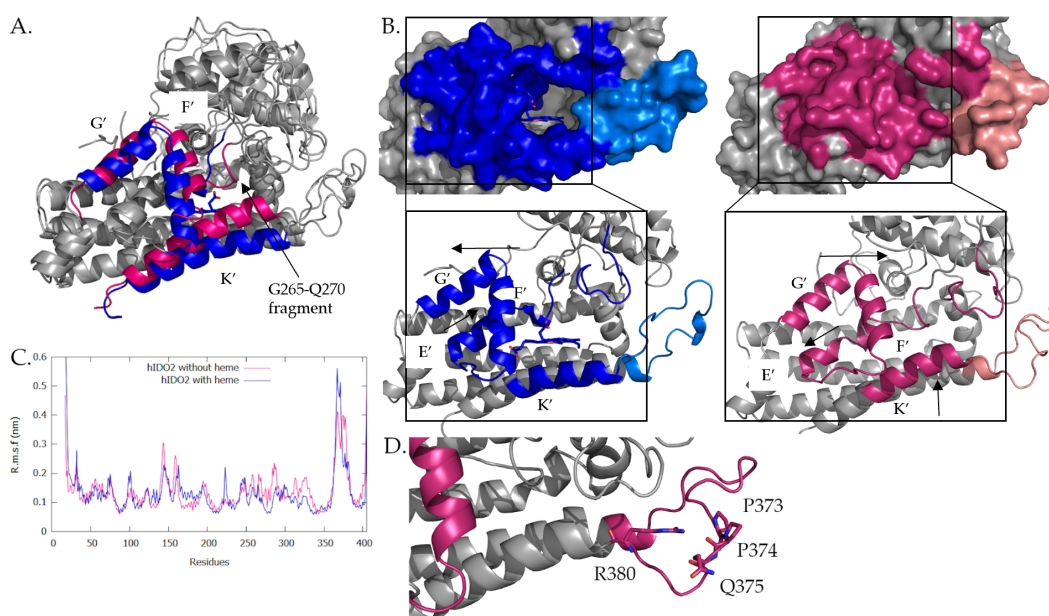


FIGURE 11.10: Characterization of the apo hIDO2 structure obtained after a 300 ns MD simulation at 310 K and 1 bar (in magenta) and comparison with the structure with the cofactor (in blue). Main differences between the apo and the holo proteins are highlighted in colors. JK'-loops are represented in the corresponding light colors. A. Global folding of the two protein forms. B. Influence of the cofactor presence on the van der Waals surface of the proteins and the corresponding secondary structure. C. R.m.s.f profiles of the apo and holo proteins. D. Interaction in the JK'-loop involving P373, P374, Q375 and R380.

Due to the concerted movement of these different secondary structure elements, a global closure of the active site is observed, thus no longer allowing the binding of a new free heme group from solution (Figure 11.10, B.). The JK'-loop is very little impacted by the absence of the cofactor. The conformation adopted by the C-terminal part is open, as in the presence of cofactor. The van der Waals surface at the level of the loop is almost identical, with and without cofactor (Figure 11.10, B.). As a result, there is no marked change in the flexibility of this residue sequence (Figure 11.10, C.). Specifically, the only difference is that, in the case of an apo protein, the polar R380 is always oriented towards the residues P373, P374, and Q375 (Figure 11.10, D.). Hydrogen bonds are established between the main chain of P373, P374, and Q375 and the polar residue. The interaction is therefore established within the JK'-loop and no longer with another partner of the protein. It can be concluded from this study that in the case of the hIDO2 apo form, the heme binding site is closed by the change of conformation of the F', G', and K' helices but not by the JK'-loop.

11.3.3 Influence of the polymorphism on the lability

In the introduction of this thesis, it was mentioned that the hIDO2 protein exists in two polymorphic forms in the Caucasian population. These forms are 1) a mutation of R235W 2) a deletion of a piece of sequence from Y346 to the end of the protein. To understand the effect of these polymorphs, 300 ns triplicate MD simulations were performed on R235 mutant, which provided similar results (Appendix E, Figure E.4). The R235W mutation affects the secondary structures of the G265-Q270 fragment, which adopting a type **III** conformation, the F' helix and the JK'-loop (Figure 11.11, A.).¹ The heme position is modified, as well it adopts a position more upstream of the active site, closer to the JK'-loop and R380. Even if the JK'-loop adopts a closed conformation at the C-terminal extremity, the disorganization of the F' helix leads to a large opening in front of the heme (Figure 11.11, B.). The motion of the JK'-loop is decreased by the mutation while the flexibility of F'-loop varies according to the replicates inducing different conformations (Appendix E, Figure E.4, B.).

To understand this change in the position of the heme, it is necessary to see from an individual point of view which amino acid is impacted by the mutation (Figure

¹The mutation also has an impact on the D' helix which contains R235. As a consequence, the helix loses its folding but this is moderate in comparison to the conformational change of the JK'-loop, the G265-Q270 fragment, and the F' helix.

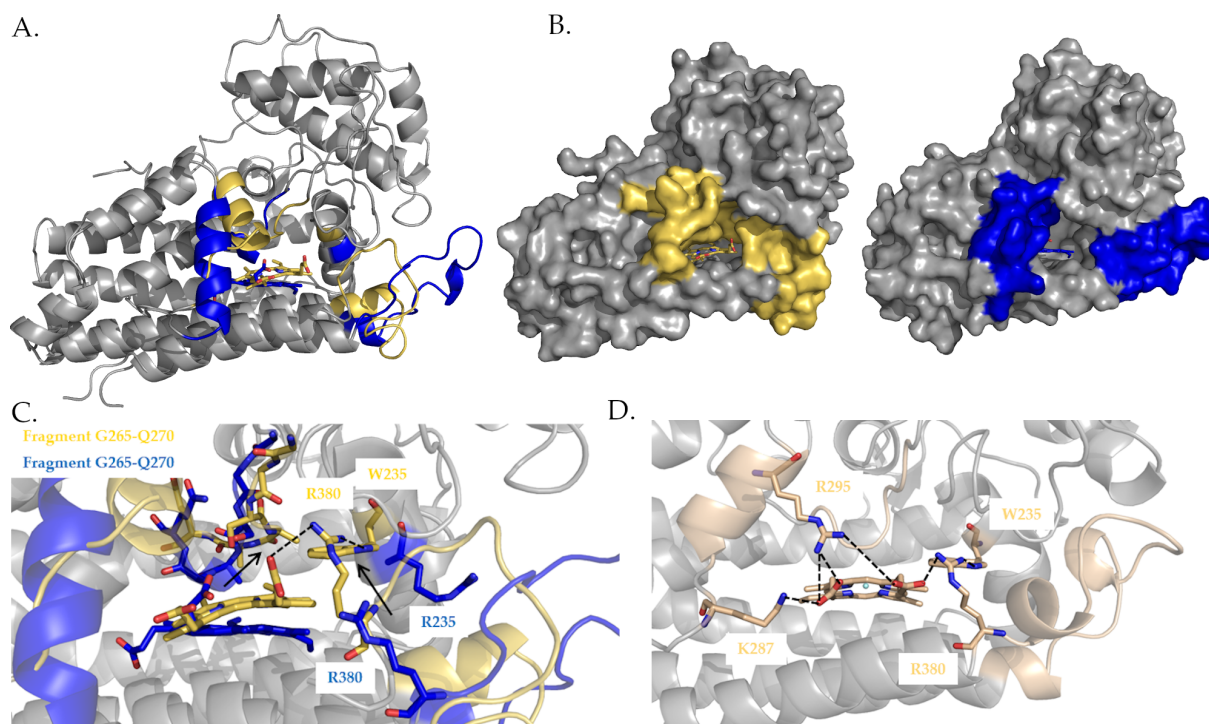


FIGURE 11.11: Characterization of the hIDO2 structure with the mutation R235W obtained after a 300 ns MD simulation at 310 K and 1 bar (R1, in yellow, R2 in wheat). A. Comparison with the structure after 300 ns for R1 with the cofactor (WT protein, in blue). Main differences between the WT protein and the R235W mutant are highlighted in blue and yellow colors respectively. B. Open surface of the mutant protein hIDO2 after 300 ns (R1) and contraction of the heme binding pocket. Comparison with the surface for WT protein after 300 ns (in blue). C. Induced-fit caused by the R235W mutation D on the JK'-loop residues (R1). D. Conformation of K287, R295 and R380 in the trajectory at 220 ns of the MD simulation of the R235W protein, at 310 K and 1 bar (R2).

11.11, C.). In the R235W mutation, R235 which brings positive charge into the active site, is replaced by W235. This aromatic residue is no longer oriented in the same way as R235 and prefers to be placed towards the highly hydrophobic active site. Because of this reorientation and the absence of a positive charge to repel R380, R380 is attracted towards the active site pocket. That leads to new interactions between R380 and the cofactor, W235, R295 (included in the helix F') or the G265-Q270 fragment. Contrary to the holo structure simulation, the orientation of R380 toward the active site is observed during the whole trajectory of each replicates. As a result, an induced fit of the entire heme binding pocket occurs and is associated with a contraction of its volume. Also, since the cofactor no longer has the binding of the iron ion to H347 in

the R235W mutant, this contraction leads to the exit of the cofactor from active site, like "a wet hand that catches a piece of soap".

This change in the cofactor position impacts the conformation of the F' helix which interacts with the heme or R380, depending on the replicate (Appendix E, Figure E.3). The positively charged amino acids of the helix F' modify their position in order to compensate for the resulting stabilization of the heme. Thus, K287 or R295, which does not interact with the cofactor in the WT protein, establishes interactions with the carboxylate groups of the cofactor and the positively charged residues in some frames of replicates. This causes a loss of helix folding between K387 and D291. It is the concerted movement of the three polar residues (K287, R295 and R380) that pulls the heme out of the active site as can be observed through the MD trajectories (Figure 11.11, D.).

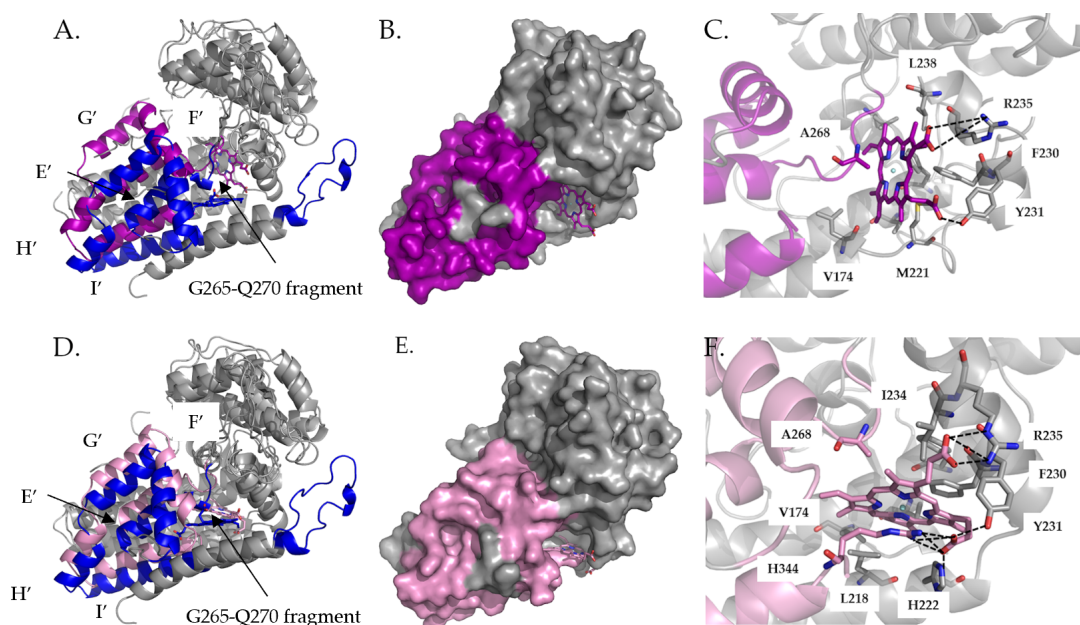


FIGURE 11.12: Characterization of the structure of hIDO2 with the deletion Y346X obtained after 300 ns MD simulation at 310 K and 1 bar for (R1: in purple, R2: in pink). A. and D. Comparison with the structure with the cofactor (WT protein, in blue). Main differences between the WT protein and the deletion polymorph are highlighted in blue and purple/pink colors respectively. B. and E. Open surface of the protein hIDO2 caused by the deletion. C. and F. Interaction between the heme cofactor and the protein in its new position.

It is also foreseen that the deletion of residues Y346 to P405 involves a displacement of the cofactor (Figure 11.12, A.). The effect of the residues deletion on the enzyme was studied through duplicate 300 ns MD simulations at 310 K and 1 bar. The r.m.s.d and r.m.s.f profiles corresponding to the different replicates are available in Appendix E, Figure E.5. In each case, there is a loss in the occupancy of the heme binding pocket. Despite the fact that trajectories followed by the heme is not identical for all, the heme trends to occupy a new pocket, formed by H222, F230, Y231, and R235. The structural differences with the WT protein are again observable at the level of the E', F', G', H' and I' helices (Figure 11.12, A. and D.) and G265-Q270 fragment (adopting a type I conformation). The van der Waals surface of the protein shows an opening of the protein (Figure 11.12, B. and E.). It is thus suggested that the heme can be free to leave its binding site for an other protein with a higher affinity. Electrostatic interactions with R235 and/or R344, which stabilize the carboxylate moiety of the cofactor (Figure 11.12, C. and F.). A hydrophobic environment formed by the residues V174, L218, M221, F230, I234, L238 and A268 also participate to the heme stabilization, as well as hydrogen bonds formed with Y231 and H222. From all these evidences, it is assumed that this hIDO2 polymorphs strongly impact the lability of the cofactor for the protein, mainly by causing conformational changes in the F' helix and, if present, the JK'-loop.

11.4 Study of the JK-loop with ligand in the active site

Following the study of the hIDO2 active site plasticity in the absence of ligand, a study of the same system with L-Trp was carried out. The experimental and the literature data indicate that L-Trp has a low affinity for hIDO2. In order to understand why, molecular docking calculations followed by a MD simulations were performed. All of the 300 ns MD simulations were performed without any constraint on the atom positions, at 310 K and 1 bar.

11.4.1 Docking of L-Trp into the active site of hIDO2

To generate a structure of hIDO2 complexed to its substrate, molecular docking of L-Trp was performed on the holo structure obtained by MD at the end of the 300 ns MD trajectory. The latter was performed using the Maestro program, through an induced fit method allowing a rearrangement of the side chains of the protein. Twenty-one docking orientations were obtained for L-Trp in hIDO2 with docking scores ranging

from $-6.84 \text{ kcal mol}^{-1}$ to $-4.835 \text{ kcal mol}^{-1}$. None of these orientations is equivalent to the reactive position observed in hIDO1. Nevertheless, two poses were analyzed, namely the best score pose (pos1) and the pose closest to a reactive position (pos6) (Figure 11.13).

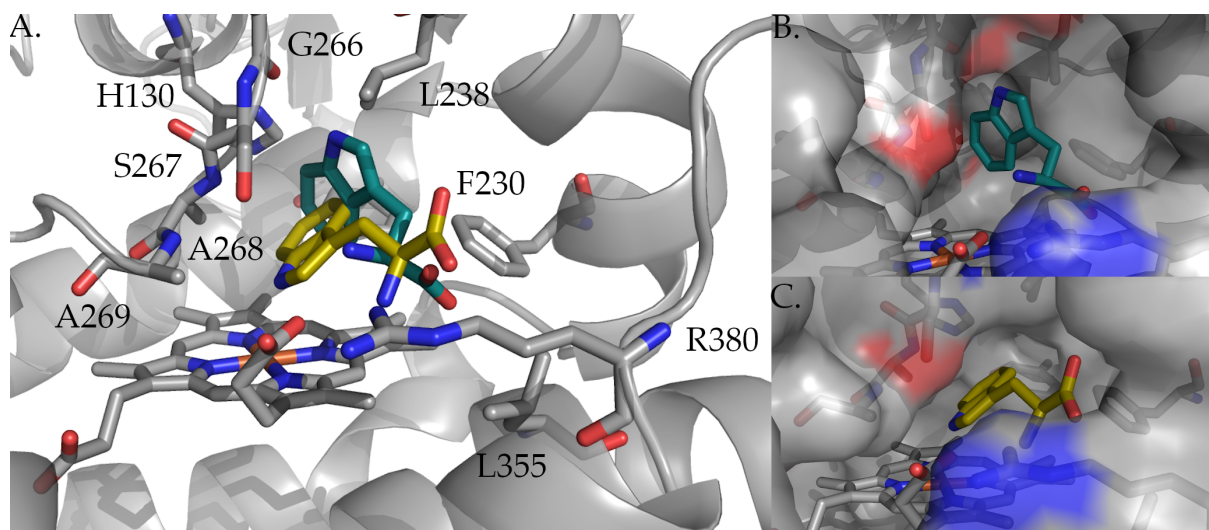


FIGURE 11.13: Two analyzed poses obtained by docking of L-Trp into hIDO2. Pos1 is in blue and pos6 in gold. A. Relative positioning according to the active site. B. van der Waals surface of the residues in the active site for pos1. C. van der Waals surface of the residues in the active site for pos6.

Pos1 shows the L-Trp in a position where the indole nitrogen atom points to the main chain carbonyl of G266. The polar part of the ligand is stabilized by the heme. The residue R235 of the protein is not oriented to stabilize the carboxylate of the substrate. Pocket A is open due to the relative position of the side chains (S267, A268 and A269) in the active site. For pos6, the orientation of the polar part of the ligand is similar to pos1 but the indole ring is flipped involving that the ring nitrogen interacts with the iron atom of the heme. The active site is closed and L-Trp cannot occupy the pocket A. Consequently, few interactions are established with the ligand. These interactions mainly occur at the G265-Q270 fragment. For both poses, F230, L238, and L355 provide a hydrophobic environment to stabilize the aromatic part. MM-GBSA calculations achieved using Maestro lead to similar binding ΔG for both poses, namely $-35.48 \text{ kcal mol}^{-1}$ for pos1 and $-34.56 \text{ kcal mol}^{-1}$ for pos6. These two positions could explain the poor activity of hIDO2. If L-Trp is positioned as in pos1,

it is clearly not ideally placed to react. If it is positioned as in pos6, the coordination with iron prevents/makes it more difficult to activate the oxygen.

11.4.2 MD simulation of hIDO2 bound to L-Trp using docked poses

To assess the molecular docking described above, 300 ns MD simulation, at 310 K and 1 bar were performed using the two docked structures. It aims at describing the evolution of the protein structure and its possible plasticity while checking the stability of the ligand in its pocket. Results are presented at Figure 11.14. During the MD simulation of pos1, L-Trp globally remains in the same position even if the orientation of the indole moiety varies slightly (Figure 11.14, A.). The mean interaction energy between the protein and L-Trp, calculated from short-range Coulomb and Lennard-Jones energies, amount to $-173.9 \text{ kJ mol}^{-1} \pm 50.7 \text{ kJ mol}^{-1}$. Despite the slight reorientation of the indole ring, L-Trp does not move towards the pocket A due to a steric hindrance at the level of the aromatic part leads to a steric hindrance. Also, the G265-Q270 fragment adopts a type II conformation, with S267 and A268 in front of the heme cofactor.

In contrast to pos1, pos6 is not stable at all during the MD simulation. From the beginning of the production stage, the ligand leaves the active site of hIDO2 (Figure 11.14, B.). Then, it moves at the surface of the protein, approaching from time to time the opening of the heme pocket.

The MD observation are consistent with the MM-GBSA calculations, i.e, pos1 is seen as more stable than pos6. Nevertheless, both MD simulations show a stabilization of the JK'-loop in the presence of L-Trp inside or outside the enzyme. In both cases, the loop is so stable that it hardly varies in conformation with time (Figure 11.14, C. and D.). This results in a clear decrease in the corresponding r.m.s.f. values. The conformation adopted by the loop is intermediate at the C-terminal extremity. To summarize, the MD results allow to exclude pos6 from the possible L-Trp binding positions and validate pos1. However, pos1 does not favor the activity of the enzyme due to the orientation of the indole ring.

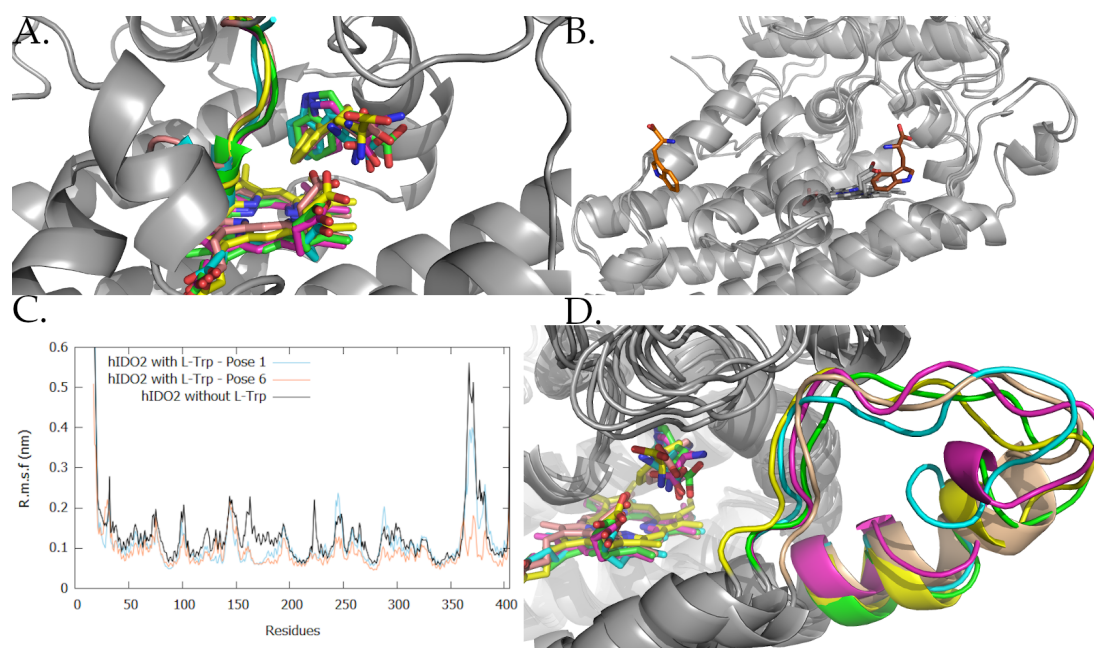


FIGURE 11.14: A. Snapshots of the 300 ns MD trajectories of the L-Trp bound to hIDO2 at 100, 150, 170, 200 and 300 ns, at 310 K and 1 bar. Pos 1 is used as the starting MD ligand position. B. Snapshots of the 300 ns MD trajectories of the L-Trp bound to hIDO2 at 10 and 300 ns, at 310 K and 1 bar. Pos 6 is used as the starting MD ligand position. C. R.m.s.f profiles of the protein residues for the two simulations. D. Conformations of the JK'-loop as obtained for the 300 ns MD trajectories of the L-Trp bound to hIDO2 at 100, 150, 170, 200 and 300 ns, at 310 K and 1 bar with Pos 1 as starting MD ligand position.

11.4.3 MD simulations of L-Trp bound to hIDO2 using hIDO1 data

To confirm the MD results, two MD simulations were performed starting with L-Trp in a reactive and an intermediate position, as achieved for the hIDO1 study (see Chapter 7, for hIDO1-closed and hIDO1-intermediate). To perform MD simulations, L-Trp was positioned exactly at the corresponding location in hIDO1. The MD simulations were then performed without position constraint for 300 ns, at 310 K and 1 bar. When L-Trp is positioned in the reactive position, a rearrangement is observed at the beginning of the production stage. It leads, after 50 ns, to the exit of the substrate from the active site (Figure 11.15, A.). This reactive position does not appear to be adequate in the case of hIDO2. The same stabilizing effect as for pos6 is observed for the JK'-loop when L-Trp is outside the protein (Figure 11.15, B.), i.e, a decrease of the flexibility and a stable position with time.

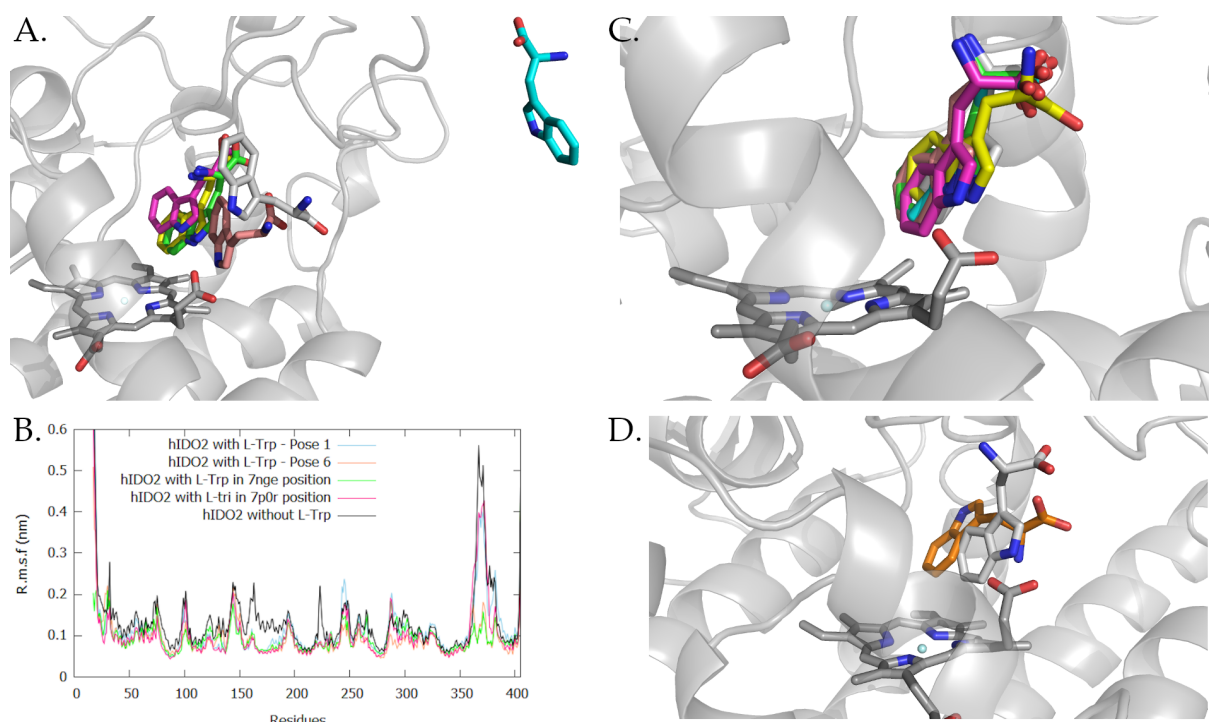


FIGURE 11.15: A. Snapshots of the 300 ns MD trajectories of the L-Trp bound to hIDO2 at 1, 10, 20, 30, 40 and 50 ns, at 310 K and 1 bar. L-Trp in hIDO1-closed (PDB: 7nge) is used as the starting MD ligand position. B. R.m.s.f profiles of the protein residues for the different simulations. C. Snapshots of the 300 ns MD trajectories of the L-Trp bound to hIDO2 at 50, 100, 150, 200, 250 and 300 ns, at 310 K and 1 bar. L-Trp in hIDO1-intermediate (PDB: 7p0r) is used as the starting MD ligand position. D. Comparison of the position of L-Trp after 300 ns of simulation in case of a starting pose 1 position (grey) and a starting hIDO1-intermediate position (PDB: 7p0r, orange).

Conversely, simulation starting from the position observed in the hIDO1-intermediate structure (PDB: 7p0r) reveals a stable substrate in the enzyme pocket (Figure 11.15, C.). The mean interaction energy between the protein and L-Trp, calculated from short-range Coulomb and Lennard-Jones energies, amount to $-266.0 \text{ kJ mol}^{-1} \pm 51.6 \text{ kJ mol}^{-1}$. The position adopted by the substrate differs from pos1 despite the fact that they both occupy the same place in the pockets A and B (Figure 11.15, D.). The stabilization of the JK'-loop is then identical in this MD simulation and in pos1 (Figure 11.15, B.). While pos1 shows L-Trp as interacting with the polar part of the heme, the present MD simulation reports that the indole nitrogen atom ensures the ligand stabilization. Thus, both positions are possible even if they do not represent L-Trp as ideally placed for a reactive process. To summarize this section, the poor activity of hIDO2 probably

comes from a less ideal positioning of L-Trp in the active site compared to hIDO1. The reasons for this poor positioning are detailed in the comparative part (Chapter 12).

11.5 Intermediate conclusions

This chapter provides first elements of the possible structure of the hIDO2 protein. The models obtained by homology and by AlphaFold are not representative enough in view of the great protein dynamics. A multidisciplinary approach is needed to study the protein. The Molecular Dynamics simulations highlight the mobility of the F' helix as well as of the JK'-loop. These parts are strongly affected by absence of cofactor, mutations or deletions.

In the holo protein, the F' helix obtained after a 300 ns of MD simulation adopts a different conformation than in the homology models. This discrepancy comes from the fact that it is shorter in hIDO2 than in the reference template hIDO1. The helix also presents a great plasticity and its role is central in the lability of the cofactor. Indeed, during the MD simulations, the position of heme cofactor varies slightly and H347 is not well oriented to perform a binding between the cofactor and the protein. It is due to a global induced fit of the protein rather than to a lack of conservation of residues close to H347 (including M350). The JK'-loop is build from alternation of apolar and polar parts in hIDO2. It can be separated into two sections: N-terminal (A358 to P374) and C-terminal (from Q375 to R380). Its flexibility is very high, with a value three fold higher than the average for the whole protein. Simulations with the cofactor did not allow to determine a common conformation for the C-terminal part between the replicates, but a tendency towards opening is still observed. Without any heme cofactor, the conformation of the JK'-loop remains open. However, due to a concerted movement of the helices F', I', and G', the heme binding site is closed. In view of the lower affinity of the cofactor for the protein observed in chapter 5, it is assumed that it is not necessarily easy to open the protein to incorporate a new cofactor. The existence of polymorphs such as the R235W mutation results in closing the dynamic loop with a displacement of R380 towards the center of the heme binding pocket. This causes, with the concerted movement of the F' helix and the G265-Q270 fragment, a contraction of the active site. Once again, this phenomenon results in a loss of heme binding. K287, R295 and R380 had a crucial role in the exit of the cofactor. At last,

the truncation of Y346X leads, by the absence of the JK'-loop, to the exit of the heme from its binding pocket.

The binding of the substrate to the enzyme has also been studied. From molecular docking and MD simulation, it was shown that the substrate does not manage with ease to position itself in a reactive state in the active site of hIDO2. This supports the fact that the affinity of L-Trp for the enzyme is low. The substrate mainly adopts an intermediate position, in pocket B, even if pocket A is open. In this case, the JK'-loop is relatively stable and adopts with an intermediate type conformation.

To conclude, the high lability of the heme and the low affinity of L-Trp explain the poor activity of the protein. Indeed, the cofactor is an essential partner to the reaction. Increasing its lability results in a decrease of the activity for the enzyme. Moreover, the positioning of L-Trp in the active site remains mostly a non-ideal one. Together with the high lability of the cofactor, it supports the poor activity of the protein.

Bibliography

- [1] The UniProt Consortium. Uniprot: the universal protein knowledgebase in 2021. *Nucleic acids research*, 49(D1):D480–D489, 2021.
- [2] A. Waterhouse, M. Bertoni, S. Bienert, G. Studer, G. Tauriello, R. Gumienny, F. T. Heer, T. A. P. de Beer, C. Rempfer, L. Bordoli, et al. Swiss-model: homology modelling of protein structures and complexes. *Nucleic acids research*, 46(W1):W296–W303, 2018.
- [3] P. Benkert, M. Biasini, and T. Schwede. Toward the estimation of the absolute quality of individual protein structure models. *Bioinformatics*, 27(3):343–350, 2011.
- [4] G. Studer, C. Rempfer, A. M. Waterhouse, R. Gumienny, J. Haas, and T. Schwede. Qmeandisco—distance constraints applied on model quality estimation. *Bioinformatics*, 36(6):1765–1771, 2020.
- [5] J. Jumper, R. Evans, A. Pritzel, T. Green, M. Figurnov, O. Ronneberger, K. Tunyasuvunakool, R. Bates, A. Žídek, A. Potapenko, et al. Highly accurate protein structure prediction with alphafold. *Nature*, 596(7873):583–589, 2021.

- [6] M. Varadi, S. Anyango, M. Deshpande, S. Nair, C. Natassia, G. Yordanova, D. Yuan, O. Stroe, G. Wood, A. Laydon, et al. Alphafold protein structure database: massively expanding the structural coverage of protein-sequence space with high-accuracy models. *Nucleic acids research*, 50(D1):D439–D444, 2022.
- [7] M. J. Abraham, T. Murtola, R. Schulz, S. Páll, J. C. Smith, B. Hess, and E. Lindahl. Gromacs: High performance molecular simulations through multi-level parallelism from laptops to supercomputers. *SoftwareX*, 1:19–25, 2015.

Part V

Comparison of the two targets and discussion

*“On a fait c’qu’on a fait comme on l’a fait, mais on l’a fait, hein
Tout s’transforme, rien n’se perd, ombre et lumière”*

Orelsan - Civilisation

Chapter 12

Comparison of hIDO1 and hIDO2 and discussion

12.1 Introduction

Throughout this thesis, various characteristics of hIDO1 and hIDO2 have been studied. This has allowed to lift the veil on the plasticity of the two proteins. With this new information in hand, it is interesting to finally answer the question of the differences and similarities between these two proteins. This is detailed in this part.

12.2 Physico-chemical characterization of the two targets

One of the most contrasting pieces of information between hIDO1 and hIDO2 mentioned in the literature prior to this thesis is the lack of activity of the latter protein. However, this is not the only difference highlighted in this thesis. Too often forgotten in the characterization of the literature for hIDO1 and hIDO2, the physicochemical study of the lability and affinity of the cofactor for the protein, the protein stability and activity have been conducted during this thesis in Chapters 4 and 5. At the end of the first two chapters of results, it is possible to conclude on this characterization part and to compare hIDO1 and hIDO2 from a point of view of their physio-chemical properties

12.2.1 Characterization of the cofactor incorporation

The first characteristic discussed is the incorporation and the lability of the cofactor. The comparison of the two therapeutic targets must be done with care. Since there is no precise technique for determining the molar extinction coefficient of the Soret band due to the presence of bounded heme in the two proteins, it is not possible to state with complete certainty that one incorporates less the cofactor than the other. The same conclusion for the cofactor affinity depending on the oxidation state is true: not knowing if the molar extinction coefficient is the same depending on the oxidation of the cofactor, we can not decide on the affinity of the protein. However, some conclusions can be drawn. Several results suggest that the heme cofactor presents a lower affinity for hIDO2 than for its paralog hIDO1 (Figure 12.1). Notably, hIDO2 can present a totally apo form, which is very difficult to isolate for hIDO1. For hIDO1, the loss of the cofactor to form the apo protein is achieved only in the presence of another hemoprotein in apo form (Appendix A), such as apo-myoglobin, to compete with heme. However, even after overnight, the loss of heme into the enzyme is never

complete. For hIDO2, loss of the cofactor is much easier, without the need for another apo hemoprotein, temperature and successive buffer changes being strong enough to reduce incorporation. As a result, hIDO2 would appear to have less affinity for its cofactor than hIDO1.

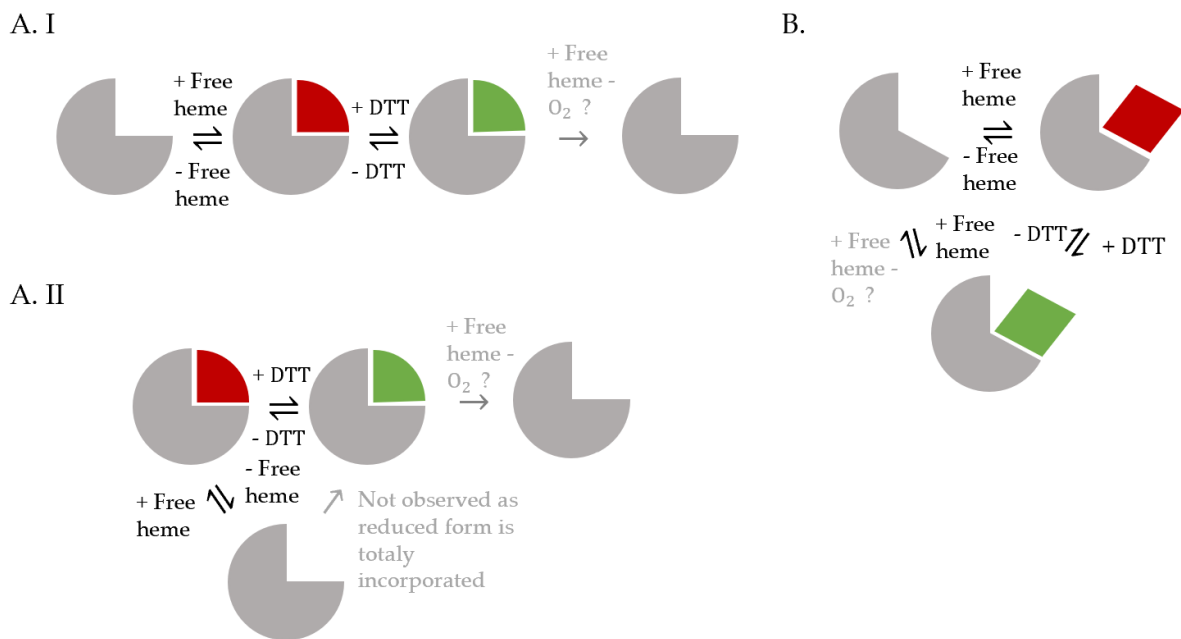


FIGURE 12.1: Equilibria established between the different forms of A. hIDO1 with the two possible hypotheses (I. and II.) and B. hIDO2. Red = oxidized cofactor, Green = reduced cofactor. The cofactor in hIDO2 are less affine than the one in hIDO1.

Another important difference between the two proteins is the ability to reincorporate the cofactor (Figure 12.1), and thus their heme lability, depending on the redox state. For hIDO1, it could be shown that the cofactor of the protein was only labile in the oxidized form. Incorporation was not significantly increased under reducing conditions, despite the addition of a large amount of cofactor. However, this could be explained by the fact that, *in vitro*, a 100% incorporation has already been achieved, even though this was fully incorporated has been proven as non-existent in the cell. For hIDO2, both oxidation states of the cofactor were found to be labile. It is thus possible to re-incorporate the cofactor into the protein under reducing or oxidizing conditions. If the hypothesis is maintained that reduced hIDO1 is not labile because it is already at 100% of incorporation, this effect could be a second indication that hIDO2 has a lower affinity and is therefore not in the form of bound heme in 100% of active sites *in vitro*. At last, it could be isolated that for both reduced forms of hIDO1

and hIDO2, an intermediate is observed in addition to the bound state. This intermediate could be a non-bound form of the heme in the active site, making the transition between the holo and apo form. This state could be due to a lability when the heme binds to dioxygen. As a result, the type of equilibrium is not the same between the different forms of hIDO1 and hIDO2 depending on the hypothesis as described at Figure 12.1.

12.2.2 Characterization of the stability

Concerning the stability, an important difference exists between the two proteins. In its native state, without the addition of heme or reducing agent, the hIDO1 protein has a much higher melting temperature than hIDO2, as summarized in Table 12.1. This difference of 10 degrees for the reduced form and almost 15 degrees for the oxidized form shows a tendency for hIDO2 to unfold easier than hIDO1. The oxidation state of the cofactor, and therefore of the protein, affects the stability of hIDO1 but not hIDO2. This is justified by the fact that the reduced cofactor of hIDO1 does not present any lability. Due to the nature of the covalent bond in ferrous hIDO1 between the cofactor and the protein, there is a stronger maintenance of the protein structure than in the absence of this bond (ferric hIDO1 or hIDO2). Consequently, unfolding occurs at higher temperature.

TABLE 12.1: Comparison of melting temperature between hIDO1 and hIDO2, according to the oxidative state of the cofactor.

Protein	T _m (°C) if oxidized	T _m (°C) if reduced
hIDO1	58.1 ± 0.2	62.4 ± 0.1
hIDO2	48.1 ± 0.1	47.7 ± 0.1

The effect of adding additives is also different between the two therapeutic targets. Indeed, while the addition of heme has almost no effect on the oxidized form of hIDO1, a stabilization of the reduced form of hIDO1 (T_m = 68.8 degrees ± 0.2) and of the reduced (T_m = 68.8 degrees ± 0.0) and oxidized (T_m = 65.3 degrees ± 0.2) forms of hIDO2, respectively, is observed when 50 μM of cofactor is added. This addition results in the appearance of a new form, doped in heme. It is also possible to see the coexistence between the two forms for a lower cofactor concentration of 30 μM.

12.2.3 Characterization of the activity

The activity of hIDO1 and hIDO2 was, prior to this thesis, the best known data in the literature. Indeed, for hIDO2, it was even one of the only known data. The present part has thus allowed to verify the enzymological data of the literature. It turns out, as expected, that hIDO1 (K_m of $40 \mu\text{M}$) is much more affine for its substrate than hIDO2 (K_m not determined in this work but known to be of low biological representative value). The hemoprotein hIDO1 presents a capacity of retro-inhibition, at high substrate concentration. This seems not the case for hIDO2, where it is difficult to achieve saturation of the reaction. This observation needs to be confirmed. The addition of hemin causes an inhibition of the activity of hIDO1 due to the competition with incorporation equilibrium. For hIDO2, the addition of the cofactor has no marked effect on the activity.

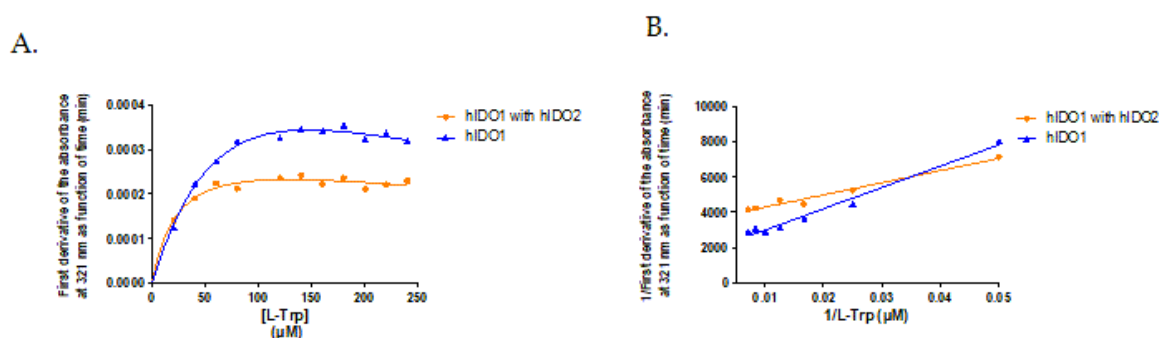


FIGURE 12.2: Enzymological assays of hIDO1 in presence of hIDO2. A. Retro-inhibition fit B. Lineweaver-Burk lines at low concentration in L-Trp.

Knowing that it was demonstrated that hIDO2 could be less complementary for its cofactor than hIDO1, enzymatic tests were performed for hIDO1, in the presence of hIDO2. Under the tested concentration in L-Trp (between $10 \mu\text{M}$ and $240 \mu\text{M}$), hIDO2 (210 nM per well) is not active. Therefore, it cannot contribute to the formation of NFK. However, we observe an effect of the presence of hIDO2 on hIDO1. In this case, the precision of the enzymological measurements makes it difficult to conclude with certainty of the effect. What is observed through the replicates is that the addition of hIDO2 leads to a decrease of the maximal speed of the reaction. No retro-inhibition is observed. The behavior is quite similar to that observed for hIDO1 when heme is

added. A tendency towards inhibition, due to the establishment of a new equilibrium, could be perceived. This research is also consistent with the research of Lee *et al.* on the decrease of hIDO1 activity in the presence of hIDO2. [1] However, as this is close to the effect when heme is added, it is possible that it is not hIDO2 that is capturing the heme from hIDO1, as discussed in the paper. [1] This would indicate that, under the reaction conditions, a heme transfer equilibrium interferes with the reaction. This must be confirmed by additional measurements, and why not, by cellular tests.

12.2.4 Conclusions of this physico-chemical comparison

This physico-chemical characterization allowed to learn more about the two proteins. From the characteristics collected, we now know that the heme cofactor in hIDO2 is more labile and less affine than the heme cofactor in hIDO1. It is also notable that hIDO2 is less stable and therefore the balance between its folded and unfolded form is more easily shifted towards unfolding of the protein. Finally, as expected, hIDO2 is less active than hIDO1. A new information being that the activity of hIDO1 in the presence of hIDO2 is impacted by the presence of the second enzyme. This is consistent with cellular results from the literature. However, the explanation that hIDO2 captures heme from hIDO1 no longer seems correct. More study on this topic should be done to understand the complex mechanism.

This new information opens up possibilities for the role of hIDO2 in the human body. It is indisputable that the protein is not there to degrade L-Trp. However, due to its greater cofactor lability, lower cofactor affinity and ease of defolding, it is a tool of choice for boosting hIDO1 activity. Being expressed in the common tissues or cells than hIDO1 and being induced by one of the products of the hIDO1 chain, it could serve as a heme stock for the protein by activating the cofactor synthesis pathway. It has indeed already been shown for hTDO2 that overexpression of the hemoprotein cancels the negative feedback controlling the heme pathway, thus allowing a small amount of free heme to be bound by the hTDO2 protein. In the way that hTDO2 is able to use this reserve, it is possible to imagine a similar mechanism for hIDO2. In this way, hIDO2 would be, by being over-expressed in cancers or COVID-19 diseases, a heme reservoir for hIDO1. In the presence of hIDO1, it would thus reload the active site and allow a better affinity of the substrate for the enzyme and a higher activity.

[2] To prove this hypothesis and better understand the complementarity of the two enzymes, a structural study is necessary.

12.3 Structural characterization of the two targets

The structural characterization of the two therapeutic targets has been focused throughout this thesis on the plasticity of the proteins. The information collected is not based on the same techniques. Indeed, where it was possible for hIDO1 to crystallize the protein in order to refine its JK dynamic loop and to study the plasticity of the active site or the existence of an exo site, the crystallization attempts of hIDO2 were not successful. As a consequence, the characterization of this enzyme was performed computationally by combining homology modeling, docking and Molecular Dynamics.

12.3.1 Crystallization and global folding information

The hIDO1 protein crystallizes relatively easily, with medium resolutions. The protein is formed of two domains, namely the small and the large subunit (Figure 12.3). The small subunit presents an exo site formed of three pockets. The large subunit presents the active site with a great plasticity to allow adaptation to the substrate. This is possible through several flexible parts, namely the JK-loop and the G261-G265 fragment. This thesis highlights the open, closed or intermediate conformation of the JK-loop depending on the positioning of the ligands or the absence of the latter in the active site. The JK-loop adapts to the ligand and is strongly stabilized when it adopts a reactive position. For the G261-G265 fragment, the adaptation is also linked to the occupancy of the active site and shows the possibility of three different conformations depending on the type of ligands. The first conformation (type **I**) presents an orientation with S263 in the reverse plan and A264 forward the plan. The fragment adopts this conformation for an empty ferric active site or for an active site occupied by poor affinity ligand. The second conformation (type **II** - "S263 forward/ A264 forward") happens when a substrate is entering the active site, regardless of the oxidation state (O₂ or L-Trp) or in the case of inhibitors of hIDO1 with less affinity for the enzyme. The last conformation (type **III**) - "S263 forward/A264 reverse") is strictly observed with L-Trp in the reactive conformation or for some very affine inhibitors of the protein. This conformation is associated with an induced-fit of the G261-G265 fragment

in order to allow the opening of the A pocket. The determination of one type of conformation to another is done by measuring the ψ dihedral angle of A264 (type II: between -65° and -85° , type III: lower than -55°)

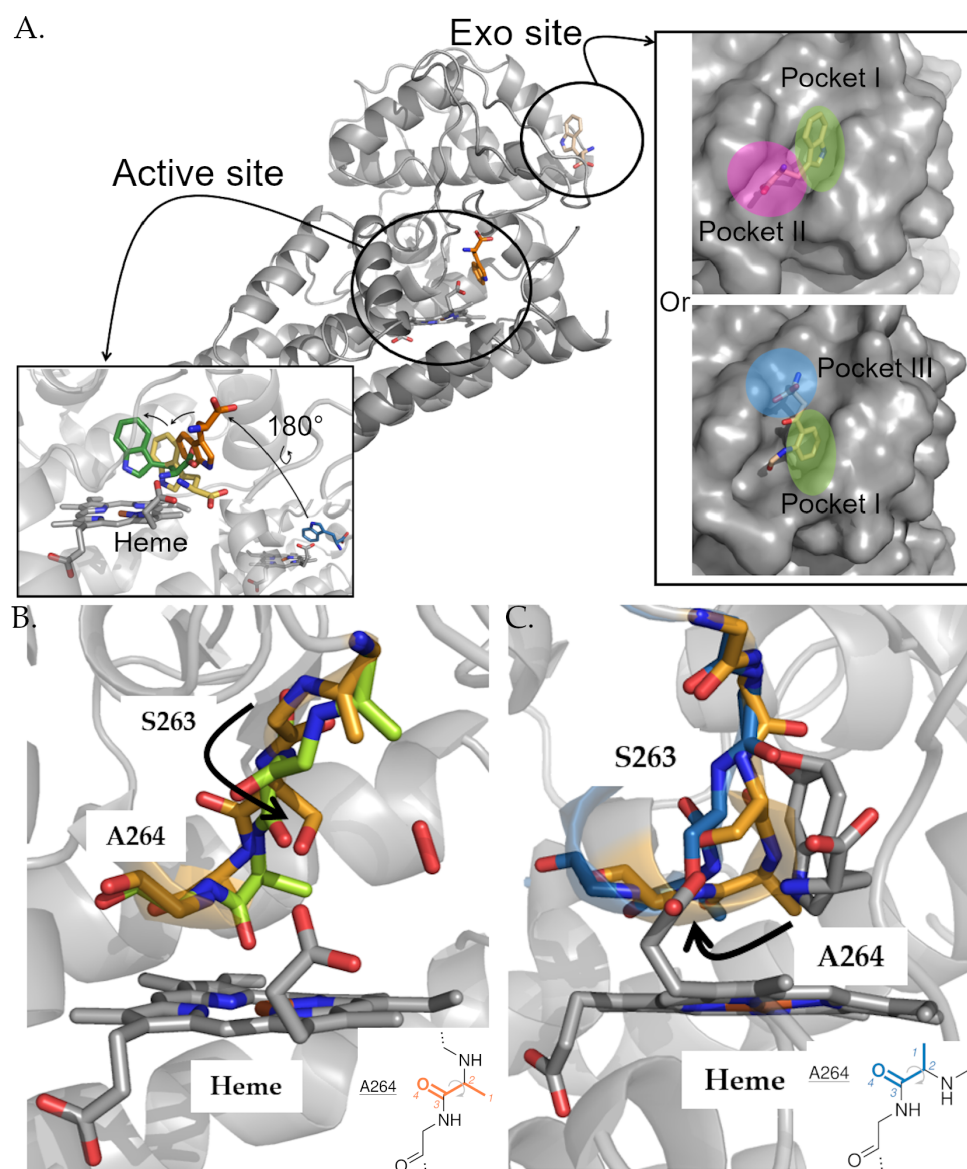


FIGURE 12.3: Global folding information collected for hIDO1 using crystallography and Molecular Dynamics. A. Relative positioning of exo and active site in small and large subunit of hIDO1. B. Conformation adopted by G261-G265 fragment in case of type I (in green) and II (in orange). C. Conformation adopted by G261-G265 fragment in case of type II (in orange) and III (in blue).

In contrast, hIDO2 is not crystallized. This may be due to a constitutional instability for the non-conserved residues. The analysis of the hIDO2 sequence could also explain the difficulties to crystallize the protein. Indeed, in the non-conserved part of the sequence, there are about a hundred changes in polarity of the residues¹ as well as 12 changes in charge among the polar residues. These changes in polarity can induce a greater difficulty in crystallization following a different surface hydrophobicity. Moreover, these local changes may, in addition to changes in protein folding, induce changes in the crystal interfaces and may not allow organized crystal packing and crystal formation. In fact, the dimeric interfaces for hIDO1 are found at the Y36-H45/Q54-K61 residues for the small subunit and at the BC, HI and pre- α -helix D for the large subunit. For hIDO2, these are areas with local changes in polarity.

As a result of these difficulties to crystallize, the study presented in this thesis is mainly focused on a computational study of the enzyme. From an overall point of view, hIDO2 is predicted to present a fold close to hIDO1 with a small and a large subunit. For the large unit, in hIDO2, plasticity is different than for hIDO1. It is not limited to the JK'-loop and the G265-Q270 fragment but is extended to all the moieties surrounding the heme. The F', G', I' and K' helices can then adopt totally different positions according to the simulations. This can be explained by the conservation of the residues of these helices. As described at Figure 12.4, the G261-G265 fragment is highly conserved between the two proteins. This conservation will lead to the possible observation of several conformations for this fragment as in the case of hIDO1. For hIDO2, a type II or III conformation is observed in the holo protein without ligand in the active site. The absence of cofactor leads to a variable conformation of the G265-Q270 fragment without preference for one of the three types. The docking of L-Trp in the active site allowed to highlight a docking of the substrate in the intermediate position. Consequently, the fragment adopts a type II conformation as was the case for hIDO1 with a substrate molecule in the active site but not in the reactive position. This conservation of the residues is not observed in the case of the helix F' and the JK'-loop. The helix F' is shortened in hIDO2 and the non-conserved residues change in terms of polarity. This induces different kind of flexibility or folding for these parts. The same observation can be done for the

¹When a residue goes from polar to apolar or vice versa. The sequence alignment of the two targets is shown in Appendix E at Figure E.6 with residues had been highlighted to differentiate polar and apolar residues.

JK'-loop which one is longer in hIDO2 than in hIDO1. There is a higher proportion of apolar residue in the N-terminal part of hIDO2 loop. The plasticity of the G', I' K' helices is not explicable by the different natures of the residues since the sequence is relatively well conserved. Their conformational change could then come from a global change of the protein by induced fit. The following sections describe the behavior of these flexible parts in hIDO2 relative to hIDO1 as a function of active site occupancy (with and without cofactor, with and without the substrate).

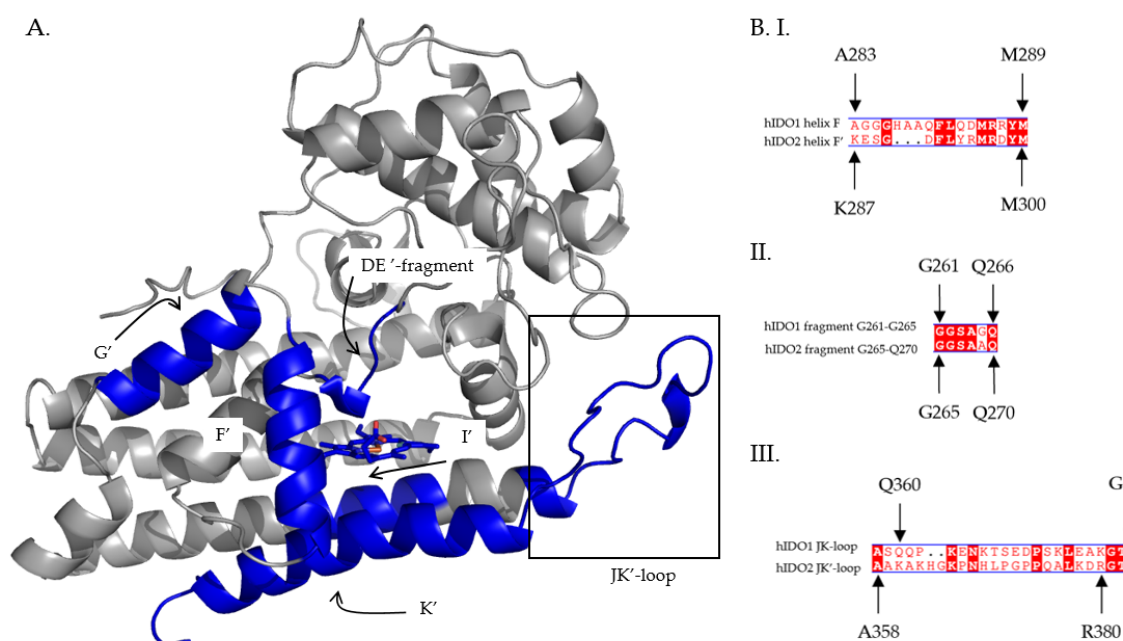


FIGURE 12.4: A. Global folding of hIDO2 with important flexible part highlighted in blue. B. Sequence alignment of the F helix as well as the JK-loop and the G261-G265 fragment in hIDO1 with the sequence of F' helix, JK'-loop and G265-Q270 fragment in hIDO2. Conserved residues are in red.

12.3.2 Study of the structural features of holo forms

By changing the dimeric interfaces, the crystal structure of holo form of hIDO1, without ligand other than the cofactor in the active site, could be obtained with a complete JK-loop at the beginning of the thesis. With the complementarity of Molecular Dynamics, it could be supported that hIDO1 holo form presented an intermediary conformation for the C-terminus, with an electrostatic interaction involving K377 (6.8

$\text{\AA} \pm 2.4\text{\AA}$ and $6.9 \text{\AA} \pm 2.4\text{\AA}$ between the carboxylate part of the cofactor and the protonated amine of K377). During the dynamics, the majority of the trajectories obtained show this conformation with a distance between K377 (NZ) and the active site (CB of A264) between 10\AA and 16\AA . The N-terminal part of the protein adopts a conformation independent of the C-terminal part. It is predominantly globular, with a number of H-bonds of 1.3 ± 1.0 established between the JK-loop and the DE-fragment. This dual conformation of the N-terminal and C-terminal parts keeps the cofactor inside the active site. After the publication of the paper associated with these results, it could be shown that hIDO1 holo replicates also gave the same tendency².

The holo hIDO2 protein definitely presents a different flexibility resulting in changes in the plasticity. For this enzyme, simulations were run in three replicates of the holo protein. The r.m.s.f profiles shows that hIDO2 has higher overall values than hIDO1, both at the protein average and the JK'-loop (Figure 12.5, A.). Significant variability in the conformation of the C-terminal JK'-loop is observed for hIDO2. In the three replicates, conformations adopted varies to open, closed or intermediate with a predominance of the more open forms. This highlights a high flexibility of the JK'-loop in the presence of cofactor. The interaction between R380 (the homologue of K377) and the heme cofactor is not always observed and the average distance between the two partners varies strongly according to the replicates. Compared to hIDO1 where the F-helix presents mainly the same folding, this one differs in hIDO2 depending on the replicates. Lastly, while in hIDO1, during MD simulations with the holo empty active site, only one conformation for the G261-G265 fragment is observed, namely a type II conformation, it can vary between type II and III in hIDO2. All of this supports an exacerbated plasticity of the enzyme. As a result, while heme remains stable and H346 remains iron-oriented in hIDO1 ($3.6 \text{\AA} \pm 0.4 \text{\AA}$ in the published results and $2.7 \text{\AA} \pm 0.3 \text{\AA}$ in the second replicate simulation performed with GROMACS 2020), plasticity of the entire active site of hIDO2 leads to rapid loss of binding (distances amount values bigger than 5.0\AA) and displacement of the cofactor into the active site pocket. The conformation adopted by the JK'-loop also lead to a greater opening of the active site in hIDO2 than in hIDO1 (Figure 12.6, B. and C.). These results support the greater lability of the cofactor in hIDO2 compared to hIDO1. While in hIDO1, the ligand-free conformation helps maintain the heme in the active site, this is not the

²In the rest of this discussion, these results will be referred to as R2 - GROMACS 2020 since they were done with the most recent version of GROMACS.

case in hIDO2. Simulations with the M350I mutant prove that the exacerbated lability of heme not explained by a lack of a conserved residue close to H347 but rather by an overall movement of the protein.

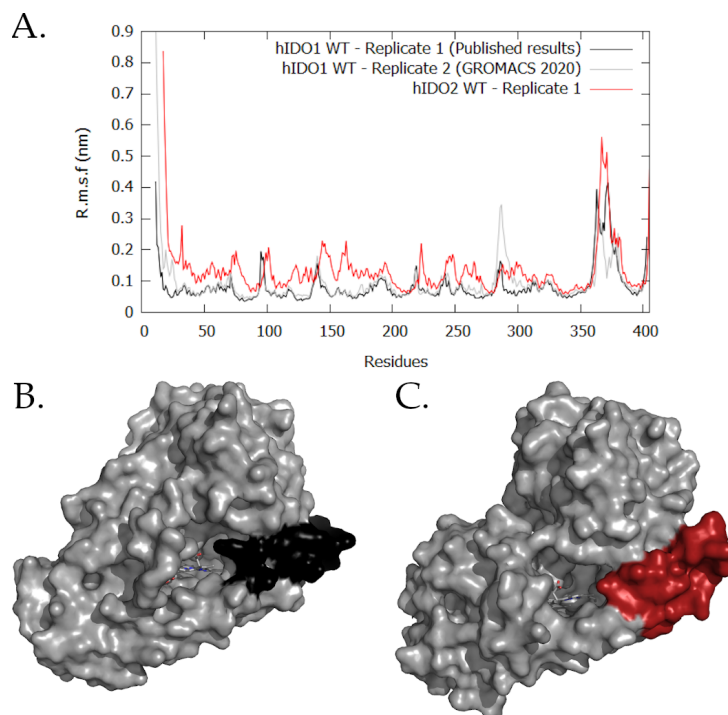


FIGURE 12.5: Comparison of the holo protein between hIDO1 and hIDO2. A. R.m.s.f profiles. B. van der Waals surface of hIDO1. C. van der Waals surface of hIDO2.

12.3.3 Study of the structural features of apo forms

The effect of removing the heme cofactor was studied on the two enzymes. For hIDO1, an opening of the dynamic loop at the C-terminal end as well as a more extended N-terminal form towards the solvent is observed. The distance between the atoms CB of A264 and NZ of K377 considerably increases to $25.5 \text{ \AA} \pm 1.3 \text{ \AA}$. This results in an increase in the number of H-bonds with water and a decrease in the number of internal H-bonds with the DE-fragment. The cofactor-free loop is also more agitated. This open conformation at both ends could then be a strategy to open the active site to accommodate a free heme from the solvent.

For hIDO2, once again, the result is contrasted with hIDO1. The flexibility of the N-terminal part of the dynamic loop tends to decrease when that of the C-terminal

part increases. They thus become almost equivalent in amplitude. The value for the C-terminal part is significantly higher than for hIDO1 (Figure 12.6, A.). The variation in conformations of the loop is small as it keeps an open conformation (distance between the atoms CB of A268 and NH1 of R380 amounts to $19.8 \text{ \AA} \pm 1.8 \text{ \AA}$ in R1, $19.2 \text{ \AA} \pm 2.9 \text{ \AA}$ in R2, $22.5 \text{ \AA} \pm 1.5 \text{ \AA}$ in R3). However, due to a global rearrangement of helices F', G' and K', the active site is closed. In this way, hIDO2 is unable to capture a free heme.

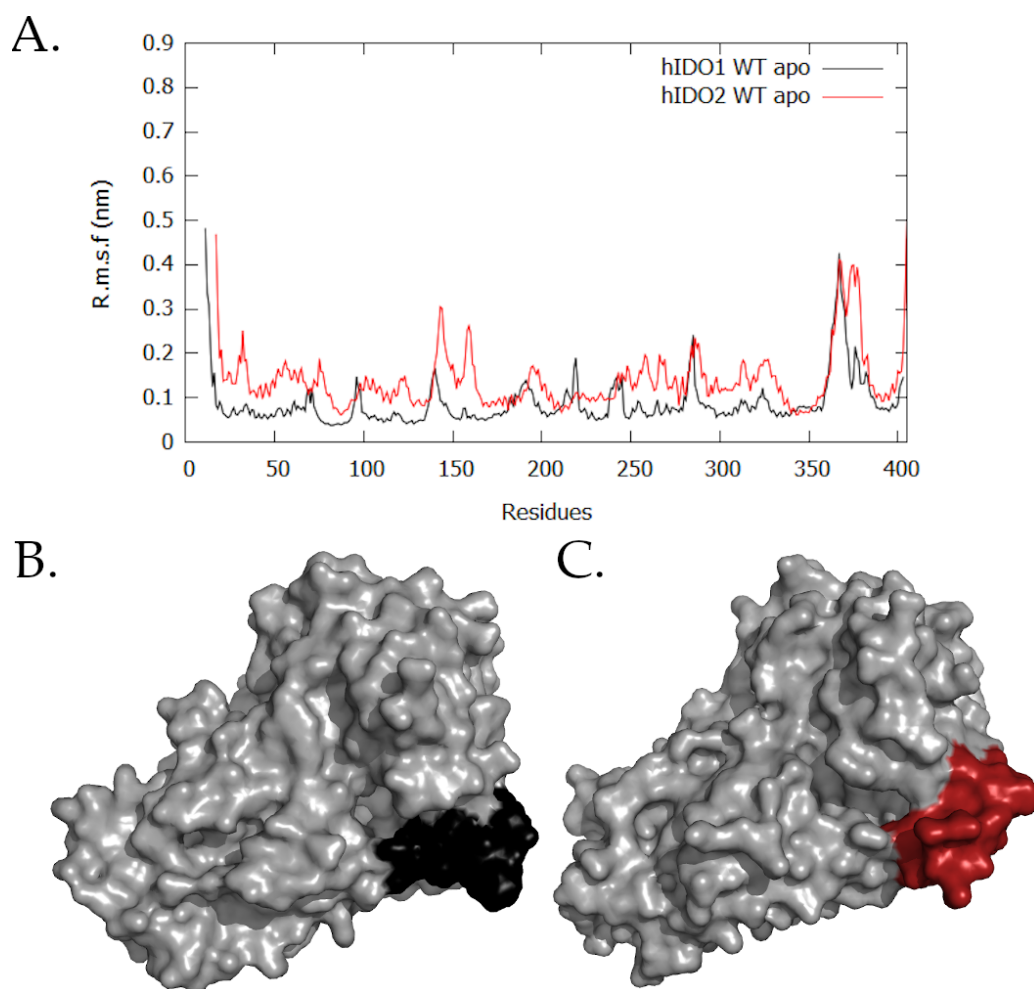


FIGURE 12.6: Comparison of the apo protein between hIDO1 and hIDO2. A. R.m.s.f. profiles. B. Van der Waals surface of hIDO1. C. Van der Waals surface of hIDO2.

The joint results of the holo and apo forms tend to indicate that while hIDO1 has a plasticity facilitating the maintenance of a heme (interaction with K377, intermediate loop structure with a globular fold) or its acceptance in the active site (open structure in the absence of heme), hIDO2 has a completely opposite action by opening its active

site in the presence of cofactor and closing it in its absence. These results may explain the poor activity of hIDO2 since if its cofactor is more labile, and the protein is not sufficient to maintain it, the reaction cannot take place. The role of hIDO2 is thus crucial in an increased lability of heme allowing potential interactions with hIDO1 through heme transfer. The polymorphic forms of hIDO2 present in the Caucasian population support this theory of increased lability for the cofactor in hIDO2 as there is a loss of cofactor coordination in the associated MD simulations.

12.3.4 Study of the structural features of L-Trp bound forms

Formally, L-Trp is the substrate of hIDO1 and hIDO2. However, it has been shown that there is almost no activity for hIDO2. This could be due to poor binding of the cofactor but also to a lack of affinity for the substrate. For this purpose, the positioning of the substrate in the two active sites was studied. For hIDO1, L-Trp could be obtained by crystallography in three distinct positions (Figure 12.7, A.). In two of them, L-Trp is in intermediate position (blue and orange) while the third one presents L-Trp in reactive position (green). The dynamic loop varies in conformation with the position of the substrate in the active site. Using a crystallographic structure with a product analogue, it was possible to reconstruct the folding mechanism of the JK-loop during the reaction. The conclusion of the study showed that the JK-loop as well as the G261-G265 fragment adapted to the arrival of the substrate by changing their conformation. To accomplish this, the G261-G265 fragment goes from conformation **I** (empty active site) to **II** (L-Trp entry into the active site) to finish in conformation **III** (L-Trp in reactive position). For the dynamic loop, the closing of the JK-loop allows the displacement of L-Trp in pocket A (or conversely, it is by moving that the ligand closes the loop). The interactions of K373 and K377 are crucial for this mechanism. Alternatively, the different conformations of the dynamic loop could be related to different values of C-terminal fluctuation, depending on the folding steps (Figure 12.7, B.). In the reactive position, the loop closes and stable. However, this motion must increase to position the ligand in comparison to the case without substrate. This flexibility is therefore essential for the completion of the reaction. In its most stable position, the ligand/protein complex has an mean interaction energy of $-327.5 \text{ kJ mol}^{-1} \pm 41.4 \text{ kJ mol}^{-1}$.

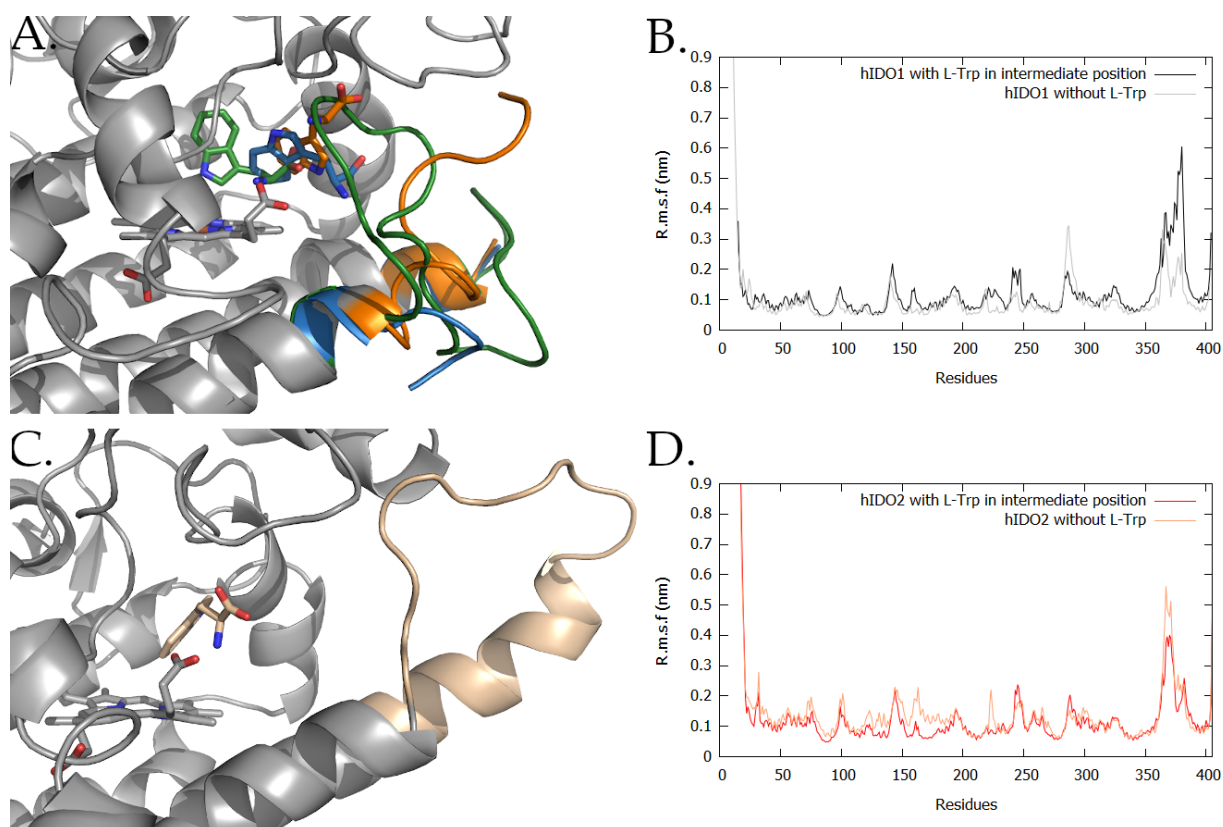


FIGURE 12.7: Comparison of the holo protein with L-Trp in the active site between hIDO1 and hIDO2. A. Position of the L-Trp observed in the three crystallographic structure and corresponding JK-loop conformation in hIDO1. B. R.m.s.f profiles of hIDO1 in presence or in absence of L-Trp in intermediate position. C. Position of the L-Trp observed in the MD simulation (300 ns) and corresponding JK-loop conformation in hIDO2. D. R.m.s.f profiles of hIDO2 in presence or in absence of L-Trp in intermediate position.

In hIDO2, it is not possible to isolate L-Trp in the reactive position by MD simulations. Indeed, it is not stable in this position and leaves the enzyme. The only stable positions are those where L-Trp is in the intermediate position, similar to the blue and orange positions of hIDO1 (Figure 12.7, C.). As a result, the ligand/protein complex has a much less negative mean interaction energy than hIDO1 with a value of $-173.9 \text{ kJ mol}^{-1} \pm 50.7 \text{ kJ mol}^{-1}$. This is, however, more stable than L-Trp in the analogous intermediate position, before displacement, in hIDO1 ($-97.3 \text{ kJ mol}^{-1} \pm 46.6 \text{ kJ mol}^{-1}$). It is difficult to justify this non-ideal binding by the residues conservation in the protein. Indeed, the active sites are conserved up to 70% between the two enzymes. [3] Only four amino acids are not conserved in this active site (Y126,

C129, F164, and S167 of hIDO1 are replaced by H130, L133, I168, and T171 for hIDO2, respectively), inducing a 15% increase in pocket size. [4] This change is not enough to explain the non-positioning of L-Trp in docking and MD. The explanation put forward could therefore come from the difference in plasticity of the two proteins. Indeed, in the dynamics of hIDO2 with L-Trp in the intermediate position, the loop is stabilized by the presence of the substrate and keeps its intermediate position (Figure 12.7, C. and D.). Conversely, for the hIDO1 homologous position, the C-terminal end was so agitated that it outperformed the ligand-free values of the N-terminal end. One hypothesis would be that the loop is too stabilized by the poorly positioned L-Trp, so it does not move to close the active site, which does not push the L-Trp into pocket A and does not lead to the conformation change of the G265-Q270 fragment. Indeed, the G265-Q270 fragment remains in type II conformation during the simulation. Moreover, since the L-Trp in intermediate position in hIDO2 is more stable in this position than that L-Trp in an analogue position in hIDO1, hIDO2 substrate remains in its local minimum. With the increased cofactor lability, this poor positioning can explain the low activity of hIDO2.

12.3.5 Study of binding sites outside the active site

With the research presented here, it was possible to investigate the presence of an exo site for the two proteins. For hIDO1, the exo site, composed of one binding pocket for the aromatic part and two binding pockets for the polar part, could then serve as a binding point for the substrate and the reaction product. It could then be brought into focus that this site could have been refined in other structures deposited in the PDB. The MD analysis indicated a possible substrate/product input/output pathway between the JK-loop and the exo site via the N-terminal part of the loop (NJK site). However, this has yet to be proven experimentally. For hIDO2, the present research did not reveal the presence of an exo site on hIDO2 with no bonding preference for L-Trp on the surface.

12.4 hIDO2 acts as a pseudo-enzyme of hIDO1

Summarizing what has been learned about hIDO1 and hIDO2, it is important to remember that both enzymes present a high degree of plasticity but that it is different between the two systems. The hIDO1 protein does everything to adapt its structure

to its cofactor or substrate/product. For this, refolding mechanisms involving the JK-loop and the G261-Q265 fragment exist. With K373 and K377, it will be possible to maintain the cofactor or ligand in the active site when the activity requires it and thus modulate the lability of the cofactor. This is consistent with the physicochemical properties measured during this thesis. Investigation of possible other binding sites highlights that hIDO1 is able to capture L-Trp in solution through its exo site. In contrast, the physicochemical characteristics of hIDO2 show a greater lability of the cofactor and a lower activity of the enzyme. It also has an ability to move more easily its equilibrium to a less folded state. This is what is observed structurally since a great plasticity of the structure is encountered. For example, the F' helix can lose its arrangement in space depending on the presence or absence of cofactor or mutation. The JK'-loop does not have the same dynamic than in its counterpart part in hIDO1. The loop has a tendency to remain globally open and not to fold. This leads to a poorer adaptation to its substrate, decreasing the activity, or its cofactor, increasing the lability of the heme. One of the essential points of this work is that the flexibility of the JK or JK' loop is essential to their folding.

In the introduction to this thesis, the hypothesis that hIDO2 is a pseudo-enzyme of hIDO1 was stated. According to this model and by the results collected during this thesis, this theory would be possible. The protein hIDO2 could, by being over-expressed, temporarily keep heme and L-Trp in its active site. The presence of L-Trp near the active site would stabilize the enzyme and prevent the substrate from being consumed. It is also interesting to note that, in their biological sequence, hIDO1 has 12 histidines while hIDO2 has 19, mostly assumed on the surface. This could then help to store free heme near hIDO2 to serve as a stock for hIDO1. Thus, with a better affinity for the substrate and the cofactor, the hIDO1 enzyme could draw on this reserve to increase its activity. A correction is made to what might be proposed in the literature: hIDO2 is not a negative regulator but its effect on the hIDO1 activity comes from the modification of the apo-holo ratio. The binding of heme could have a retarding effect on the kinetics which was seen as inhibition. More studies should be done with hIDO1 in the presence of heme and/or hIDO2 to investigate this effect.

Bibliography

- [1] Y.-K. Lee, H. B. Lee, D.-M. Shin, M. J. Kang, E. C. Yi, S. Noh, J. Lee, C. Lee, C.-K. Min, and E. Y. Choi. Heme-binding-mediated negative regulation of the tryptophan metabolic enzyme indoleamine 2, 3-dioxygenase 1 (ido1) by ido2. *Experimental & Molecular Medicine*, 46(11):e121–e121, 2014.
- [2] A. Badawy. Kynurenine pathway of tryptophan metabolism: regulatory and functional aspects. *International Journal of Tryptophan Research*, 10:1–20, 2017.
- [3] C. J. D. Austin and L. M. Rendina. Targeting key dioxygenases in tryptophan–kynurenine metabolism for immunomodulation and cancer chemotherapy. *Drug discovery today*, 20(5):609–617, 2015.
- [4] U. F. Röhrig, S. R. Majjigapu, D. Caldelari, N. Dilek, P. Reichenbach, K. Ascencao, M. Irving, G. Coukos, P. Vogel, V. Zoete, et al. 1, 2, 3-triazoles as inhibitors of indoleamine 2, 3-dioxygenase 2 (ido2). *Bioorganic & Medicinal Chemistry Letters*, 26(17):4330–4333, 2016.

Part VI

Conclusions and outlooks

*“Des expériences qui ont toutes foirées
Je n’sais pas ce qu’il y a devant
Une chose est sûre j’cours après
J’mesens plus adulte maintenant
Qu’j’ai fait d’mes rêves d’enfant une réalité.”*

Georgio - Les anges dans des robes rouges

Chapter 13

Conclusions and outlook

13.1 To conclude

This thesis has been rich in new results and discoveries. On the one hand, it was undoubtedly possible to learn more about the plasticity of hIDO1. In this way, the folding mechanism of the JK-loop could be explained for the first time. It was then possible to demonstrate that the plasticity of hIDO1 was not only represented by the JK-loop but also by the G261-G265 fragment and an exo site. For hIDO2, in spite of a non-accomplished crystallization, important information on the physico-chemical characterization of the enzyme could be brought to light for the first time. Computationally, it was possible to study the structure and dynamics of the protein in the presence or absence of its cofactor or substrate. The findings are summarized in the different sections of this chapter.

13.2 The plasticity of hIDO1

The plasticity of hIDO1 is a complex subject. In the first part of this thesis, it was possible to verify the physicochemical characterizations of the literature. Thus, it was shown that hIDO1 was a relatively stable protein with a melting temperature of 58.1 °C for the oxidized form and 62.4 °C for the reduced form. This different stability can be related to a lability of the cofactor in oxidized state, thus not serving as a scaffold for the maintenance of the protein structure as the heme is not labile for the reduced form. From an activity point of view, the protein has a K_m of 40 μM with a retro-inhibition by the substrate. Addition of hemin to the protein affects the activity but the mechanism of action is still not understood.

Once these characteristics were verified, the question was to understand how the plasticity of the enzyme helps to its biological function. To achieve this, the folding mechanism of the JK-loop was first studied. This required the collection of structural information on the positioning of the ligand in the active site. By changing the crystal packing of the protein during its crystallization, new interfaces were created which allowed to refine the dynamic loop of hIDO1 twice, with or without L-Trp in the active site. Three other structures were obtained with partially refined loop position but with L-Trp as temporary intermediate in the active site or a product analogue, L-Kynurenine.

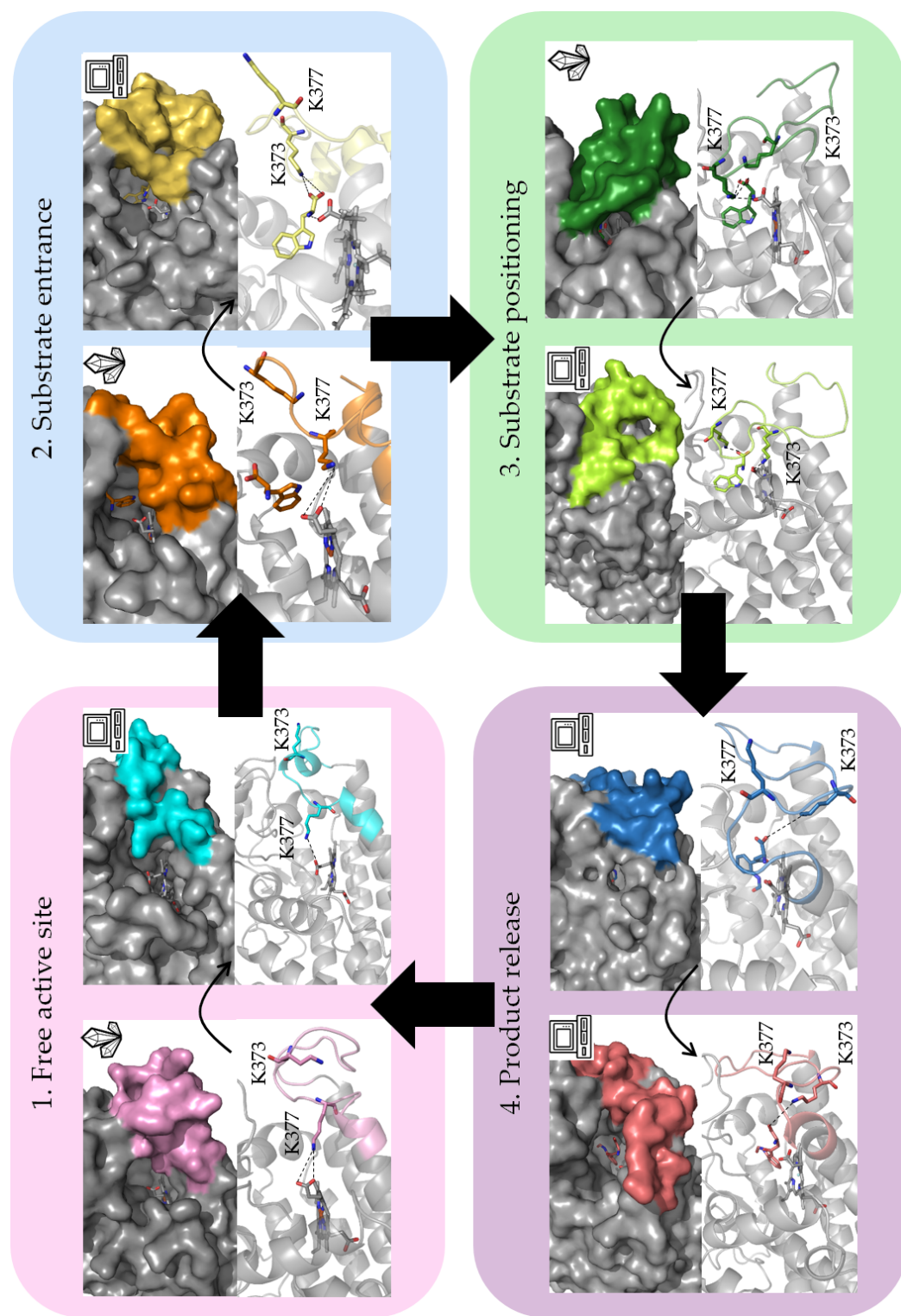


FIGURE 13.1: Final refolding mechanism for the JK-loop realized by combining the experimental (symbolized by a crystal) and MD results (symbolized by a computer).

It was possible to relate the conformational change of the C-terminus part of the loop to the positioning of the ligand in the active site. Three residues were found to be essential for ligand positioning and loop folding: K373, K377 and T379. Molecular Dynamics studies were run to complete the information on the refolding of the JK-loop and to arrive at the proposed mechanism of the Figure 13.1 involving K373 and K377. It appears from this study that the flexibility of the C-terminal part of the JK-loop is one of the phenomena allowing its closing or opening. Indeed, the intermediary steps go through an intense motion of the C-terminal part to allow its movement. Without ligand in the active site, the loop is used to keep the heme in the active site and thus regulates lability. The residues K373 and K377 do not exert the same role in this mechanism. While K373 allows to bring the substrate to the reactive position or to exit the product, K377 helps to maintain the cofactor during the substrate positioning. The importance of the F helix that interacts with T379 and closes totally the active site was also demonstrated.

Nevertheless, the plasticity of hIDO1 is not limited to the JK-loop. This thesis revealed two other plastic sites, namely the G261-G265 fragment and the exo site. This G261-G265 fragment adapts its conformation according to the occupancy of the active site. Consequently, three possible conformations exist for these residues (Figure 13.2). The first conformation (type **I**) is a so-called "S263 reverse/A264 forward" conformation obtained with ferric empty active site or with heme coordination by A264, with O₂ in the process of being positioned or "foreign" molecules not having a good affinity for the active site (glycerol, products of the kynurenine pathway, etc.). The second conformation (type **II**) presents an organization called "S263 forward/ A264 forward". In this case, the heme is never coordinated by the carbonyl of A264. This conformation is observed 1) when a substrate is entering the active site, regardless of the oxidation state (O₂ or L-Trp) 2) in the case of holo inhibitors of hIDO1 with less affinity or apo inhibitors of the enzyme. The last conformation (type **III**) is called "S263 forward/A264 reverse". This conformation is strictly observed with L-Trp in the reactive conformation or for some very affine inhibitors of the protein (Epacadostat, NLG-919, Amg-1 or MMG-0358 and analogs). This conformation is associated with an induced-fit of the fragment in order to allow the opening of the A pocket. It is possible that this plasticity, associated with the reorganization of the JK-loop, is at the origin of the positioning of the substrate in the A pocket.

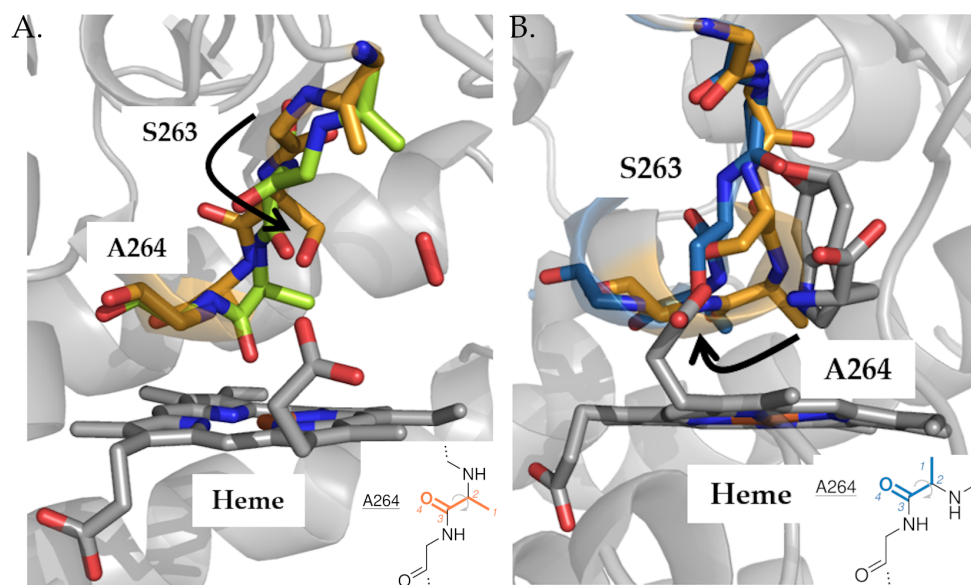


FIGURE 13.2: A. Conformation adopted by G261-G265 fragment in case of type I (in green) and II (in orange). B. Conformation adopted by G261-G265 fragment in case of type II (in orange) and III (in blue)

At last, this work leads to the localization of a *exo* site in hIDO1, consistent with experimental evidence of its existence. This site is located at the level of the small subunit, near amino acids R100, D94, E56 and G53. It is composed of a binding pocket for the apolar part (pocket I) and two possible pockets for the polar part (pockets II and III). The occupancy of these two pockets differs according to the monomers studied. As the role of the *exo* site is still unknown, Molecular Dynamics studies were performed to try to understand this latter. It would appear that it may be involved in a pathway to bring the substrate to the active site or bring out the product. Taken together, the flexibility of the JK-loop, the G261-G265 fragment adaptation, and the *exo* site points to the importance of protein plasticity to perform the reaction. The hIDO1 protein is a protein that adapts to its ligand or cofactor by slightly changing its conformations in order to stabilize the ligands.

13.3 The plasticity of hIDO2

For the hIDO2 protein, physico-chemical characterization was an essential step in view of the almost complete absence of information on the enzyme in the literature. This characterization highlighted the increased lability of the heme cofactor in the enzyme as well as its lower affinity for the cofactor in comparison to hIDO1. This

lability, unlike for hIDO1, exists for the reduced and the oxidized form. That results in the same stability for both forms. The studied protein is active but the activity is really low. These differences in term of lability and activity intrigue and raise questions about the structural differences of hIDO2 compared to hIDO1. To answers to these questions, crystallization assays were performed, without success. Consequently, the fundamental deep study was performed using the Molecular Dynamic and the biological modeling.

Since homology modeling does not sufficiently account for the dynamics present in hIDO2, MD simulations were performed (Figure 13.3, A.). Multiple parts present flexibility in hIDO2: the JK'-loop but also the helix F' and the fragment G265-Q270. The helices G', I' and K' can be impacted by the conformation of these parts. This results in a general plasticity of the protein, being able to adapt the size of its active site according to the presence of heme, L-Trp or mutations. Compared to hIDO1, the F' helix is shortened and its flexibility could be related to high lability of the cofactor in the protein. The helix can unfold or fold, influencing the size of the cofactor binding pocket. During the simulation, the heme cofactor moves in its pocket and H347 is not oriented to interact with the iron. Concerning the JK'-loop, the loop is longer in hIDO2 and presents an alternation of polar and no polar residues. The flexibility of the loop is different in hIDO2 since the fluctuation of the residues is quite high but is little influenced by the presence or not of cofactor or mutation (Figure 13.3, A., II.). Mainly, the loop adopts a open conformation. The absence of cofactor leads to a closure of the active site by a concerted move of helices F', G' and I' that do not allow the incorporation of a new free heme. The existing polymorphs of hIDO2 present a exacerbated lability of the cofactor, which one try to exit the protein. For example, in R235W polymorph, a contraction of the active site is observed due to the movement of F' helix and G265-Q270 fragment (Figure 13.3, A., III.). The residues K287, R295 and R380 bring the cofactor outside the enzyme.

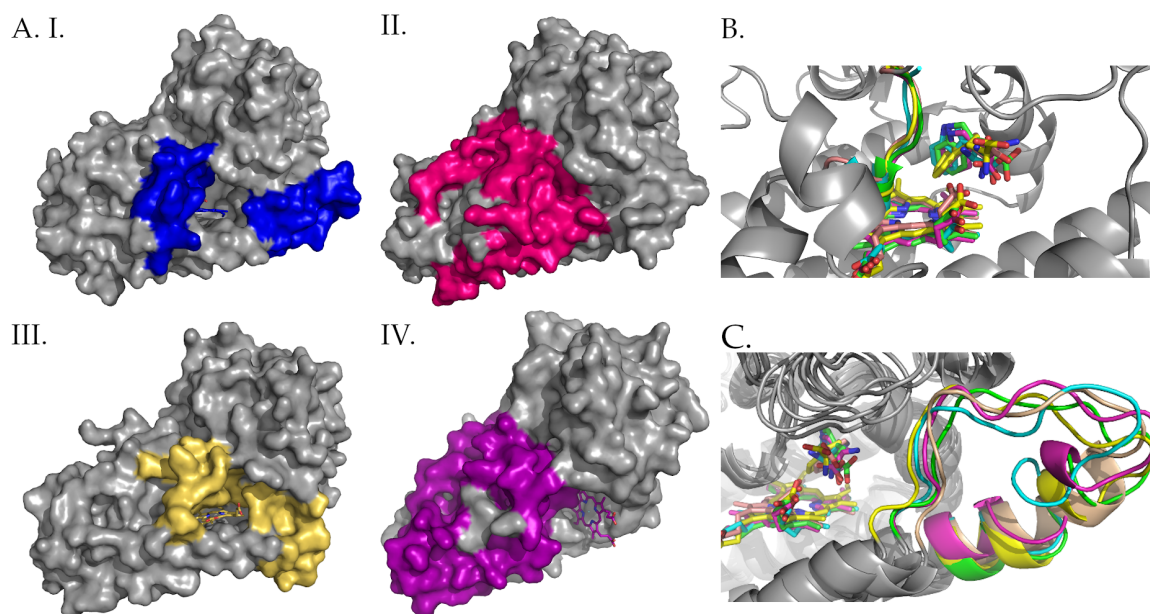


FIGURE 13.3: A. Summary of the van der Waals surface adopted for the hIDO2 protein studied during the thesis (I. = holo protein, II. apo protein, III. R235W polymorph, IV. H346X polymorph). Flexible parts are highlighted in colors. B. Conformation adopted by L-Trp in the active site and C. Related conformation for the JK'-loop.

The G265-Q270 fragment is able to adopt different conformations like in hIDO1 (type I, II or III). However, these will be less fixed. For the holo protein, type II or III conformations are observed and all conformations are observed for the apo protein. Polymorph R235W presents a type III conformation while polymorph Y346X adopts a type I conformation. The great flexibility of this fragment is mainly used to move forward or not in the active site in order to close, or not, the heme binding pocket. Simulations with L-Trp highlight the difficulties to position the substrate in the active site. To prove that, L-Trp was docked in the active site of hIDO2 and, after that, subjected to a 300 ns MD simulation. The substrate adopts an intermediate position in pocket B even if the pocket A is open (Figure 13.3, B.). In the presence of a substrate in such a position, the G265-Q270 fragment adopts a type II conformation. The JK'-loop remains in intermediate position with a stable conformation at the C-terminal extremity, which does not allow its refolding and the closure of the active site (Figure 13.3, C.). For the protein, the high lability of the cofactor in addition to the difficulty to position the substrate can explain the low activity. As polymorphs exist in 50% of the Caucasian population, having a protein hIDO2 with exacerbated cofactor lability could be an evolutionary advantage.

13.4 Comparison of the plasticity for hIDO1 and hIDO2

In terms of the thesis, it is clear that both enzymes present a high degree of plasticity. The JK/JK'-loops and the G261-G265/G265-Q270 fragments are two common plastic parts. In addition, hIDO1 presents an exo site while hIDO2 owns a flexible F' helix. The roles of this plasticity change in the two systems. While hIDO1 adapts its structure to bind its cofactor or substrate/product through G261-G265 fragment reorganization and JK-loop closure, hIDO2 is not designed to bind its cofactor or substrate easily due to a large flexibility of F' helix and G265-Q270 fragment. Moreover, the increase of the JK-loop motion during the substrate entrance in hIDO1 allows to refold the loop and position the substrate whereas the JK'-loop remains open and stable in presence of L-Trp intermediate in hIDO2. Modulating the flexibility of these loops could then be an inhibition strategy in drug design. The theory that hIDO2 is a pseudo-enzyme of hIDO1 could then be possible since hIDO2, by being overexpressed, could serve as a heme or L-Trp stock for hIDO1 which has more affinity for the cofactor or substrate.

13.5 What to do in terms of prospects?

Several perspectives can be considered with the results of this thesis. A first, more general perspective, is the reparameterization of the CHARMM27 force field in a short-term perspective for the heme cofactor. Indeed, as the lability appears to be a redox-dependent phenomenon, it could be interesting to perform the simulations with a force field containing a ferric heme to see the effect on hIDO1 and hIDO2. The help of quantum chemistry will be important for this in order to be able to recalculate the charges, distances and angles on the different atoms during the reparameterization. Making quantum calculations of the energy would allow to investigate further the transition mechanism from the apo to the holo state for both proteins. However, preliminary results show the importance of a high level of description of the system (more than one heme and one histidine analogue) to have values closer to the protein reality. Indeed, if the system is too simple, there is not even a stabilizing binding energy of the two partners.

For hIDO1, perspectives are divided into two parts: 1) to investigate the role of K373 and K377 2) to better understand the role of the exo site. The first outlook, to

understand the role of K373 and K377, could be achieved with a multidisciplinary approach. From an experimental point of view, K373 and K377 mutants as well as double mutants could be made to see the impact on the stability, cofactor lability or activity of the enzyme. This has already been done for K377 and was able to show an effect on cofactor lability. However, the latter was not significant, which could indicate the importance of other partners in lability, such as K373. A T379 mutant or triple mutant could also be interesting to investigate the combined effect of K373, K377 and T379. From a computational point of view, K373A/K377A mutant models or with modifications of the dynamic loop structure, especially by deleting the lysines K373 and K377, could be studied. This has been done preliminary using Maestro and shows an effect on the affinity of the heme for the protein. It could be interesting to make further calculations with a ferric and ferrous force field. This research would complement the current research in order to, in the final perspective, allow the design of drugs based on altering the motion of the JK-loop or the interaction with K373 and K377 to prevent its folding. The second objective would be to investigate the exo site to provide more information on its role and to see if it could serve as an action point for future inhibitors. This could be done first with mutants of the central amino acids of pockets I, II and III to see the effect of mutation on the physicochemical properties of the enzyme. From a more general point of view, it could be interesting to implement time resolved serial femtosecond crystallography measurements for the study of hIDO1 plasticity. This technique requiring free electron lasers is a powerful technique to study the reactions and the structural changes of a protein, by crystallography, without radiation damage and at room temperature.

Concerning the hIDO2 protein, it would be really interesting to have an idea of the veracity of the computational models. As the lack of conservation of the crystal interfaces could be the cause of the non-crystallization of hIDO2, tests with a crystallophore could be a first prespective in the short term. In this perspective, the "Polyvalan Crystallophore number 1" [1] is a terbium-based crystallophore known to help the formation of crystalline interface. It is also a tool of choice because it allows experimental phasing of structures. Lastly, it would allow to determine if the observed crystals are protein crystals even before the synchrotron analysis since the latter is a luminescent compound. The observation of drops is thus a simple preliminary tool of determination. Under the 584 commercial screen conditions tested, this compound does not precipitate or self-crystallize, thus avoiding false positives. However, due

to the price of the material, its use requires the use of a crystallization robot. A domain crystallization approach or by binding hIDO2 to a fusion protein could also be considered. If it passes by techniques that do not require the crystallization of the protein, the perspectives could be to either 1) go through a SAXS analysis 2) bind the hIDO2 protein to a larger molecule (like antibodies) in order to increase the size and to allow a Cryo-EM analysis of the system.

13.6 The final words

This thesis has made progress in the research on hIDO1 and hIDO2 in terms of understanding their plasticity. Methodologically, the multidisciplinary approach used has proven its strength and can be transferred to other projects. Taken together, the prospects for hIDO1 and hIDO2 could complete this work and help to understand the underlying apo/holo transition mechanisms of hIDO1 and hIDO2 as well as their complementarity in order to create effective inhibitors for these two systems.

Bibliography

- [1] S. Engilberge, T. Wagner, G. Santoni, C. Breyton, S. Shima, B. Franzetti, F. Riobé, O. Maury, and E. Girard. Protein crystal structure determination with the crystallophore, a nucleating and phasing agent. *Journal of Applied Crystallography*, 52(4):722–731, 2019.

Part VII

Appendices

Appendix A

Materials and methods

A.1 Introduction

During the thesis, several protocols had to be established and optimized in order to obtain the results mentioned in this manuscript. This appendix presents all these protocols in their most efficient version.

A.2 Proteins production and purification

The production of the proteins of interest and their different mutants was carried out during the thesis in the Research Unit in Microorganism Biology (URBM). The detailed production and purification protocols can also be found in the different articles mentioned in this thesis. [1, 2] For the rest of the appendix, it is important to have in mind the molecular weight values and the molar extinction coefficient of the two proteins. These values are shown in Table A.1.

TABLE A.1: Molecular weight and extinction coefficient at 280 nm of hIDO1 and hIDO2 calculated according ProtParam software. [3]

Protein	Construction	Molecular weight (kDa)	Extinction coefficient if cys are oxidized	Extinction coefficient if cys are reduced
hIDO1	Nterm	45.24	45880	45380
hIDO2	Nterm full	47.59	42860	42985
hIDO2	Nterm cleaved	45.70	42860	42985

A.2.1 Production of hIDO1 in a holo form

The production of hIDO1 WT¹ was made from *E. coli* BL21 DE3 bacteria transformed with a pET-28a plasmid provided by Tong *et al.* [4] containing the sequence coding for the interest protein with an N-terminal histag.² This protein sequence contains two surface mutations (K116A, K117A) to improve the crystallization. The production was

¹The production of hIDO1 mutants (K377X) was done in an identical manner, without any protocol modification.

²The sequence used is as follows: MGSSHHHHHH SSGSAAYHID EEVGFALPNP QENLPDFYND WMFIAKHLPD LIESGQLRER VEKLNMLSID HLTDHKSQRL ARLVLGCITM AYVWVGKGHGD VRKVLPRNIA VPYCQLSAAL ELPPILVYAD CVLANWKKKD PNKPLTYENM DVLFSFRDGD CSKGFFLVSL LVEIAAASAI KVIPTVFKAM QMQRDTLLK ALLEIASCLE KALQVFHQIH DHVNPKAFFS VLRIYLSGWK GNPQLSDGLV YEGFWEDPKE FAGGSAGQSS VFQCFDVLG IQQTAGGGHA AQFLQDMRRY MPPAHRNFLC SLESNPSVRE FVLSKGDAGL REAYDACVKA LVSLRSYHLQ IVTKYILIPA SQPKENKTS EDPSKLEAKG TGGTDLMNFL KTVRSTTEKS LLKEG

launched in liquid LB with Kanamycin as antibiotic. The growth of bacteria was performed at 37 °C to reach an optical density of 0.6. The protein was induced with a T7 polymerase induction system activated by the addition of IPTG (0.4 mM in final concentration). The cofactor was introduced during induction using the heme precursor, the δ -aminolevulinic acid (0.75 mM in final concentration). The induction occurred at 20 °C overnight. After production, the bacteria were pelleted by centrifugation on Beckmann centrifuge at 4500 rpm and stored at -20 °C pending purification.

Prior protein purification, the bacterial pellets were lysed by sonication, under ice, at a power of 20 Watts. The lysate was then filtered and loaded onto a His-trap column. The purification buffer and the lysis buffer were composed of 50 mM Tris, 200 mM NaCl, 5% glycerol supplemented with imidazole. At the beginning of the purification, an imidazole concentration of 20 mM (buffer A) was used. That allows the elution of the flow through (the 50 first minutes at Figure A.1). After the elution of the flow through, a gradient in buffer B (500 mM in imidazole) was necessary to elute the protein. The protein eluted at 30% in buffer B (around 90 and 110 minutes, at Figure A.1). The elution peak can be separated into two peak parts. Based on an analysis by SDS-page gels (Fig. A.1, (b)), only the second part was retained because the first one comes out with a lot of impurities for few hIDO1 protein.

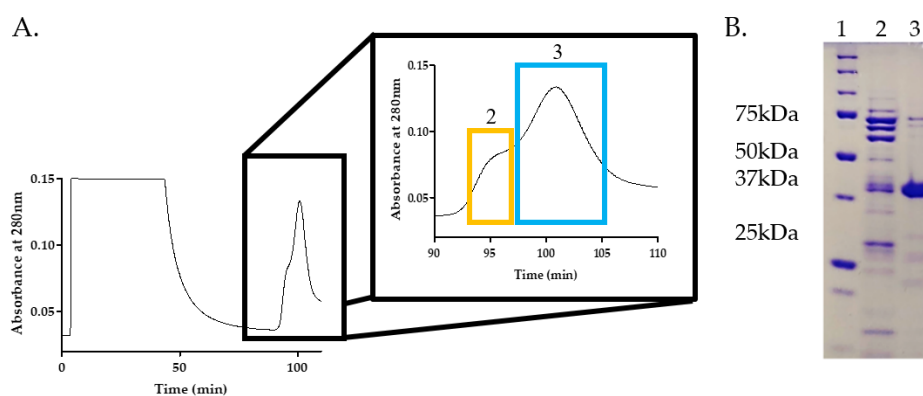


FIGURE A.1: IMAC purification of hIDO1 A. Chromatogram from IMAC purification of hIDO1. Zoom on the outgoing peak during the gradient in buffer B. B. SDS-PAGE analysis of the fractions collected during the purification. 1 = Ladder; 2 = first part of the peak; 3 = second part of the peak.

This second part of the peak allowed to obtain, without cleavage, a protein with sufficient purity, homogeneity and stability for the characterizations. The collected fraction presented a red color and contained around 15 mg of protein for three liters of culture. After purification, a buffer exchange was performed as different buffers were used depending on the analysis:

- Buffer C : 5 mM HEPES at pH = 6.5, 200 mM NaCl and 5 mM DTT. This buffer is used for the crystallization assays.
- Buffer D : 50 mM Tris at pH = 6.5. This buffer is used for characterization of the activity.
- Buffer D + DTT : 50 mM TRIS at pH = 6.5 and 5 mM DTT. This buffer is used for characterization of the stability.
- Buffer E : 50 mM KH_2PO_4 at pH = 7.5, 100 mM NaCl and 20% of glycerol. This buffer is used for characterization of the stability.
- Buffer E + DTT : 50 mM KH_2PO_4 at pH = 7.5, 100 mM NaCl, 20% of glycerol and 5 mM DTT. This buffer is used for characterization of the stability.

A.2.2 Production of hIDO1 in an apo form

In order to produce the apo form of hIDO1, several protocols were tested and optimized. The most efficient in terms of yield was to produce the protein in holo form and then removed the cofactor rather than to make a production without δ -aminolevulinic acid. Consequently, the production and the purification started with a standard production of the protein, in the presence of 0.4 mM of IPTG and 0.75 mM of δ -aminolevulinic acid. The resulting pellets were then lysed and purified with a first IMAC, as described in the previous section. After the first IMAC, pure holo hIDO1 was dialyzed overnight, at 6 °C, in the presence of apo-myoglobin under stoichiometric conditions. As apo-myoglobin had a better affinity for the heme cofactor, it allowed to remove the remaining heme bound to hIDO1. Subsequently, the hIDO1 apo protein was harvested by a second IMAC in the same way as IMAC1. During this IMAC2, myoglobin eluted in flow through while hIDO1 apo eluted around 30% in buffer B. The harvested fractions were almost colorless and, after exchange in buffer D, presented an absorbance ratio lower than 0.5.

A.2.3 Production of hIDO2 in a holo form

Production of hIDO2 WT³ was performed from *E. coli* BL21 DE3 bacteria transformed with a pET-28a plasmid, ordered from GenScript. The plasmid presented the gene coding for the protein of interest with a poly-histidine tail in N-terminal⁴ and a kanamycin resistance gene. Since it is possible to find two probable sequences for hIDO2 on UniProt [5] (there are two possible methionine starts at positions 1 and 14), in the present work, the so-called "active" form is used by starting the sequence with methionine 14.⁵ Bacterial growth was performed in a liquid LB medium until a turbidity of 0.6 was reached. Once this value was observed, protein induction was started by adding 1.0 mM of IPTG. In order to produce also the heme cofactor, 0.75 mM of aminolevulinic acid was added to the mixture at this time. The induction was then performed overnight under stirring at 20 °C. The next day, the bacterial pellets were collected at 4500 rpm on a Beckmann centrifuge. They were stored at –20 °C before purification.

In order to isolate the protein of interest, an IMAC purification was performed based on the affinity of the protein for the column by the presence of an N-terminal tail. For this purpose, bacterial lysis was performed by sonication, on ice and at 20Watts, in a buffer composed of 50 mM TRIS, 300 mM NaCl and 5% glycerol supplemented with 10 mM of imidazole (buffer A). After lysis, the lysate was loaded on His-Trap column in the same buffer as the lysis buffer. The elution of the flow through protein (peak 1, Figure A.2), which contains all of the proteins not bound to the column, was observed. After this elution, the imidazole concentration was increased with 15% with a second buffer (buffer B corresponding to the same concentration in TRIS, NaCl and glycerol than buffer A but with 250 mM in imidazole). The resulting concentration was 47.5 mM of imidazole and allowed the removal of impurity having

³The productions of hIDO2 with a truncated construction or with mutants were done in an identical manner, without any protocol modification.

⁴The construction with a poly-histidine tail at the C-terminal position did not result in the expression of the protein in stable form. The position of the tag is therefore essential in this type of system.

⁵The sequence used is as follows: MGSSHHHHHHH SGLVPRGSH MEPHRPNVKT AVPLSLESYH ISEYGFLLP DSLKELPDHY RPWMEIANKL PQLIDAHQLQ AHVDKMPLLS CQFLKGHREQ RLAHLVLSFL TMGYVWQEGE AQPAEVLPRN LALPFVEVSR NLGLPPILVH SDLVLTNWTK KDPDGFLEIG NLETIISFPG GESLHGFILV TALVEKEAVP GIKALVQATN AILQPNQEAL LQALQRLRLS IQDITKTLGQ MHDYVDPDIF YAGIRIFLSG WKDNPAMPAG LMYEGVSQEP LKYSGGSAAQ STVLHAFDEF LGIRHSKESG DFLYRMRDYM PPSHKAFIED IHSAPSLRDY ILSSGQDHLL TAYNQCVQAL AELRSYHITM VTKYLITAAA KAKHGKPNHL PGPPQALKDR GTGGTAVMSF LKSVRDKTLE SILHPRG

a low affinity for the column (peak 2, Figure A.2). Finally, in order to recover the protein of interest, the imidazole concentration was gradually increased up to 250 mM. A jump in absorbance was observable at 80% in buffer B before the main peak (peak 3, Figure A.2). The majority of the protein hIDO2 eluted at 100% in buffer B (peak 4, Figure A.2). The purity of the different fractions could be checked on SDS-PAGE gel (Figure A.2, B.). The fraction with 15% and 80% of buffer B contained a small quantity of hIDO2 in addition to impurity. This was similar to a poorly folded protein, having a lower affinity for the column. For the rest of the characterization, fraction at 100% in buffer B (VII) is used.

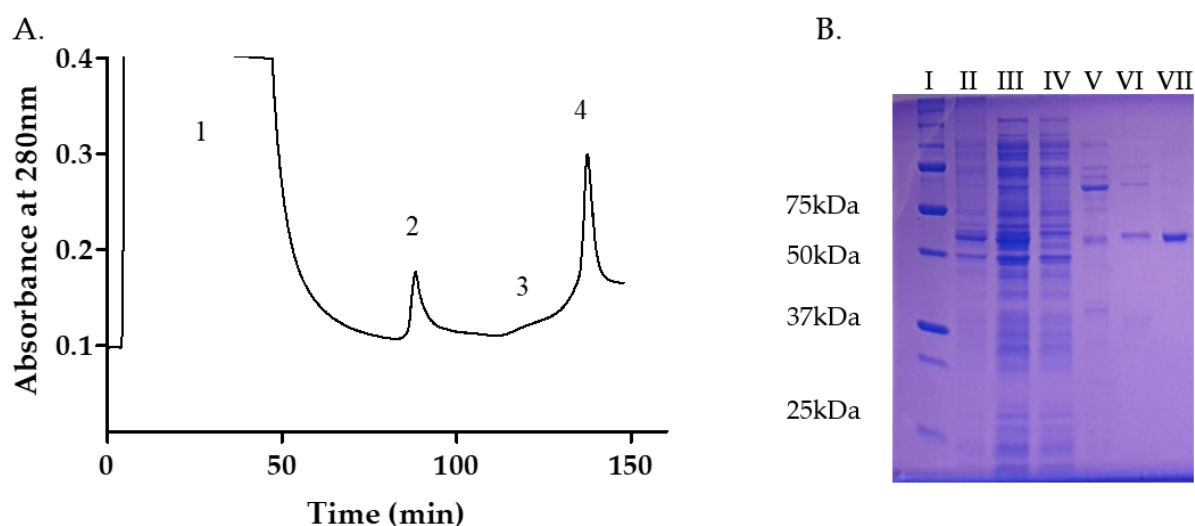


FIGURE A.2: IMAC purification of hIDO2 A. Chromatogram from IMAC1 purification of hIDO2. B. SDS-PAGE analysis of the fractions collected during the purification. I: Ladder, II bacterial pellet, III: lysate, IV: Flow-Through, V: peak at 15% in buffer B, VI: sight peak at 80% in buffer B, VII: Major peak at 100% in buffer B.

During the optimization of the crystallization conditions for hIDO2, thrombin cleavage was performed. This also required optimization of the cleavage protocol. In the designated sequence of hIDO2, between the poly-histidine tail and the protein, a thrombin-specific cleavage sequence is present (LVPR|GS). In order to remove the tag, 15 units of thrombin per milligram of protein were thus left in contact with pure hIDO2 overnight, after fractionation in eppendorfs of 1 mL. The following day, fractions were pooled together and a second IMAC purification was then performed to

separate the thrombin from the protein of interest. After loading the sample, the purification was performed using buffer A until the thrombin exited the column (Figure A.3, A.). Then, an imidazole gradient was introduced (final concentration: 250 mM in imidazole) until the elution of the studied protein. The elution of cleaved hIDO2 at a concentration of 85 mM in imidazole was observed. This was explained by the presence of histidine clusters on the surface of hIDO2 (20 histidines residues in the cleaved sequence), allowing an affinity for the column. The protein obtained after IMAC1 and after cleavage was pure according to SDS-PAGE analysis (Figure A.3, B.). The efficiency of hIDO2 cleavage was verified by Western-Blot with an anti-his antibody (Figure A.3, C.).

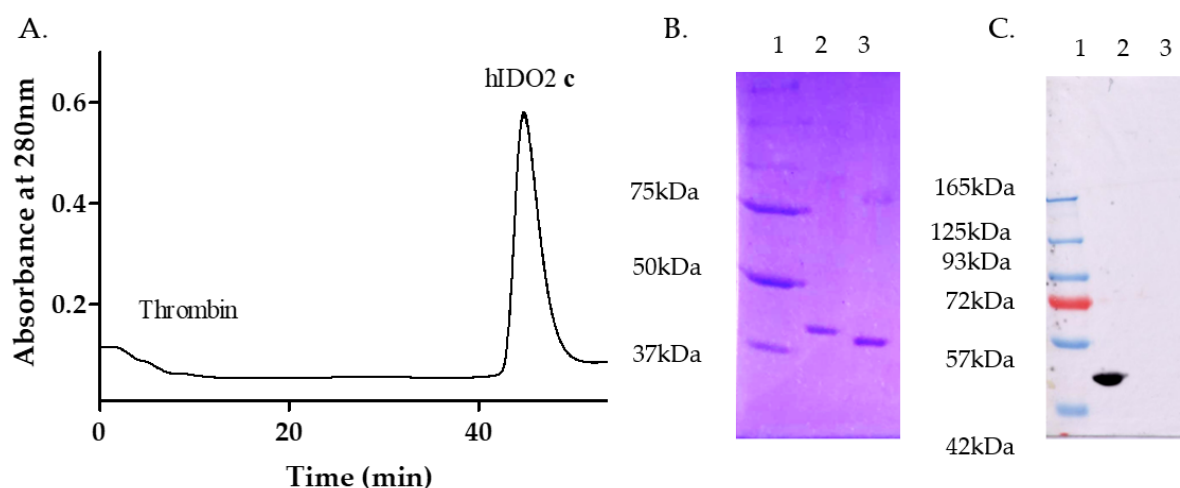


FIGURE A.3: IMAC2 purification of hIDO2 A. Chromatogram from IMAC2 purification of hIDO2. B. SDS-PAGE analysis of the fractions collected during the purification. 1: Ladder, 2: full hIDO2, 3: cleaved hIDO2. C. Western-blot analysis with anti-his antibody of hIDO2 before and after cleavage. 1: Ladder, 2: full hIDO2, 3: cleaved hIDO2.

A.2.4 Production of hIDO2 in an apo form

The production of the apo form of hIDO2 was achieved simply at a higher induction temperature compared to the holo form (between 20 °C and 25 °C). In these conditions, the protein obtained incorporated almost no cofactor. The stability and activity tests having validated the folding of the protein, this protein could be used for the lability tests.

A.3 Characterization of the cofactor incorporation

In order to study the incorporation of the heme cofactor in the two proteins, UV-Visible spectra were performed using the NanoDrop 2000 from Thermo Scientific. Molecular weights and extinction coefficients used for the two proteins were extracted from ProtParam and listed in the Table A.1. During the measurement, the absorbance spectrum of the incorporated protein was measured between 250 nm and 600 nm. The absorbance value of the Soret peak, characteristic of hemoproteins and located at a maximum absorbance value near 400 nm, gives access to the ratio of cofactor absorbance by Equation A.1.

$$A_i = \frac{A(\lambda_{max:400-450nm})}{A(280nm)} \quad (A.1)$$

The lability study was performed in a similar manner but at 25 °C. For this purpose, protein aliquots with a final concentration of 25 µM were prepared with different heme cofactor concentrations. The protein was then added just before the first measurement. The blank was made with an aliquot of the same cofactor concentration, where the protein was replaced by an equivalent volume of buffer E. The protein and the blank aliquots were incubated with a heating bench for eppendorfs. The absorbance spectra of each solution were measured every 15min. The results were processed and visualized with Microsoft Excel and GraphPad [6] softwares.

A.4 Characterization of the stability

To assess the stability of hIDO1 and hIDO2, Differential Scanning Fluorimetry (DSF) analyses using nanoDSF form NanoTemper™ were performed. The protein samples were studied at a initial concentration, verified at the NanoDrop, of 1.0 mg mL⁻¹. The studied additives were prepared in stock solutions, stored at -20 °C, with the following concentrations: 600 µM of hemin, 40 mM of L-Trp and 0.1 M of K₃Fe(CN)₆. On ice, test aliquots were prepared with 48 µL of the protein solution supplemented with a variable volume of additive to test different concentrations. The volume was adjusted to 60 µL by adding the buffer in which the protein solution was located. Each 60 µL test aliquot was used to make three technical replicates for measurement.

Each replica was analyzed with an individual capillary of 10 μL . The temperature of the system then increased from 35 $^{\circ}\text{C}$ to 95 $^{\circ}\text{C}$ with a heating rate of 0.1 $^{\circ}\text{C min}^{-1}$ – 7 $^{\circ}\text{C min}^{-1}$. The accuracy of the temperature was about $\pm 1^{\circ}\text{C}$. During the experiment, LED light at an excitation wavelength of 280nm was applied to the individual capillary and fluorescence signals at 330nm and 350nm were recorded.

A.5 Characterization of the activity

The activity of hIDO1 and hIDO2 was tested by monitoring the production of N-formyl-kynurenine over time at 321 nm. For this purpose, a SpectraMaxTM equipment was used. The study was carried out on a 96-well plate adapted to the UV reading. Each well was filled with 220 nM of protein of interest (2 μL of hIDO1 1 mg mL^{-1} in Buffer D or 2 μL of hIDO2 1 mg mL^{-1} in Buffer E), supplemented with 250 nM of catalase (0.6 μL). The volume was adjusted to 80 μL by a 100 mM phosphate buffer with a pH depending on the protein studied to ensure maximum activity. For hIDO1, the pH was 6.5 while for hIDO2 it was 7.5. In the first part of the enzyme assay, a mixture of ascorbic acid and methylene blue (20 mM and 10 μM respectively, final concentrations of 8 mM and 4 μM respectively) was added to each well to reduce the protein. An incubation time of 6 minutes was observed before the addition of 40 μL of the protein substrate, L-Trp, at varying concentrations. The final concentration ranges studied for hIDO1 were from 5 μM to 240 μM in final concentrations while the hIDO2 studies were concerned with final concentrations in substrate from 100 μM to 8 mM. NFK production was then monitored at 321 nm. The slopes obtained under linear velocity conditions were processed by GraphPad [6] to obtain the Michaelis-Merten curves.

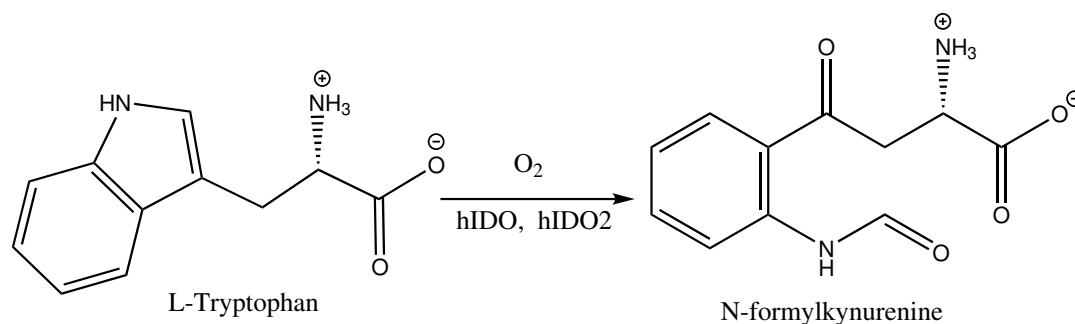


FIGURE A.4: Enzymatic reaction catalyzed by hIDO1 and, to a lesser extent, by hIDO2. The formation of NFK is followed at 321 nm.

A.6 Characterization of the structure by crystallography

The crystallization assays for hIDO1 and hIDO2 proteins required careful optimization of the different protocols. Therefore, in this section, the hIDO1 crystallization and co-crystallization protocols as well as the hIDO2 crystallization assay protocols are detailed separately. The rest of the section also details the data processing protocols, after collection at the Soleil synchrotron. The tables of crystallization data are the object of another appendix (Appendix E). All figures were generated using PyMOL (version 0.99; Schrodinger) or Maestro for the interaction maps. [7]

A.6.1 Crystallization assay of hIDO1

After exchanged into a crystallization buffer containing 5 mM of HEPES/NaOH pH 7.6, 200 mM NaCl and 5 mM DTT, the protein was concentrated using amicon with a 10 kDa molecular-weight cutoff membrane to reach a concentration of 16 mg/ml. Crystallization assays were carried out with the hanging-drop vapor-diffusion method at 293 K. The wells contained a solution made of 14% of polyethylene glycol 3350 and 0.1 M in $\text{KH}_2\text{PO}_4/\text{NaOH}$ buffer at a pH of 6.25. Drops were made with 1 μL of the well solution and 1 μL of the protein solution. Red crystals appeared within one day. Before data collection, crystals were soaked for 2 min with the well solution supplemented with a cryo-solution at a final concentration of 20% of glycerol and 20 mM of sodium dithionite. Sodium dithionite allowed the reduction of the heme iron into the ferrous state. Subsequently, the crystals were flash-cooled in liquid nitrogen.

A.6.2 Co-crystallization assays of hIDO1

Before proceeding to co-crystallization assays, the reduced protein (in buffer C) was incubated on ice with L-Trp or L-kynurenine at a final concentration of 2 mM for, at least, 15 minutes. After incubation, using the hanging-drop vapor diffusion method at 293 K, drops were made with 1 μL of the well solution and 1 μL of the protein/L-Trp solution. The wells contained a solution consisting of 14-15% polyethylene glycol 3350, 0.1 M $\text{KH}_2\text{PO}_4/\text{NaOH}$ at pH 6.25-6.50. The red crystals appeared in one day and were left for at least two weeks before the diffraction experiment and data collection. Prior data collection, crystals were soaked for at maximum 2 min in well solution supplemented with a cryo-solution at a final concentration of 20% glycerol and 20 mM sodium dithionite. The crystals were subsequently flash-cooled in liquid nitrogen.

A.6.3 Crystallization screenings of hIDO2

Investigations of the crystallization conditions of hIDO2 were conducted using commercially available screening kits on Molecular Dimension (PACT, JCSG+ and the BCS screen). [8, 9] In parallel, the crystallization conditions of hIDO1 were also tested on hIDO2. The crystallization study of hIDO2 was conducted using full or cleaved proteins, with or without truncations, at a concentration of 18 mg mL^{-1} . Each protein was then tested in buffer E, with or without DTT, to assess the crystallizability of both redox forms of the cofactor. Additive addition was also studied by adding excess hemin to the sample (1.0 mM), prior to crystallization tests.

A.6.4 X-ray collection and model refinement of hIDO1

The resources of the SOLEIL synchrotron (Gif-sur-Yvette, France) allowed the collection of data on the PROXIMA-1 (PX1) or PROXIMA-2 (PX2) beamlines using a DECTRIC EIGER X 16M detector at 100K and at a single wavelength of 0.980 \AA . Data indexation was performed with XDS suite. [10] Molecular replacement using Phaser [11] solved the phase problem in each data set. For the structure 7a62, the structure was solved by molecular replacement with a monomer from the PDB entry 6e43 as the model. [4] For the structure 7nge, 7p0n and 7p0r, monomer C from 7a62 structure was used as model for the replacement. At last, the molecular replacement in 7yxt and 7z2l structure was based on monomer A form 7nge structure.

Model building and structure refinement were performed using Coot [12] and Phenix. [13] For the structure 7a62, the refinement was performed under NCS restraint on torsion-angles. In this case, anisotropy in the data was removed using the extension Morph model on Phenix. [14] The heme cofactor, L-Trp, NFK or L-kynurenine molecules were added to the monomers using eLBOW. [15] For structures 7nge, 7p0n and 7p0r, crystallographic maps (2Fo-Fc) are cut around the L-Trp using adequate Phenix module and a model cut method. [13] In the case of structure with L-Kynurenine, crystallographic maps (2Fo-Fc) are defined with the Polder Map module. [13] The cavity volumes in the active site were calculated using the POCASA 1.1 server with a grid of 1 \AA and a probe radius of 1.0 \AA .

A.7 Characterization by computational study

The characterization of the two therapeutic targets by computational methods was based on the different analyses performed by Maestro. This includes docking, homology modeling, binding site analysis and MM-GBSA analysis.

A.7.1 Analyses using MM-GBSA calculation of hIDO1

In order to evaluate the affinity of L-Trp and the heme cofactor depending on the different crystal structures, MM-GBSA calculations were performed using the Maestro Prime tool. [7, 16, 17] The monomers from the PDB structures were first prepared with the heme group and, if present, the ligand inside by the Protein Preparation Wizard tool of the Biologics suite from Maestro program. [7, 18] In order to properly define the coordinative bonds between the iron ion and the nitrogen atoms of the porphyrin ring, a preprocessing of the macromolecule was performed. The addition of hydrogen atoms was also done at this stage with a validation of the protonation states by the program Epik. [7, 19, 20] The ferrous redox state was retained for iron in agreement with the crystallization conditions. The final model was optimized with the OPLS3e force field. [7, 21] Separate structure files were then obtained for the ligand and/or the cofactor and the enzyme. The MM-GBSA calculations were run using the VSGB solvation model [7, 22] together with the OPLS3e force field. The enzyme was kept rigid to preserve a conformation close to the crystal conformation. Prior to the calculation using Prime MM-GBSA, validation tests on the system against known data have been done using human hemoglobin and sperm whale myoglobin to validate the ranking of affinity for the heme cofactor (data not shown).

A.7.2 Binding site studies of hIDO1

The enzyme binding sites were determined with the SiteMap tool of the Maestro suite. [7] For this purpose, the crystal structures were prepared with Protein Preparation Wizard tool. [7, 18] The different ligands were removed manually in order to leave the pockets empty. The analysis was run to determine at least 10 top-ranked binding sites with 10 site points per site using a fine grid method.

A.7.3 Homology modeling of hIDO1

To study the dynamics of the JK-loop of hIDO1 in presence of ligands (section A.8), the crystal structures 7p0r, 7p0n and 7z2l were completed by means of a homology model. The model was constructed with the Maestro program using Prime and the Structure Prediction Wizard with the sequence from the structure 7a62 as the starting model. [7, 16, 17] Sequences were aligned with ClustalW alignment method. Model building method used was the knowledge-based method. The heme cofactor and the L-Trp molecule were then added to the resulting homology model at a position observed by crystallography. This completes the gap between the N-terminus and C-terminus of the JK-loop exclusively, without modification of any other structure.

A.7.4 Homology modeling of hIDO2

The model by homology of hIDO2 was designated by the Swiss Model program [23–25] from the 7a62 structure available in the PDB. The starting sequence of hIDO2 was the one described in UniProt [5], with M14 as the starting point in order to have the active form of the enzyme. The heme, missing from the model, was added from the known position of hIDO1, with an initial distance between iron and H347 of 2.2 Å.

A.7.5 Docking study of hIDO2

Docking of L-Trp in the active site of hIDO2 was performed with the holo structure of hIDO2 obtained after 300 ns of production by Molecular Dynamics as starting model (see point A.8). First, the Protein Preparation Wizard [7, 18] was used to prepare the protein of interest. A preprocessing of the structure was performed in order to assign the binding orders, to add the hydrogens to the structure and to create the possible disulfide bonds [7, 19, 20]. This step also allowed to define the binding between the heme cofactor and the protein as well as its redox state. After optimization of the hydrogen bonds contained in the protein, a general minimization was then performed in the OPLS3e force field. [7, 21] The ligand was prepared with the LigPrep tool with force field OPLS3e and by generating the possible ionization state by Epik. [7, 19–21] The docking was then done with the Induced fit Docking tool [26–28] and with the OPLS3e force field. [21] The heme cofactor present in the active site of the protein then served as the center for the box defining the volume where docking was performed. The size of the box was defined as less than or equal to 20Å. The ligand was docked in

a flexible way, by evaluating the different possible conformations within $2.5 \text{ kcal mol}^{-1}$ of the minimum. The docking allowed an automatic adjustment of the side chains within 5 \AA of the ligand, based on the B-factor. The results showed the 20 best ligand positions. The poses with the best glide score and the closest pose to the known reactive position of hIDO1 were kept in order to perform MMGBSA analyses as well as a further investigation by Molecular Dynamics.

A.8 Characterization by Molecular Dynamics

Molecular Dynamics modeling has been a tool of choice during the thesis to further understand hIDO1 or hIDO2. However, this required the establishment of protocols from the beginning of the thesis. These are described in their most optimized version in this section. However, the discussion on the definition of the covalent link between the histidine and the cofactor is the subject of Appendix B.

A.8.1 Molecular Dynamics studies of hIDO1 in absence of ligand

Molecular Dynamics simulations of the apo and holo forms of hIDO1 were run using the program GROMACS 2016 (5.1.4) [29] with the CHARMM27 force field [30] and the CMAP corrections for the protein. The monomer C of the crystal structure (PDB entry: 7a42) was used as starting model. For the simulation without the heme cofactor, the construction of the model was performed by removing the heme group of the chain C of the crystal structure. A r.m.s.d analysis between the chain and the monomers of the apo-forms reported in the PDB yields values of 0.3 \AA for the structure 6e43, 0.5 \AA for 6azv, and 0.6 \AA for 6azw, showing that the unbound chain C of 7a62 was a good model of the apo-form. H atoms were added using GROMACS. [29] The systems were solvated using all-atom TIP3P and coarse-grained SIRAH water particles. [31, 32] A cubic box was built around the protein with at least 2.0 nm between the box and the protein atoms. TIP3P water molecules were placed in a shell of 1.0 nm thickness around the molecular system. The space between the shell and the box was completed with coarse-grained SIRAH water particles. The use of a hybrid all-atom/coarse grained water solvent allows to model a protein system which remains fully surrounded by all-atom water molecules. SIRAH water were constrained with position restraint for each water oxygen atom to avoid direct interaction with the protein during the simulation. Finally, the total charge of the system was neutralized

with sodium ions randomly placed into the SIRAH water.

The optimization and MD trajectories were generated under the particle mesh Ewald (PME) periodic boundary conditions (PBC). A cut-off value of 1.2 nm was applied for Coulomb and van der Waals interactions. Temperature and pressure were fixed using the V-Rescale [34] and the Parrinello-Rahman [33] algorithms, respectively. Covalent bonds involving hydrogen atoms were constrained using the LINCS algorithm. [35] The resulting system was optimized using the steepest descent algorithm for a maximal number of 2500 steps and an initial step size of 0.05 nm. During the equilibration stage of the system, the temperature was progressively increased from 50 K to 310 K using short MD runs. The first run consisted of a 10 ps simulation at 50 K on the system obtained after optimization. Afterwards, the system was relaxed for two runs of 20 ps at 150 K and 310 K. Finally, a run of 50 ps at 310 K and 1 bar was performed to finalize the relaxation of the system. The equilibration was extended during 60 ns with a time step of 2 fs at 310 K and 1 bar. The production step was run for 200 ns (100×10^6 steps) with a time step of 2 fs.

A.8.2 Molecular Dynamics studies of hIDO1 in presence of ligands

To study the dynamics of the JK-loop of hIDO1 in presence of ligands, each monomer with a L-Trp or a L-Kynurenine molecule in the active site was used as the starting model. The crystal structures without a complete refined JK-loop were filled by means of a homology model as described in Section A.7.3. The resulting structures were used as starting points for the MD simulations in complement to the structure hIDO1-closed (7nqe). MD simulations of the different protein/ligand complexes were run using GROMACS 2020 [29] with the CHARMM27 force field [36] and CMAP corrections for the protein. H atoms were added using GROMACS.

The ligand-specific topology files were created using the SwissParam software [37] based on the position in the protein and the protonation state of the molecule at pH 7.0. The starting file is a file with the exact coordinates of the ligand in the protein, saved as .mol, isolated with Pymol. [38] The ligand molecule was allowed to move from its original position during the simulations. The solvation, the optimization and the equilibration of the models were performed as described in the previous section.

In the present dynamics, the production stage was run for 300 ns with a time step of 2 fs.

A.8.3 Molecular Dynamics studies of hIDO2 in absence of ligands

Molecular dynamics analysis of hIDO2 was performed on the basis of the structure obtained by homology. Thus, it was possible to study the apo and holo form of the protein. Using Pymol [38], the two polymorphs known from the literature for hIDO1 (R231W and Y346X) were designated. All dynamics on these models were run by GROMACS 2020 [29] with the CHARMM27 force field [36] and the CMAP correction for the protein. Hydrogen atoms were added using GROMACS. The solvation of the models was performed in a hybrid way, with TIP3P and SIRAH waters according to the same methodology detailed for hIDO1. For the sake of future comparison, the same methodology was also used for system minimization, equilibration steps and trajectory productions stage. All models were analyzed as triplicates, with three different random velocity sets at the beginning of the equilibration. Production steps lasted 300 ns, with a time step of 2 fs.

A.8.4 Molecular Dynamics studies of hIDO2 in presence of L-Trp

Based on the coordinated file of the holo protein after 300 ns of production, the analysis of the evolution of L-Trp in the active site of hIDO2 was performed by Molecular Dynamics. For this purpose, several starters were chosen. In a first step, simulations were launched on the positions resulting from the docking with 1) the best score or 2) the best orientation based on the knowledge of the system. On the other hand, simulations by taking the exact position of the reactive L-Trp in hIDO1 and transposing it to hIDO2 are also performed. The ligand topology files were created from Swiss-Param software. [37] The methodology followed is exactly the same as in the case of ligand-based simulations for hIDO1 for model building, minimization, equilibration and production. The ligands are free to move during the whole simulation.

Bibliography

- [1] M. Mirgaux, L. Leherte, and J. Wouters. Influence of the presence of the heme cofactor on the JK-loop structure in indoleamine 2,3-dioxygenase 1. *Acta Crystallographica Section D: Structural Biology*, 76:1211–1221, 2020.

- [2] M. Mirgaux, L. Leherter, and J. Wouters. Temporary intermediates of L-Trp along the reaction pathway of human indoleamine 2, 3-dioxygenase 1 and identification of an exo site. *International Journal of Tryptophan Research*, 14:1–11, 2021.
- [3] E. Gasteiger, C. Hoogland, A. Gattiker, M. R. Wilkins, R. D. Appel, A. Bairoch, et al. Protein identification and analysis tools on the expasy server. *The Proteomics Protocols Handbook*, pages 571–607, 2005.
- [4] S. Luo, K. Xu, S. Xiang, J. Chen, C. Chen, C. Guo, Y. Tong, and L. Tong. High-resolution structures of inhibitor complexes of human indoleamine 2, 3-dioxygenase 1 in a new crystal form. *Acta Crystallographica Section F: Structural Biology Communications*, 74(11):717–724, 2018.
- [5] The UniProt Consortium. Uniprot: the universal protein knowledgebase in 2021. *Nucleic Acids Research*, 49(D1):D480–D489, 2021.
- [6] A. M. Brown. A new software for carrying out one-way anova post hoc tests. *Computer Methods and Programs in Biomedicine*, 79(1):89–95, 2005.
- [7] Schrodinger. Schrodinger release 2021-2. SiteMap. LLC, New-York, NY, 2021.
- [8] J. Newman, D. Egan, T. S. Walter, R. Megeed, I. Berry, M. Ben Jelloul, J. L. Sussman, D. I. Stuart, and A. Perrakis. Towards rationalization of crystallization screening for small-to medium-sized academic laboratories: the pact/jcsg+ strategy. *Acta Crystallographica Section D: Biological Crystallography*, 61(10):1426–1431, 2005.
- [9] A. Chaikuad, S. Knapp, and F. von Delft. Defined peg smears as an alternative approach to enhance the search for crystallization conditions and crystal-quality improvement in reduced screens. *Acta Crystallographica Section D: Biological Crystallography*, 71(8):1627–1639, 2015.
- [10] W. Kabsch. Xds. *Acta Crystallographica Section D: Biological Crystallography*, 66(2):125–132, 2010.
- [11] A. J. McCoy, R. W. Grosse-Kunstleve, P. D. Adams, M. D. Winn, L. C. Storoni, and R. J. Read. Phaser crystallographic software. *Journal of Applied Crystallography*, 40(4):658–674, 2007.
- [12] P. Emsley, B. Lohkamp, W. G. Scott, and K. Cowtan. Features and development of coot. *Acta Crystallographica Section D: Biological Crystallography*, 66(4):486–501, 2010.

- [13] P. D. Adams, P. V. Afonine, G. Bunkóczi, V. B. Chen, I. W. Davis, N. Echols, J. J. Headd, L.-W. Hung, G. J. Kapral, R. W. Grosse-Kunstleve, et al. Phenix: a comprehensive python-based system for macromolecular structure solution. *Acta Crystallographica Section D: Biological Crystallography*, 66(2):213–221, 2010.
- [14] T. C. Terwilliger, R. J. Read, P. D. Adams, A. T. Brunger, P. V. Afonine, R. W. Grosse-Kunstleve, and L.-W. Hung. Improved crystallographic models through iterated local density-guided model deformation and reciprocal-space refinement. *Acta Crystallographica Section D: Biological Crystallography*, 68(7):861–870, 2012.
- [15] N. W. Moriarty, R. W. Grosse-Kunstleve, and P. D. Adams. electronic ligand builder and optimization workbench (elbow): a tool for ligand coordinate and restraint generation. *Acta Crystallographica Section D: Biological Crystallography*, 65(10):1074–1080, 2009.
- [16] M. P. Jacobson, D. L. Pincus, C. S. Rapp, T. J.F. Day, B. Honig, D. E. Shaw, and R. A. Friesner. A hierarchical approach to all-Atom protein loop prediction. *Proteins: Structure, Function and Genetics*, 55(2):351–367, 2004.
- [17] M. P. Jacobson, R. A. Friesner, Z. Xiang, and B. Honig. On the role of the crystal environment in determining protein side-chain conformations. *Journal of Molecular Biology*, 320(3):597–608, 2002.
- [18] G. Madhavi Sastry, M. Adzhigirey, T. Day, R. Annabhimoju, and W. Sherman. Protein and ligand preparation: Parameters, protocols, and influence on virtual screening enrichments. *Journal of Computer-Aided Molecular Design*, 27(3):221–234, 2013.
- [19] J. R. Greenwood, D. Calkins, A. P. Sullivan, and J. C. Shelley. Towards the comprehensive, rapid, and accurate prediction of the favorable tautomeric states of drug-like molecules in aqueous solution. *Journal of Computer-Aided Molecular Design*, 24(6):591–604, 2010.
- [20] J. C. Shelley, A. Cholleti, L. L. Frye, J. R. Greenwood, M. R. Timlin, and M. Uchi-maya. Epik: A software program for pKa prediction and protonation state generation for drug-like molecules. *Journal of Computer-Aided Molecular Design*, 21(12):681–691, 2007.

- [21] E. Harder, W. Damm, J. Maple, C. Wu, M. Reboul, J. Y. Xiang, L. Wang, D. Lupyan, M. K. Dahlgren, J. L. Knight, J. W. Kaus, D. S. Cerutti, G. Krilov, W. L. Jorgensen, R. Abel, and R. A. Friesner. OPLS3: A Force Field Providing Broad Coverage of Drug-like Small Molecules and Proteins. *Journal of Chemical Theory and Computation*, 12(1):281–296, 2016.
- [22] J. Li, R. Abel, K. Zhu, Y. Cao, S. Zhao, and R. A. Friesner. The VSGB 2.0 model: A next generation energy model for high resolution protein structure modeling. *Proteins: Structure, Function and Bioinformatics*, 79(10):2794–2812, 2011.
- [23] A. Waterhouse, M. Bertoni, S. Bienert, G. Studer, G. Tauriello, R. Gumienny, F. T. Heer, T. A. P. de Beer, C. Rempfer, L. Bordoli, et al. Swiss-model: homology modelling of protein structures and complexes. *Nucleic Acids Research*, 46(W1):W296–W303, 2018.
- [24] N. Guex, M. C. Peitsch, and T. Schwede. Automated comparative protein structure modeling with swiss-model and swiss-pdbviewer: A historical perspective. *Electrophoresis*, 30(S1):S162–S173, 2009.
- [25] G. Studer, C. Rempfer, A. M. Waterhouse, R. Gumienny, J. Haas, and T. Schwede. Qmeandisco—distance constraints applied on model quality estimation. *Bioinformatics*, 36(6):1765–1771, 2020.
- [26] W. Sherman, H. S Beard, and R. Farid. Use of an induced fit receptor structure in virtual screening. *Chemical Biology & Drug Design*, 67(1):83–84, 2006.
- [27] W. Sherman, T. Day, M. P. Jacobson, R. A. Friesner, and R. Farid. Novel procedure for modeling ligand/receptor induced fit effects. *Journal of Medicinal Chemistry*, 49(2):534–553, 2006.
- [28] R. Farid, T. Day, R. A. Friesner, and R. A. Pearlstein. New insights about herg blockade obtained from protein modeling, potential energy mapping, and docking studies. *Bioorganic & Medicinal Chemistry*, 14(9):3160–3173, 2006.
- [29] M. J. Abraham, T. Murtola, R. Schulz, S. Páll, J. C. Smith, B. Hess, and E. Lindah. Gromacs: High performance molecular simulations through multi-level parallelism from laptops to supercomputers. *SoftwareX*, 1:19–25, 2015.

- [30] A. D. MacKerell, N. Banavali, and N. Foloppe. Development and current status of the charmm force field for nucleic acids. *Biopolymers: Original Research on Biomolecules*, 56(4):257–265, 2000.
- [31] L. Darre, A. Tek, M. Baaden, and S. Pantano. Mixing atomistic and coarse grain solvation models for md simulations: let wt4 handle the bulk. *Journal of Chemical Theory and Computation*, 8(10):3880–3894, 2012.
- [32] H. C. Gonzalez, L. Darre, and S. Pantano. Transferable mixing of atomistic and coarse-grained water models. *The Journal of Physical Chemistry B*, 117(46):14438–14448, 2013.
- [33] M. Parrinello and A. Rahman. Polymorphic transitions in single crystals: A new molecular dynamics method. *Journal of Applied physics*, 52(12):7182–7190, 1981.
- [34] G. Bussi, D. Donadio, and M. Parrinello. Canonical sampling through velocity rescaling. *The Journal of Chemical Physics*, 126(1):014101, 2007.
- [35] B. Hess, H. Bekker, H. J. C. Berendsen, and J. Fraaije. Lincs: a linear constraint solver for molecular simulations. *Journal of Computational Chemistry*, 18(12):1463–1472, 1997.
- [36] A. D. MacKerell, N. Banavali, and N. Foloppe. Development and current status of the CHARMM force field for nucleic acids. *Biopolymers*, 56(4):257–265, 2000.
- [37] V. Zoete, M. A Cuendet, A. Grosdidier, and O. Michielin. Swissparam: a fast force field generation tool for small organic molecules. *Journal of Computational Chemistry*, 32(11):2359–2368, 2011.
- [38] Schrödinger, LLC. The PyMOL molecular graphics system. Version 1.7.4.4, November 2015.

Appendix B

Methodological development for the fundamental study: definition of the histidine /heme link

B.1 Introduction

The definition of the covalent bond linking histidines H346/H347 to the central iron atom is an important methodological feature for hIDO1/hIDO2 research. This comes from the recent discovery of the lability of the cofactor in the protein and the existence of intermediate states at the apo and holo forms. Two possibilities exist 1) consider this bond as rigid and covalently defined during the dynamics 2) consider that an interaction is possible but do not fix the bond. Although this may seem like a detail, the choice of the methodology adopted can have great consequences on the outcome of the Molecular Dynamics. In particular, it is justified by a rigidification of the system in case of choice of the first hypothesis. Moreover, the histidine/heme distances are also impacted because the nature of the interaction, and thus of the atomic radii, changes according to the adopted methodology (ranging from covalent to van der Waals type radii). In this appendix, the two methodological possibilities have been investigated and the results obtained have been compared.

B.2 Influence of the covalent link on hIDO1

Knowledge prior to this thesis demonstrated that the ferric heme of hIDO1 was labile in the active site. [1] This thesis confirmed this information and again demonstrated that the apo form was the main form in hIDO1. In addition, a state with unbound ferrous heme but in the active site seems to exist in addition to the apo and holo states. A question therefore arises in the methodology adopted for the MD simulations of hIDO1: how to define the link between H346 and iron? In order to evaluate the influence of this choice, Molecular Dynamics simulations were performed with several different protocols. The first possibility is the absence of covalent bonding and the mention in GROMACS that H346 is a heme-coordinated histidine D (for consistency of charges and hydrogen placement). This is compared to the same situation but with motion restraints on the NE atom from this H346 and the iron (the force constant applied on the heavy atoms varies between $1000 \text{ kJ mol}^{-1} \text{ nm}^{-2}$ and $10000 \text{ kJ mol}^{-1} \text{ nm}^{-2}$). At last, a simulation where a covalent bond is directly established has been performed. This last simulation requires more pre-processing than the others. To define the covalent link, a program had to be designed, by Dr. Leherte, to create the topology file containing all the information of this link (distance, angles).

All simulations are run with the version of GROMACS 2020. For the unrestrained simulation which has previously performed with GROMACS 2016, all trends are consistent in terms of quantitative and qualitative values between the two version of GROMACS (2016 and 2020). These results have been compared to results with restraints. The differentiation of the results was analyzed in two parts: the quantifiable results (r.m.s.d, r.m.s.f, distances, etc.) and qualifiable (loop position, observation of the dynamics, etc.). Two methodologies are considered similar as long as there is no significant variation in the quantitative data. The comparison of the r.m.s.f values shows that the imposition of constraints has few influences on this value, either for the overall plasticity or the loop motion. The simulation with a force constant of $10000 \text{ kJ mol}^{-1} \text{ nm}^{-2}$ slightly diverges from this trend. Since the starting structure is identical in all simulations, the deviation over time from this initial common structure was calculated (Figure B.2). The simulations that differs the least for the initial structure are the simulation without constraint, the simulation with a force constant of $1000 \text{ kJ mol}^{-1} \text{ nm}^{-2}$ and the simulation with the covalent bond.

TABLE B.1: Distances (H346(NE)-Fe, in Å) and angles (H346(NE)-Fe-NA(Heme), in °) with standard deviation (indicated with the \pm) between the NE atom of H346 and the heme cofactor according to the different models for hIDO1.

Restraint	Distance H346(NE)-Fe (Å)	Angle H346(NE)-Fe-NA (°)
No restraint	2.7 ± 0.3	92.3 ± 8.5
Covalent bond	2.2 ± 0.1	90.3 ± 3.0
Force constant of $1000 \text{ kJ mol}^{-1} \text{ nm}^{-2}$	2.6 ± 0.4	93.3 ± 8.6
Force constant of $10000 \text{ kJ mol}^{-1} \text{ nm}^{-2}$	3.1 ± 0.5	80.9 ± 6.0

For all, the heme and H346 move slightly from the initial position (Table B.1). Taking as reference the distance of the covalent bond, fixed on the basis of crystallography, in the simulation of the unconstrained protein or with force constant on the heavy atoms, this distance is greater than a covalent bond. The distances closest to these values are for the models without restraints or with a force constant of $1000 \text{ kJ mol}^{-1} \text{ nm}^{-2}$. The angle formed between porphyrin and histidine is ideally close to 90 degrees. For this characteristic, the value for the simulation without restraint is the closest to the one with the covalent bond, despite a greater deviation due

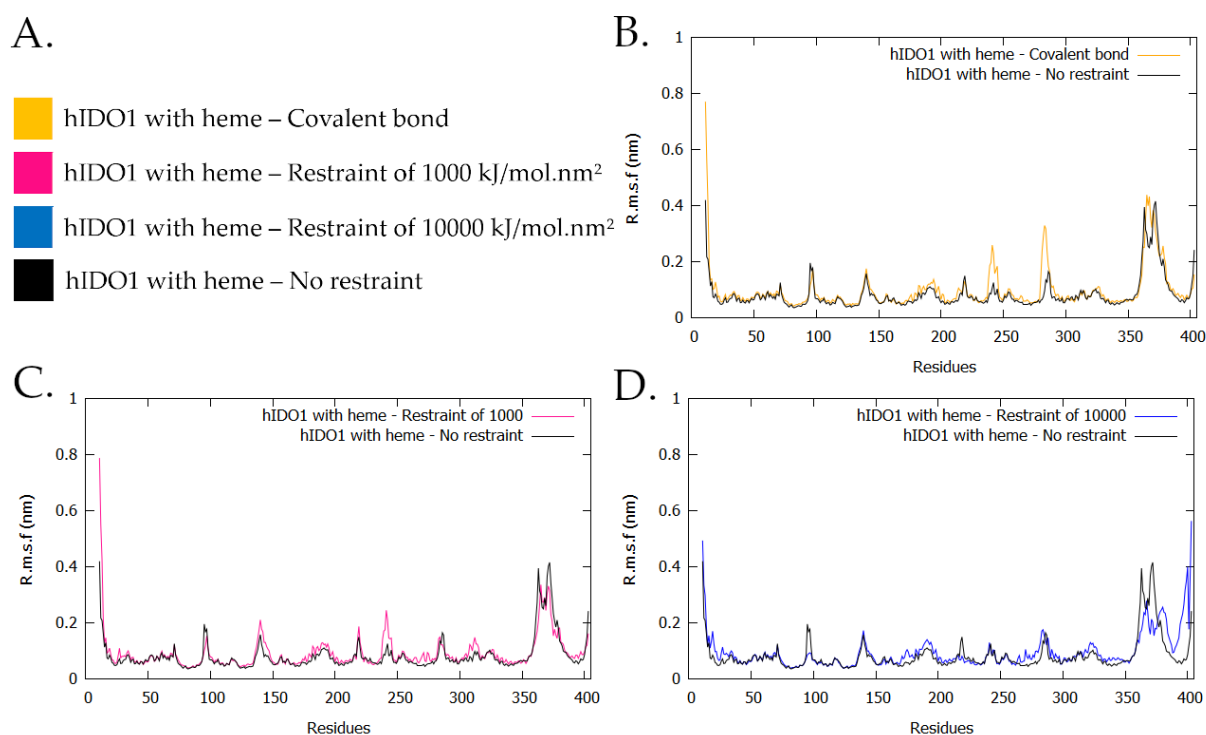


FIGURE B.1: R.m.s.f profiles of the holo hIDO1 structure according to the kind of restraint for the bond between H346 and the heme cofactor. A. Legend. B. Comparison between the simulation with covalent bond and without restraint. C. Comparison between the simulation with a force constant of 1000 kJ mol⁻¹ nm⁻² and without restraint. D. Comparison between the simulation with a force constant of 10000 kJ mol⁻¹ nm⁻² and without restraint.

to the flexibility left of the residue.

From a qualitative point of view, all simulations show an intermediate type conformation. However, the introduction of position restraints can, for the covalent bond and the 1000 kJ mol⁻¹ nm⁻² constraint in particular, induces a turn in addition to the K helix and a stabilization of the cofactor by K373 rather than by K377. The divergence of the structures with a force constant 10000 kJ mol⁻¹ nm⁻² is established only in the fact that H346 orientates differently during the dynamics and thus increases the distance between H346 and the iron. Consequently, the overall plasticity of the protein changes, without changing its folding. In view of the limited change caused by the presence of the covalent bond, it was then decided not to impose any constraint on this histidine/heme distance in order not to distort the conformation trend adopted by H346. It also makes sense that it is then possible to compare the unconstrained

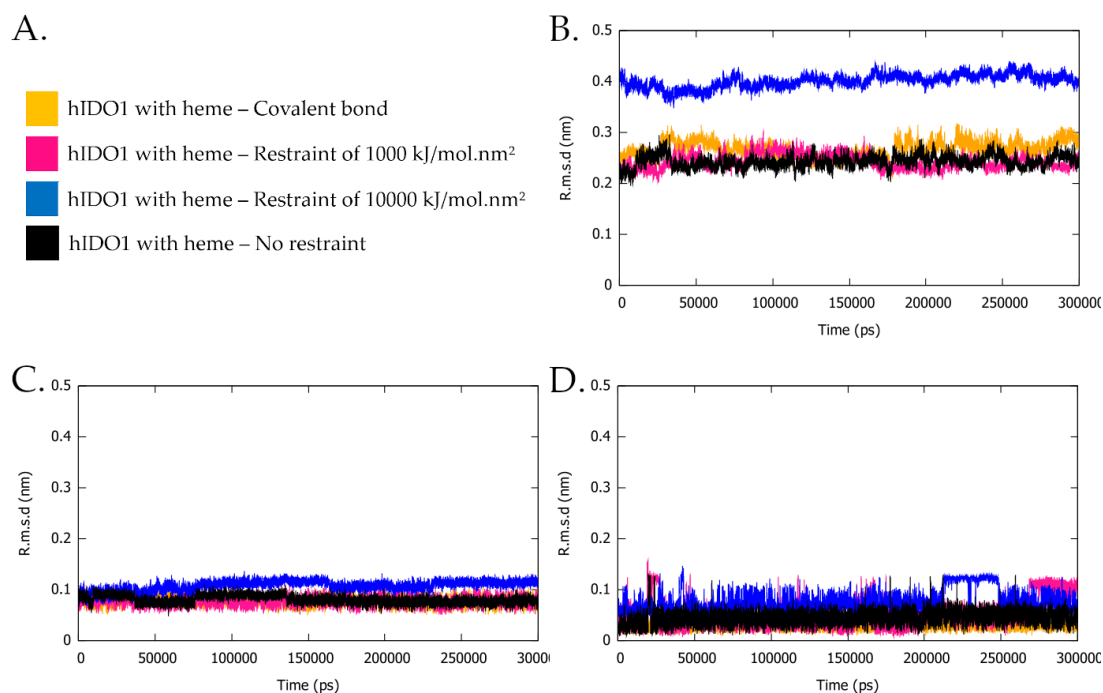


FIGURE B.2: R.m.s.d profiles of protein residues, heme cofactor and H346 for holo hIDO1 structure according to the kind of restraint for the bond between H346/Fe. The r.m.s.d were calculated in comparison to the initial common structure in each case. A. Legend for the graphs. B. r.s.m.d for the overall protein. C. r.s.m.d for the heme cofactor. D. r.s.m.d for H346.

simulations of hIDO1 with the unconstrained one of hIDO2 in this way.

B.3 Influence of the covalent link on hIDO2

Due to the experimental findings detailed in the characterization part of this thesis, the definition of lability in hIDO2 is even more central. It has been shown that both forms of the enzyme are labile. Moreover, the apo form but with unbound heme in the active site exists. Thus, it may make less sense to rigidly fix the link between the heme and the protein. The section here details the influence of the H347(NE)-Fe constraint on the dynamics results. Several types of simulations are performed, as for hIDO1: one simulation with an unconstrained protein, one simulation with an imposed covalent bond between iron and H347, and two simulations with a variable force constant imposed on the iron atom and the NE atom of H347. The H347(NE)-iron distance is impacted by the type of methodology. With a covalent bond definition, this distance

is $2.2 \text{ \AA} \pm 0.1 \text{ \AA}$, as fixed by the topology file (Table B.2). The simulation of the unconstrained protein or the simulations with a force constant do not show such a result since no distance imposition is performed. In this case, the obtained values of the distance between NE and iron increase drastically to values higher than 5.0 \AA (Table B.2). There is no change in the type of coordination as the ND atom remains around 4 or 5 \AA from the iron. There is therefore a loss of H347 binding for hIDO2, which was not observed for hIDO1. Logically, the $1000 \text{ kJ mol}^{-1} \text{ nm}^{-2}$ force constant looks more like the unconstrained form while the $10000 \text{ kJ mol}^{-1} \text{ nm}^{-2}$ force constant has values that tend towards the covalent form. The angles (Table B.3) follow the same trend with a marked deviation of H347 from the covalent bond and the theoretical angle of 90 degrees, showing a disorientation of H347.

TABLE B.2: Distances (H347(NE)-Fe, in \AA) with standard deviation (indicated with the \pm) between the NE atom of H347 and the heme cofactor according to the different models for hIDO2.

Restraint	Distance H347(NE)-Fe (\AA)	Distance H347(ND)-Fe (\AA)
No restraint	5.3 ± 1.3	5.0 ± 1.0
Covalent bond	2.2 ± 0.1	4.2 ± 0.01
Force constant of $1000 \text{ kJ mol}^{-1} \text{ nm}^{-2}$	5.2 ± 0.9	5.0 ± 0.4
Force constant of $10000 \text{ kJ mol}^{-1} \text{ nm}^{-2}$	3.3 ± 0.5	4.4 ± 0.2

TABLE B.3: Angles (H347(NE)-Fe-NA(Heme), with standard deviation (indicated with the \pm), in $^\circ$) between the NE atom of H347 and the heme cofactor according to the different models for hIDO2.

Restraint	Angle H347(NE)-Fe-NA ($^\circ$)
No restraint	73.1 ± 8.1
Covalent bond	87.9 ± 4.2
Force constant of $1000 \text{ kJ mol}^{-1} \text{ nm}^{-2}$	137.4 ± 6.8
Force constant of $10000 \text{ kJ mol}^{-1} \text{ nm}^{-2}$	84.0 ± 7.2

Regarding the quantifiable results, the analyses of the r.m.s.f. show that flexibility of the unrestrained protein or the protein with the covalent bond is relatively close (Figure B.3, A.). The mobility is sometimes slightly more marked in the case of the constrained simulation, mainly at the level of folds with known dynamics (helix F'

and heme binding site). Conversely, a force constant on the iron ion and the NE atom of histidine leads to more aberrant values and an increase in fluctuation values for H347 if the force constant is low ($1000 \text{ kJ mol}^{-1} \text{ nm}^{-2}$). This effect is no longer visible when the force constant increases. Another quantitative characteristic is the variation of r.m.s.d (Figure B.4). As for hIDO1, the deviation over time from this initial common structure was calculated. In all cases, the variation of r.m.s.d for heme or H347 is negligible. However, there is a difference on the r.m.s.d on the protein residues. This implies different folding depending on the type of definition for the link between H346 and heme.

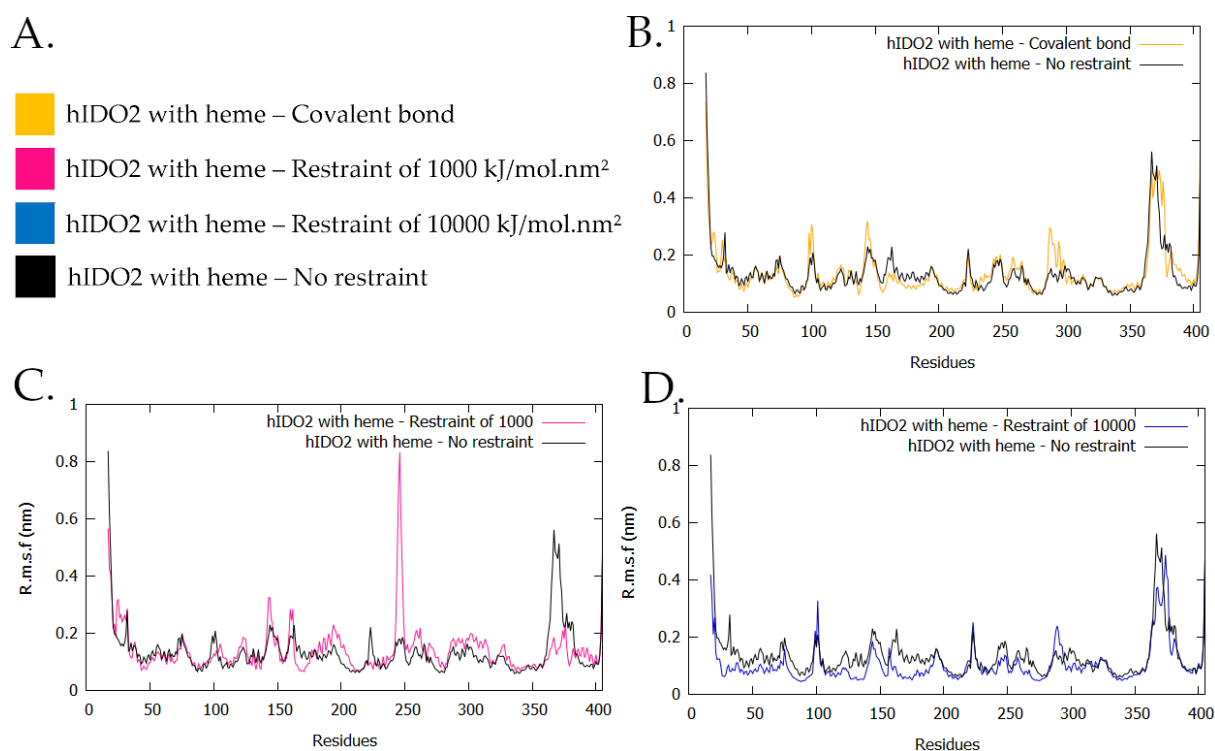


FIGURE B.3: R.m.s.f profiles of the holo hIDO2 structure according to the kind of restraint for the bond between H347 and the heme cofactor. A. Legend. B. Comparison between the simulation with covalent bond and without restraint. C. Comparison between the simulation with a force constant of $1000 \text{ kJ mol}^{-1} \text{ nm}^{-2}$ and without restraint. D. Comparison between the simulation with a force constant of $10000 \text{ kJ mol}^{-1} \text{ nm}^{-2}$ and without restraint.

For the covalent simulation, in Figure B.5, A., r.m.s.d profiles in comparison to the final 300 ns structure without restraint show that this effect is especially marked for the JK'-loop and the helix F'. The core of the active site is, however, insignificantly

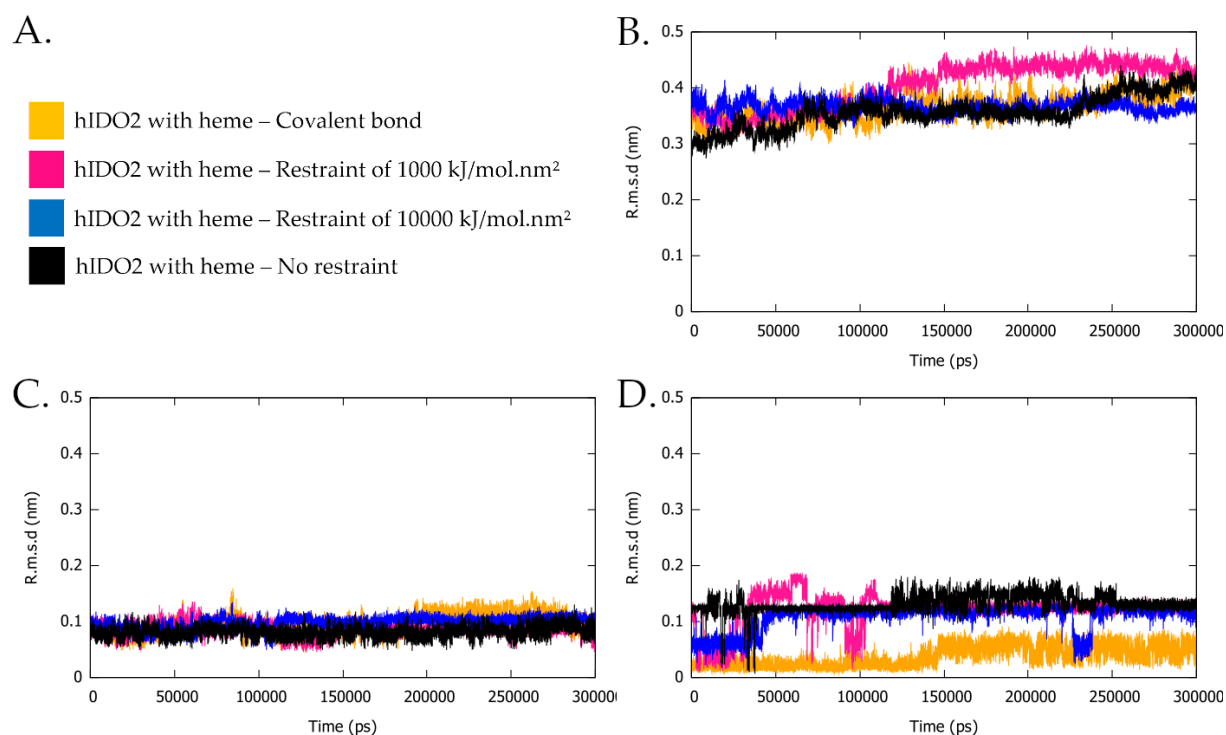


FIGURE B.4: R.m.s.d profiles of protein residues, heme cofactor and H347 for holo hIDO2 structure according to the kind of restraint for the bond between H347/Fe. The r.m.s.d were calculated in comparison to the initial common structure in each case. A. Legend for the graphs. B. r.s.m.d for the overall protein. C. r.s.m.d for the heme cofactor. D. r.s.m.d for H347.

impacted (fragment G265-Q270, in green lines). The same observation is made for the simulation with a force constant of 10000 kJ mol⁻¹ nm⁻² (Figure B.5, B.).

Qualitatively, a force constant of 10000 kJ mol⁻¹ nm⁻² or a covalent bond results in an important rigidification of the system. As a result, there is a change of secondary structure at the level of the F' helix, located between residues E288 and M300 (Figure B.6, A. and B.). This is already appear at the beginning of the production as observed in Figure B.6, B. after 1ns. In this case, the helix folding is shorter, involving an isolated helix turn (S286-S289) occurring before the main helix (D291-M300). The JK'-loop is not impacted by the restraints and adopt almost similar conformations at the C-terminal extremity, with an open conformation without interaction between R380 and the cofactor (Figure B.6, C.). The N-terminal conformation is also identical to the unconstrained simulation, with a rather globular conformation and close to the DE'-loop (Figure B.6, D.). When the system has time to relax, the folding is changed

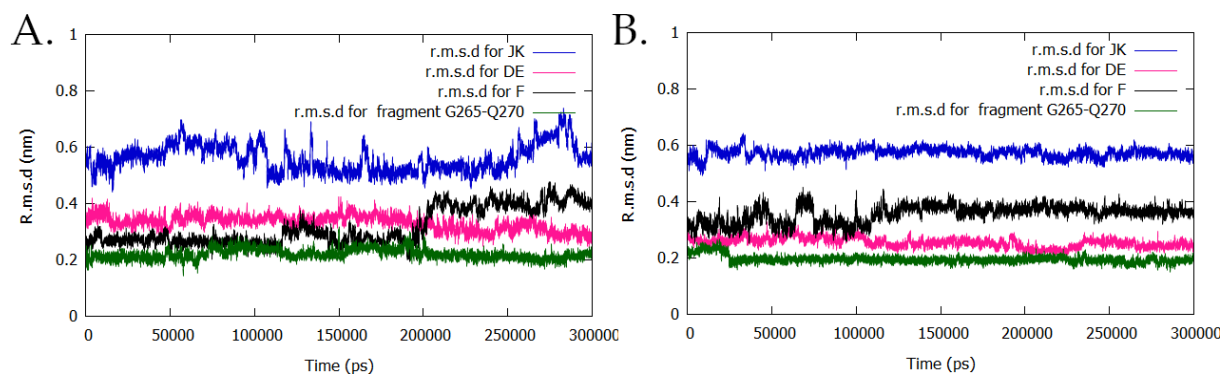


FIGURE B.5: R.m.s.d profiles of helix F', DE'-loop, active site and JK'-loop for holo hIDO2 structure according to the kind of restraint for the bond between H347/Fe. The r.m.s.d is performed against the final structure after 300 ns of simulation at 310 K and 1 bar for hIDO2 without restraints. A. for covalent restrained protein. B. for protein with a $10000 \text{ kJ mol}^{-1}$ force constant.

during the simulation (Figure B.7, A.). For the simulation with a covalent bond, the F' helix is still defined by an isolated turn (H285-E288) followed by a main α -helix (G290-M300) (Figure (Figure B.7, B.)). The fold is positioned closer to the heme binding pocket. This change is linked to the repositioning of the heme and the fragment G265-Q270 as to avoid a clash with the position of the heme. The JK'-loop remains in an open conformation at the C-terminal extremity (Figure B.7, C.). For the N-terminal extremity, the JK'-loop adopts a helix folding for the N-terminal part during the production stage (Figure B.7, D.). This is due to the rigidification of H347 surrounding stabilizing the conformation of J' helix. This folding leads to a longer conformation extended towards the solvent.

In conclusion, although this slightly different conformation for the N-terminal part, the conformation at the C-terminal extremity of the JK'-loop is open, regardless of the type of constraints imposed during the simulation. The methodology adopted to define the bond between H347 and the iron ion does not impact the analysis of the JK'-loop dynamics. However, if a constraint is applied, either force constant or covalent, essential information about the folding of the helix F' is lost, with a restructuring of the active site. The constrained simulations are close to the structures adopted in hIDO1 for this helix. Knowing that 1) experimental data indicates that the protein has a high cofactor lability, 2) this helix F' is involved in the maintenance of the cofactor in the active site, and 3) imposing a covalent bond for hIDO2 would be to consider

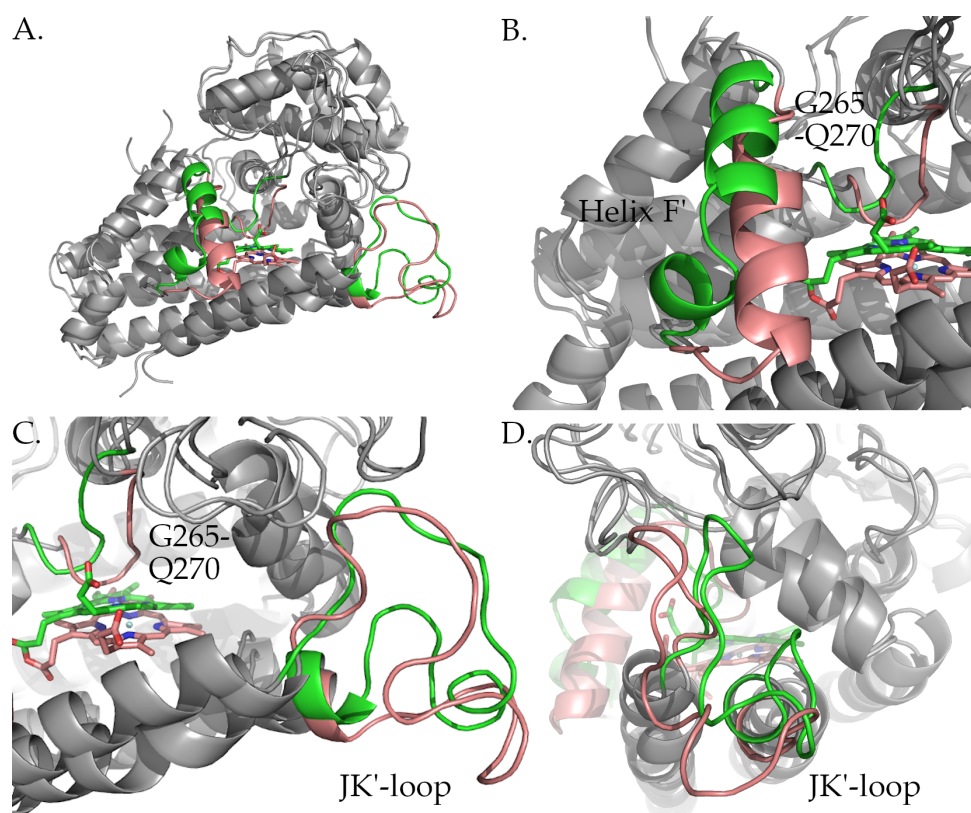


FIGURE B.6: Influence of covalent bond between H347(NE) and iron atom on the hIDO2 structure after 1 ns of production stage, at 310 K and 1 bar. Conformation changes of the F' helix, the fragment G265-Q270 and the JK'-loop are highlighted in colors (in green). Comparison with the unconstrained structure (in pink). A. Global folding for the two structures. B. Folding of the F'-helix according to the simulation. C. Folding of the C-terminal extremity of the JK'-loop according to the simulation. D. Folding of the N-terminal extremity of the JK'-loop according to the simulation.

that these cofactor lability characteristics are identical to hIDO1, the dynamics of the thesis were performed without constraints in order to explore new conformational possibilities for the enzyme.

B.4 Conclusions of the appendix

In conclusion, this part of the methodology has shown the effect of constraints on H346 or H347 on the general dynamics of the two proteins. For hIDO1, the imposition of a constraint is not necessary to maintain the orientation of H346. In order not to distort the structure of the hIDO1 protein and to be able to compare the behavior

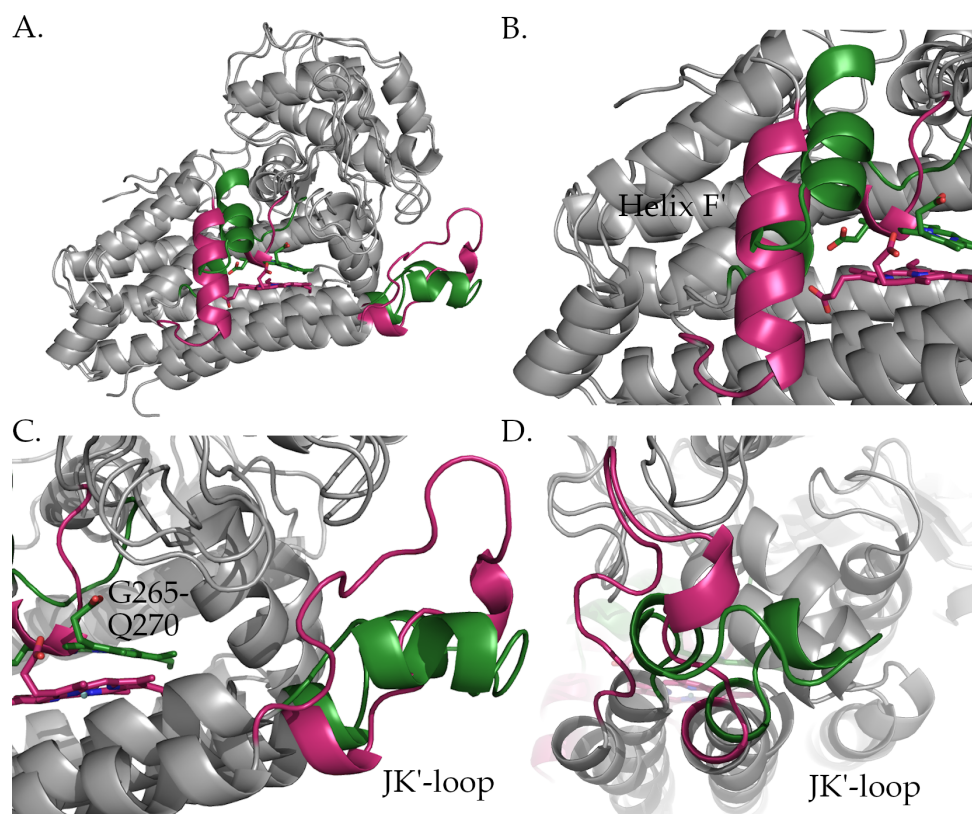


FIGURE B.7: Influence of covalent bond between H347(NE) and iron atom on the hIDO2 structure after 300 ns of production stage, at 310 K and 1 bar. Conformation changes of the F' helix, the fragment G265-Q270 and the JK'-loop are highlighted in colors (in green). Comparison with the unconstrained structure (in pink). A. Global folding for the two structures. B. Folding of the F'-helix according to the simulation. C. Folding of the C-terminal extremity of the JK'-loop according to the simulation. D. Folding of the N-terminal extremity of the JK'-loop according to the simulation.

with hIDO2, the simulations are therefore performed without constraints, with the definition of H346 as a D-type histidine. For hIDO2, the link between H347 and the heme is lost quickly during the MD simulations if the link is not forced as a covalent bond. The constraints greatly influence the conformation adopted by the F' helix and the G265-Q270 fragment but not the JK'-loop. In view of the high cofactor lability observed experimentally, it is therefore chosen not to impose any constraint, in order not to lose important information on this loop.

Bibliography

- [1] M. T. Nelp, P. A. Kates, J. T. Hunt, J. A. Newitt, A. Balog, D. Maley, X. Zhu, L. Abell, A. Allentoff, R. Borzilleri, et al. Immune-modulating enzyme indoleamine 2,3-dioxygenase is effectively inhibited by targeting its apo-form. *Proceedings of the National Academy of Sciences*, 115(13):3249–3254, 2018.

Appendix C

Physico-chemical characterization of hIDO1 and hIDO2: Supporting information

C.1 Absorbance of free hemin in solution

Free hemin absorbs in solution has a different maximum absorbance value than bound hemin. To see this, Figure C.1 aligns the different spectra and also shows the typical absorbance spectra of free hemin, depending on the oxidation state.

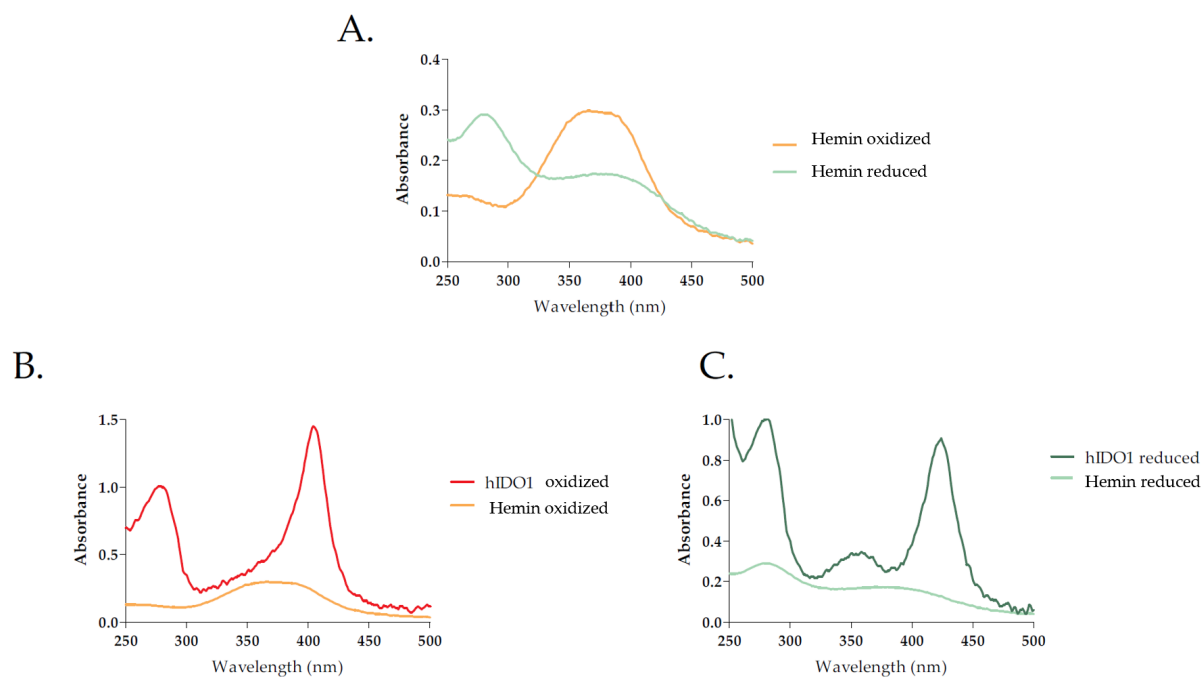


FIGURE C.1: UV-Visible absorption spectroscopy spectra of free hemin in solution at a concentration of $100\ \mu\text{M}$. A. Oxidated and reduced free hemin B. Comparison of free oxidated hemin with oxidated hIDO1. C. Comparison of free reduced hemin with reduced hIDO1.

The figure C.2 below shows the heme calibration line, in ferric and ferrous condition. Thus, the molar extinction coefficient could be determined at $30000\ \text{M}^{-1}\ \text{cm}^{-1}$. It is also notable that this coefficient is not influenced by the redox state of the cofactor.

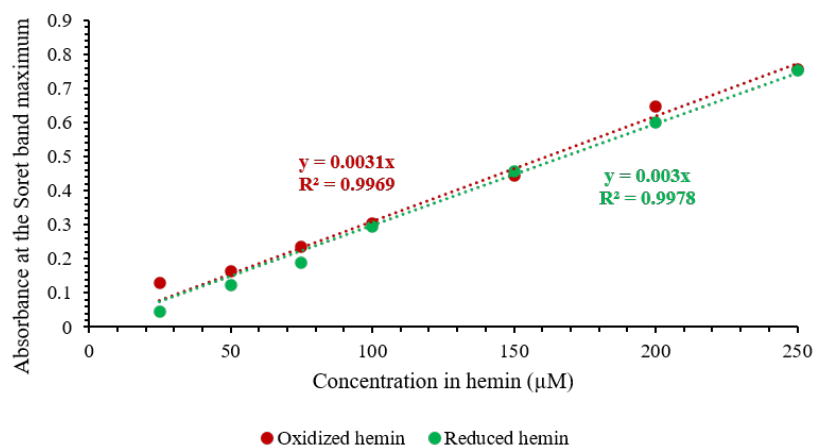


FIGURE C.2: Calibration line for absorbance of free hemin in phosphate buffer (with 5 mM DTT for reduced hemin and without for oxidized hemin) measured at the maximum of the Soret band.

C.2 UV-Visible absorption spectroscopy analyses of lability in hIDO1 at 25 °C

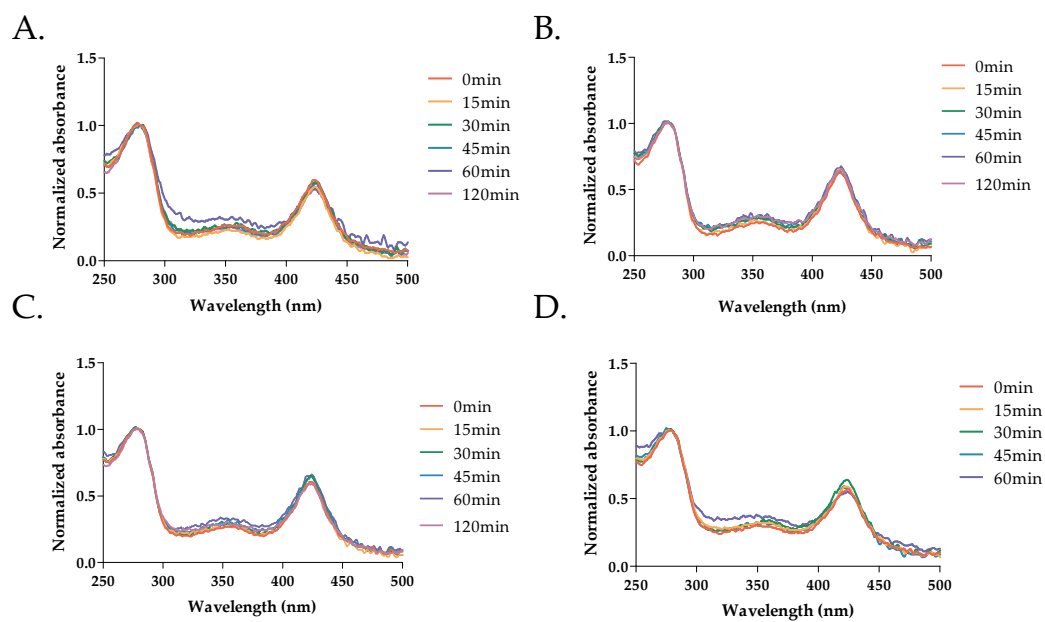


FIGURE C.3: Re-incorporation experiment in hIDO1 of reduced hemin at 25 degrees and for a final protein concentration of 25 μM . A. Spectrum with 25 μM of hemin. B. Spectrum with 75 μM of hemin. C. Spectrum with 100 μM of hemin. D. Spectrum with 125 μM of hemin.

C.3 UV-Visible absorption spectroscopy analyses of lability in hIDO2 at 25 °C

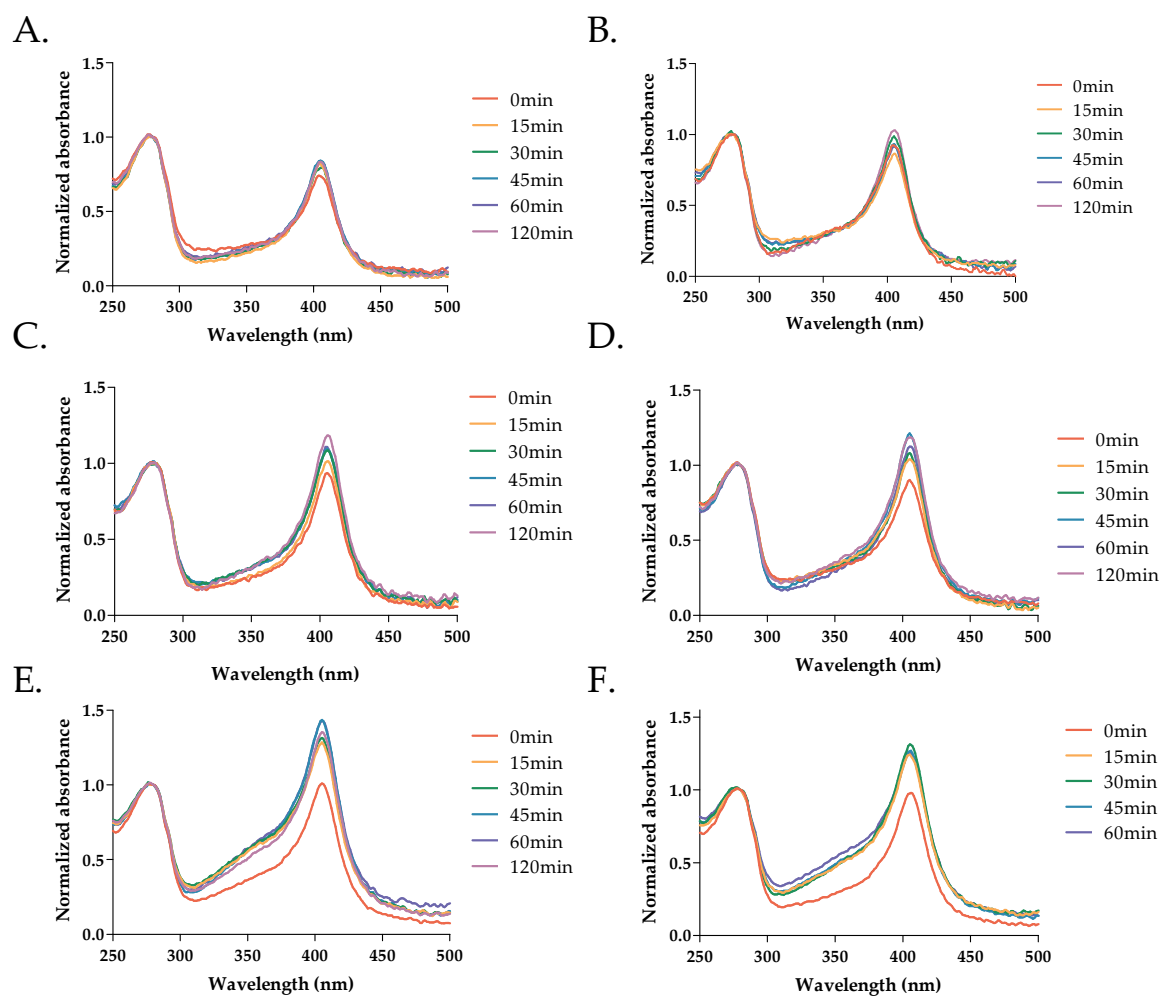


FIGURE C.4: Re-incorporation experiment in hIDO1 of oxidized hemin at 25 degrees and for a final protein concentration of 25 μM . A. Reference spectrum without addition of hemin. B. Spectrum with 25 μM of hemin. C. Spectrum with 75 μM of hemin. E. Spectrum with 100 μM of hemin. F. Spectrum with 125 μM of hemin.

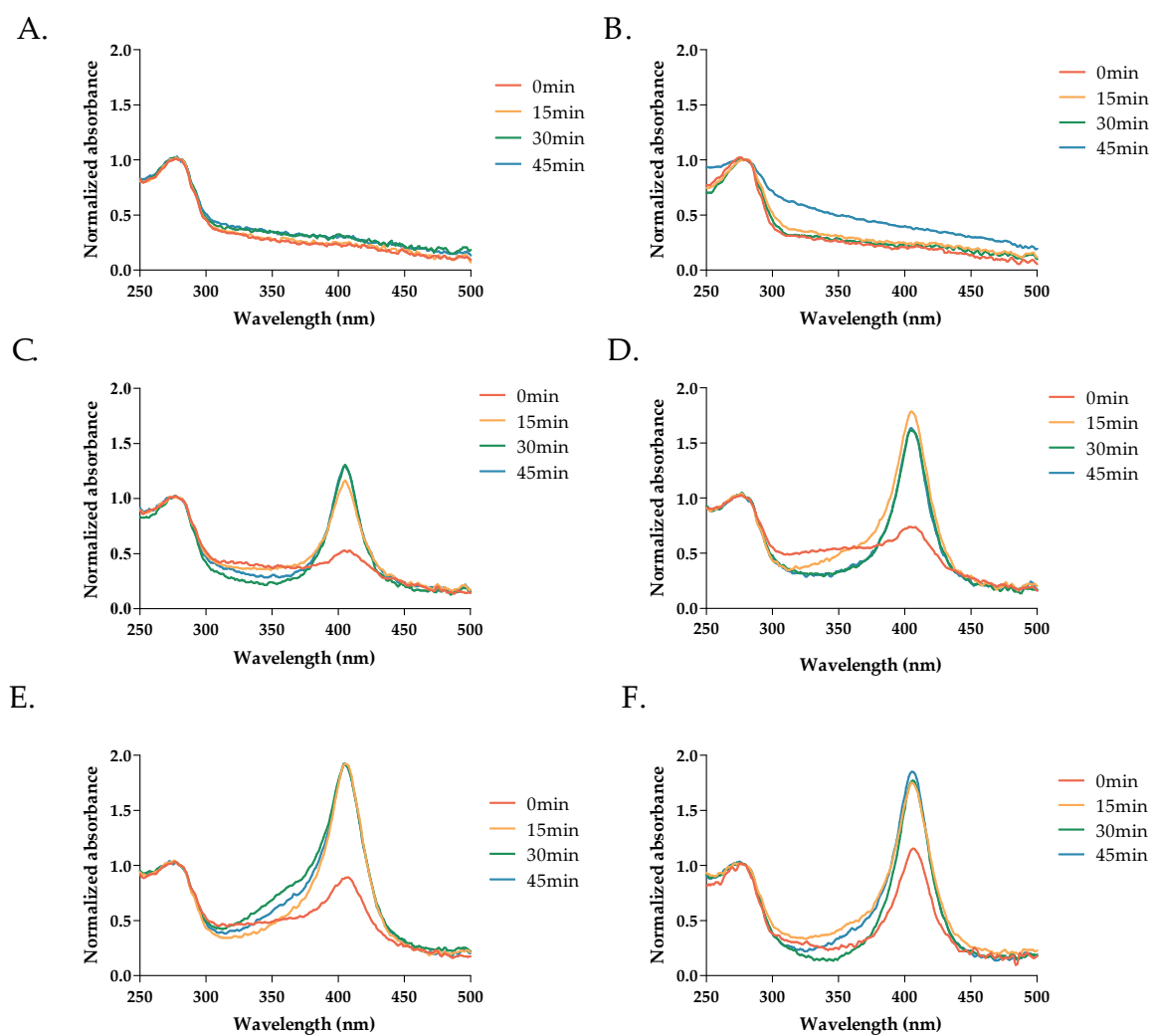


FIGURE C.5: Re-incorporation experiment in hIDO2 of oxidized hemin at 25 degrees and for a final protein concentration of 20 μM . A. Reference spectrum without addition of hemin. B. Spectrum with 25 μM of hemin. C. Spectrum with 50 μM of hemin. D. Spectrum with 75 μM of hemin. E. Spectrum with 100 μM of hemin. F. Spectrum with 125 μM of hemin.

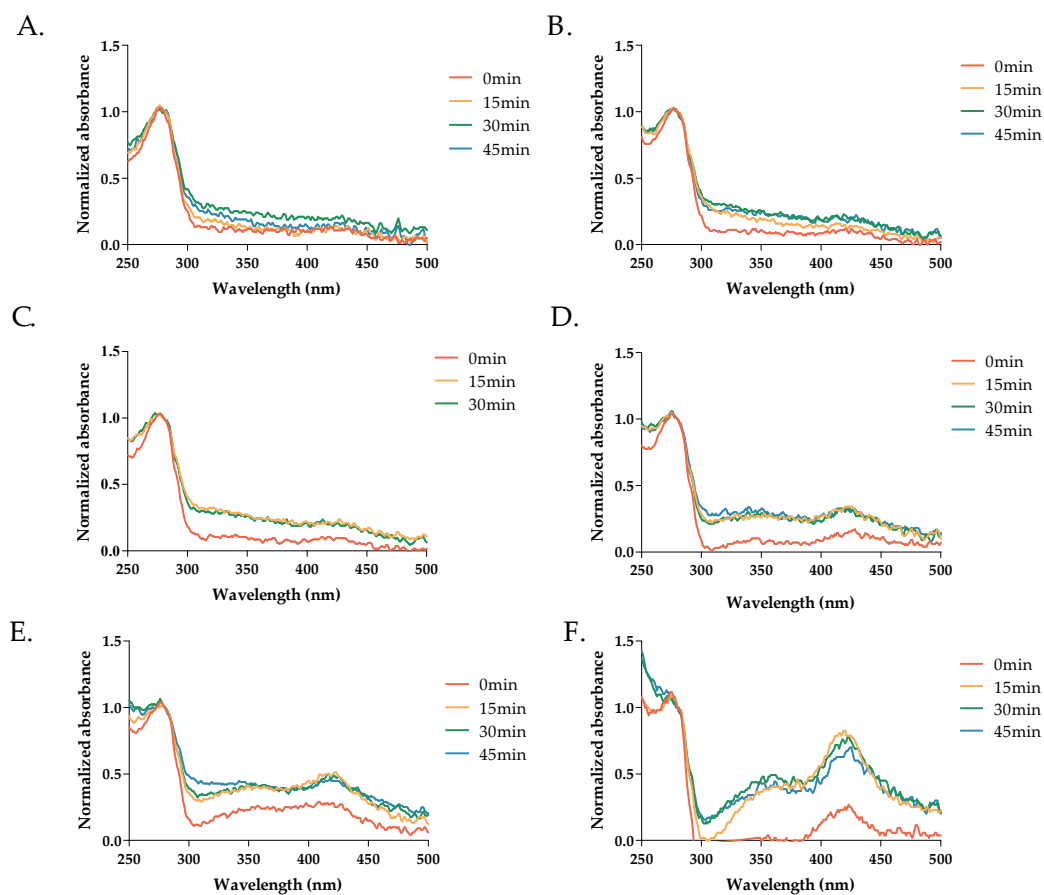


FIGURE C.6: Re-incorporation experiment in hIDO2 of reduced hemin at 25 degrees and for a final protein concentration of 25 μM . A. Reference spectrum without addition of hemin. B. Spectrum with 25 μM of hemin. C. Spectrum with 50 μM of hemin. D. Spectrum with 75 μM of hemin. E. Spectrum with 100 μM of hemin. F. Spectrum with 125 μM of hemin.

Appendix D

Comprehensive study of hIDO1 plasticity: Supporting information

D.1 JK-loop plasticity study by means of crystallographic snapshots

This section contains additional information to chapter 6.

D.1.1 JK-loop behavior without ligand in the active site

Data-collection and refinement statistics of structure 7a62

TABLE D.1: Data collection and refinement statistics for crystal structure 7a62. Values in parentheses are for the highest resolution shell.

PDB code	7A62
Data collection	
Wavelength (Å)	0.979
Resolution (Å)	49.18-2.44 (2.53-2.44)
Space group	$P2_12_12$
a, b, c (Å)	80.96 117.95 216.41
α, β, γ (°)	90 90 90
Total reflections	1067214 (93823)
Unique reflections	77982 (4879)
R_{merge}	0.1677 (1.828)
R_{meas}	0.1742 (1.907)
$CC_{1/2}$	0.998 (0.753)
CC^*	1 (0.927)
I/σ (I)	8.81 (0.84)
Completeness (%)	84.0 (98.0)
Multiplicity	13.7 (12.4)
Wilson B-factor (Å^2)	38.98
Refinement	
No. of reflections	65724 (4878)
No. of reflection used for R_{free}	3301 (255)
R_{work}	0.2118 (0.3717)
R_{free}	0.2579 (0.4351)
CC(work)	0.941 (0.665)
CC(free)	0.923 (0.745)

TABLE D.2: Data collection and refinement statistics (continued) for crystal structure 7a62. Values in parentheses are for the highest resolution shell.

PDB code	7A62
No. of non-hydrogen atoms	
Total	12873
Protein	11962
Ligands/ions	216
Protein residues	1533
B factors (\AA^2)	
Overall	39.83
Protein	39.71
Ligands/ions	45.98
Water	40.14
R.M.S deviations	
Bond lengths (\AA)	0.014
Bond angles ($^\circ$)	1.05
Ramachandran plot	
Favored (%)	96
Allowed (%)	3.7
Outliers (%)	0.33
Rotamers outliers (%)	1.3
Clash score	6.46

Interaction in the different dimerization interface

TABLE D.3: Distances involved in dimeric interaction in the small unit of structure 7a62.

Dimerization interface	Monomer	Amino acids (atoms)	Monomer	Amino acids (atoms)	Distances (\AA)
P104-E119	A	D68 (OD2)	D	M64 (SD)	3.9
	A	M64 (SD)	D	D68 (OD1)	3.8
	A	M64 (SD)	D	D68 (OD2)	3.6
	A	D68 (OD2)	D	R105 (NH2)	3.9
	A	Q113 (NE2)	D	Q113 (OE1)	3.8
	A	Q113 (OE1)	D	Q113 (NE2)	3.9
	A	K257 (NZ)	D	E119 (OE1)	3.6
	A	K257 (NZ)	D	E119 (OE2)	3.6

TABLE D.4: Distances involved in dimeric interaction in the small unit of structure 7a62. (continued)

Dimerization interface	Monomer	Amino acids (atoms)	Monomer	Amino acids (atoms)	Distances (Å)
Y36-H45 and Q54-K61	A	N37 (OD1)	D	R58 (NH2)	2.6
	A	D38 (OD1)	D	W609 (O)	2.7
	D	W609 (O)	D	R58 (NH2)	3.6
	D	W609 (O)	D	Q54 (OE1)	2.3
	D	W608 (O)	D	R58 (NH1)	2.3
	D	W608 (O)	D	E57 (OE2)	2.9
	D	R58 (NH1)	D	E57 (OE2)	4.2
	A	R58 (NH1)	D	E57 (OE1)	2.9
	A	R58 (NH1)	D	E57 (OE2)	3.4
	A	R58 (NH2)	D	E57 (OE1)	2.3
	A	R58 (NH2)	D	E57 (OE2)	3.5
	D	E57 (OE1)	D	K61 (NZ)	3.0

Volume of pocket B as induced by the conformation of the JK-loop in 7a62

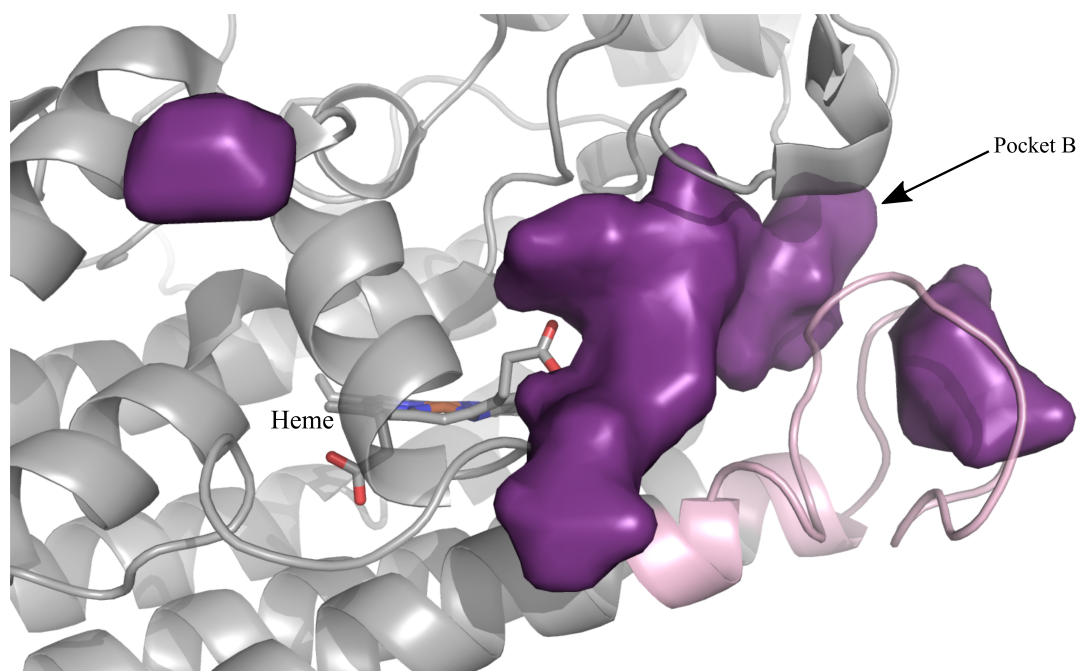


FIGURE D.1: Volume of the pocket B resulting from the JK-loop conformation. The cavities were generated using the POCASA 1.1. server [1].

TABLE D.5: Distances involved in dimeric interaction in the large unit from structure 7a62.

Dimerization interface	Monomer	Amino acids (atoms)	Monomer	Amino acids (atoms)	Distances (Å)
Helix D	A	D219 (OD1)	A	W613 (O)	2.4
	A	D219 (OD1)	A	W745 (O)	3.7
	A	D219 (OD2)	A	W745 (O)	3.8
	A	D219 (OD1)	A	W735 (O)	2.4
	A	W745 (O)	D	W735 (O)	3.4
	A	W745 (O)	D	W718 (O)	2.2
	D	W718 (O)	D	H220 (O)	3.6
	A	D219 (OD2)	D	W621 (O)	3.5
	D	W612 (O)	D	W718 (O)	3.6
	A	W612 (O)	D	H218 (O)	2.4
	A	W612 (O)	D	E146 (OE2)	3.2
	A	W612 (O)	D	H220 (NE2)	3.2
	D	W614 (O)	D	E146 (OE1)	2.4
	D	W614 (O)	D	E146 (OE2)	2.6
	D	W614 (O)	D	W732 (O)	2.4
	D	W614 (O)	D	W603 (O)	2.5
	D	W603 (O)	D	H220 (NE2)	3.8
	A	H218 (NE2)	D	D219 (OD1)	3.8
	A	H218 (ND1)	D	D219 (OD2)	4.0
	A	H218 (ND1)	D	D219 (OD1)	4.1
A	H218 (NE2)	D	D219 (OD2)	4.9	
BC-loop and HI-loop	A	R193 (NH1)	A	D325 (OD1)	2.8
	A	R193 (NH1)	A	D325 (OD2)	3.3
	A	R193 (NE)	A	D325 (OD2)	2.7
	A	D325 (OD2)	C	R193 (NE)	4.7
	A	Q191 (OE1)	C	K323 (NZ)	4.1
	A	K323 (NZ)	C	Q191 (OE1)	4.3
	C	K323 (NZ)	C	Q191 (OE1)	4.1
	C	D325 (OD2)	C	R193 (NH1)	3.4
	C	D325 (OD1)	C	R193 (NH1)	2.9
	C	D325 (OD2)	C	R193 (NE)	2.7

D.1.2 JK-loop behavior in the presence of L-Trp in the active site

Data-collection and refinement statistics

TABLE D.6: Data-collection and refinement statistics for 7nge, 7p0r and 7p0n. Statistics for the highest-resolution shell are in parentheses.

		hIDO1-closed	hIDO1-intermediate	hIDO1-opened	
PDB code		7NGE	7P0R	7P0N	
Diffraction data	Resolution (Å)	46.87 - 2.30 (2.38 - 2.30)	49.22 - 2.5 (2.59 - 2.50)	46.84 - 2.50 (2.59 - 2.50)	
	Space group	P 21 21 2	P 21 21 2	P 21 21 2	
	a, b, c (Å)	81.36, 114.67, 219.67	80.89, 115.72, 217.53	81.36, 114.57, 220.98	
	α, β, γ (°)	90, 90, 90	90, 90, 90	90, 90, 90	
	Total reflections	1120575 (103662)	829135 (84007)	503416 (44769)	
	Unique reflections	91724 (8917)	71454 (7008)	71786 (7022)	
	CC1/2	0.998 (0.541)	0.997 (0.59)	0.995 (0.606)	
	CC*	0.999 (0.838)	0.999 (0.861)	0.999 (0.869)	
	I/ σ	10.43 (0.97)	7.21 (0.79)	6.70 (0.95)	
	Completeness (%)	99.56 (97.63)	99.65 (99.42)	99.34 (97.88)	
	Multiplicity	12.2 (11.6)	11.6 (12.0)	7.0 (6.4)	
	Wilson B factor	46.97	54.62	52.26	
	Refinement	No. of reflections	91721 (8849)	71273 (6995)	71579 (6965)
		No. of reflections used for Rfree	1999 (194)	3560 (350)	3582 (348)
Rwork		0.2147 (0.3644)	0.2185 (0.3723)	0.2151 (0.3738)	
Rfree		0.2702 (0.3770)	0.2855 (0.4251)	0.2794 (0.4137)	
CC(work)		0.956 (0.765)	0.967 (0.814)	0.961 (0.787)	
CC(free)		0.954 (0.870)	0.953 (0.620)	0.937 (0.616)	
B factors	Overall	54.55	61.98	58.73	
	Macromolecule	53.94	61.67	58.28	
	Ligands/ions	60.59	69.62	65.99	
	Water	60.84	63.81	63.07	
R.m.s. deviations	Bond lengths (Å)	0.010	0.009	0.009	
	Bond angles (°)	1.12	1.08	1.13	
Rama. plot	Favored (%)	94.28	94.18	94.05	
	Allowed (%)	5.32	5.69	5.82	
	Outliers (%)	0.40	0.13	0.14	
Rotamer (%) outliers	0.16	0.70	0.55		
Clashscore	8.87	8.73	7.86		

Relatives positions of L-Trp

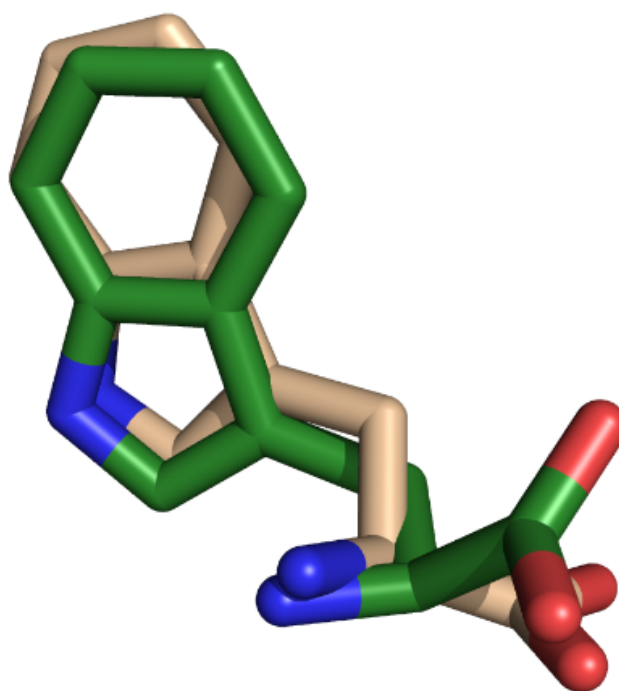


FIGURE D.2: Alignment of L-Trp in the hIDO1-closed structure (in green) with the structure from Luo *et al* (in wheat, PDB code: 6e46).

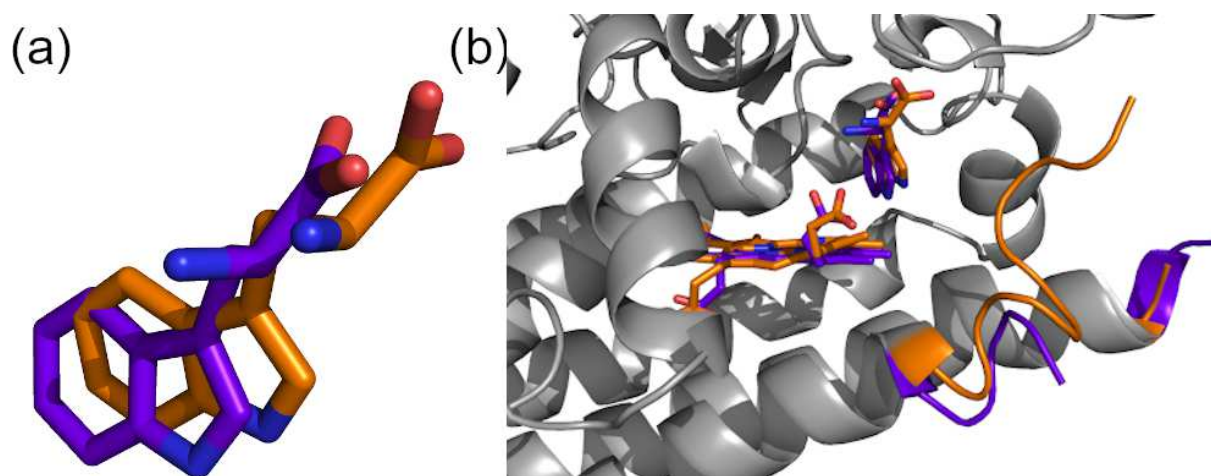


FIGURE D.3: Alignment of L-Trp in the hIDO1-intermediate structure (in orange) with the structure from Pharm *et al.* (in purple, PDB code : 6ubp). (a) Comparison of the position of L-Trp after alignment of the two structures (b) JK-loop conformation in the two structures.

D.1.3 JK-loop behavior in the presence of L-Kynurenine

Data-collection and refinement statistics of structure 7z12

TABLE D.7: Data collection and refinement statistics for crystal structure 7zl2. Values in parentheses are for the highest resolution shell.

PDB code	7zl2
Data collection - Resolution (Å)	47.23 - 2.56 (2.65 - 2.56)
Space group	$P2_12_12$
a, b, c (Å)	81 116.28 217.59
α , β , γ (°)	90 90 90
Total reflections	904254 (82903)
Unique reflections	66614 (6308)
CC _{1/2}	0.998 (0.855)
CC*	0.999 (0.96)
I/ σ (I)	13.33 (2.22)
Completeness (%)	99.18 (93.96)
Multiplicity	13.6 (13.1)
Wilson B-factor (Å ²)	42.15
Refinement - No. of reflections	66416 (6228)
No. of reflection used for R _{free}	3316 (309)
R _{work}	0.1802 (0.2795)
R _{free}	0.2441 (0.3263)
CC(work)	0.972 (0.909)
CC(free)	0.945 (0.847)
No. of non-hydrogen atoms - Total	13073
Protein	11903
Ligands/ions	266
Protein residues	1500
B factors (Å ²) - Overall	46.40
Protein	45.92
Ligands/ions	53.53
Water	50.74
R.M.S deviations	
Bond lengths (Å)	0.009
Bond angles (°)	1.00
Ramachandran plot - Favored (%)	95.47
Outliers (%)	0.14
Rotamers outliers (%)	0.62
Clash score	7.20

D.2 The JK-loop plasticity study by MD from crystallography snapshots

This section provides additional information to chapter 7.

D.2.1 JK-loop behavior without ligand in the active site

Structural comparison of the holo/apo form

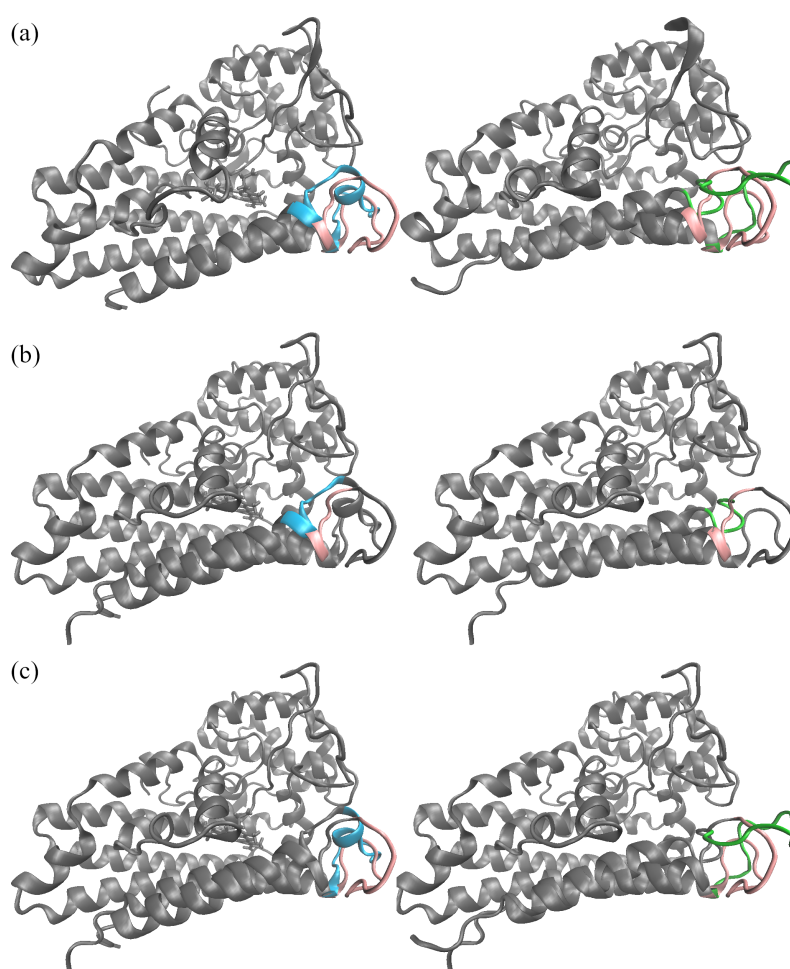


FIGURE D.4: Superimposition of the crystal (pink), MD simulation with the heme cofactor at $t = 200$ ns (cyan), and MD simulation structure without the heme cofactor at $t = 200$ ns (green) (a) Overall view (b) C-terminal part of the JK-loop (E375 to G380) (c) N-terminal part of the JK-loop (Q360 to E374).

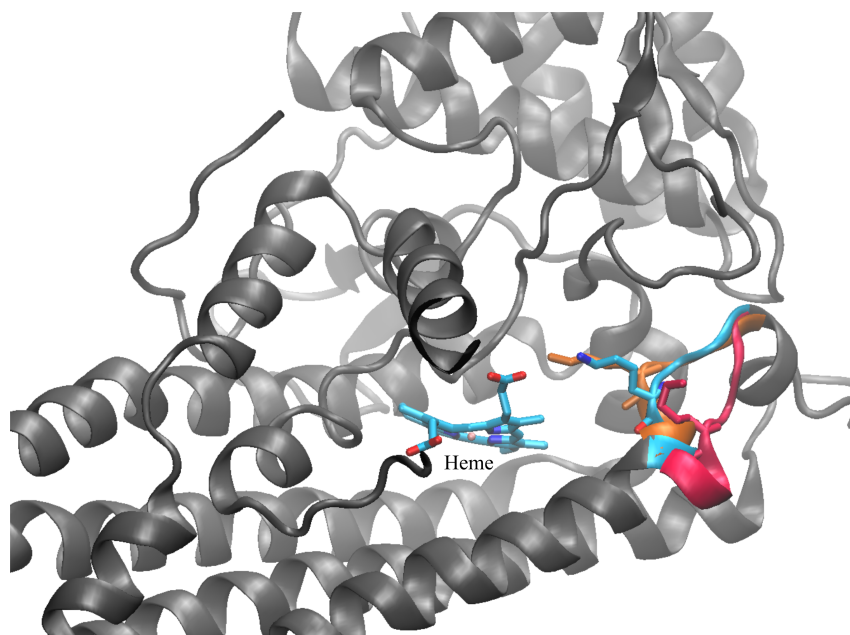


FIGURE D.5: Superimposition of different locations of K377 obtained from the MD simulation with the heme cofactor. Conformations are clustered in three groups: closed (in orange, the distance between K377 and A264 varies from 6 Å to 10 Å, 16.1% of the conformations), intermediate (in cyan, the distance between K377 and A264 varies from 10 Å to 16 Å, 79.3% of the conformations) and open (in red, the distance between K377 and A264 is larger than 16 Å, 4.6% of the conformations). Percentages were calculated over a 200 ns MD simulation at 300 K and 1 bar.

D.2.2 JK-loop behavior with NFK in the active site

TABLE D.8: Distances between K377 or T379 and the ligand or cofactor. The analysis was performed from the 300 ns MD simulations at 310 K and 1 bar, for each replicate.

Distances	Replicate 1	Replicate 2	Replicate 3
K377 (N) - NFK (O1)	13.5 ± 1.4	15.6 ± 2.6	16.0 ± 2.1
K377 (N) - NFK (O2)	14.5 ± 1.5	17.3 ± 2.6	16.1 ± 2.4
T379 (O) - NFK (O1)	12.4 ± 1.5	19.4 ± 2.2	18.7 ± 1.5
T379 (O) - NFK (O2)	13.0 ± 1.5	21.1 ± 2.1	18.7 ± 1.9
T379 (O) - NFK (N)	11.4 ± 1.9	18.5 ± 2.1	17.3 ± 1.5
K377 (N) - Heme (O1)	17.1 ± 1.1	17.5 ± 2.2	17.1 ± 2.3
K377 (N) - Heme (O2)	17.4 ± 1.3	18.1 ± 2.2	17.1 ± 2.3
T379 (N) - Heme (O1)	11.7 ± 1.5	17.7 ± 1.9	17.2 ± 1.5
T379 (N) - Heme (O2)	12.0 ± 2.1	18.4 ± 2.0	16.1 ± 1.1

D.3 G261 to G265 as sensor of ligand entrance

TABLE D.9: Mean correlation coefficient observed in ferric active sites in presence of substrates for structures with two monomers in the asymmetric unit.

Kind of ligands	PDB code	Resolution (Å)	CC for monomer A	CC for monomer B
O ₂	6mq6	3.1 [2]	0.89 ± 0.11	0.91 ± 0.03
	6dpq ³	2.9 [2]	0.94 ± 0.04	0.92 ± 0.03
CN	2d0u	2.3 [3]	0.91 ± 0.01	0.89 ± 0.04
TRP	6ubp	3.0 [4]	0.94 ± 0.02	0.93 ± 0.01
	6e35	2.8	0.93 ± 0.01	0.93 ± 0.01
	6cxv	2.6 [5]	0.96 ± 0.01	0.96 ± 0.01
	6cxu ⁵	2.5 [5]	0.95 ± 0.01	0.95 ± 0.01
	5wmx	2.7 [6]	0.93 ± 0.01	0.93 ± 0.02
	5wmw	3.0 [6]	0.94 ± 0.01	0.92 ± 0.03
	5wmv	2.6 [6]	0.95 ± 0.01	0.96 ± 0.01
	5wmu	2.4 [6]	0.97 ± 0.01	0.96 ± 0.02

TABLE D.10: Mean correlation coefficient observed in ferric active sites in presence of apo inhibitors for structures with two monomers in the asymmetric unit.

PDB code	Resolution (Å)	Ligand code	CC for monomer A	CC for monomer B
7rrc	2.2 [7]	6RI	0.93 ± 0.02	0.91 ± 0.04
7rrb	2.7 [7]	6ZI	0.93 ± 0.02	0.93 ± 0.03
7b1o	2.6 [8]	SLW	0.94 ± 0.03	0.94 ± 0.02
7m63	3.1 [8]	YRP	0.88 ± 0.03	0.91 ± 0.02
6x5y	2.7	URJ	0.91 ± 0.03	0.92 ± 0.03
6wpe	2.4 [9]	UG6	0.95 ± 0.01	0.95 ± 0.02
6wjy	1.9 [10]	U41	0.95 ± 0.01	0.95 ± 0.02
6v52	1.8 [11]	QPV	0.95 ± 0.01	0.94 ± 0.01
6mq6	3.1 [2]	H7P	0.89 ± 0.11	0.91 ± 0.03
6dpr ¹	3.2 [2]	H7P	0.93 ± 0.02	0.91 ± 0.03
6dpq	2.9 [2]	GOL, H7P	0.94 ± 0.04	0.92 ± 0.03
6azw	2.8 [12]	C51	0.93 ± 0.02	0.93 ± 0.04

TABLE D.11: Mean correlation coefficient observed in ferric active sites in presence of holo inhibitors for structures with two monomers in the asymmetric unit.

PDB code	Resolution (Å)	Ligand code	CC for monomer A	CC for monomer B
6pz1 ¹	2.7 [13]	AOJ	0.94 ± 0.02	0.96 ± 0.01
5whr ¹	2.3 [14]	AOJ	0.96 ± 0.01	0.96 ± 0.01
6pu7	2.4 [15]	OY4	0.94 ± 0.02	0.94 ± 0.01
5wn8	2.5 [6]	BBJ	0.92 ± 0.02	0.93 ± 0.02
5xe1	3.2 [16]	IUU	0.96 ± 0.02	0.96 ± 0.01
7m7d	2.6 [8]	YRM	0.95 ± 0.02	0.93 ± 0.03
7e0u	2.3 [17]	HUC	0.96 ± 0.02	0.96 ± 0.01
7e0t	2.3 [17]	HU9	0.93 ± 0.01	0.93 ± 0.03
7e0s	2.7 [17]	HU6	0.96 ± 0.01	0.95 ± 0.01
7e0q	2.5 [17]	HU3	0.95 ± 0.02	0.95 ± 0.03
7e0p	2.6 [17]	HU0	0.94 ± 0.02	0.95 ± 0.02
7e0o	3.3 [17]	HS0	0.94 ± 0.02	0.93 ± 0.03
6o3i	2.7 [18]	LKP	0.96 ± 0.02	0.95 ± 0.02
5etw	2.7 [19]	XNL	0.91 ± 0.04	0.93 ± 0.01
5ek4	2.6 [19]	5PF	0.93 ± 0.03	0.94 ± 0.01
5ek3	2.2 [19]	5PK	0.95 ± 0.02	0.94 ± 0.01
5ek2	2.7 [19]	5PJ	0.93 ± 0.03	0.92 ± 0.03
4u74 ²	2.3	PIM	0.97 ± 0.01	0.97 ± 0.01
4u72 ³	2.0	PIM	0.97 ± 0.01	0.97 ± 0.01
2d0t	3.4 [3]	PIM	0.98 ± 0.01	0.97 ± 0.01
7ah6	3.0 [20]	RCW	0.94 ± 0.02	0.91 ± 0.01
7ah5	2.9 [20]	RCQ	0.94 ± 0.02	0.94 ± 0.03
7ah4	2.4 [20]	RCN	0.95 ± 0.02	0.95 ± 0.02
6r63	2.9 [21]	JTB	0.92 ± 0.02	0.91 ± 0.04
6f0a	2.3 [22]	C82	0.96 ± 0.01	0.96 ± 0.01
6kw7	3.0 [23]	DYC	0.89 ± 0.01	0.92 ± 0.04
6kps	2.3 [23]	DU6	0.95 ± 0.02	0.94 ± 0.01
6kof	2.3 [23]	D09	0.95 ± 0.02	0.93 ± 0.02
4pk6	2.8 [24]	PKL	0.93 ± 0.01	0.91 ± 0.03
4pk5	3.5 [24]	PKJ	0.95 ± 0.02	0.95 ± 0.02

Bibliography

- [1] Y. J. Yu, I. Zhou, and M. Yao Tanaka. Roll: A new algorithm for the detection of protein pockets and cavities with a rolling probe sphere. *Bioinformatics*, 26(1):46–52, 2010.

TABLE D.12: Mean correlation coefficient observed in ferric active sites for structures with four monomers in the asymmetric unit.

PDB code	Resolution (Å)	Ligand code	CC for monomer A	CC for monomer B	CC for monomer C	CC for monomer D
6e44 ¹	1.9 [25]	No ligand	0.92 ± 0.02	0.88 ± 0.04	0.94 ± 0.01	0.86 ± 0.04
6e40	2.7 [25]	No ligand	0.90 ± 0.02	0.93 ± 0.02	0.88 ± 0.05	0.93 ± 0.03
6azu	2.8 [12]	No ligand	0.92 ± 0.02	0.93 ± 0.03	0.90 ± 0.01	0.91 ± 0.02
6e43	1.7 [25]	HQM (apo)	0.96 ± 0.01	0.96 ± 0.01	0.96 ± 0.01	0.97 ± 0.01
6azv	2.8 [12]	C4V (apo)	0.93 ± 0.02	0.93 ± 0.04	0.73 ± 0.06	0.92 ± 0.02
6e40	2.7 [25]	BBJ (holo)	0.90 ± 0.02	0.93 ± 0.02	0.88 ± 0.05	0.92 ± 0.03
6e41	2.1 [25]	HQJ (holo)	0.93 ± 0.01	0.93 ± 0.03	0.94 ± 0.01	0.92 ± 0.04
6e42	2.1 [25]	HQJ (holo)	0.96 ± 0.01	0.96 ± 0.02	0.96 ± 0.01	0.95 ± 0.03

- [2] K. N. Pham and S.-R. Yeh. Mapping the binding trajectory of a suicide inhibitor in human indoleamine 2, 3-dioxygenase 1. *Journal of the American Chemical Society*, 140(44):14538–14541, 2018.
- [3] H. Sugimoto, S.-i. Oda, T. Otsuki, T. Hino, T. Yoshida, and Y. Shiro. Crystal structure of human indoleamine 2, 3-dioxygenase: catalytic mechanism of o₂ incorporation by a heme-containing dioxygenase. *Proceedings of the National Academy of Sciences*, 103(8):2611–2616, 2006.
- [4] K. N. Pham, A. Lewis-Ballester, and S.-R. Yeh. Conformational plasticity in human heme-based dioxygenases. *Journal of the American Chemical Society*, 143(4):1836–1845, 2020.
- [5] A. Lewis-Ballester, S. Karkashon, D. Batabyal, T. L. Poulos, and S.-R. Yeh. Inhibition mechanisms of human indoleamine 2, 3 dioxygenase 1. *Journal of the American Chemical Society*, 140(27):8518–8525, 2018.
- [6] A. Lewis-Ballester, K. N. Pham, D. Batabyal, S. Karkashon, J. B. Bonanno, T. L. Poulos, and S.-R. Yeh. Structural insights into substrate and inhibitor binding sites in human indoleamine 2, 3-dioxygenase 1. *Nature communications*, 8(1):1–8, 2017.
- [7] D. Li, D. L. Sloman, A. Achab, H. Zhou, M. A. McGowan, C. White, C. Gibeau, H. Zhang, Q. Pu, I. Bharathan, et al. Oxetane promise delivered: Discovery of

- long-acting ido1 inhibitors suitable for q3w oral or parenteral dosing. *Journal of Medicinal Chemistry*, 2022.
- [8] M. M. Hamilton, F. Mseeh, T. J. McAfoos, P. G. Leonard, N. J. Reyna, A. L. Harris, A. Xu, M. Han, M. J. Soth, B. Czako, et al. Discovery of iacs-9779 and iacs-70465 as potent inhibitors targeting indoleamine 2, 3-dioxygenase 1 (ido1) apoenzyme. *Journal of Medicinal Chemistry*, 64(15):11302–11329, 2021.
- [9] D. Li, Y. Deng, A. Achab, I. Bharathan, B. A. Hopkins, W. Yu, H. Zhang, S. Sanyal, Q. Pu, H. Zhou, et al. Carbamate and n-pyrimidine mitigate amide hydrolysis: structure-based drug design of tetrahydroquinoline ido1 inhibitors. *ACS Medicinal Chemistry Letters*, 12(3):389–396, 2021.
- [10] Q. Pu, H. Zhang, L. Guo, M. Cheng, A. C. Doty, H. Ferguson, X. Fradera, C. A. Lesburg, M. A. McGowan, J. R. Miller, et al. Discovery of potent and orally available bicyclo [1.1. 1] pentane-derived indoleamine-2, 3-dioxygenase 1 (ido1) inhibitors. *ACS Medicinal Chemistry Letters*, 11(8):1548–1554, 2020.
- [11] C. White, M. A. McGowan, H. Zhou, N. Sciammetta, X. Fradera, J. Lim, E. M. Joshi, C. Andrews, E. B. Nickbarg, P. Cowley, et al. Strategic incorporation of polarity in heme-displacing inhibitors of indoleamine-2, 3-dioxygenase-1 (ido1). *ACS medicinal chemistry letters*, 11(4):550–557, 2020.
- [12] M. T. Nelp, P. A. Kates, J. T. Hunt, J. A. Newitt, A. Balog, D. Maley, X. Zhu, L. Abell, A. Allentoff, R. Borzilleri, et al. Immune-modulating enzyme indoleamine 2, 3-dioxygenase is effectively inhibited by targeting its apo-form. *Proceedings of the National Academy of Sciences*, 115(13):3249–3254, 2018.
- [13] K. N. Pham, A. Lewis-Ballester, and S.-R. Yeh. Structural basis of inhibitor selectivity in human indoleamine 2, 3-dioxygenase 1 and tryptophan dioxygenase. *Journal of the American Chemical Society*, 141(47):18771–18779, 2019.
- [14] S. Crosignani, P. Bingham, P. Bottemanne, H. Cannelle, S. Cauwenberghs, M. Cordonnier, D. Dalvie, F. Deroose, J. L. Feng, B. Gomes, et al. Discovery of a novel and selective indoleamine 2, 3-dioxygenase (ido-1) inhibitor 3-(5-fluoro-1 h-indol-3-yl) pyrrolidine-2, 5-dione (eos200271/pf-06840003) and its characterization as a potential clinical candidate. *Journal of Medicinal Chemistry*, 60(23):9617–9629, 2017.

- [15] H. Zhang, K. Liu, Q. Pu, A. Achab, M. J. Ardolino, M. Cheng, Y. Deng, A. C. Doty, H. Ferguson, X. Fradera, et al. Discovery of amino-cyclobutarene-derived indoleamine-2, 3-dioxygenase 1 (ido1) inhibitors for cancer immunotherapy. *ACS medicinal chemistry letters*, 10(11):1530–1536, 2019.
- [16] Y. Wu, T. Xu, J. Liu, K. Ding, and J. Xu. Structural insights into the binding mechanism of ido1 with hydroxylamide based inhibitor incb14943. *Biochemical and Biophysical Research Communications*, 487(2):339–343, 2017.
- [17] X.-L. Ning, Y.-Z. Li, C. Huo, J. Deng, C. Gao, K.-R. Zhu, M. Wang, Y.-X. Wu, J.-L. Yu, Y.-L. Ren, et al. X-ray structure-guided discovery of a potent, orally bioavailable, dual human indoleamine/tryptophan 2, 3-dioxygenase (hido/htdo) inhibitor that shows activity in a mouse model of parkinson’s disease. *Journal of Medicinal Chemistry*, 64(12):8303–8332, 2021.
- [18] S. Kumar, J. P. Waldo, F. A. Jaipuri, A. Marcinowicz, C. Van Allen, J. Adams, T. Kesharwani, X. Zhang, R. Metz, A. J. Oh, et al. Discovery of clinical candidate (1 r, 4 r)-4-((r)-2-((s)-6-fluoro-5 h-imidazo [5, 1-a] isoindol-5-yl)-1-hydroxyethyl) cyclohexan-1-ol (navoximod), a potent and selective inhibitor of indoleamine 2, 3-dioxygenase 1. *Journal of Medicinal Chemistry*, 62(14):6705–6733, 2019.
- [19] Y.-H. Peng, S.-H. Ueng, C.-T. Tseng, M.-S. Hung, J.-S. Song, J.-S. Wu, F.-Y. Liao, Y.-S. Fan, M.-H. Wu, W.-C. Hsiao, et al. Important hydrogen bond networks in indoleamine 2, 3-dioxygenase 1 (ido1) inhibitor design revealed by crystal structures of imidazoleisoindole derivatives with ido1. *Journal of medicinal chemistry*, 59(1):282–293, 2016.
- [20] U. F. Röhrig, S. R. Majjigapu, A. Reynaud, F. Pojer, N. Dilek, P. Reichenbach, K. Ascencao, M. Irving, G. Coukos, P. Vogel, et al. Azole-based indoleamine 2, 3-dioxygenase 1 (ido1) inhibitors. *Journal of Medicinal Chemistry*, 64(4):2205–2227, 2021.
- [21] U. F. Röhrig, A. Reynaud, S. R. Majjigapu, P. Vogel, F. Pojer, and V. Zoete. Inhibition mechanisms of indoleamine 2, 3-dioxygenase 1 (ido1). *Journal of medicinal chemistry*, 62(19):8784–8795, 2019.
- [22] J. A. C. Alexandre, M. K. Swan, M. J. Latchem, D. Boyall, J. R. Pollard, S. W. Hughes, and J. Westcott. New 4-amino-1, 2, 3-triazole inhibitors of indoleamine 2,

- 3-dioxygenase form a long-lived complex with the enzyme and display exquisite cellular potency. *ChemBioChem*, 19(6):552–561, 2018.
- [23] Y.-H. Peng, F.-Y. Liao, C.-T. Tseng, R. Kuppusamy, A.-S. Li, C.-H. Chen, Y.-S. Fan, S.-Y. Wang, M.-H. Wu, C.-C. Hsueh, et al. Unique sulfur–aromatic interactions contribute to the binding of potent imidazothiazole indoleamine 2, 3-dioxygenase inhibitors. *Journal of Medicinal Chemistry*, 63(4):1642–1659, 2020.
- [24] S. Tojo, T. Kohno, T. Tanaka, S. Kamioka, Y. Ota, T. Ishii, K. Kamimoto, S. Asano, and Y. Isobe. Crystal structures and structure–activity relationships of imidazothiazole derivatives as ido1 inhibitors. *ACS medicinal chemistry letters*, 5(10):1119–1123, 2014.
- [25] S. Luo, K. Xu, S. Xiang, J. Chen, C. Chen, C. Guo, Y. Tong, and L. Tong. High-resolution structures of inhibitor complexes of human indoleamine 2, 3-dioxygenase 1 in a new crystal form. *Acta Crystallographica Section F: Structural Biology Communications*, 74(11):717–724, 2018.

Appendix E

**Comprehensive study of hIDO2
plasticity: Supporting
information**

E.1 Investigation of the hIDO2 structure by MD

This appendix contains additional information to chapter 7.

E.1.1 Study of the JK-loop in the absence of ligand in the active site

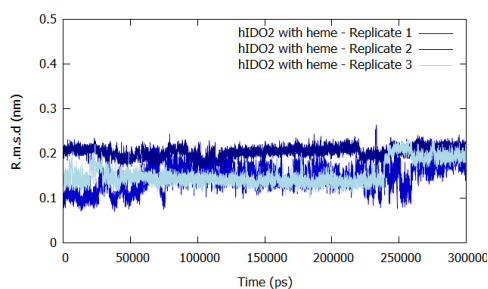


FIGURE E.1: R.m.s.d profiles of the fragment G265-Q270 into the different 300 ns MD replicates at 310 K and 1 bar.

E.1.2 Study of the JK-loop with M350I mutation

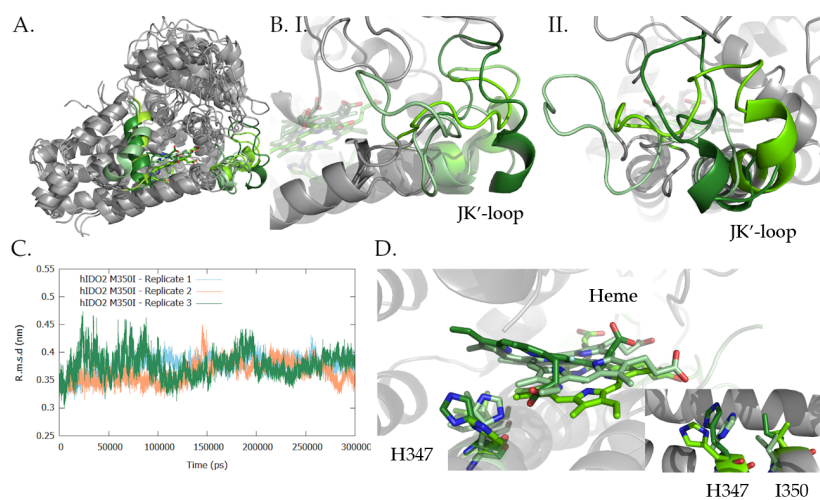


FIGURE E.2: Conformation of the protein after a 300 ns MD simulation at 310 K and 1 bar. A. Global folding. B. Structural divergence at the level of the JK'-loop (Two perpendicular views (I. and II.)). C. R.m.s.d profiles in comparison to the starting structure for each replicate. D. Structural divergence at the level of the heme cofactor, H347 and I350.

E.1.3 Influence of the polymorphism on the lability

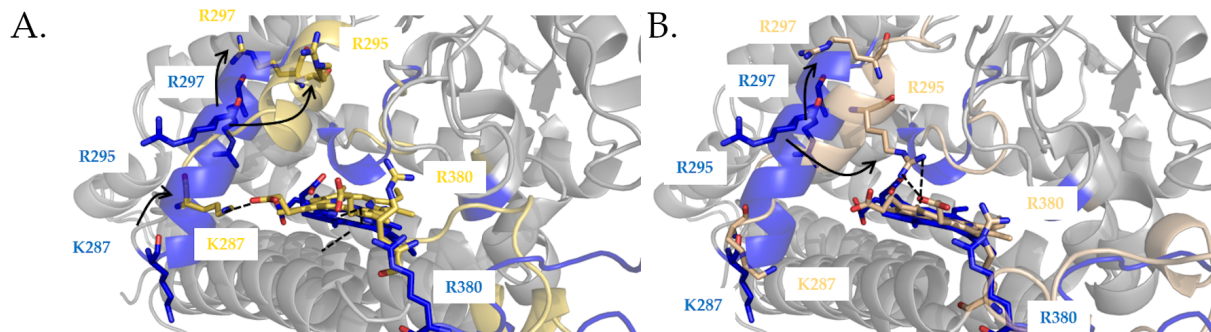


FIGURE E.3: Induced-fit caused by the R235W mutation in the F' helix. Conformation of the protein after a 300 ns MD simulation, at 310 K and 1 bar. A. For R1. B. For R2.

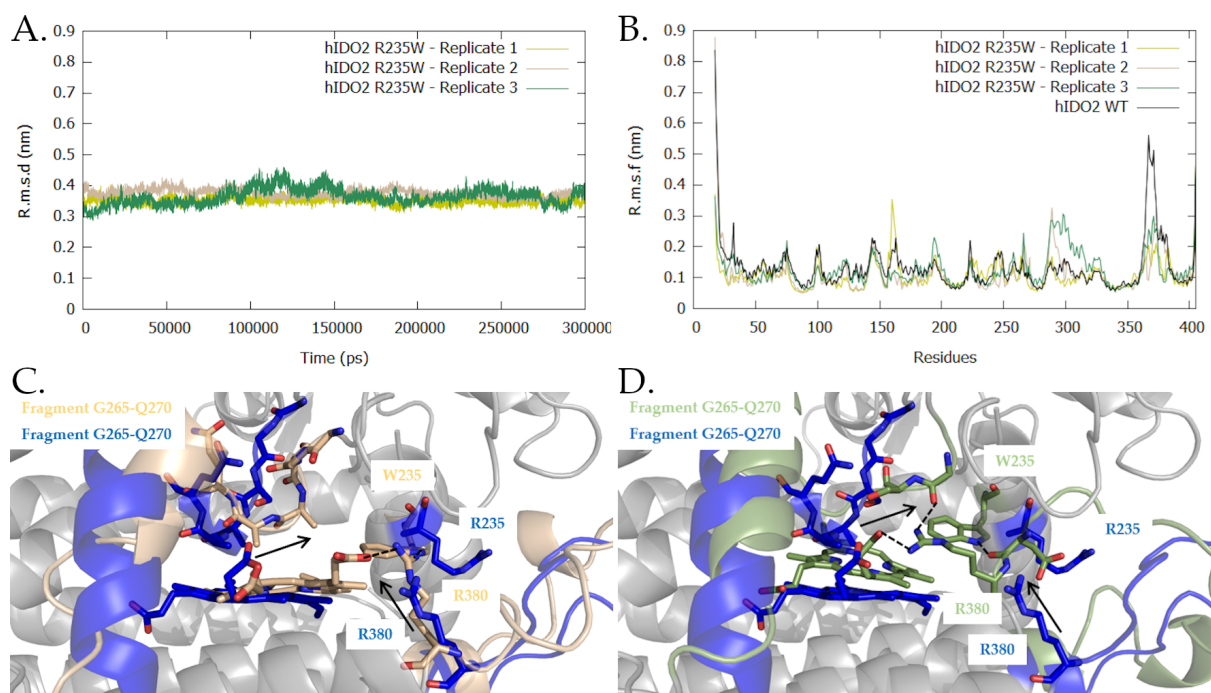


FIGURE E.4: Conformation of the R235W protein after a 300 ns MD simulation, at 310 K and 1 bar. A. R.m.s.d of the protein in comparison to the starting structure B. R.m.s.f profiles on the protein for the three replicates and comparison with WT protein. C. Induced-fit caused by the R235W mutation on the JK'-loop residues for R2. D. Induced-fit caused by the R235W mutation on the JK'-loop residues for R3.

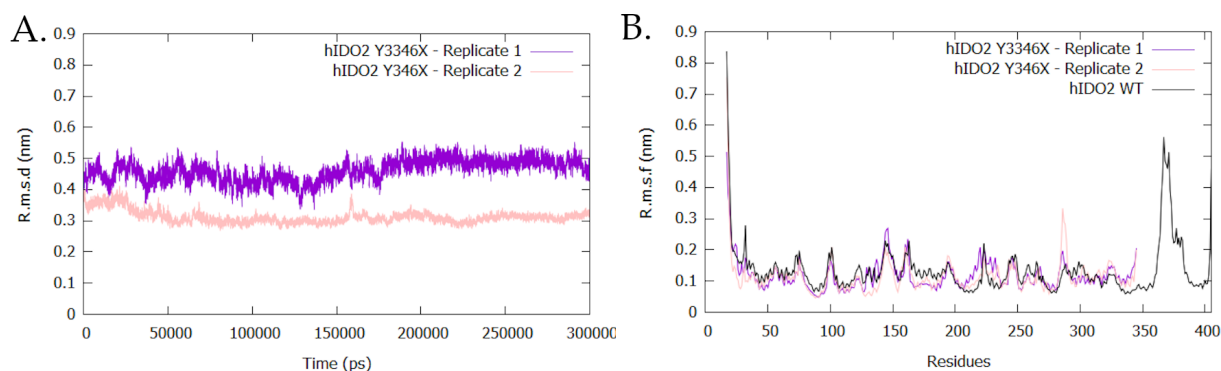


FIGURE E.5: Conformation of the Y346X protein after a 300 ns of MD simulation, at 310 K and 1 bar. A. R.m.s.d in comparison to the starting structure. B. R.m.s.f profiles on the protein residues for the three replicates and comparison with WT protein.

E.2 Polarity changes between hIDO1 and hIDO2 in the sequence alignment

Bibliography

- [1] F. Corpet. Multiple sequence alignment with hierarchical clustering. *Nucleic acids research*, 16(22):10881–10890, 1988.

```

      1      10      20      30      40      50
hIDO1  ...MAHAMENSWITSEYHIDEVGFALPNPQILPDPYIWMFIAKLP LITSGQLR
hIDO2  MPPFPNVKAVPLSLESYHISEEYGFLLPDSIKLPLDYRFWMIAKLP LITDAQLR
consensus>50 mepmahnvenavpiSLeSYHIdEEvGFLLP#ple#LPDfYndWMfIANhLP#LI#agQLq

      60      70      80      90      100     110
hIDO1  ERVEKLNMLSIDHLLHKSQRLLALVVLGCI TMAVYVWGKGGIVRKLPRNIAVPCQLSA
hIDO2  AIVDKMFLLSCOFLKGRQRLLALVVLGFI TMCYVWQGGGAPAVLPRNLAIPFVLSA
consensus>50 ehV#K$n$LSi#fLkdHkeQRLLhLVLGfiTMAVYVWqeGea#vaeVLPRNiAvP%v#vSa

      120     130     140     150     160     170
hIDO1  AL LPPILVYADQVLANWKKDPNKKPLIYNNMIVLRFSDGDCSKGFILVSLLVEIAAAS
hIDO2  NLGLPPIVYADHVLNWKKDPNCFLEIGNLIIISFPGGSLIGFLLVILVKEAVE
consensus>50 nLeLPPILVyaDlVLaNwKkKDP#gfLeieN$#viiSFpdG#clhGFILVslLVEieAvp

      180     190     200     210     220     230
hIDO1  AIKVIPLVFRAMQMQRHLLKALLETASCLERKALQVHQHDHVNPKAFFSVIRIYLSG
hIDO2  GKALVQATNAHLPNDEALLOALQRLLSICDITRLGQHDYVDPIFYAGIRIFLSG
consensus>50 aIKvIvqvfnAilmq#q#aLLqALLeialci#dilqvlqQiHDyV#PdiF%aviRI%LSG

      240     250     260     270     280     290
hIDO1  WKGNPQLISGLVYEGRWHPKFAAGGSAQSSVFCDFVLLGICQTAGGGAAAFLOIMR
hIDO2  WAKNPAMPAGLVYEGVSCPLIYAGGSAQSSVLAFAFDFLGIKSKSG...FLYMR
consensus>50 WKdNPq$pdGLvYEGvs##Ple%aGGSAaQSSVlqaFDvllGIqqsaegGhaa#FLydMR

      300     310     320     330     340     350
hIDO1  FYMPPAHKAFICSLSPSVRFVLSKGDAGLREAYACVVALVLSYHLQIVTKYIIL
hIDO2  dYMPPAHKAFIDISAPSLRDIYLSGGLLILAYNOCVAAALRSYHITVTKYIIT
consensus>50 dYMPPaHknFiedieSnPSvR##!LSkG#dgLleAY#qCVqALveLRSYHiqIVTKYiii

      360     370     380     390     400
hIDO1  FASQDP..KENHISEDPKLLAAGTGGTDIMFLKVRSTTEKSLKKG.
hIDO2  AAAKARLGGKPNLPGPPALKLRGTGGTAVMSFLKVRRTTEHSILPRG
consensus>50 aAaqqkhgKeNhlpedPqaLedkGTGGTdvMnFLKsVRdkTleSiLhegg

```

FIGURE E.6: Sequence alignment of hIDO2 with hIDO1 considering a start at M14 for hIDO2, without any tag, realized by Multialign software [1] with Blosum62 matrix. Highlighting of polar (green) and apolar (pink) residues.

Appendix F

List of publications

F.1 Publications

- Haufroid, M., Mirgaux, M., Leherte, L., & Wouters, J. Crystal structures and snapshots along the reaction pathway of human phosphoserine phosphatase. *Acta Crystallographica Section D: Structural Biology*, 2019, 75(6):592-604.
- Leherte, L., Haufroid, M., Mirgaux, M., & Wouters, J. Investigation of bound and unbound phosphoserine phosphatase conformations through Elastic Network Models and Molecular Dynamics simulations. *Journal of Biomolecular Structure and Dynamics*, 2020, 39(11):3958-3974.
- Mirgaux, M., Leherte, L., & Wouters, J. Influence of the presence of the heme cofactor on the JK-loop structure in indoleamine 2, 3-dioxygenase 1. *Acta Crystallographica Section D: Structural Biology*, 2020, 76(12):1211-1221.
- Mirgaux, M., Leherte, L & Wouters, J. Temporary intermediates of L-Trp along the reaction pathway of human indoleamine 2,3- dioxygenase 1 and identification of an exo site. *International Journal of Tryptophan Research*, 2021, 14:1-11.
- Mirgaux, M., Scaillet, T., Kozlova, A., Tumanov, N., Frederick, R., Bodart, L., & Wouters, J. Structural study of bioisosteric derivatives of 5-(1H-indol-3-yl)-benzotriazole and their ability to form chalcogen bonds. *Acta Crystallographica Section E: Crystallographic Communications*, 2022, 78(4):418-424.

F.2 Conferences

- M. Mirgaux, L. Leherte, J. Wouters, A structural study by crystallography and Molecular Dynamics of hIDO to assist design of original inhibitors, Young SRC, 6th March 2020, Namur, Belgium. (Flash presentation and poster)
- M. Mirgaux, L. Leherte, J. Wouters, A structural study by crystallography and Molecular Dynamics of hIDO1 to assist design of original inhibitors, ReNaForBis Workshop, October 2020, Oléron, France. (Poster)
- M. Mirgaux, A structural study by crystallography and Molecular Dynamics of hIDO1 to assist design of original inhibitors, NISM Annual Meeting 2020, 20th November 2020, Namur, Belgium. (Online presentation)

- M. Mirgaux, Crystallography and Molecular Dynamics of hIDO1 to assist structure based drug design, 28th Young Research Fellows Meeting 2021, 12sd February 2021, Paris, France. (Online presentation)
- M. Mirgaux, Crystallography and Molecular Dynamics to improve the fundamental understanding of therapeutic targets for cancer, 11th Belgian Crystallography Symposium, 17th March 2021, Namur, Belgium. (Poster)
- M. Mirgaux, Importance of protein loop dynamics and plasticity in drug development, Young Chemists' Conference Day 2022, 1st April 2022, Liege, Belgium. (Oral presentation)
- Fundamental study of hIDO1 and hIDO2 proteins to aid drug design for immunotherapy, Women in Science, 28th April 2022, Namur, Belgium.
- M. Mirgaux, Unraveling hIDO1 conformational dynamic to guide the discovery of new inhibitors, 3rd FNRS Med Chem Symposium, 19th May 2022, Namur, Belgium. (Oral presentation)
- M. Mirgaux, A fundamental study of protein dynamism to the rescue of drug design: application to hIDO1, 33rd European Crystallography Meeting, 23-27th Augustus 2022, Versailles, France. (Poster)
- M. Mirgaux, Unraveling hIDO1 conformational dynamic to guide the discovery of new Inhibitors, NISM Annual Meeting 2022, 6th September 2022, Namur, Belgium. (Oral presentation)
- M. Mirgaux, Unraveling hIDO1 Conformational Dynamic to Guide the Discovery of New Inhibitors, 9th EFMC Young Medicinal Chemists' Symposium, 8-9th September 2022, Nice, France. (Oral presentation)

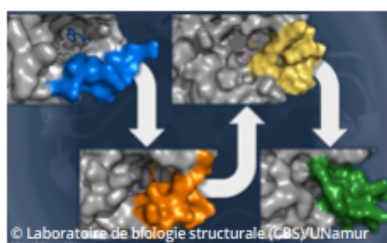
F.3 PDB structures

- 2019: 6Q6J, 6HYY, 6HYJ
- 2020: 7A62
- 2021: 7NGE, 7P0R, 7P0N
- 2022: 7XYT, 7ZL2

F.4 Prizes

- " Étude mécanistique de la phosphosérine phosphatase humaine, une enzyme impliquée dans la chimiorésistance au 5-Fluorouracile dans le cancer du côlon : approches expérimentale et computationnelle. " - Prize of the master thesis in Chemistry - University of Namur, Namur, Belgium, 2019.
- " Mechanistic study of the human phosphoserine phosphatase (hPSP): crystallographic and computational approaches " - Prize of the best oral presentation - SFMBBM, Bruxelles, Belgium 2019.
- " Unravelling hIDO1 conformational dynamic to guide the discovery of new inhibitors" - Prize of the best oral presentation - 3rd FNRS Med Chem Symposium, Namur, Belgium, 2022.

F.5 Publications in web media



Une recherche dynamique pour aider la conception de futurs médicaments

Dans le corps humain, de nombreuses fonctions biologiques sont assurées au moyen de protéines dont la structure en trois dimensions peut se réarranger

au gré des besoins de la réaction qu'elles provoquent. La dynamique des protéines est ainsi la pierre angulaire régissant la plupart des réactions métaboliques. Malheureusement, il arrive que des protéines interviennent dans certaines maladies. C'est le cas de l'hémoprotéine indoleamine 2,3-dioxygénase 1 humaine (hIDO1). En effet, une plus grande proportion de cette protéine dans les cellules cancéreuses provoque une résistance à l'immunothérapie. La compréhension de son fonctionnement est donc un défi essentiel et nécessite souvent une approche innovante et multidisciplinaire. Dans ce contexte, les auteurs de cette publication ont étudié le comportement dynamique de hIDO1 en laboratoire par cristallographie et dynamique moléculaire. Les recherches ont permis une meilleure compréhension des étapes de positionnement du substrat ainsi que la détermination d'un nouveau site de liaison dans cette protéine. Tous ces résultats constituent une base solide pour aider à la conception future de médicaments ciblant hIDO1.

« Temporary Intermediates of L-Trp Along the Reaction Pathway of Human Indoleamine 2,3-Dioxygenase 1 and Identification of an Exo Site », *International Journal of Tryptophan Research*, décembre 2021.

 **Manon Mirgaux**, Aspirante FNRS, CBS, UNamur
Et al.

FIGURE F.1: Publication in the FNRS.news of February 2022.

narilis NAMUR RESEARCH INSTITUTE FOR LIFE SCIENCES

HOME MEMBERS RESEARCH FACILITIES OPEN POSITIONS BOARD CONTACT GALLERY

Home News "Young Medicinal Chemist Award in Belgium (SRC)" awarded to PhD student Manon Mirgaux

"YOUNG MEDICINAL CHEMIST AWARD IN BELGIUM (SRC)" AWARDED TO PHD STUDENT MANON MIRGAUX

Manon Mirgaux is a PhD candidate in the Laboratory of Structural Biological Chemistry (CBS) led by Prof. Johan Wouters (UNamur, NARILIS/NISM institutes). Her doctoral thesis aims at understanding the functioning of dynamic loops in proteins considered as potential targets for cancer immunotherapy. Her work focuses specifically on the dynamic behavior of the JK-loop of the human indoleamine 2,3-dioxygenase 1 (IDO) hemoprotein, a protein exerting an immunosuppressive effect and facilitating immune escape of tumors. The research conducted by Manon relies on the use of a multidisciplinary approach mixing protein crystallography, biochemistry and computational modelling techniques (Mirgaux et al., 2021; Mirgaux et al., 2020). Her findings will form a solid basis for the design of novel IDO inhibitors able to effectively restore anti-tumor immune defenses.

On May 19, 2022, Manon Mirgaux had the opportunity to present her work during the 3rd symposium of the FNRS contact group "Medicinal Chemistry" at the UNamur. With her brilliant talk entitled "A fundamental study of protein dynamism to the rescue of drug design: application to hIDO1", she was selected as the winner of the **Young Medicinal Chemist Award in Belgium (SRC)**. Thanks to this prize, Manon is now invited to give an oral communication at the international conference "EFMC Young Medicinal Chemists' Symposium" to be held in September 2022 in Nice!

FIGURE F.2: Publication in the highlight of the Narilis newsletter of June 2022.



UNIVERSITÉ DE NAMUR

Accueil | Accès | Annuaire | Contacts

Accueil UNamur > Nouvelles > Manon Mirgaux récompensée par le « Young Medicinal Chemist Award in Belgium » de la SRC

NOUVELLE

MANON MIRGAUX RÉCOMPENSÉE PAR LE « YOUNG MEDICINAL CHEMIST AWARD IN BELGIUM » DE LA SRC

Le 19 mai 2022, Manon Mirgaux a eu l'opportunité de présenter ses travaux lors du 3eme colloque du groupe de contact FNRS « Chimie Médicinale » à l'UNamur. Avec son brillant exposé, elle a remporté le « Young Medicinal Chemist Award in Belgium » de la Société Royale de Chimie (SRC).

Manon Mirgaux est doctorante sous contrat d'aspirante FNRS au Laboratoire de Chimie Biologique Structurale (CBS) du département de chimie de l'UNamur, dirigé par le Professeur Johan Wouters (Instituts NARILIS et NISM). Sa présentation, intitulée « Une étude fondamentale du dynamisme des protéines au secours de la conception de médicaments : application à hIDO1 » s'appuie sur l'utilisation d'une approche multidisciplinaire mêlant cristallographie des protéines, biochimie et techniques de modélisation computationnelle. Ses découvertes constitueront une base solide pour la conception de nouveaux inhibiteurs capables de restaurer efficacement les défenses immunitaires pour combattre des tumeurs.

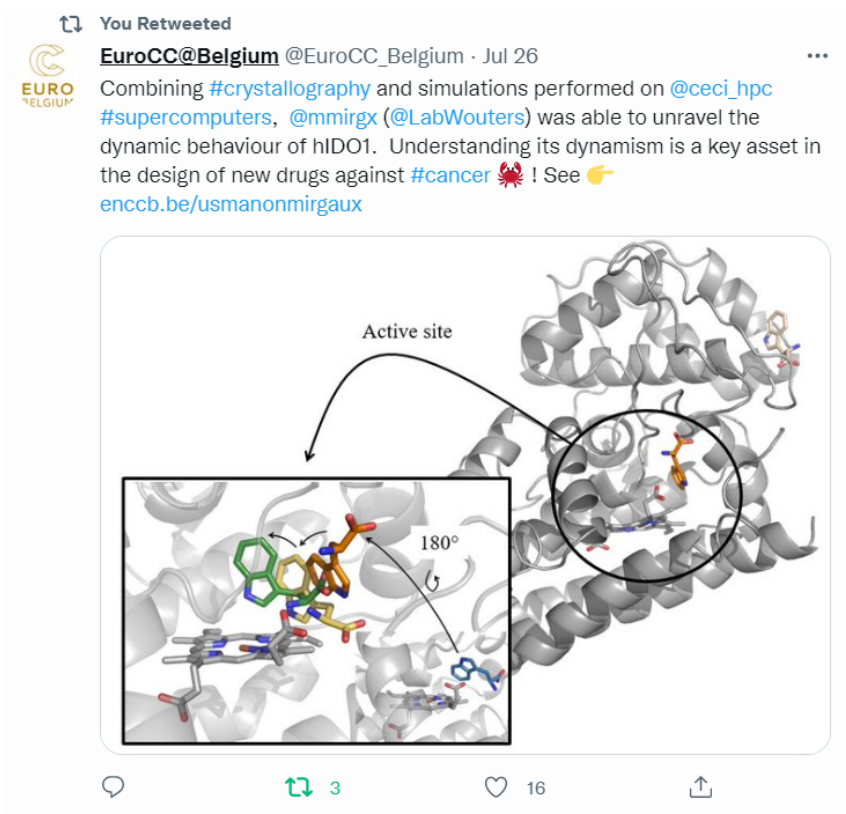
La Société Royale de Chimie (SRC) a pour objectif prioritaire de rassembler les chimistes belges et de favoriser les échanges interdisciplinaires générateurs d'idées et d'innovations.

Grâce à ce prix, elle est invitée à présenter une communication orale au colloque international « EFMC Young Medicinal Chemists' Symposium » qui se tiendra en septembre 2022 à Nice !

Félicitations à elle !

Contact : Manon Mirgaux - manon.mirgaux@unamur.be

FIGURE F.3: Publication in the "Nouvelles" of the UNamur in June 2022.



You Retweeted

EuroCC@Belgium @EuroCC_Belgium · Jul 26

Combining #crystallography and simulations performed on @ceci_hpc #supercomputers, @mmirgx (@LabWouters) was able to unravel the dynamic behaviour of hIDO1. Understanding its dynamism is a key asset in the design of new drugs against #cancer 🦋 ! See 👉 [enc.cb.be/usmanonmirgaux](https://www.enc.cb.be/usmanonmirgaux)

Active site

180°

3

16

FIGURE F.4: Publication in the User Story of the EuroCC in February 2022.
Full link: <https://www.enc.cb.be/usmanonmirgaux>